UNIVERSITÀ DEGLI STUDI DI NAPOLI "FEDERICO II"

Tesi di Dottorato

"Clinical application of multiparametric imaging in the evaluation of the canine reproductive tract"

Coordinatore
Chiar.mo Prof.
Paolo De
Girolamo

Candidato
Dott. Stefano Spada

Tutor
Chiar.mo Prof.
Marco Russo

List of Chapters

Preface

The present manuscript endeavors to elucidate and explore the scientific pathway undertaken during the three-years PhD program of the candidate, focusing on investigating innovative and evidence-based clinical approaches to small animal reproduction clinical issues. The thesis comprises an introductory section (Chapter 1 - 2), where the candidate's primary areas of interest have been meticulously analyzed and discussed. Additionally, a collection of the scientific studies (Chapter 3 – 10) conducted during the PhD has been provided. A final chapter (Chapter 11) concerning the future perspective and the main outcomes of the present thesis.

The goal of the present thesis is to acquire data on innovative diagnostic tools capable of evaluating and assessing the canine reproductive status and potential, in the context of a multiparametric diagnostic approach to canine fertility. Moreover, part of the thesis is dedicated into describing and investigating novel methods aimed to improve male fertility.

List of abbreviations

AD Abdominal diameter
AF Abnormal fetus
AI Artificial insemination
ALH Amplitude of lateral head
ANOVA Analysis of variance
ATP Adenosine triphosphate
AUC Area under the curve
AV Area of vascularization
BCF beat cross frequency
BCS Body condition score
BD Body diameter
BP Biparietal diameter
BPD Biparietal diameter
BPH Benign prostatic hyperplasia
CEUA Committee on the Use of Animals
CEUS Contrast-enhanced ultrasound
CI Confidence interval
CLAHE Contrast limited adaptive histogram equalization
CLIA Chemiluminescence immunoassay
CnTI Contrast Tuned Imaging
CPS Contrast pulse sequencing
CRL Crown-rump length
CT Computerized tomography
CTRL Control
CV Cohort value
DAPI 4′,6-diamidino-2-phenylindole
DCF Dichlorofluorescein
DCFH-DA Dichlorofluorescein diacetate
DHT dihydrotestosterone
DICOM Digital imaging and communication in medicine
DL longitudinal depth
DNA Deoxyribonucleic acid
DPTV diencephalo-telencephalic vesicle
DT Tansverse depth
DV Diastolic velocity
EC European conformity

List of abbreviations

ECAR European college of animal reproduction
EDTA Ethylenediamine tetraacetic acid
EDV End diastolic velocity
EYT-G egg-yolk TRIS-citrate glucose
FDA Food and drug administration
FITC Fluorescein isothiocyanate
FNA Fine needle aspiration
GGc Greenhouse-Geisser correction
HD High definition
HMMP High mitochondrial membrane potential
HOST hyposmotic swelling test
HR Hear rate
IBM International business machine
ICC Inner chorionic cavity
IQR Interquartile range
L Length
LDL low density lipoprotein
LH Luteinizing hormone
LIN Linearity
LMMP Low mitochondrial membrane potential
LN Liquid nitrogen
LSD Least square difference
MDA Malondialdehyde
MI Mechanical index
MR Magnetic resonance
mTT Medium transit time
NF Normal fetus
NPV Negative predictive value
OS Oxidative stress
OUD Outer uterine diameter
PA Prostate area
PBS Phosphate buffered saline
PI Pulsatility index
PN Prostate neoplasia
PPI Perfusion peak intensity
PPV Positive predictive value
PRF Pulse repetition frequency
PSV Peak systolic velocity
PV Prostate volume

List of abbreviations

PW Pulsed-wave Doppler
RBF Regional blood flow
RBV Regional blood volume
RI Resistivity index
ROC receiver operating characteristic
ROI Region of interest
ROIS Region of interests
ROS Reactive oxygen species
RT Room temperature
SCA Sperm class analyzer
SD Standard deviation
SE Standard error
SF6 sulfur hexafluoride
SPSS Statistical Package for the Social Sciences
SPV Systolic peak velocity
STR Straightness
SV Systolic velocity
TaMAX time-averaged maximum velocity
TaMIN time-averaged minimum velocity
TBA thiobarbituric acid
TCG Tris citric acid glucose
TIC Time-intensity curves
TmT Transmission time
TTP Time to peak
TUNEL Terminal deoxynucleotidyl transferase dUTP nick end labeling
UCA Ultrasound contrast agent
US Ultrasound
UWN Ultra-Wideband Non-linear
VA Vascularization area
VAP Average path velocity
VCL Curvilinear velocity
VEGF Vascular endothelial growth factor
VR Vascularization ratio
VSL Straight-line velocity
W Width
WOB Wobble

List of figures

List of figures

List of tables

Abstract

Canine infertility has posed considerable financial challenges to the expanding breeding industry, especially in the past decades. Assessing fertility in dogs may be challenging due to the absence of standardized tests for both males and females. A comprehensive clinical approach to evaluate canine fertility should include an accurate physical and ultrasonographic examination of the reproductive tract, hormonal tests and semen analysis. While B-mode ultrasound (US) is an excellent tool at detecting reproductive conditions, a multiparametric ultrasonographic approach is recommended due to the limited specificity of two-dimensional ultrasound in the differentiation of pathologic conditions or in the monitoring of physiologic reproductive processes. Contrast-enhanced ultrasound (CEUS) emerged as a promising technique involving an intravenous contrast-agent capable of assessing the microvascularization of an organ, resulting a suitable method in distinguishing benign from malignant lesions giving superior information compared to colour and power Doppler ultrasound.

The primary focus of the current thesis is to evaluate the application of a multiparametric ultrasonographic approach for both male and female reproductive conditions, including CEUS. Prostatic neoplasia (PN), though uncommon in canines, tends to be more prevalent in castrated dogs. The assessment of prostate malignancies may be challenging due to low specificity of B-mode ultrasonographic signs and to the few information available in literature. CEUS revealed to be a suitable method to differentiate benign from malignant lesions in prostate of intact dogs. The first study of the current thesis was to assess prostatic perfusion in castrated dogs using CEUS. CEUS was performed in 64 neutered dogs, using a 5–7.5 MHz linear transducer with coded harmonic capability, dedicated analytical software, and a second-generation contrast agent, SonoVue. B-mode evaluation was performed to assess mean prostate volume and, subsequently a CEUS examination was undertaken. It was possible to detect the vascular prostatic flow in all specimens and quantitative parameters such as peak perfusion intensity (PPI) and time to peak (TTP) were measured using a dedicated software to analyse contrast enhancement (Qontrast). The parameters were compared with the one from previous studies revealing a higher PPI when compared to intact dogs. CEUS showed promising results indicating potential diagnostic applications for PN diagnosis in neutered dogs. The parameters derived from the present studies exhibited a high

standard deviation among specimens, possibly indicative of the considerable variability in size, age, age at castration, and time elapsed since castration. Therefore, another study was undertaken to assess potential variations in prostatic vascularization detected using CEUS in dogs. Image analysis was performed by using a digital software (ImageJ), able in objectivize measurement of tissue characteristics, favouring the detection of changes in echogenicity or vascular blood supply which may not be distinguished by the human eye. Twenty-three neutered dogs underwent B-mode and CEUS of the prostate using the same methodology as the previous study. Videoclips were analysed with both software (Qontrast and ImageJ) and the following parameters were calculated: PPI, TTP and Vascularization Ratio (VR). Correlation tests revealed higher vascularization in younger compared with older dogs ($p < 0.05$) and in smaller compared with larger dogs ($p < 0.05$). Time elapsed since orchiectomy ($p > 0.05$) had no effect on prostatic perfusion. CEUS and the post-processing analysis tool ImageJ allowed analysis of vascular perfusion in all dogs and showed the potential to improve the diagnostic possibilities for andrological examination. The lack of correlation with time elapsed since castration may contribute to the high variability observed in the specimens. Consequently, a preliminary study was conducted to describe vascular regression after at least 3 months since castration, aiming to determine whether vascular regression persists beyond this timeframe. Ten neutered dogs were evaluated twice six years apart using the same techniques (B-mode and CEUS) to detect morphologic and vascular involution of the prostate after castration. The prostate exhibited similarity in terms of morphology and echotexture on B-mode US, minimally decreasing in volume over time. Prostate perfusion significantly decreased in all dogs between T0 and T1, with a PPI reduction from 54.9 to 29.6 % and an increase in TTP from 26.3 to 47 s. These preliminary data suggest that prostatic involution after neutering is not a short-term process and may be of clinical relevance.

Another section of the present thesis was conducted in female dogs, aiming to address the knowledge gap concerning uterine and ovarian changes during oestrus using a multiparametric ultrasonographic approach. A study employing high definition (HD) US was conducted to assess the reproductive tract of female dogs during follicular development. Eight females were examined at five different time points during the follicular phase, determined through vaginal cytology and blood progesterone concentrations. US examinations were performed using the ACUSON S2000/SIEMENS device equipped with a multifrequency HD transducer

(5.5-18 MHz). The ovarian structures were evaluated and measured throughout the oestrus cycle. A correlation was observed between uterine thickness increase and the rise in ovarian and follicular dimensions. The HD ultrasonography technique, with its excellent image resolution, favoured a more precise characterization of the reproductive structures in female dogs and the changes occurring during the follicular phase of the estrous cycle.
In the context of a multiparametric approach to the detection of ovulation in dogs, an additional study was conducted, integrating pulsed wave Doppler and CEUS in the evaluation of follicular development. Eight healthy bitches were enrolled in the study and were evaluated by using B-mode, Pulsed wave Doppler and CEUS at five different timepoints (T1 – T5) of the estrous cycle established by vaginal cytology and serum progesterone concentration. Ovarian vascular blood supply evaluated with Pulsed wave Doppler and CEUS evaluation increased across all the timepoints. Quantitative CEUS analysis revealed a statistical difference in PPI (%), MTT (s) and AUC (%) in particular at T5. CEUS evaluation of the ovaries was feasible and demonstrated a marked increase in perfusion parameters in the late postovulatory period, demonstrating its applicability in the assessment of canine corpora lutea development.
Another focal point of the current thesis centered on placental hemodynamics, aiming to determine quantitative and qualitative parameters for pregnant brachycephalic bitches. Moreover, it wants to describe placental vascularization and perfusion in females with fetal abnormalities close to delivery. Previous studies found an increase incidence of fetal anomalies in brachicephalic dogs, but it is not known if placental function could play a role in the occurrence of these conditions. The study involved forty-four healthy fetuses from 22 brachycephalic bitches and 9 fetuses with gestational abnormalities (anasarca and hydrocephalus) from 8 brachycephalic bitches. Evaluations were conducted at days 25 (M1), 45 (M2), and 58 (M3) of gestation in normal pregnancies, whereas fetuses with gestational abnormalities were evaluated at the last time point. Biometric values of the fetuses were determined through B-mode, and vascular indices by Doppler fluxometry of the umbilical artery, whereas qualitative assessment of contrast filling and quantitative parameters of placental perfusion were performed using CEUS. Contrast distribution remained uniformly homogeneous in placental tissues and CEUS filling parameters exhibited consistency throughout the evaluated periods ($P < 0.05$). In fetuses with hydrops, Doppler values were similar to those obtained in healthy subjects ($P > 0.05$), while CEUS evaluation revealed a heterogeneous

distribution with lower intensity of placental tissue filling and a delay in perfusion time ($P < 0.05$) exhibiting a diagnostic accuracy of 75%. CEUS showed demonstrated its applicability in detecting failures in placental vascular filling (tissue dysfunction) in fetuses with anasarca and hydrocephalus.

The concluding section of the present thesis was dedicated to exploring innovative approaches to enhance canine fertility and semen quality, with a specific focus on the use of antioxidants. Artificial insemination is a routinely performed method in canine breeding programme and semen evaluation results crucial for the successful achievement of a pregnancy. Insemination can be performed by using fresh, chilled or frozen semen. However, semen storage should be performed with the presence of antioxidants, which helps in preventing damaging processes to spermatozoa. The aim of these studies was to evaluate the effect of two antioxidants, Maca and Crocin, in the supplementation of semen extender on quality-related canine semen parameters during cooling and freezing. The first experiment aimed to evaluate the effect of Maca on frozen-thawed sperm quality in canine semen. Ejaculates from ten dogs were frozen in the absence (control group) or the presence of 10, 20 and 50 µL/mL of an aqueous extract of Maca and were evaluated immediately after thawing and after 1h and 2 h at 37 C° for sperm viability, motility, DNA fragmentation and lipid peroxidation. Canine sperm cells frozen with an extender supplemented with Maca exhibited higher total motility. Moreover, the supplementation of Maca was responsible for a surge in hyperactivation and WOB of sperm cells after one hour at 37°C. What emerges from this study is the protective role of Maca against lipid membrane peroxidation of canine spermatozoa, which is a primary marker of oxidative stress.

The second experiment evaluated the effect of Crocin supplementation extender at three different concentrations (C0,5, C1 e C2) on quality-related canine semen parameters after cooling. Ejaculates from ten dogs were evaluated for sperm viability, sperm motility, membrane integrity and lipid peroxidation after 3 h, 24 h, 4 days and 7 days of storage at 4 C°. the addition of 0.5 mM crocin in the extender significantly increased the proportion of spermatozoa with intact membranes at both 4 and 7 days compared to the control group and despite similar values of total motility and progressive motility most of the sperm kinetic parameters improved in C0.5 group compared to the control after 4 days of storage. The present findings suggested that the enrichment of the extender with the crocin improves to a

certain improved canine semen quality, particularly after 4 days of storage at 4 °C.

Introduction

Results of canine breeding soundness evaluation should give reliable insights into the breeding potential of a dog. Different definitions and explanations of terms such as fertility, fecundity, subfertility, and infertility have been provided in human and veterinary literature (Zegers-Hochschild et al. 2017). The term fertility refers to the ability to produce offspring through reproduction after reaching sexual maturity (Tanga et al. 2021). In human medicine, it has also been addressed to the circumstances under which livebirths occur, as the term is often used by demographs in the context of predicting the development of a population in a specific area (Leridon, 2007). The fertility rate is the average number of offspring that an individual gives birth to during its lifetime (Tanga et al. 2021). Indeed, the term fecundity refers to the biological theoretical ability and capacity to reproduce (Wood, 1989). Infertility in humans has been defined as the failure to achieve a pregnancy after 12 months or more of regular unprotected sexual intercourse (Zegers-Hochschild et al. 2017; Vander Borght & Wyns, 2018) and may be commonly caused by problems in ejaculating or reduced quality of sperm (Tanga et al. 2021). In dogs, infertility has been defined as conception failure of at least three (Domoslawska et al. 2020) or four (de Souza et al. 2015) matings with different bitches. The term infertility may generally be used interchangeably with the term subfertility, as the latter does not define a different or less severe fertility status than infertility, nor is subfertility a condition that exists before infertility is diagnosed (Zegers-Hochschild et al. 2017). Actually, in human subfertility describes any form of reduced fertility with prolonged time of unwanted non-conception (Gnoth et al. 2005), whereas in dogs a clear definition has never been reported. Infertility in dogs may present as failure to produce pregnancy after mating, inability to mate or ejaculate, or presenting seminal abnormalities, pathologic condition of the genitourinary tract, or reproductive physical defects. In dogs, infertility may progress slowly, even though often the onset of signs may be rapid (Lopate, 2012). The causes may be divided into two groups: congenital and acquired infertility (Domoslawska et al. 2020). Congenital defects are present at birth, whereas acquired infertility occurs later in a previously diagnosed fertile dog (Fontbonne, 2011; Gobello & Corrada, 2004).

Several diagnostic tests have been described in male and female dogs to assess canine fertility, but their predictive accuracy is not enough to determine the potential for present and future breeding (Arlt et al. 2023).

Ultrasound is one of the most reliable diagnostic tools, used to evaluate the canine reproductive tract (Davidson et al. 2009; Mantziaras, 2020), being able to provide interesting information about morphologic and physiologic changes associated to reproductive status and fertility (Moxon et al. 2015; England et al. 2009). Ultrasound allows evaluation of the size, shape, margins, echogenicity and echotexture of a given parenchyma and can guide fine-needle aspiration or core biopsy from a tissue or a lesion. It is the method of choice to assess prostate and testis to detect pathological condition and to assess fertility in terms of sperm production and quality in males (Moxon et al. 2015; de Souza et al. 2015; Smith, 2008). It is noteworthy that several prostate and testicular diseases may directly affect dog fertility impairing spermiogenesis, quality of semen and semen viability (Lopate, 2012; Kime et al. 2002; Krakowski et al. 2015), making early diagnosis important to save future breeding potential.

Ultrasound in female dogs is highly used to image the reproductive tract and is the method of choice to detect ovarian (Wilborn & Maxwell, 2012; Troisi et al. 2023) and uterine pathologies (Hagman, 2022). Ultrasound has the ability to detect changes during the oestrus cycle involving the reproductive tract, in particular being able to recognize follicular development and monitor ovulation timing (England et al. 2009; Tsuchida et al. 2022). Mistake during ovulation timing detection is the major factor impairing breeding success in canines (Wilborn & Maxwell, 2012). Ultrasound showed an accuracy of 93.6 % in identifying the day of ovulation in dogs (Tsuchida et al. 2022). However, its interpretation is strictly correlated to a well experienced operator, a cooperative patient and to the number of evaluations required to accurately detect the ovulation itself (Tsuchida et al. 2022). B-mode and colour doppler ultrasound are able to detect anomalies of the reproductive tract in both males and females, but the differentiation between benign and malignant lesions, often requires the use of cytology, biopsy or advanced imaging such as CT (Mantziaras, 2020; Russo et al. 2009).

Infertility may be also due to conditions affecting the development of the fetus during pregnancy, determining early resorption or abortion of the fetus (Fontbonne, 2023). Ultrasound is a suitable method to detect pregnancy in the bitch and is able to determine fetal gestational age, monitor fetal development and placental function (Siena & Milani, 2021). Few studies have evaluated the characteristics of prenatal death using ultrasound (England & Russo, 2006), and just case reports have described the appearance of specific foetal development abnormalities using ultrasound

(Hopper et al. 2004). Early diagnosis of foetal diseases or death remains challenging and subjective due to the lack of specific ultrasonographic signs using B-mode and Colour Doppler.

Several ultrasonographic techniques with different peculiarities and characteristics have been described in veterinary clinical practice. Besides the excellent application of b-mode and colour ultrasound into the evaluation of the reproductive tract, the main disadvantage is that image quality, reproducibility and measurements depend mainly on the operator (Mantziaras, 2020). A multiparametric approach consisting of more than one ultrasonographic technique, such as conventional B-mode, Pulsed-wave Doppler, Contrast-enhanced and elastography ultrasound is increasingly being used in human medicine (Auer et al. 2017) and in veterinary medicine as well (Orlandi et al. 2022). In particular, contrast-enhanced ultrasound (CEUS) is able in assessing the vascular blood supply, especially for the differentiation of benign and malignant lesions in different tissues and organs (Canejo-Teixeira et al. 2022; Burti et al. 2020; Vignoli et al. 2011; Orlandi et al. 2022). CEUS evaluates vessels under the resolution of conventional colour doppler, providing information about microvascularization of the evaluated structure (Dietrich et al. 2018). Several studies have been conducted about the use of CEUS in small animal reproduction, providing information about prostate (Russo et al. 2009; Vignoli et al. 2011; Troisi et al. 2016), testes (Volta et al. 2014; Orlandi et al. 2022), ovaries (Nogueira Aires et al. 2022), uterus (Quartuccio et al. 2020) and placenta (Orlandi et al. 2019; Silva et al. 2021). The technique provided new and auspicious insights about malignant lesions in prostate and testes, reporting different vascular characteristics between benign and malignant conditions (Vignoli et al. 2011; Volta et al. 2014). Prostate gland appearance after castration have not been fully investigated, even though previous studies reported a high incidence of prostate neoplasia after gonadal removal in dogs (Teske et al. 2002; Bryan et al. 2007). CEUS has the potential to improve the diagnostic approach in the detection of ovulation timing, placental disfunction and differentiating malignant from bening lesions in reproductive tissues, in the context of a multiparametric clinical approach to canine infertility and genital diseases.

Nevertheless, the quantity of studies about normal and abnormal findings of the reproductive tract using CEUS techniques are still scant (Sinagra et al. 2023).

The present thesis aims to provide new insight into canine reproductive tract features using a multiparametric approach, including CEUS technique.

References

Arlt SP, Reichler IM, Herbel J, Schäfer-Somi S, Riege L, Leber J, Frehner B. Diagnostic tests in canine andrology - What do they really tell us about fertility? Theriogenology. 2023 Jan 15;196:150-156. doi: 10.1016/j.theriogenology.2022.11.008. Epub 2022 Nov 12. PMID: 36423509.

Auer, T.; De Zordo, T.; Dejaco, C.; Gruber, L.; Pichler, R.; Jaschke, W.; Dogra, V.S.; Aigner, F. Value of Multiparametric US in the assessment of Intratesticular Lesions. Radiology 2017, 285, 640–649.

Bryan JN, Keeler MR, Henry CJ, Bryan ME, Hahn AW, Caldwell CW. A population study of neutering status as a risk factor for canine prostate cancer. Prostate. 2007 Aug 1;67(11):1174-81. doi: 10.1002/pros.20590. PMID: 17516571.

Burti S, Zotti A, Rubini G, Orlandi R, Bargellini P, Bonsembiante F, Banzato T. Contrast-enhanced ultrasound features of malignant focal liver masses in dogs. Sci Rep. 2020 Apr 8;10(1):6076. doi: 10.1038/s41598-020-63220-3. PMID: 32269300; PMCID: PMC7142119.

Canejo-Teixeira R, Lima A, Santana A. Applications of Contrast-Enhanced Ultrasound in Splenic Studies of Dogs and Cats. Animals (Basel). 2022 Aug 17;12(16):2104. doi: 10.3390/ani12162104. PMID: 36009694; PMCID: PMC9404716.

de Souza MB, England GC, Mota Filho AC, Ackermann CL, Sousa CV, de Carvalho GG, et al. Semen quality, testicular b-mode and Doppler ultrasound, and serum testosterone concentrations in dogs with established infertility. Theriogenology 2015;84:805-10.

Davidson A.P., Baker T.W. Reproductive Ultrasound of the Dog and Tom. Top. Companion Anim. Med. 2009;24:64–70. doi: 10.1053/j.tcam.2008.11.003.

Dietrich CF, Averkiou M, Nielsen MB, Barr RG, Burns PN, Calliada F, Cantisani V, Choi B, Chammas MC, Clevert DA, Claudon M, Correas JM, Cui XW, Cosgrove D, D'Onofrio M, Dong Y, Eisenbrey J, Fontanilla T, Gilja OH, Ignee A, Jenssen C, Kono Y, Kudo M, Lassau N, Lyshchik A, Franca Meloni M, Moriyasu F, Nolsøe C, Piscaglia F, Radzina M, Saftoiu A, Sidhu PS, Sporea I, Schreiber-Dietrich D, Sirlin CB, Stanczak M, Weskott HP, Wilson SR, Willmann JK, Kim TK, Jang HJ, Vezeridis A, Westerway S. How to perform Contrast-Enhanced Ultrasound

(CEUS). Ultrasound Int Open. 2018 Jan;4(1):E2-E15. doi: 10.1055/s-0043-123931. Epub 2018 Feb 7. PMID: 29423461; PMCID: PMC5802984.

Domoslawska A, Zdunczyk S. Clinical and spermatological findings in male dogs with acquired infertility: a retrospective analysis. Andrologia 2020;52:e13802.

England GC, Russo M. Ultrasonographic characteristics of early pregnancy failure in bitches. Theriogenology. 2006 Oct;66(6-7):1694-8. doi: 10.1016/j.theriogenology.2006.01.028. Epub 2006 Mar 22. PMID: 16554089.

England GC, Russo M, Freeman SL. Follicular dynamics, ovulation and conception rates in bitches. Reprod Domest Anim. 2009 Jul;44 Suppl 2:53-8. doi: 10.1111/j.1439-0531.2009.01416.x. PMID: 19754536.

Fontbonne, A. (2011). Infertility in male dogs: Recent advances. Revista Brasiliera Reproduction in Animals, 35, 266–273.

Fontbonne A. Causes of pregnancy arrest in the canine species. Reprod Domest Anim. 2023 Sep;58 Suppl 2:72-83. doi: 10.1111/rda.14407. Epub 2023 Jul 20. PMID: 37312645.

Gnoth C, Godehardt E, Frank-Herrmann P, Friol K, Tigges J, Freundl G. Definition and prevalence of subfertility and infertility. Hum Reprod. 2005 May;20(5):1144-7. doi: 10.1093/humrep/deh870. Epub 2005 Mar 31. PMID: 15802321.

Gobello, C., & Corrada, Y. (2004). Acquired infertility in male dogs with normal libido. Compendium on Continuing Education for the Practising Veterinarian –. North American Edition, 26(1), 18–27.

Hagman R. Pyometra in Small Animals 2.0. Vet Clin North Am Small Anim Pract. 2022 May;52(3):631-657. doi: 10.1016/j.cvsm.2022.01.004. PMID: 35465903.

Hopper BJ, Richardson JL, Lester NV. Spontaneous antenatal resolution of canine hydrops fetalis diagnosed by ultrasound. J Small Anim Pract. 2004 Jan;45(1):2-8. doi: 10.1111/j.1748-5827.2004.tb00187.x. PMID: 14756202.

Kime DE, Tveiten H. Unusual motility characteristics of sperm of the spotted wolffish. J. Fish Biol. 2002;61:1549–1559.

Krakowski, L., Wachocka, A., Brodzki, P., Wrona, Z., Piech, T., Wawron, W., Chalabis-Mazurek, A., 2015. Sperm quality and selected biochemical parameters of seminal fluid in dogs with benign prostatic hyperplasia. Anim. Reprod. Sci. 160, 120–125.

References

Leridon H. Studies of fertility and fecundity: comparative approaches from demography and epidemiology. C R Biol. 2007 Apr;330(4):339-46. doi: 10.1016/j.crvi.2007.02.013. Epub 2007 Apr 3. PMID: 17502290.

Lopate C. The problem stud dog. Vet Clin North Am Small Anim Pract 2012;42:469e88 [vi].

Mantziaras G. Imaging of the male reproductive tract: Not so easy as it looks like. Theriogenology. 2020 Jul 1;150:490-497. doi: 10.1016/j.theriogenology.2020.03.009. Epub 2020 Mar 14. PMID: 32241560.

Moxon R., Bright L., Pritchard B., Bowen I.M., Souza M.B.d., Silva L.D.M.d., England G.C.W. Digital Image Analysis of Testicular and Prostatic Ultrasonographic Echogencity and Heterogeneity in Dogs and the Relation to Semen Quality. Anim. Reprod. Sci. 2015;160:112–119. doi: 10.1016/j.anireprosci.2015.07.012.

Nogueira Aires LP, Gasser B, Silva P, Del'Aguila-Silva P, Yamada DI, Carneiro RK, Bressianini Lima B, Padilha-Nakaghi LC, Ramirez Uscategui RA, Spada S, Russo M, Rossi Feliciano MA. Ovarian contrast-enhanced ultrasonography and Doppler fluxometry in bitches during the postovulatory estrus and corpora lutea formation. Theriogenology. 2022 Dec;194:162-170. doi: 10.1016/j.theriogenology.2022.10.009. Epub 2022 Oct 13. PMID: 36265337.

Orlandi R, Vallesi E, Boiti C, Polisca A, Troisi A, Righi C, Bargellini P. Contrast-enhanced ultrasonography of maternal and fetal blood flows in pregnant bitches. Theriogenology. 2019 Feb;125:129-134. doi: 10.1016/j.theriogenology.2018.10.027. Epub 2018 Oct 30. PMID: 30414566.

Orlandi R, Vallesi E, Boiti C, Polisca A, Bargellini P, Troisi A. Characterization of Testicular Tumor Lesions in Dogs by Different Ultrasound Techniques. Animals (Basel). 2022 Jan 17;12(2):210. doi: 10.3390/ani12020210. PMID: 35049832; PMCID: PMC8773431.

Quartuccio M, Liotta L, Cristarella S, Lanteri G, Ieni A, D'Arrigo T, De Majo M. Contrast-Enhanced Ultrasound in Cystic Endometrial Hyperplasia-Pyometra Complex in the Bitch: A Preliminary Study. Animals (Basel). 2020 Aug 7;10(8):1368. doi: 10.3390/ani10081368. PMID: 32784584; PMCID: PMC7460530.

Russo M., Vignoli M., Catone G., Rossi F., Attanasi G., England G.C.W. Prostatic perfusion in the dog using contrast-enhanced doppler ultrasound. Reprod. Domest. Anim. 2009;44:334–335. doi: 10.1111/j.1439-0531.2009.01442.x.

References

Siena, G.; Milani, C. Usefulness of Maternal and Fetal Parameters for the Prediction of Parturition Date in Dogs. Animals 2021, 11, 878. https://doi.org/10.3390/ani11030878

Silva P, Maronezi MC, Padilha-Nakaghi LC, Gasser B, Pavan L, Nogueira Aires LP, Russo M, Spada S, Ramirez Uscategui RA, Moraes PC, Rossi Feliciano MA. Contrast-enhanced ultrasound evaluation of placental perfusion in brachicephalic bitches. Theriogenology. 2021 Oct 1;173:230-240. doi: 10.1016/j.theriogenology.2021.08.010. Epub 2021 Aug 10. PMID: 34399387.

Sinagra L, Orlandi R, Caspanello T, Troisi A, Iannelli NM, Vallesi E, Pettina G, Bargellini P, De Majo M, Boiti C, Cristarella S, Quartuccio M, Polisca A. Contrast-Enhanced Ultrasonography (CEUS) in Imaging of the Reproductive System in Dogs: A Literature Review. Animals (Basel). 2023 May 11;13(10):1615. doi: 10.3390/ani13101615. PMID: 37238045; PMCID: PMC10215906.

Smith J. Canine prostatic disease: a review of anatomy, pathology, diagnosis, and treatment. Theriogenology. 2008 Aug;70(3):375-83. doi: 10.1016/j.theriogenology.2008.04.039. Epub 2008 Jun 2. PMID: 18514299.

Tanga BM, Qamar AY, Raza S, Bang S, Fang X, Yoon K, et al. Semen evaluation: methodological advancements in sperm quality-specific fertility assessment - a review. Animal bioscience 2021;34:1253e70.

Teske E, Naan EC, van Dijk EM, Van Garderen E, Schalken JA. Canine prostate carcinoma: epidemiological evidence of an increased risk in castrated dogs. Mol Cell Endocrinol. 2002 Nov 29;197(1-2):251-5. doi: 10.1016/s0303-7207(02)00261-7. PMID: 12431819.

Troisi A, Orlandi R, Bargellini P, Menchetti L, Borges P, Zelli R, Polisca A. Contrast-enhanced ultrasonographic characteristics of the diseased canine prostate gland. Theriogenology. 2015 Nov;84(8):1423-30. doi: 10.1016/j.theriogenology.2015.07.029. Epub 2015 Jul 29. PMID: 26277703.

Troisi A, Orlandi R, Vallesi E, Pastore S, Sforna M, Quartuccio M, Zappone V, Cristarella S, Polisca A. Clinical and ultrasonographic findings of ovarian tumours in bitches: A retrospective study. Theriogenology. 2023 Oct 15;210:227-233. doi: 10.1016/j.theriogenology.2023.07.020. Epub 2023 Jul 22. PMID: 37540955.

Tsuchida M, Komura N, Yoshihara T, Kawasaki Y, Sakurai D, Suzuki H. Ultrasonographic observation in combination with progesterone monitoring for detection of ovulation in Labrador Retrievers. Reprod

Domest Anim. 2022 Feb;57(2):149-156. doi: 10.1111/rda.14035. Epub 2021 Nov 8. PMID: 34724259.

Vander Borght M, Wyns C. Fertility and infertility: Definition and epidemiology. Clin Biochem. 2018 Dec;62:2-10. doi: 10.1016/j.clinbiochem.2018.03.012. Epub 2018 Mar 16. PMID: 29555319.

Vignoli M., Russo M., Catone G., Rossi F., Attanasi G., Terragni R., Saunders J.H., England G.C. Assessment of Vascular Perfusion Kinetics Using Contrast-enhanced Ultrasound for the Diagnosis of Prostatic Disease in Dogs. Reprod. Domest. Anim. 2011;46:209–213. doi: 10.1111/j.1439-0531.2010.01629.x.

Volta A., Manfredi S., Vignoli M., Russo M., England G.C.W., Rossi F., Bigliardi E., Di Ianni F., Parmigiani E., Bresciani C., et al. Use of contrast-enhanced ultrasonography in chronic pathologic canine testes. Reprod. Dom. Anim. 2014;49:202–209. doi: 10.1111/rda.12250.

Wilborn RR, Maxwell HS. Clinical approaches to infertility in the bitch. Vet Clin North Am Small Anim Pract. 2012 May;42(3):457-68, v. doi: 10.1016/j.cvsm.2012.01.016. PMID: 22482812.

Wood JW. Fecundity and natural fertility in humans. Oxf Rev Reprod Biol 1989;11:61-109.

Zegers-Hochschild F, Adamson GD, Dyer S, Racowsky C, de Mouzon J, Sokol R, Rienzi L, Sunde A, Schmidt L, Cooke ID, Simpson JL, van der Poel S. The International Glossary on Infertility and Fertility Care, 2017. Fertil Steril. 2017 Sep;108(3):393-406. doi: 10.1016/j.fertnstert.2017.06.005. Epub 2017 Jul 29. PMID: 28760517.

Chapter 1

Ultrasonographic examination of the canine reproductive tract
B-mode and Pulsed wave Doppler ultrasound

1.1 B-mode and Doppler ultrasound of the male reproductive tract

1.1.1 Ultrasound of the prostate gland

Ultrasound is the imaging modality of choice for the male reproductive system (Smith, 2008) and the most commonly used imaging technique, due to its advantages. It is a quick, non-invasive, inexpensive method, widely available in small animal practice. Sedation is rarely needed, while the owner can safely be present. Ultrasound allows evaluation of the size and parenchyma of organs and can guide fine-needle aspiration or core biopsy from a tissue or a lesion (Mantiaras, 2020).
The male reproductive system of dogs consists of the testes, spermatic cord, excurrent duct system, scrotum, accessory sex glands, penis and muscles for protrusion, erection and ejaculation. The prostate is the only accessory sex glands in dogs and may be assessed by using digital rectal palpation in terms of location, size and pain (Smith, 2008). Ultrasound allows an improved evaluation of the gland in terms of dimensions, integrity of the capsule and parenchymal changes (Gunzel-Apel et al. 2001; Levy et al. 2014). The prostate is an ovoid-shape bilobed gland positioned at the bladder neck which encircles the proximal urethra. The normal prostate is positioned within or immediately cranial to the pelvis and is bordered dorsally by the rectum. The prostate may be imaged in longitudinal and transverse plan where the urethra results to be as a hypoechoic line and circle, respectively. The prostate is characterized by a hyperechoic capsule and a homogeneous echogenic parenchyma. The size of the gland can be assessed by single measurements (Levy et al. 2014; Bosma et al. 2021) or by using prostate volume (Atalan et al. 1999b). The prostate dimensions may vary depending on the size and age of the dog (Atalan et al. 1999a; Ruel et al. 1998; de Freitas et al. 2015). After castration prostate goes through a volumetric involution, becoming an ellipsoid shaped structure with a hypoechoic parenchyma (Cazzuli et al. 2022; Bosma et al. 2021; Angrimani et al 2020). Deprivation of androgen action performed by using treatments such as finasteride, osaterone acetate and deslorelin acetate, affect both prostate dimensions and vascularization having similar effect reported after neutering (Niżański et al. 2020; Lima et al. 2021; Angrimani et al. 2020). The combination of reduced size and reduced echogenicity often makes it difficult to differentiate the gland margins from the periprostatic fat (Russo

& Vignoli, 2023). The two lobes of the dog's prostate gland each have an independent vascular supply. The prostatic artery has an anatomically variable origin, but commonly arises from the internal pudendal artery. For each lobe various vessels can be identified: cranial, dorsal and ventral subcapsular also called lateral by some authors, caudal, and parenchymal (Stefanov, 2004; Sun et al. 2017). Blood flow from the prostate can be detected only in short segments of the relevant vein.

Pulsed-wave Doppler (PW) ultrasound is useful for identification of the location of the prostatic arterial supply and vessels may be imaged in the transverse or longitudinal plane. Flow characteristics vary according to the region of the prostate artery (Gunzel Apel, 2001; Zelli et al. 2013). In PW mode, a sample volume is placed to surround the entire lumen of a vessel and the waveforms are recorded. The blood flow parameters determined are peak systolic velocity (PSV), end diastolic velocity (EDV), (RI) (PSV-EDV)/PSV) (Pourcelot 1974) and Pulsatility Index (PI) (PSV-EDV)/mean velocity) (Gosling and King 1974). Prostatic evaluation through Doppler combined with two-dimensional ultrasound provides dynamic and specific information related to the anatomy and morphology of the studied organ and also enables localization, characterization, and quantification of vascular hemodynamics (de Freitas et al. 2015).

Prostate appearance may change according to the presence of diseases such as BPH, prostatitis and prostatic neoplasia. In most of the condition prostate may appear enlarged. However, B-mode ultrasound did not show specificity to distinguish benign from malignant conditions (Bradbury et al. 2009). Dogs affected by BPH may have an enlarged prostate gland with dis-homogenous prostatic parenchyma, characterized by the presence of hyperechoic foci with shadowing effects, representing mineralization and several parenchymal cysts, with variable dimensions, representing the prostatic ducts with an accumulation of prostatic fluid (de Freitas et al. 2015, Vignoli et al. 2011). When cysts become very large, they may have a similar appearance to a true paraprostatic cyst (fluid distention of a remnant uterus masculinus, Müllerian ducts), and can be difficult to differentiate, although the former is usually associated with other prostatic parenchymal changes typical of BPH, and in some cases the wide base of attachment/origin of the cyst within the prostate can be detected (in true paraprostatic cysts the cyst is attached only by a thin stalk-like structure). Large prostatic retention cysts or paraprostatic cysts have fluid that is anechoic but may become more echogenic and have obvious sediment consisting in mineralization with shadowing effect (Renfrew et al. 2008; Russo & Vignoli, 2022). Prostatitis

may occur together with BPH, therefore prostate may be increased in size and a hypoechoic band surrounding the prostatic capsule may be found as a result of the prostatic oedema, above all in acute prostatitis (Lea et al. 2022). The parenchyma is usually heterogenous and in acute prostatitis has a hypoechoic appearance, which is followed in more chronic cases by increased echogenicity, with focal echogenic regions (Russo & Vignoli, 2022). Steatitis or peritonitis affecting the periprostatic fat causes a hyperechoic and hyperattenuating appearance (Russo & Vignoli, 2022). Prostatic mineralization may occur in BPH, prostatitis and prostatic neoplasia even though it was found that this feature was more frequent in the latter condition (Bradbury et al. 2009; Lea et al. 2022; Russo et al. 2012). In case of prostatitis, prostatic abscesses may be present, and could be distinguished by cysts by a hypoechoic content and a thicker wall. Occasionally, ruptured abscess may be found, being an emergency situation (Lea et al. 2022).

Prostatic neoplasia may be characterized by several signs, but none of them is specific of malignant condition. Bradbury and colleagues found that mineralization in neutered dogs had a positive predictive value (PPV) of 100% for prostate neoplasia, a negative predictive value (NPV) of 50%, and a sensitivity and specificity of 84% and 100%, respectively, whereas in intact dogs had a PPV of 22%, an NPV of 96%, and a sensitivity and specificity of 67% and 77%, respectively (Bradbury et al. 2009). The development of prostatic pathology is in many cases associated with changes in the vascular supply to the prostate as well as changes to the prostatic parenchyma (Russo et al. 2012). The study of blood flow velocity by PW could not determine the true flow values due to its dependence on the angle of insonation, while indices (RI and PI), expressed by relationships between the velocity (PSV, EDV and V means) being independents of this parameter, are not affected by any sampling errors (Zelli et al. 2013a; Moll et al. 2017). In dogs affected by BPH, there is an overall increase in prostatic vascular blood supply, even though specific parameters calculated by using PW are not directly influenced. In human medicine, RI is considered an important parameter to detect benign prostate hyperplasia. However, this was not found in dogs, probably due to a different composition of the prostatic capsule, inducing less intraprostatic pressure in canines (Zelli et al. 2013). Vascularization of the prostate may be affected by ejaculation in the previous 6 hours (Alonge et al. 2018a,b). Prostate vascularization is affected by androgen action and castration leads to a decrease in terms of overall vascularization (Lima et al. 2021).

1.1.2 Ultrasound of the testis

Testicles in dogs are within the scrotal sac, have a homogenous parenchyma and are characterized by the presence of a central hyperechoic line or circle, in longitudinal and transverse view, respectively, representing the mediastinum testis (Russo & Vignoli, 2022). The testicular capsule surrounds the parenchyma and is a dynamic "sub-organ" (Mantziaras, 2020). Ultrasound examination of the testes is part of the breeding soundness evaluation of the dog, as there is a good correlation between testicular volume and total sperm output (England, 1991). Testicular volume may be calculated by using ultrasound, which resulted to be more accurate when compared with orchidometry (Paltiel, 2002). Interestingly, the estimation of the normal testicular size is not always easy and requires knowledge of the body weight of the dog, as it is positively correlated with testicular weight and volume (Johnston et al. 1991). However, even though testicular size should be taken into account during a breeding soundness examination, no differences in terms of testicular volume were noticed between fertile and infertile dogs (de Souza et al. 2015). The age of the animal should also be considered, as the size of the testicles increases only during the juvenile period, until puberty (James & Heywood, 1979) and moreover, in prepubertal dogs, the testes tend to have a more hypoechoic echogenicity compared to adult dogs (Bracco et al. 2023). Estimating testicular volume can be useful in demonstrating asymmetry or reduction, as some authors have reported that testicular volume is age-related, with the maximum size reached at 6 years, followed by a progressive decrease (Mantziaras et al. 2014). Subtle generalized changes may be difficult to detect; dogs with testes that are more echogenic and less homogeneous have poorer semen quality (Moxon et al. 2015).

The epididimys consists of head, body and tail, located cranially, dorsally and caudally, respectively and it appears hypoechoic when compared to testicular echogenicity (Russo & Vignoli, 2022). Microlithiases are commonly seen following testicular inflammation or in early-stage testicular degeneration, often associated with poor sperm morphology and poor sperm motility (Kim et al. 2003). Testicular or epididymal cysts are an occasional incident finding. They appear anechoic, well circumscribed, round areas, often with distal acoustic enhancement (Russo & Vignoli, 2022).

Vascularization of the testicles can be assessed by using colour Doppler ultrasound. In particular, the supra-testicular artery, that is part of the pampiniform plexus, the marginal testicular artery at the cranial pole of the

testis, marginal testicular artery at the caudal pole of the testis, and intratesticular artery, comprising the centripetal branches and recurrent rami, can be identified and evaluated by using this technique (Gunzel-Apel 2001; Bracco et al. 2023; Venianaki et al. 2023; Gumbsch et al. 2002).

Characteristics of blood flow within the testicular artery, assessed by pulsed-wave Doppler ultrasound, vary depending on the segment (de Souza et al. 2014). Among the haemodynamic parameters of blood flow evaluated during Doppler examination of the testicular artery, the resistance index (RI) and the pulsatility index (PI) have been studied widely and have been considered as possible indicators of semen quality in dogs (Gloria et al. 2020; Zelli et al. 2013b). Of note, however, is that England and colleagues, in dogs, found no associations between these two parameters and future semen quality (England et al. 2017). In the testes, the increase in these indices characterises disruption in the microcirculation and thus a significant reduction in the testicular blood flow. Spermatogenesis is a highly sensitive process in which blood supply is of particular importance, and changes in the blood flow of the area could lead to impairment in sperm production (Lemos et al. 2020; Srivastava et al. 2021). Vascularization is directly correlated to the age and healthy status of the testes. Venianaki and colleagues have reported changes occurring to the testicular vascularization from the 4th to the 40th week of age in Beagle puppies, finding that the most adequate size and clear spectral waveforms of the testicular arteries may be assessed as early as the 12th week of age (Venianaki et al. 2023). Moreover, Brito and colleagues found that testicular vascularization results to be reduced when compared to young dogs. Ageing seems to cause natural hemodynamical changes to the testicular artery, resulting in reduced blood flow (ischemia) and tissue damage. Testes and epididymis vascular characteristics, therefore, may represent the causal factors for changes in spermatogenesis and, as a consequence, negatively affect the sperm quality of older dogs (Brito et al. 2021).

Ultrasound is the method of choice to detect (England et al. 1991) and assess most of the canine testicular disorders (Orlandi et al. 2022; Bracco et al. 2023; Russo & Vignoli, 2022). Ultrasound is the most used method to identify and locate cryptorchid testes in dogs (Felumlee et al. 2012). However, testicular atrophy or reduced dimensions of the undescended testes could make the location challenging (Khan et l. 2018; Russo & Vignoli, 2022). The condition occurs more often on the right side with the inguinal canal location being the most frequent. Moreover, cryptorchidism seems to be more common in the inguinal region of dog of small sized

breeds and in the abdominal region in dogs of medium- and large-sized breeds (Tannouz et al. 2019). Vascular blood supply evaluation by using colour doppler may reveal a displacement of the pampiniform plexus (Russo & Vignoli, 2022). Criptorchid dogs may be normal, atrophied or may present signs of neoplastic degeneration (Khan et al. 2018). When the cryptorchid neoplastic testis exceeds 8 cm it may not be possible to confirm the origin with ultrasound, and CT is preferred (Russo & Vignoli, 2022).

Orchitis, as inflammation of the testis, can occur acutely or chronically. Acute orchitis may present with variable ultrasonographic characteristics, ranging from irregular and poorly defined anechoic areas to a diffuse patchy hypoechoic echo pattern, and focal abscessation may be evident (Davidson et al. 2009; Mattoon et al. 2020; Bigliardi et al. 2019). Typically, the testis and epididymis enlarge, and fluid may accumulate between the visceral and parietal tunic within the scrotum, being a hydrocele (Bigliardi et al. 2019). The fluid may be anechoic or hypoechoic depending on the nature of the fluid accumulation. Chronic orchitis and epididymitis is less obvious in terms of ultrasonographic features and may reveal hyperechoic or mixed echogenic parenchyma, often associated with a reduction in testicular size. In the case of chronic progression of orchitis, abscess formation may occur, characterized by an irregular hyperechoic wall and anechoic to hypoechoic central contents (Mattoon et al. 2020). In acute conditions, vascularization is generally increased when compared to normal testes (Bigliardi et al. 2019).

Testicular tumour may be diagnosed by using B-mode ultrasound and colour doppler, even though some lesions may be hysoechoic and low vascularized, that may require other techniques to be identified (Orlandi et al. 2022). Besides B-mode and Colour Doppler are able to identify the most of testicular tumour lesions, there are no typical features that may help in distinguishing tumour types (Orlandi et al. 2022). Testicular tumours can range from circumscribed small nodules to large complex masses with heterogeneous echo-pattern and disruption of normal anatomy. At the time of diagnosis, Sertoli cell tumours and seminomas are usually large with mixed echogenicity, resulting sometimes in generalised testicular enlargement (Russo et al. 2021). Interstitial cell tumours may appear as well-defined focal hypoechoic lesions. However, areas of haemorrhage and necrosis may occur in all tumour types and may be seen ultrasonographically as disorganised hyperechoic and hypoechoic regions. Other findings that may be associated with testicular neoplasia include areas of calcification within the testicular parenchyma that appear as hyperechoic foci producing

acoustic shadowing. There are few descriptions of testicular blood flow in abnormal testes. Colour Doppler ultrasonography shows an increase in blood flow within and around most tumours (Bigliardi et al. 2019). While this is useful for tumour detection, the changes noted are not specific for tumour type (Russo et al. 2021; Orlandi et al. 2022).

1.1.3 Ultrasound of the penis

Ultrasound findings of the normal canine penis have been described. The anatomical parts of the penis, such as corpora cavernosa, corpus spongiosum, os penis and bulbus glandis were all demonstrated in ultrasound images (Payan-Carreira & Bessa, 2008; Goericke-Pesch et al. 2013). It may aid in discerning the etiology of priapism, distinguishing between nonischemic (arterial, high flow) or ischemic (veno-occlusive, low flow) condition (Lavely, 2009).
Within the penis, the penile bone can be identified as a hyperechoic structure with back acoustic shadowing. The Corpus spongiosum is slightly hyperechoic and is mainly delimited by the hyperechoic penile bone, housing the urethra. Evaluating the urethra is crucial for identifying obstructions such as calculi or clots. Corpora cavernosa, encompassing the corpus spongiosum, exhibit a heterogeneous parenchyma due to multiple hypoechoic areas representing blood storage chamber, filled during erection (Goericke-Pesch et al. 2013). Various os penis tumors, including haemangiosarcoma, osteochondrosarcoma, osteosarcoma, and lymphosarcoma, have been visualized using ultrasound and radiography, although requiring histological confirmation. Neoplasia like transmissible venereal tumor, squamous cell carcinoma, lymphosarcoma, adenocarcinoma, and mast cell tumor in the canine penis lack specific imaging findings in the literature (Mantziaras, 2020).

1.2 B-mode and Doppler ultrasound of the female reproductive tract

1.2.1 Ultrasound of the ovaries

The ovaries are located in the dorsal abdomen slightly lateral to the caudal poles of the kidneys. Multifrequency curvilinear or linear 5–11 MHz transducers are the standard equipment for ovarian examination. High-resolution probes (i.e., 18 MHz or more) are currently available and may

maximise the ability to visualise subtle changes in the ovary. The caudal pole of the kidneys and the adjacent area are examined in sagittal and transverse planes to localise the ovaries (Davidson, 2009). Their identification may be facilitated by the appearance of marginal artefacts dorsal to each ovary. The appearance varies according to the stage of the oestrous cycle when follicular growth can be readily detected. Multiple anechoic structures can be observed during proestrus and oestrus; after ovulation, thicker-walled corpora lutea are present during late oestrus and the first phase of dioestrus. Round and hypoechoic corpora lutea are easily detectable in mid-dioestrus when they deform the otherwise oval profile of the ovary (Russo et al. 2021; Russo & Vignoli, 2022). Follicles are recruited during in the last phase of anoestrus, when few and small follicles may be found until 100 days before ovulation (England et al. 2009). However, the number of follicles remains scant until the onset of proestrus, where follicular development increase dramatically from 1.3 ± 0.6 per ovary to a peak of 7.6 ± 0.5 per ovary (England et al. 2009). Number of follicles is directly correlated to the breed examined, as a consequence of the number of puppies expected by the bitch. Large follicles with a mean diameter of 4 mm can be detected from 10 days before ovulation (England et al. 2009). They tend to increase in size reaching a mean of 6-7 mm during ovulation. From the day of the LH peak to the ovulation time there is a constant increase of follicle diameter (Tsuchida et al. 2022). Nevertheless, it has been reported that follicles may ovulate any time once reaching 5 mm (Tsuchida et al. 2022). Moreover, the size of preovulatory follicles seem to change significantly from one breed to another (England & Allen, 1989; England et al. 2009; Tsuchida et al. 2022) as in giant breeds, they may reach up to 9 mm in diameter (Fontbonne & Malandian, 2006). In 5% of bitches, detection of ovulation is extremely difficult, mainly due to technical problems (Domosławska et al., 2014). From these findings, it can be assumed that ultrasound is a feasible method to detect follicle development, but the detection of the day of ovulation remains challenging.

After ovulation follicles does not collapse as in other species, and may be seen as fluid filled cavities, whose diameter tends to increase reaching a peak of 1.2 cm at day 6 after ovulation, during the formation of the corpora lutea (Tsuchida et al 2022). The early corpora lutea are often cavitated and contain anechoic fluid and as such can be difficult to differentiate from a follicle. They do however have thick walls and the diameter of the lumen is smaller than the follicle that they replaced. Central cavities may persist for up to 25 days and do not compact until day 28. After that time, they may be seen as

hypoechoic structure with smooth margins, whose diameter tends to reduce throughout the diestrus phase (Russo & Vignoli, 2022).
Ovarian cysts may be found in dogs and may be identified as anechoic fluid-filled structures of variable size, several of which are commonly greater than 1 cm in diameter. Luteal cysts may present thicker wall when compared to follicular one (Knauf et al. 2014).
Ovarian tumours are uncommon in bitches and information regarding their ultrasonographic appearance are scant (Diez-Bru et al. 1998; Sehgal, 2019; Russo et al. 2021; Troisi et al. 2023). Confirmation that a mass is ovarian in origin is based on its appropriate location, being caudal to the kidneys, and ideally having an association with an adjacent uterine horn. The adjacent uterus can be confirmed by imaging the ovarian veins with Colour Doppler. Ultrasonographically, ovaries in bitches with ovarian tumours may appear unilaterally enlarged, with regional or focal lesions that may be solid or cystic. Frequently there is a significant disruption of the normal appearance with an inhomogeneous echotexture. Tumours may be small or large, with size ranging from 1.5 to 15 cm (Troisi et al. 2023) and may be solid, contain small cysts, or be primarily cystic in appearance (Russo et al. 2021). Ovarian masses may be classified as follows: solid masses (less than 10% anechoic cavities), solid masses with a cystic component (from 10% to 50%), or cystic masses (greater than 50%). The size of cysts may range from 0.2 to 3.5 cm in diameter (Russo et al. 2021). Troisi and colleagues found that granulosa cell tumours and adenocarcinoma shape were irregular in 69% and 60% respectively (Troisi et al. 2023) in accordance with previous findings (Diez-Bru et al. 1998; Madewell & Theilen, 1987). In contrast to the data published by Diez-Bru et al. 1998, they found an irregular shape in 100% of adenomas. The other neoplasia did not show any typical shape (Troisi et al. 2023). Teratomas are often cystic and may show partial mineralisation with distal shadowing, due to structures such as hair, skin, sweat glands, cartilage, bone, and teeth, which might help to distinguish these tumours from other ovarian masses (Russo et al. 2021). The presence of free fluid may be associated with peritoneal dissemination, and careful evaluation for metastatic disease should be performed. Colour Doppler ultrasound may help identify solid, vascularised components in an ovarian mass (Rowan et al. 2017).

1.2.2 Ultrasound of the uterus

The canine uterus is Y-shaped organ composed by four parts: uterine tubes, uterine horns, uterine body and cervix. The uterine horns extends from the

ovaries, positioned proximally and close to the abdominal wall converging distally in the midline at the uterine body (Russo et al. 2021).

The uterine tubes are generally not visible unless enlarged due to fluid accumulation or neoplasia. Uterine tube neoplasia are rare condition and ultrasound may be helpful in assessing the origin of the mass. Leiomyoma of the mesosalpinx has been described as a solid mass (Eker et al. 2006). Large adenomas have been described as unilocular cystic or cavernous masses (Marino et al. 2007; Plagge & Bali, 2018). In one case, an adenocarcinoma was described as an ovoid mass with a moderately vascularised heterogenous parenchyma and hypoechoic cystic areas.

The uterine body and uterine horns are composed of two distinct layers: a central homogeneous relatively hypoechoic region surrounded by a peripheral hyperechoic layer, representing the serosa (Russo & Vignoli, 2022). The lumen is generally not seen but may be visible as a bright echogenic central line, which represents the mucosal–luminal interfaces (Davidson et al. 2009; Russo et al. 2021). During oestrus, the uterus becomes thicker, more hypoechoic and the layers may be more distinct. During ovulation period a small anechoic endoluminal content may be found (Freitas et al. 2017; Russo & Vignoli, 2022). The uterine artery (positioned lateral to the uterine vein) may be detected adjacent to the mid uterine body and may be confirmed using the colour Doppler setting. Previous studies found an increase in RI of the uterine artery from 2 days prior to the day of ovulation (Freeman et al. 2013). However, it seems that parity and breed may directly influence the vascular blood supply indices (Freitas et al. 2017). In the post-partum period, the uterine layers are more evident. In the first weeks, it is possible to identify the three layers of the myometrium, whereas the endometrium appears echogenic (Barbosa et al. 2013). Vascular blood supply tends to decrease during the weeks (Barbosa et al. 2013), with a reduction in PSV and EDV and an increase in vascular resistance RI (Batista et al. 2013).

Uterine layers integrity may be damaged by the presence of multiple cysts in case of cystic endometrial hyperplasia. The size of the cysts may be highly variable and mainly with an anechoic content. The incidence of these cystic lesions increases with age, with most bitches over seven years having some changes (Russo & Vignoli, 2022).

The uterine horns may be filled with fluid of different echogenicity: anechoic fluid filled uterus is generally compatible with hydrometra or mucometra, whereas hypo- or echogenic content may be representative of pyometra or hemometra. Small echogenic particles and luminal echogenic

bodies may be identified, which probably represent inflammatory debris or hemorrhage, although mucus may have a similar ultrasonographic appearance (Russo & Vingoli, 2022). However, the evaluation of echogenicity remains subjective, therefore the diagnosis should be accompanied by clinical signs and other tests (Hagman, 2022). During pyometra, endometrial thickness increase and peritoneal effusion and reactivity may occur (Bigliardi et al. 2004). The uterine horns may severly enlarge causing organ displacement and may be folded upon itself (Russo & Vignoli, 2022). Vascular hemodynamics of uterine arteries is significantly influenced by uterine conditions. Pyometra bitches showed increase vascular blood flow and velocity when compared to dogs affected by cystic endometrial hyperplasia and healthy dogs. Moreover, endometrial hyperplasia, accompanied or not by luminal contents, seems to have a higher blood flow velocity than normal uterus. (Batista et al. 2016). Treatment with aglepristone and prostaglandin (Rodrigues da Rosa Filho et al. 2021) or cabergoline and prostaglandin (Batista et al. 2022) tends to reduce vascular perfusion of the uterus.

Uterine neoplasia may appear as endoluminal or intramural, homogeneous or heterogeneous, mass lesions with a possible amount of uterine fluid. Leiomyoma, fibroleiomyoma, and leiomyosarcoma have been described as solid masses, but anechoic ischemic cavities are often observed in the mass, giving a mixed to cystic pattern (Patsikas et al. 2014; Tsioli et al., 2011). Occasionally, hyperechoic foci have been reported and are thought to be a sign of calcification, fibrosis, or metaplasia found in this category of tumours. Poorly differentiated sarcomas have been described as solid masses. Adenocarcinomas are rare and occasionally present as masses of mixed echogenicity with solid areas, hyperechoic foci, and cystic components (Patsikas et al. 2014; Kokkinos et al. 2019). Endometrial polyps have been reported as endoluminal, projecting, well-demarcated masses, solid or with anechoic multiple cystic glands surrounded by a large amount of luminal fluid (Marino et al. 2013; Schlafer et al. 1997; Chambers et al. 2011). Despite some distinguishable patterns, most masses are described as solid with cystic areas, making diagnosis difficult unless biopsy samples are collected (Russo et al. 2021).

1.3 B-mode and Doppler ultrasound of the pregnant dog and fetus

1.3.1 Gestational age determination

Ultrasound is highly used for pregnancy diagnosis and is of great advantage in evaluating fetal development and abnormalities and determining the date of parturition (Lopate et al. 2008; Siena & Milani, 2021). Estimating gestational age allows to predict time of parturition, favouring a correct management in case of c-section scheduling. Gestational age can be determined and calculated based on several biometric values reported in literature but also on the first appearance of specific organs or fetal structures (Beccaglia et al. 2016; Arlt, 2020). Using biometric values may be important especially in case the time of ovulation and mating is not known. The most important measurements performed in clinical practice are: inner corionic cavity (ICC), representing the distance inner diameter of corionic cavity; biparietal diameter (BP), representing the distance between the parietal bones; outer uterine diameter (OUD), representing the maximal diameter of the uterus, measured in the region of the conceptus; body diameter (BD) representing the largest diameter of the abdomen, having in the scan both the fetal stomach and liver; deep portion of diencephalo-telencephalic vesicle (DPTV); crown-rump length (CRL), representing the distance from the anus to the head (Lopate, 2008). Measurements should be performed on at least two fetuses, due to the in-homogeneous development of the fetuses, to increase the accuracy of the prediction (Luvoni & Beccaglia, 2006; Beccaglia et al. 2008; Beccaglia et al. 2012; Alonge et al. 2016; Sridevi, 2013). Size and breed seems to influence significantly the accuracy of the measurements in the determination of the gestational age (Socha & Janowski, 2014; Socha & Janowski, 2015; Socha & Janowski, 2017). Specific formulas have been reported to be associated to a single breed, as it has been found that age and breed of the dog may influence gestational length (Son et al. 2001; Groppetti et al. 2015).
ICC and OUD are generally evaluated in the first half of pregnancy. ICC is the most used parameters with its best accuracy detected at 20-25 days of gestation. OUD tends to be highly inaccurate, due to the undefined measurement marker (Luvoni & Grioni, 2000). BP, BD, DPTV and CRL are used in the second half of pregnancy (Lopate, 2008; Beccaglia & Luvoni, 2006). CRL may be used from day 26 until day 45 after LH peak, since after this time the body starts to flex its shape, influencing negatively the accuracy of the measurements (England et al. 1990; Luvoni & Beccaglia, 2006). BD may be measured 26 days after the LH peak (Kutzler et al. 2003). BP may be identified as earlier as day 30 of pregnancy, although a better

visualization of parietal bones may occur after day 35 (Kutzler et al. 2003). Even though BP is considered the most reliable parameter to assess the gestational age, its accuracy may change during the weeks, being higher between the 5th and 6th week of pregnancy. However, recent studies investigating the reliability of the present parameter found a reduced accuracy in the last week of pregnancy for C-section planning (de Cramer et al 2018; Beccaglia & Luvoni, 2012). DPTV may be used from the 30th day of pregnancy, even though the best moment to assess the diencephalo-telencephalic vesicle is 7 days before parturition, because of the increased consistency of its measurement and the lower standard deviation on this date (Beccaglia et al. 2008). Recent studies reported that the combined use of ICC in early pregnancy and BP in late pregnancy showed no statistically significant differences in the prediction of parturition day (within ±1 and ±2 days), except for small-size bitches (78.9% and 42.3% within ±1, respectively) (Beccaglia & Luvoni, 2006; Socha & Janowski, 2014).
The use of placental measurements for estimating gestational age is controversial. Recent studies found a positive correlation between placental thickness and gestational age regardless of breed and body weight (Maldonado et al. 2012; Pollis et al. 2023).

1.3.2 Fetal development and maturity

Pregnancy diagnosis may be performed on the 19th or 20th, even though an early diagnosis at 17th days has been reported (Aissi & Slimani, 2008; Lopate, 2008; Kim & Son, 2007). The gestational chambers may be recognized as lemon-shaped anechoic structure distributed within the two uterine horns. The chamber turns into a spheroidal shape at 20th days of gestation, and the first embryonic echoes may be seen at 23rd day (Lopate, 2008; Aissi & Slimani, 2008). The zonary placenta may be seen as early on the 23rd of pregnancy as an echogenic band surrounding the inner corionic cavity in trasverse view and as a linear structure located dorsally and ventrally to the cavity when the fetus is scanned in longitudinal view (Kim & Son, 2007; Yeager et al. 1992). The placenta is a transient and unique organ of metabolic interchange between the conceptus and the dam and is composed by a fetal (the corion) and a maternal (the endometrium) component. Placental changes are reported during pregnancy in terms of vascular blood supply, as a result of the increasing metabolic demnand of the fetus. A recent study analyzed placental ultrasonographic changes in terms of echogenicity during pregnancy finding a more inhomogenous

parenchyma in late compared to early gestation (Zabitler et al. 2022). Between 23 and 25 days of pregnancy fetal heartbeat can be detected and measured with pulsed wave doppler (Siena & Milani, 2021). Fetal heart rate is a critical sign that should be assessed in every pregnancy check to verify the viability of the fetuses. The normal heart rate is generally above 220 bpm. A decrease of the heart rate may be sign of fetal distress, which can be defined as mild (between 220 and 180 bpm) or severe (<180 bpm). A heart rate decrease below 140 bpm may indicate fetal hypoxia and serious risk for the viability of the fetus (Lopate, 2008). However, the heart rate seems not to be constant throughout pregnancy. A recent study reported phenomena of heartbeat acceleration and deceleration during the last weeks two weeks of pregnancy (Gil et al. 2014). At 27-28 days of gestation the embryo moves from the periphery to the centre of the gestational chamber, suspended by the fetal membranes, with the yolk sac being the largest of the two cavities. The yolk sac become tubular and is resorbed within 30th day of pregnancy (Lopate, 2008). From at least day 30th several organs start to develop and may be recognized with ultrasound examination (Siena & Milani, 2021).
The assessment of fetal maturity is necessary to determine the ability of the fetus to survive in the extrauterine life. Recent studies reported the usefulness of intestinal evaluation, in terms of morphological development and peristaltic movement, as a tool to detect fetal maturity (Gil et al. 2015). The intestinal area may be visualized caudally to the fetal liver as a homogeneously echogenic region from 40 to 44 days of pregnancy (23–19 days before parturition), the intestinal wall may be visualized in some intestinal portions from 44 to 48 days (19–15 days before parturition). The intestinal wall and its mucosal surface may be easily identified from day 50 to day 54 (13–9 days before parurition). Fetal gastrointestinal movement may be detected from at least 10 days before parturition, with an increase in percentage in the following days in the number of peristaltic movements, in particular 5 days before the delivery (Milani et al. 2020; Siena et al. 2022b). Fetal kidney evaluation has been reported to be a suitable method to determine gestational age. Gil and colleagues proposed the use of a specific formula, involving the kidney length in order to detect the gestational age, whose best accuracy reported was between 15 and 11 days before parturition (Gil et al. 2018). Nevertheless, a recent study partially disagrees with the present findings, since the kidney formula did not show good accuracyin estimating the days before parturition (Siena et al. 2023a). Another study proposed the use of single parameters such as cortical and medullary thickness in a comprehensive evaluation of the estimated day of parturition

(Siena et al. 2022c). The development and ultrasonographic features of kidneys in canine fetus have been reported to be influenced by maternal and litter size, and days before parturition. In particular, both the cortex and the medulla present a more homogeneous parenchyma approaching the date of parturition (Siena et al. 2023b).
The use of Doppler evaluation has been reported and proposed during pregnancy diagnosis and evaluation. The use of doppler ultrasound may be use for the assessment of uterine and umbilical artery blood flow. The increasing metabolic request exhibits as an increase vascular blood supply of the placenta and uterus. Uterine artery perfusion increases in the last two trimesters of pregnancy, and the indices associated with blood flow velocities (resistive index, RI and pulsatility Index, PI) decrease as gestational age advances (Lopate, 2018; Blanco et al. 2008; Miranda & Domingues, 2010). Peak systolic (PSV) and end diastolic velocities (EDV), but not RI, are affected by litter size (Batista et al. 2018). An equation describing the correlation between uterine artery RI and gestational age has been calculated for small-size bitches, together with a RI reference range values during the second half of pregnancy (Batista et al. 2018) Variations in the previously described parameters are due to increased fetal needs for blood flow as pregnancy advances. During mid-late pregnancy, an influence of litter and maternal size on RI is reported, with lower values observed in large-size bitches compared with small-size bitches (Blanco et al. 2020).
Umbilical artery RI could be useful for parturition timing and early fetal distress assessment (Giannico et al. 2015). Giannico and colleagues reported that normal parturition is likely to occur within 12 h when all fetuses show a RI < 0.7 (Giannico et al. 2015).

1.3.3 Fetal abnormalities and death

The term “pregnancy loss” is generraly used to indicate early embryonic, or fetal resorption and abortion. The choice of these terms should be performed based on the moment of pregnancy, where fetal death occurs (Fontbonne, 2023). Several causes of pregnancy arrest are reported in literature, which may be divided in infectious causes, both bacterial and viral, and non-infectious causes, comprising diseases of the uterus, nutritional, environmental, toxic and hormonal causes (Schlafer, 2005; Root Kustritz, 2005; Fontbonne, 2023).
Embryonic or fetal resorption is a process that exhitates in the disintegration of the conceptus until the 30-40th day of pregnancy, which may be not

diagnosed, unless an ultrasonographic evaluation is not performed. Undeveloped bones and soft tissue may be detected by using ultrasound (England & Russo, 2006, Fontbonne, 2023). The resorption rate in canines is 14.2 % and may be influenced by several factors such as age and size of the dam, litter size and the presence of previous reproductive problems (Lascialfari et al. 2023).

The term abortion is usually reserved to indicate expulsion of a dead fetus or a living one unable to survive in the extrauterine life. The abortion may occur from the 35th day of pregnancy until the day of parturition (Johnston et al. 2001). However, its diagnosis may remain unnoticed due to cannibalism behaviour of the mother, which may eat the dead fetus (Odendaal et al. 1994). Late pregnancy arrest, especially in large sized dogs may exhitates in retained fetus, which could undergo mummification or maceration in the uterus, determining uterine diseases (Fontbonne, 2023).

The diagnosis of fetal death may be easily performed based on the absence of fetal heartbeat (Lopate, 2008). If an early embryonic resorption occurs, a gestational chamber, with reduced quantity of echogenic amniotic fluid may be found. Throughout the pregnancy the resorbed chambers tend to collapse on themselves, until no signs of amniotic fluid or embryonic membranes or echoes may be detected (Russo & Vignoli, 2022). When an abortion occurs and organs such as bones and soft tissue started their development, the latters may be recognized also in late pregnancy even though sometimes may present with a collapsed, deformed, or undeveloped shape. The amniotic fluid become echogenic with a crenulated appearance. Moreover, a dead fetus is generally smaller when compared to the rest of the litter due to an interrupted development (Russo & Vignoli, 2022, Lascialfari et al. 2023). Uterine pathologies may be determined by fetal death, especially when late abortion occurs, with retained fetus and placenta, that may act as a perfect pabulum for bacterial growing. Occasionally, anaerobic gas producing bacteria may grow within the chamber of the aborted fetus determing a localized uterine emphysema. In severe cases, where the entire litter does not survive the emphysema may occur within the entire uterus (Russo & Vignoli, 2022). Doppler ultrasound has been applied to assess the role of vascularization in the development of the fetus. Blanco and colleagues found that RI of the uterine, umbilical, and fetal renal arteries in bitches increases in abnormal pregnancies (Blanco et al. 2011). Similar results were reported in another recent study (Gaikwad et al. 2020). It cannot be excluded that pregnancy arrest may be a result of placental failure, due to vascular conditions.

When the term abnormal pregnancy is used, cases of development abnormalities and fetal diseases should be considered. Anasarca and hydrocephalus are one of the most represented fetal abnormalities reported in dogs, where prenatal diagnosis may be performed. However, the causes of these diseases is still unknown. Fetuses affected by anasarca may present an accumulation of anechoic fluid in the subcutaneous space, thorax, and abdominal cavity (Siena et al. 2022a). Occasionally, the condition may solve spontaneously (Hopper et al. 2004). Hydrocephalus may present a symmetrical or asymmetrical dilatation of cerebral ventricles, appearing anechoic surrounding the choroid plexus (foetal ventriculomegaly) (Sannmuang et al. 2020).

1.4 References

Aissi A, Slimani C. Time of initial detection of fetal structures and anatomic differentiation by using B-mode ultrasound examination in bitches. Pak J Biol Sci. 2008 Jul 1;11(13):1750-3. doi: 10.3923/pjbs.2008.1750.1753. PMID: 18819632.Alonge, S.; Beccaglia, M.; Melandri, M.; Luvoni, G.C. Prediction of whelping date in large and giant canine breeds by ultrasonography foetal biometry. J. Small Anim. Pr. 2016, 57, 479–483.

Alonge S, Melandri M, Fanciullo L, Lacalandra GM, Aiudi G. Prostate vascular flow: The effect of the ejaculation on the power doppler ultrasonographic examination. Reprod Domest Anim. 2018a Feb;53(1):110-115. doi: 10.1111/rda.13078. Epub 2017 Sep 11. PMID: 28891218.

Alonge S, Melandri M, Leoci R, Lacalandra GM, Aiudi G. Ejaculation effect on blood testosterone and prostatic pulsed-wave Doppler ultrasound in dogs. Reprod Domest Anim. 2018b Sep;53 Suppl 2:70-73. doi: 10.1111/rda.13277. PMID: 30238660.

Angrimani DSR, Francischini MCP, Brito MM, Vannucchi CI. Prostatic hyperplasia: Vascularization, hemodynamic and hormonal analysis of dogs treated with finasteride or orchiectomy. PLoS One. 2020 Jun 25;15(6):e0234714. doi: 10.1371/journal.pone.0234714. PMID: 32584842; PMCID: PMC7316311.

Arlt, S.P. The bitch around parturition. Theriogenology 2020, 150, 452–457.

Atalan G, Holt PE, Barr FJ. Ultrasonographic estimation of prostate size in normal dogs and relationship to bodyweight and age. J Small Anim Pract. 1999a Mar;40(3):119-22. doi: 10.1111/j.1748-5827.1999.tb03052.x. PMID: 10200922.

Atalan G, Holt PE, Barr FJ, Brown PJ. Ultrasonographic estimation of prostatic size in canine cadavers. Res Vet Sci. 1999b Aug;67(1):7-15. doi: 10.1053/rvsc.1998.0267. PMID: 10425234.

Barbosa Cda C, de Souza MB, de Freitas LA, da Silva TF, Domingues SF, da Silva LD. Assessment of uterine involution in bitches using B-mode and Doppler ultrasonography. Anim Reprod Sci. 2013 Jun;139(1-4):121-6. doi: 10.1016/j.anireprosci.2013.02.027. Epub 2013 Mar 16. PMID: 23602011.

Batista PR, Gobello C, Corrada Y, Pons E, Arias DO, Blanco PG. Doppler ultrasonographic assessment of uterine arteries during normal canine puerperium. Anim Reprod Sci. 2013 Oct;141(3-4):172-6. doi: 10.1016/j.anireprosci.2013.07.013. Epub 2013 Aug 6. PMID: 23968999.

References

Batista PR, Gobello C, Rube A, Corrada YA, Tórtora M, Blanco PG. Uterine blood flow evaluation in bitches suffering from cystic endometrial hyperplasia (CEH) and CEH-pyometra complex. Theriogenology. 2016 Apr 15;85(7):1258-61. doi: 10.1016/j.theriogenology.2015.12.008. Epub 2015 Dec 20. PMID: 26810829.

Batista, P.; Gobello, C.; Rube, A.; Barrena, J.; Re, N.; Blanco, P. Reference range of gestational uterine artery resistance index in small canine breeds. Theriogenology 2018, 114, 81–84.

Batista PR, Gobello C, Rube A, Barrena JP, Arioni S, Blanco PG. Doppler ultrasonographic evaluation of medically treated female dogs with cystic endometrial hyperplasia-pyometra complex. Vet Radiol Ultrasound. 2022 Jul;63(4):490-497. doi: 10.1111/vru.13079. Epub 2022 Mar 13. PMID: 35279908.

Beccaglia, M.; Luvoni, G.C. Comparison of the accuracy of two ultrasonographic measurements in predicting the parturition date in the bitch. J. Small Anim. Pr. 2006, 47, 670–673

Beccaglia, M.; Faustini, M.; Luvoni, G. Ultrasonographic Study of Deep Portion of Diencephalo-Telencephalic Vesicle for the Determination of Gestational Age of the Canine Foetus. Reprod. Domest. Anim. 2008, 43, 367–370.

Beccaglia, M.; Luvoni, G.C. Prediction of Parturition in Dogs and Cats: Accuracy at Different Gestational Ages. Reprod. Domest. Anim. 2012, 47, 194–196

Beccaglia, M.; Alonge, S.; Trovo', C.; Luvoni, G.C. Determination of gestational time and prediction of parturition in dogs and cats: An update. Reprod. Domest. Anim. 2016, 51, 12–17.

Bigliardi E, Parmigiani E, Cavirani S, et al. Ultrasonography and cystic hyperpla- sia- pyometra complex in the bitch. Reprod Domest Anim 2004;39:136–40.

Bigliardi E., Denti L., De Cesaris V., Bertocchi M., Di Ianni F., Parmigiani E., Bresciani C., Cantoni A.M. Colour Doppler Ultrasound Imaging of Blood Flows Variations in Neoplastic and Non-Neoplastic Testicular Lesions in Dogs. Reprod. Dom. Anim. 2019;54:63–71. doi: 10.1111/rda.13310.

Blanco, P.G.; Arias, D.O.; Gobello, C. Doppler ultrasound in canine pregnancy. J. Ultrasound Med. 2008, 27, 1745–1750.

Blanco PG, Rodríguez R, Rube A, Arias DO, Tórtora M, Díaz JD, Gobello C. Doppler ultrasonographic assessment of maternal and fetal blood flow in abnormal canine pregnancy. Anim Reprod Sci. 2011 Jun;126(1-

2):130-5. doi: 10.1016/j.anireprosci.2011.04.016. Epub 2011 May 4. PMID: 21616613.

Blanco, P.G.; Huk, M.; Lapuente, C.; Tórtora, M.; Rodríguez, R.; Arias, D.O.; Gobello, C. Uterine and umbilical resistance index and fetal heart rate in pregnant bitches of different body weight. Anim. Reprod. Sci. 2020, 212, 106255

Bosma F, Wijsman S, Huygens S, Passon-Vastenburg M. Ultrasonographic measurements of the prostate gland in castrated adult dogs. Acta Vet Scand. 2022 Jul 8;64(1):15. doi: 10.1186/s13028-022-00634-1. PMID: 35804438; PMCID: PMC9264550.

Bracco C, Gloria A, Contri A. Ultrasound-Based Technologies for the Evaluation of Testicles in the Dog: Keystones and Breakthroughs. Vet Sci. 2023 Dec 1;10(12):683. doi: 10.3390/vetsci10120683. PMID: 38133235; PMCID: PMC10747277.

Bradbury CA, Westropp JL, Pollard RE. Relationship between prostatomegaly, prostatic mineralization, and cytologic diagnosis. Vet Radiol Ultrasound. 2009 Mar-Apr;50(2):167-71. doi: 10.1111/j.1740-8261.2009.01510.x. PMID: 19400462.

Brito MM, da Rosa Filho RR, Losano JDA, Vannucchi CI. Ageing changes testes and epididymis blood flow without altering biometry and echodensity in dogs. Anim Reprod Sci. 2021 May;228:106745. doi: 10.1016/j.anireprosci.2021.106745. Epub 2021 Mar 22. PMID: 33770706.

Cazzuli G, Damián JP, Molina E, Pessina P. Post-castration prostatic involution: A morphometric and endocrine study of healthy canines and those with benign prostatic hyperplasia. Reprod Domest Anim. 2022 Feb;57(2):157-164. doi: 10.1111/rda.14036. Epub 2021 Nov 9. PMID: 34724270.

Chambers, B.A.; Laksito, M.A.; Long, F.; Yates, G.D. Unilateral uterine torsion secondary to an inflammatory endometrial polyp in the bitch. Aust. Vet. J. 2011, 89, 380–384.

Davidson A.P., Baker T.W. Reproductive Ultrasound of the Dog and Tom. Top. Companion Anim. Med. 2009;24:64–70. doi: 10.1053/j.tcam.2008.11.003.

De Cramer, K.; Nöthling, J. Is the biparietal diameter of fetuses in late gestation too variable to predict readiness for cesarean section in dogs? Theriogenology 2018, 113, 50–55.

de Freitas LA, Pinto JN, Silva HV, da Silva LD. Two-dimensional and Doppler sonographic prostatic appearance of sexually intact French

Bulldogs. Theriogenology. 2015 Apr 15;83(7):1140-6. doi: 10.1016/j.theriogenology.2014.12.016. Epub 2014 Dec 18. PMID: 25623230.

de Souza MB, da Cunha Barbosa C, Pereira BS, Monteiro CL, Pinto JN, Linhares JC, da Silva LD. Doppler velocimetric parameters of the testicular artery in healthy dogs. Res Vet Sci. 2014 Jun;96(3):533-6. doi: 10.1016/j.rvsc.2014.03.008. Epub 2014 Mar 28. PMID: 24684894.

de Souza MB, England GC, Mota Filho AC, Ackermann CL, Sousa CV, de Carvalho GG, Silva HV, Pinto JN, Linhares JC, Oba E, da Silva LD. Semen quality, testicular B-mode and Doppler ultrasound, and serum testosterone concentrations in dogs with established infertility. Theriogenology. 2015 Sep 15;84(5):805-10.

Diez-Bru, N.; Garcia-Real, I.; Martinez, E.M.; Rollan, E.; Mayenco, A.; Llorens, P. Ultrasonographic appearance of ovarian tumors in 10 dogs. Vet. Radiol. Ultrasound 1998, 39, 226–233.

Domosławska, A., Jurczak, A., & Janowski, T. (2014). Progesterone level does not distinguish the different course of canine ovulation deter-mined by ultrasonography. Polish Journal of Veterinary Sciences, 17, 2 9 3 – 2 9 7 .

Eker, K.; Salmanoğlu, M.R.; Vural, S.A. Unilateral leiomyoma in the mesosalpinx of a dog. J. Am. Anim. Hosp. Assoc. 2006, 42, 392–394.

England, G. C., & Allen, W. E. (1989). Real-time ultrasonic imaging of the ovary and uterus of the dog. Journal of Reproduction and Fertility Supplement, 39, 9 1– 10 0 .

England, G.; Allen, W.E.; Porter, D.J. Studies on canine pregnancy using B-mode ultrasound: Development of the conceptus and determination of gestational age. J. Small Anim. Pr. 1990, 31, 324–329

England G. Relationship between ultrasonographic appearance, testicular size, spermatozoal output and testicular lesions in the dog. J Small Anim Pract 1991;32:306e11.

England, G.; Russo, M. Ultrasonographic characteristics of early pregnancy failure in bitches. Theriogenology 2006, 66, 1694–1698.

England GC, Russo M, Freeman SL. Follicular dynamics, ovulation and conception rates in bitches. Reprod Domest Anim. 2009 Jul;44 Suppl 2:53-8. doi: 10.1111/j.1439-0531.2009.01416.x. PMID: 19754536.

England G., Bright L., Pritchard B., Bowen I., de Souza M., Silva L., Moxon R. Canine Reproductive Ultrasound Examination for Predicting Future Sperm Quality. Reprod. Dom. Anim. 2017;52:202–207. doi: 10.1111/rda.12825.

References

Felumlee A.E., Reichle J.K., Hecht S., Penninck D., Zekas L., Dietze Yeager A., Goggin J.M., Lowry J. Use of Ultrasound to Locate Retained Testes in Dogs and Cats: Location of Retained Testes. Vet. Radiol. Ultrasound. 2012;53:581–585. doi: 10.1111/j.1740-8261.2011.01943.x.

Fontbonne, A., & Malandian, E. (2006). Ovarian ultrasonography and follow-up of estrus in the bitch and queen. Waltham Focus, 16, 2 2– 29

Fontbonne A. Causes of pregnancy arrest in the canine species. Reprod Domest Anim. 2023 Sep;58 Suppl 2:72-83. doi: 10.1111/rda.14407. Epub 2023 Jul 20. PMID: 37312645.

Freeman SL, Russo M, England GC. Uterine artery blood flow characteristics assessed during oestrus and the early luteal phase of pregnant and non-pregnant bitches. Vet J. 2013 Aug;197(2):205-10. doi: 10.1016/j.tvjl.2013.02.015. Epub 2013 Jun 14. PMID: 23770397.

Freitas LA, Mota GL, Silva HVR, Silva LDM. Two-dimensional sonographic and Doppler changes in the uteri of bitches according to breed, estrus cycle phase, parity, and fertility. Theriogenology. 2017 Jun;95:171-177. doi: 10.1016/j.theriogenology.2017.03.012. Epub 2017 Mar 15. PMID: 28460672.

Gaikwad SM, Gulavane SU, Kumbhar UB, Shelar RR, Chaudhari RJ, Ribeiro RA. Doppler evaluation of maternal vessels in normal gestation and threatened abortion in canines. Ir Vet J. 2020 Aug 1;73:15. doi: 10.1186/s13620-020-00169-9. PMID: 32774843; PMCID: PMC7395967.

Giannico, A.T.; Gil, E.M.U.; Garcia, D.A.A.; Froes, T.R. The use of Doppler evaluation of the canine umbilical artery in prediction of delivery time and fetal distress. Anim. Reprod. Sci. 2015, 154, 105–112.

Gil, E.; Garcia, D.; Giannico, A.; Froes, T. Canine fetal heart rate: Do accelerations or decelerations predict the parturition day in bitches? Theriogenology 2014, 82, 933–941.

Gil, E.M.U.; Garcia, D.A.A.; Giannico, A.T.; Froes, T.R. Early results on canine fetal kidney development: Ultrasonographic evaluation and value in prediction of delivery time. Theriogenology 2018, 107, 180–187.

Gloria A, Di Francesco L, Marruchella G, Robbe D, Contri A. Pulse-wave Doppler pulsatility and resistive indexes of the testicular artery increase in canine testis with abnormal spermatogenesis. Theriogenology. 2020 Dec;158:454-460. doi: 10.1016/j.theriogenology.2020.10.015. Epub 2020 Oct 8. PMID: 33049570.

Gosling RG, King DH, 1974: Arterial assessment by Doppler-shift ultrasound. Proc R Soc Med67, 447–449.

References

Groppetti D, Vegetti F, Bronzo V, Pecile A. Breed-specific fetal biometry and factors affecting the prediction of whelping date in the German shepherd dog. Anim Reprod Sci. 2015 Jan;152:117-22. doi: 10.1016/j.anireprosci.2014.11.018. Epub 2014 Dec 4. PMID: 25510562.

Gumbsch P., Holzmann A., Gabler C. Colour-Coded Duplex Sonography of the Testes of Dogs. Vet. Rec. 2002;151:140–144. doi: 10.1136/vr.151.5.140.

Günzel-Apel AR, Möhrke C, Poulsen Nautrup C. Colour-coded and pulsed Doppler sonography of the canine testis, epididymis and prostate gland: physiological and pathological findings. Reprod Domest Anim. 2001 Oct;36(5):236-40. doi: 10.1046/j.1439-0531.2001.00288.x. PMID: 11885739.

Hagman R. Pyometra in Small Animals 2.0. Vet Clin North Am Small Anim Pract. 2022 May;52(3):631-657. doi: 10.1016/j.cvsm.2022.01.004. PMID: 35465903.

Hopper BJ, Richardson JL, Lester NV. Spontaneous antenatal resolution of canine hydrops fetalis diagnosed by ultrasound. J Small Anim Pract. 2004 Jan;45(1):2-8. doi: 10.1111/j.1748-5827.2004.tb00187.x. PMID: 14756202.

James RW, Heywood R. Age-related variations in the testes and prostate of beagle dogs. Toxicology. 1979 Mar-Apr;12(3):273-9. doi: 10.1016/0300-483x(79)90073-8. PMID: 494308.

Johnston G.R., Feeney D.A., Johnston S.D., O'Brien T.D. Ultrasonographic Features of Testicular Neoplasia in Dogs: 16 Cases (1980–1988) J. Am. Vet. Med. Assoc. 1991;198:1779–1784.

Johnston, S.D., Root Kustritz, M.V. & Olson, P.N.S. Canine pregnancy. In: Canine and feline theriogenology. Ed. WB Saunders. 2001 Ch.5; p. 66-104

Khan F.A., Gartley C.J., Khanam A. Canine Cryptorchidism: An Update. Reprod. Domest. Anim. 2018;53:1263–1270. doi: 10.1111/rda.13231.

Kim B., Winter T.C., Ryu J. Testicular Microlithiasis: Clinical Significance and Review of the Literature. Eur. Radiol. 2003;13:2567–2576. doi: 10.1007/s00330-003-2014-5.

Kim, Y.; Travis, A.J.; Meyers-Wallen, V.N. Parturition prediction and timing of canine pregnancy. Theriogenology 2007, 68, 1177–1182.

Knauf Y, Bostedt H, Failing K, et al. Gross pathology and endocrinology of ovarian cysts in bitches. Reprod Dom Anim 49:463–468, 2014

Kokkinos, P.; Ververidis, C.; Patsikas, M.; Kritsepi-Konstantinou, M.; Kazakos, G.M.; Psalla, D. Uterine stump adenocarcinoma in a bitch with

an ovarian remnant: A case report. J. Hellenic. Vet. Med. Soc. 2019, 70, 1583–1588.

Kutzler, M.A.; Mohammed, H.O.; Lamb, S.V.; Meyers-Wallen, V.N. Accuracy of canine parturition date prediction from the initial rise in preovulatory progesterone concentration. Theriogenology 2003, 60, 1187–1196.

Lascialfari P, Tesi M, Manetti C, Fanelli D, Rota A. Embryonic resorption rates at canine pregnancy diagnoses: A retrospective evaluation. Theriogenology. 2023 Aug;206:71-77. doi: 10.1016/j.theriogenology.2023.05.009. Epub 2023 May 11. PMID: 37201297.

Lea C, Walker D, Blazquez CA, Zaghloul O, Tappin S, Kelly D. Prostatitis and prostatic abscessation in dogs: retrospective study of 82 cases. Aust Vet J. 2022 Jun;100(6):223-229. doi: 10.1111/avj.13150. Epub 2022 Feb 17. PMID: 35176814.

Lemos H, Dorado J, Hidalgo M, Gaivão I, Martins-Bessa A. Assessment of Dog Testis Perfusion by Colour and Pulsed-Doppler Ultrasonography and Correlation With Sperm Oxidative DNA Damage. Top Companion Anim Med. 2020 Nov;41:100452. doi: 10.1016/j.tcam.2020.100452. Epub 2020 Jun 5. PMID: 32823153.

Lévy X, Niżański W, von Heimendahl A, Mimouni P. Diagnosis of common prostatic conditions in dogs: an update. Reprod Domest Anim. 2014 Jun;49 Suppl 2:50-7. doi: 10.1111/rda.12296. PMID: 24947861.

Lima CB, Angrimani DSR, Flores RB, Vannucchi CI. Endocrine, prostatic vascular, and proapoptotic changes in dogs with benign prostatic hyperplasia treated medically or surgically. Domest Anim Endocrinol. 2021 Apr;75:106601. doi: 10.1016/j.domaniend.2020.106601. Epub 2020 Nov 23. PMID: 33333452.

Lopate, C. Estimation of gestational age and assessment of canine fetal maturation using radiology and ultrasonography: A review. Theriogenology 2008, 70, 397–402

Lopate, C. Gestational Aging and Determination of Parturition Date in the Bitch and Queen Using Ultrasonography and Radiography. Veter Clin. N. Am. Small Anim. Pr. 2018, 48, 617–638.

Luvoni, G.C.; Grioni, A. Determination of gestational age in medium and small size bitches using ultrasonographic fetal measurements. J. Small Anim. Pr. 2000, 41, 292–294.

Luvoni, G.C.; Beccaglia, M. The Prediction of Parturition Date in Canine Pregnancy. Reprod. Domest. Anim. 2006, 41, 27–32.

Madewell BR, Theilen GH. Tumors of the genital system. In: Theilen GH, editor. Madewell BR. Veterinary cancer medicine. Philadelphia: Lea & b'ebiger; 1987.

Maldonado, A.L.L.; Júnior, E.A.; Mendonça, D.S.; Nardozza, L.M.M.; Moron, A.F.; Ajzen, S.A. Ultrasound Determination of Gestational Age Using Placental Thickness in Female Dogs: An Experimental Study. Veter Med. Int. 2012, 2012, 1–6.

Mantziaras G., Alonge S., Luvoni G.C. Ultrasonographic Study of Age-Related Changes on the Size of Prostate and Testicles in Healthy German Shepherd Dogs; Proceedings of the 17th Congress EVSSAR; Wroclaw, Poland. 26 September 2014; p. 150.

Mantziaras G. Imaging of the male reproductive tract: Not so easy as it looks like. Theriogenology. 2020 Jul 1;150:490-497. doi: 10.1016/j.theriogenology.2020.03.009. Epub 2020 Mar 14. PMID: 32241560.

Marino, G.; Quartuccio, M.; Cristarella, S.; Nicòtina, P.A.; Zanghì, A. Adenoma of the uterine tube in the bitch: Two case reports. Vet. Res. Comm. 2007, 31, 173–175.

Marino, G.; Barna, A.; Rizzo, S.; Zanghì, A.; Catone, G. Endometrial polyps in the bitch: A retrospective study of 21 cases. J. Comp. Path 2013, 149, 410–416.

Mattoon J.S., Sellon R., Berry C. Small Animal Diagnostic Ultrasound. 4th ed. Elsevier, Inc.; Philadelphia, PA, USA: 2020.

Milani C, Artusi E, Drigo M, Mateus L, Siena G, Gelli D, Falomo ME, Romagnoli S. Ultrasonographic analysis of fetal gastrointestinal motility during the peripartum period in the dog. Anim Reprod Sci. 2020 Aug;219:106514. doi: 10.1016/j.anireprosci.2020.106514. Epub 2020 Jun 2. PMID: 32828400.

Miranda, S.; Domingues, S. Conceptus ecobiometry and triplex Doppler ultrasonography of uterine and umbilical arteries for assessment of fetal viability in dogs. Theriogenology 2010, 74, 608–617.

Moll X, Aguilar A, García F, Ferrer R, Andaluz A. Validity and reliability of Doppler ultrasonography and direct arterial blood pressure measurements in anaesthetized dogs weighing less than 5 kg. Vet Anaesth Analg. 2018 Mar;45(2):135-144. doi: 10.1016/j.vaa.2017.08.006. Epub 2017 Sep 15. PMID: 29246711.

Moxon R., Bright L., Pritchard B., Bowen I.M., Souza M.B.d., Silva L.D.M.d., England G.C.W. Digital Image Analysis of Testicular and Prostatic Ultrasonographic Echogencity and Heterogeneity in Dogs and

the Relation to Semen Quality. Anim. Reprod. Sci. 2015;160:112–119. doi: 10.1016/j.anireprosci.2015.07.012.

Niżański W, Ochota M, Fontaine C, Pasikowska J. B-Mode and Doppler Ultrasonographic Findings of Prostate Gland and Testes in Dogs Receiving Deslorelin Acetate or Osaterone Acetate. Animals (Basel). 2020 Dec 11;10(12):2379. doi: 10.3390/ani10122379. PMID: 33322633; PMCID: PMC7763262.

Odendaal MW, de Cramer KG, van der Walt ML, Botha AD, Pieterson PM. First isolation of Campylobacter jejuni from the vaginal discharge of three bitches after abortion in South Africa. Onderstepoort J Vet Res. 1994 Jun;61(2):193-5. PMID: 7596570.

Orlandi R., Vallesi E., Boiti C., Polisca A., Bargellini P., Troisi A. Characterization of Testicular Tumor Lesions in Dogs by Different Ultrasound Techniques. Animals. 2022;12:210. doi: 10.3390/ani12020210.

Paltiel HJ, Diamond DA, Di Canzio J, Zurakowski D, Borer JG, Atala A. Testicular volume: comparison of orchidometer and US measurements in dogs. Radiology. 2002 Jan;222(1):114-9. doi: 10.1148/radiol.2221001385. PMID: 11756714.

Patsikas, M.; Papazoglou, L.G.; Jakovljevic, S.; Papaioannou, N.G.; Papadopoulou, P.L.; Soultani, C.B.; Chryssogonidis, I.A.; Kouskouras, K.A.; Tziris, N.E.; Charitanti, A.A. Radiographic and ultrasonographic findings of uterine neoplasms in nine dogs. J. Am. Anim. Hosp. Assoc. 2014, 50, 330–337.

Plagge, J.; Bali, M. Adenoma of the fallopian tube in a 12-year-old bitch. Kleintierpraxis 2018, 63, 272–277.

Pollis ESC, Padilha FGF, Campos IS, Bartz C, Silva FBF, Pinna AE, Leite JDS, Ferreira AMR. Establishment of a new equation to estimate gestational age in female dogs. Reprod Domest Anim. 2023 Nov;58(11):1576-1582. doi: 10.1111/rda.14473. Epub 2023 Sep 15. PMID: 37715455.

Pourcelot L, 1974: Applications cliniques del'examen Doppler transcutané. In: Peronneau P (ed), Velocimetre ultrasonore Doppler. Inserm, Paris, pp. 213–240.

Renfrew H, Barrett EL, Bradley KJ, Barr FJ. Radiographic and ultrasonographic features of canine paraprostatic cysts. Vet Radiol Ultrasound. 2008 Sep-Oct;49(5):444-8. doi: 10.1111/j.1740-8261.2008.00404.x. PMID: 18833951.

References

Rodrigues da Rosa Filho R, Morales Brito M, Gomes Faustino T, Lima de Almeida L, Correia Manoel V, Cogliati B, Vannucchi CI. Prostaglandin and antigestagen in pyometra bitches: vascular and stereological effect. Reprod Fertil. 2021 Apr 19;2(2):95-105. doi: 10.1530/RAF-20-0020. PMID: 35128446; PMCID: PMC8812451.

Root Kustritz MV. Pregnancy diagnosis and abnormalities of pregnancy in the dog. Theriogenology. 2005 Aug;64(3):755-65. doi: 10.1016/j.theriogenology.2005.05.024. PMID: 15936810.

Rowan, C.; Cuddy, L.; Bryan, J.; Shiel, R.; Hoey, S. Imaging diagnosis—Computed tomography findings in a case of metastatic ovarian adenocarcinoma in a dog. Vet. Radiol. Ultrasound 2017, 50, E60–E63.

Ruel Y, Barthez PY, Mailles A, Begon D. Ultrasonographic evaluation of the prostate in healthy intact dogs. Vet Radiol Ultrasound. 1998 May-Jun;39(3):212-6. doi: 10.1111/j.1740-8261.1998.tb00342.x. PMID: 9634189.

Russo M, Vignoli M, England GC. B-mode and contrast-enhanced ultrasonographic findings in canine prostatic disorders. Reprod Domest Anim. 2012 Dec;47 Suppl 6:238-42. doi: 10.1111/rda.12059. PMID: 23279509.

Russo M., England G.C.W., Catone G., Marino G. Imaging of Canine Neoplastic Reproductive Disorders. Animals. 2021;11:1213. doi: 10.3390/ani11051213.

Russo M, Vignoli M. Prostate, testicles, ovaries, and uterus. In: Atlas of diagnostic imaging of dogs and cats. Palm Beach Gardens, FL (USA): Edra Publishing US LLC; 2022. Ch. 37; p. 1113-1149.

Sananmuang T, Mankong K, Jeeratanyasakul P, Chokeshai-Usaha K, Ponglowhapan S. Prenatal diagnosis of foetal hydrocephalus and suspected X-linked recessive inheritance of cleft lip in a Chihuahua. J Vet Med Sci. 2020 Feb 18;82(2):212-216. doi: 10.1292/jvms.18-0516. Epub 2019 Dec 27. PMID: 31902834; PMCID: PMC7041993.

Schlafer, D.H.; Yeager, A.E.; Concannon, P.W. Theriogenology question of the month. Endometrial polyp in a beagle. J. Am. Vet. Med. Assoc. 1997, 210, 759–761.

Schlafer DH. Canine and feline abortion diagnostics. Theriogenology. 2008 Aug;70(3):327-31. doi: 10.1016/j.theriogenology.2008.05.036. Epub 2008 Jun 9. PMID: 18541293.

Sehgal, N. Efficacy of color doppler ultrasonography in differentiation of ovarian masses. J. Midlife Health 2019, 10, 22–28.

References

Siena, G.; Milani, C. Usefulness of Maternal and Fetal Parameters for the Prediction of Parturition Date in Dogs. Animals 2021, 11, 878. https://doi.org/10.3390/ani11030878

Siena G, Corrò M, Zanardello C, Foiani G, Romagnoli S, Ferré-Dolcet L, Milani C. A case report of a rapid development of fetal anasarca in a canine pregnancy at term. Vet Res Commun. 2022 Jun;46(2):597-602. doi: 10.1007/s11259-021-09860-w. Epub 2021 Dec 2. PMID: 34855120.

Siena G, Romagnoli S, Drigo M, Contiero B, di Nardo F, Milani C. Ultrasonographic changes in fetal gastrointestinal motility during the last ten days before parturition in dogs. Front Vet Sci. 2022b Oct 19;9:1000975. doi: 10.3389/fvets.2022.1000975. PMID: 36337211; PMCID: PMC9628212.

Siena G, di Nardo F, Romagnoli S, Mollo A, Contiero B, Milani C. Relationship between days before parturition and fetal kidney length, cortical thickness, medullary thickness and their ratio in dogs. Theriogenology. 2022c Dec;194:58-63. doi: 10.1016/j.theriogenology.2022.09.021. Epub 2022 Sep 27. PMID: 36209545.

Siena G, di Nardo F, Contiero B, Milani C. Clinical use of the canine foetal kidney formula in dogs of different maternal sizes during the last ten days before parturition. Vet Res Commun. 2023a Sep;47(3):1653-1663. doi: 10.1007/s11259-023-10120-2. Epub 2023 Apr 24. PMID: 37095415.

Siena G, di Nardo F, Contiero B, Banzato T, Milani C. Preliminary Evaluation of Cortical and Medullary Echogenicity in Normal Canine Fetal Kidneys during the Last 10 Days of Pregnancy. Vet Sci. 2023b Oct 31;10(11):639. doi: 10.3390/vetsci10110639. PMID: 37999462; PMCID: PMC10675300.

Smith J. Canine prostatic disease: a review of anatomy, pathology, diagnosis, and treatment. Theriogenology. 2008 Aug;70(3):375-83. doi: 10.1016/j.theriogenology.2008.04.039. Epub 2008 Jun 2. PMID: 18514299.

Socha, P.; Janowski, T. Predicting the Parturition Date in Bitches of Different Body Weight by Ultrasonographic Measurements of Inner Chorionic Cavity Diameter and Biparietal Diameter. Reprod. Domest. Anim. 2014, 49, 292–296.

Socha, P.; Janowski, T.; Bancerz-Kisiel, A. Ultrasonographic fetometry formulas of inner chorionic cavity diameter and biparietal diameter for medium-sized dogs can be used in giant breeds. Theriogenology 2015, 84, 779–783.

References

Socha, P.; Janowski, T. Specific fetometric formulas of ICC and BP for calculating the parturition date in the miniature breeds of canine. Reprod. Domest. Anim. 2018, 53, 545–549.

Son CH, Jeong KA, Kim JH, Park IC, Kim SH, Lee CS. Establishment of the prediction table of parturition day with ultrasonography in small pet dogs. J Vet Med Sci. 2001 Jul;63(7):715-21. doi: 10.1292/jvms.63.715. PMID: 11503898.

Sridevi, P. Ultrasonographic diagnosis and monitoring of pregnancy in the bitch—A review. J. Vet. Anim. Sci. 2013, 44, 1–7.

Srivastava S., Panchal S., Nagori C., Thaker M. Doppler parameters of intratesticular vessels in male factor sub fertility. Andrology. 2021;10:1000230.

Stefanov M. Extraglandular and intraglandular vascularization of canine prostate. Microsc Res Tech. 2004 Mar 1;63(4):188-97. doi: 10.1002/jemt.20028. PMID: 14988915.

Sun F, Báez-Díaz C, Sánchez-Margallo FM. Canine prostate models in preclinical studies of minimally invasive interventions: part I, canine prostate anatomy and prostate cancer models. Transl Androl Urol. 2017 Jun;6(3):538-546. doi: 10.21037/tau.2017.03.61. PMID: 28725597; PMCID: PMC5503961.

Tannouz VGS, Mamprim MJ, Lopes MD, Santos-Sousa CA, Souza Junior P, Babinski MA, Abidu-Figueiredo M. Is the right testis more affected by cryptorchidism than the left testis? An ultrasonographic approach in dogs of different sizes and breeds. Folia Morphol (Warsz). 2019;78(4):847-852. doi: 10.5603/FM.a2019.0022. Epub 2019 Mar 5. PMID: 30835343.

Troisi A, Orlandi R, Vallesi E, Pastore S, Sforna M, Quartuccio M, Zappone V, Cristarella S, Polisca A. Clinical and ultrasonographic findings of ovarian tumours in bitches: A retrospective study. Theriogenology. 2023 Oct 15;210:227-233. doi: 10.1016/j.theriogenology.2023.07.020. Epub 2023 Jul 22. PMID: 37540955.

Tsioli, V.G.; Gouletsou, P.G.; Loukopoulos, P.; Zavlaris, M.; Galatos, A.D. Uterine leiomyosarcoma and pyometra in a dog. J. Small Anim. Pract. 2011, 52, 121–124.

Tsuchida M, Komura N, Yoshihara T, Kawasaki Y, Sakurai D, Suzuki H. Ultrasonographic observation in combination with progesterone monitoring for detection of ovulation in Labrador Retrievers. Reprod Domest Anim. 2022 Feb;57(2):149-156. doi: 10.1111/rda.14035. Epub 2021 Nov 8. PMID: 34724259.

References

Venianaki AP, Barbagianni MS, Fthenakis GC, Galatos AD, Gouletsou PG. Doppler Examination of the Testicular Artery of Beagle-Breed Dogs from Birth to Puberty. Tomography. 2023 Jul 23;9(4):1408-1422. doi: 10.3390/tomography9040112. PMID: 37489480; PMCID: PMC10366859.

Vignoli M, Russo M, Catone G, Rossi F, Attanasi G, Terragni R, Saunders J, England G. Assessment of vascular perfusion kinetics using contrast-enhanced ultrasound for the diagnosis of prostatic disease in dogs. Reprod Domest Anim. 2011 Apr;46(2):209-13. doi: 10.1111/j.1439-0531.2010.01629.x. PMID: 20546182.

Yeager AE, Mohammed HO, Meyers-Wallen V, Vannerson L, Concannon PW. Ultrasonographic appearance of the uterus, placenta, fetus, and fetal membranes throughout accurately timed pregnancy in beagles. Am J Vet Res. 1992 Mar;53(3):342-51. PMID: 1595959.

Zabitler F, Aslan S, Darbaz I, Ergene O, Schäfer-Somi S. Computerized histogram analysis of the canine placenta during normal pregnancy. Theriogenology. 2022 Apr 1;182:96-102. doi: 10.1016/j.theriogenology.2022.01.008. Epub 2022 Jan 12. PMID: 35144180.

Zelli R, Orlandi R, Troisi A, Cardinali L, Polisca A. Power and pulsed Doppler evaluation of prostatic artery blood flow in normal and benign prostatic hyperplasia-affected dogs. Reprod Domest Anim. 2013a Oct;48(5):768-73. doi: 10.1111/rda.12159. Epub 2013 Mar 18. PMID: 23505997.

Zelli R., Troisi A., Elad Ngonput A., Cardinali L., Polisca A. Evaluation of Testicular Artery Blood Flow by Doppler Ultrasonography as a Predictor of Spermatogenesis in the Dog. Res. Vet. Sci. 2013b;95:632–637. doi: 10.1016/j.rvsc.2013.04.023.

Chapter 2

Contrast-enhanced ultrasound
Possibilities and limitations in small animal reproduction

2.1 Contrast-enhanced ultrasound: technique and clinical use

2.1.1 CEUS examination: technique, settings and contrast agents

The CEUS technique is an ultrasonographic diagnostic tool, which involves the use of an intravenous contrast agent to highlight the vascular blood supply, in particular the microvascularization of a targeted tissue (Dietrich et al. 2018). Even though Colour Doppler technique is an efficient method to detect vascular blood supply, additional contrast agent may be needed in case of poorly vascularized tumors or regions with many small vessels with slow blood flow. Hence CEUS is an option and was shown to improve cancer detection and tumor characterization, decreasing the number of biopsies, or during surgery in brain cancer patients (Kitano et al., 2012; Uemura et al., 2013; Prada et al., 2014). Application of CEUS started in the late 1960s after finding that the injection of agitated saline caused a detectable signal change during US examination (Gramiak and Shah, 1968). Contrast enhancement was caused by the compressible gas core of saline bubbles, enabling the bubble to backscatter the applied US wave (Paefgen et al. 2015). The first application of CEUS was performed in human medicine, by using agitated saline solution for the detection of intra and extra cardiac shunts (Kienle & Thomas, 2002). However, the bubbles created had not enough lifetime and were poorly stable in the vascular blood flow. It took more than 20 years to develop the first stable, commercially available and FDA-approved ultrasound contrast agent (Feinstein et al., 1990), Albunex®, an albumin-coated and air-filled microsphere.
Technology allowed to design and create proper and stabilized contrast agents, able in crossing the respiratory barrier, and being able to be detected in a specific region. All contrast agent consists in microbubbles full of a specific gas injected in the venous flow, through an intravenous catheter. The more recent and advanced microbubbles do not cross the endothelial barrier, being exclusively intravascular (Freccero et al. 2017). The size of the microbubbles is similar to the erythrocites (Burns et al. 2007) and no mutagenic or teratogenic effect have ever been reported in the past studies (Murotsuki, 2007). Different contrast agents are commercially available having similar characteristics. In particular, the one that has been used the most in veterinary medicine is the Sonovue® (Bracco Imaging SpA), which is characterized by an external phospholipidic shell and a gas core represented by sulfur hexafluorid (SF6) (Dietrich et al. 2018). The Sonovue® is generally used in human medicine for left ventricular

opafication and endocardial border definition, but in some countries also have approval for general vessel diagnostic or imaging of microvascular structures in the breast or differentiation of lesions in the liver (Claudon et al., 2013; Appis et al., 2015). Apart from that, SonoVue® has also been tested in clinical trials for monitoring of uterine fibroid vascularization and improved ablation (Henri et al., 2014; Jiang et al., 2014).

Transducers that have specific CEUS optimized settings able in detecting the second harmonic signal are recommended. Linear probes with higher transmit frequencies may be useful in cases of superficial lesions and when more spatial resolution is necessary. In this case, higher contrast doses may be beneficial (e. g., thyroid, breast, lymph nodes, prostate), as the agents become less efficient nonlinear scatterers at higher frequencies (Dietrich et al. 2018).

Ultrasound waves impact the microbubbles, deforming the shell and producing a back scattered signal. Specific settings are required to correctly perform CEUS, in particular the acoustic power should be adjusted. All clinically approved microbubbles, regardless of whether they are reticuloendothelial or purely blood pool, can easily be destroyed by ultrasound energy, in case the acoustic power is too high. The destruction of bubbles determines an increased back scatter when compared to when deformation occurs, improving the signal detection. However, once the shell is disrupted, the gas from the microbubbles diffuses, and the contrast agent loses its scattering properties, being no longer effective. The acoustic power may be regulated in every machine, by setting the Mechanical Index (MI) (Dietrich et al. 2014). The use of a dual-image display format is essential in CEUS studies, and it is recommended especially in examining small lesions. In this display format, a conventional B-mode low MI fundamental image and a bubble-only contrast image are displayed side-by-side. Having the conventional image displayed simultaneously allows the operator to keep the lesion in the imaging plane. Using the B-mode image for guidance, place calipers on the target lesion on both screens simultaneously to facilitate enhancement characterization (Dietrich et al. 2018).

CEUS allows real-time recording and evaluation of the wash-in and wash-out phases of the ultrasound contrast agent (UCA) over several minutes. “Wash-in”, used for both qualitative and quantitative analyses, refers to the progressive enhancement within a region of interest from the arrival of microbubbles in the field of view, to “peak enhancement”, and “wash-out” to the reduction in enhancement which follows peak enhancement (Claudon et al. 2012). The timing (early versus late onset, fast versus slow), degree

(complete, incomplete) and pattern should be described in comparison to the surrounding "normal" parenchyma. CEUS examination is considered a real time evaluation, though being extremely subjective in terms of interpretation. However, specific software for the quantitative analysis of the tissue perfusion have been developed, in order to increase repetibility and reproducibility of the results. The present softwares are able to design time-intensity curves which analyses the contrast enhancement in a specific region of interest (ROI), providing parameters, which describe tissue perfusion (Schwarz et al. 2021). The most important contrast parameters are: perfusion peak intensity (PPI), that describes the intensity of the contrast enhnancement, time to peak (TTP), that describes the time necessary to reach the peak, the area under the curve (AUC), which describes the distribution amplitude of the contrast agent, and the medium transit time (mTT), which describes the time of distribution of the contrast throughout the entire examination (Dietrich et al. 2018).

The intravenous catheter should be inserted into a peripheral vein, generally on the cephalic for its increased diameter and accessibility. At least 20 Guage catheter is required to avoid and reduce the microbubble destruction when injected. However, a recent study evidenced that the use of a 24 Gauge intravemous catheter did not alter the renal contrast perfusion in dogs (Hwang et al. 2019). A three-way stopcock may be valuable, especially if multiple injections are anticipated, as this facilitates sequential administration of the contrast material and then the saline flush, without removal of either syringe.

The dosage reported in the majority of the studies performed in dogs is 0.03 ml/kg (Russo et al. 2009; Vignoli et al. 2011; Sinagra et al. 2023). Multiple dosage in dogs have been described and can be performed in different circumstances such as: additional nodules or observations, which require characterization or in case the initial injection may not provide the full answer to the characterization of a lesion. Recent studies conducted in veterinary medicine described and suggested to inject the contrast agent at least twice and to consider the perfusion of the second injection for the study evaluation, as it shows a stronger enhancement (Stock et al. 2017; Simeoni et al. 2020; Simeoni et al. 2021). Even though for the study of specific lesion a bolus injection is enough, measurement of blood flow parameters for assessment of oncologic response to therapy is also possible with an infusion and the destruction-replenishment technique. In this case the agent is, depending on the contrast agent, suspended in saline or other media and intravenously infused with controlled pressure, to avoid bubble destruction

and at a constant rate to permit prolonged scanning (Dietrich et al. 2018). However, there are no studies which describes the use of this specific use of the CEUS in veterinary medicine.
Even though CEUS does not require sedation or anesthesia, in case of uncooperative patient, necessity of bioptic or cytologic sampling and pre-surgical evaluation, it may be necessary. However, contrast agent perfusion may be affected by heart pressure and frequency, which are significantly reduced during anesthesia and sedation (Choi et al. 2016).
The contrast agent showed to be highly tolerated and safe both in dogs and human. In a study conducted by Seiler and colleagues, Of the 411 case dogs, 3 had immediate adverse events (vomiting or syncope) and 1 had a delayed adverse event (vomiting) (Seiler et al. 2013).

2.1.2 Clinical use of CEUS in veterinary medicine

The main diagnostic goals of CEUS are studying vascular architecture and comparing the enhancement of the lesions with the surrounding normal parenchyma (Dietrich et al. 2018). In human medicine extravascular (intracavitary) CEUS (EV-CEUS) has been proposed and used for imaging physiological and non-physiological body cavities. Physiological cavities include the peritoneal cavity, pleural cavity, biliary tract, gastrointestinal tract, urinary tract, etc. and pathological cavities include abscesses, cysts, diverticula, etc. to detect rupture, drainage, fistula, etc. (Piscaglia et al. 2011; Ignee et al. 2013). The contrast agent is injected through a needle or catheter, for instance, at cholangiography or nephrostomy. Oral administration in human or as an enema for imaging the upper and lower gastrointestinal tract has also been described (Dietrich et al. 2018). No studies are available concerning the use of EV-CEUS in dogs and cats, even though its use could be helpful in the management of organs rupture (e.g. bladder or intestine) in emergency cases.
Paralleling human applications, the use of CEUS in veterinary medicine has been pursued, but, despite some research papers regarding the use of CEUS in small animals and equines (Stock et al. 2018; Mantziaras & Luvoni, 2020; Freccero et al. 2017; Seiler et al. 2016; Canejo-Teixeira et al. 2022), veterinary literature is much scarcer and based on a smaller number of cases and diseases.
CEUS found application in several domestic species for research (Roberts et al. 2016; Wilson et al. 2023; Hagen et al. 2023; Larson et al. 2022) and clinical activities (Santos et al. 2023). A clinical use also in farm animals

has been proposed in particular in ewes, where vascular characterization of utero-placental binome (Santos et al. 2023), corpora lutea (Sboros et al. 2011), and mammary glands (Mantziaras et al. 2018) has been reported. Vanderperren and colleagues reviewed the potential use of CEUS in clinical practice in sheeps, reporting interesting future perspectives concerning the application of the technique (Vanderperren et al. 2017).

In horses CEUS has been applied for several clinical reasons, in particular for the assessment of ocular vascularization (Blohm et al. 2020), intrasynovial inoculation for the assessment of traumatic injuries (Ogden et al. 2021) and for the study of distal limb (Seiler et al. 2016).

As a tool for imaging diagnosis in veterinary applications, CEUS holds several advantages, and it has been described as ideally suited for small animal imaging by several authors thanks to its very broad range of applications and its high spatial and temporal resolution and low cost (Haers & Saunders, 2009). It has the advantage of avoiding the use of sedation or anesthesia in case of cooperative patient for the study of specific organs and lesions, unlike CT or MR, having higher resolution in the evaluation of vascular blood supply.

Veterinary clinical applications of CEUS in particular for cats and dogs focus mostly on the liver (Salwey et al. 2005; Nyman et al. 2005; Wdowiak et al. 2010; Burti et al. 2020) lymph nodes (Stan et al. 2020), pancreas (Rademacher et al. 2016), gallbladder (Bargellini et al. 2016), kidneys (Waller et al. 2007; Choi et al. 2016), several types of neoplasias (Rick et al. 2009; Laluhovà et al. 2003; Orlandi et al. 2022), portosystemic shunts (Salwei et al. 2003), and last, but not the least, the spleen (Ohlerth et al. 2005; Caneijo Teixeira et al. 2022).

Guidelines concerning the vascular features of splenic lesions have been reported. B-mode ultrasound is a suitable method to identify and describe splenic focal lesions, however, the characterization and differentiation between benign and malignant conditions may be challenging due to their overlapping nature. Splenic malignant lesions during CEUS are generally hypoechoic in a specific contrast phase, are inhomogeneous and have tortous vessels inside in some cases (Canejo-Teixeira et al. 2022). Concerning liver lesions higher variability concerning the enhancement pattern of malignant lesions has been registered (Burti et al. 2020)

Few studies have been conducted concerning the use of CEUS in the evalution of the genital tract both in male and female studies.

2.2 Contrast-enhanced ultrasound in male reproduction

2.2.1 Contrast-enhanced ultrasound of the prostate gland

Most of the studies concerning the use of CEUS to assess the reproductive tract have been performed to image and evaluate the prostate gland. The first studies have been conducted to assess contrast characteristics in animal model studies (Forsberg et al. 2002; Feng et al. 2017; Jia et al. 2021). Different studies have been performed in intact dogs to evaluate both normal (Russo et al. 2009; Bigliardi & Ferrari, 2010) and abnormal (Russo et al. 2012; Vignoli et al. 2011; Troisi et al. 2015) prostate. Fewer studies have been conducted to evaluate prostate gland in neutered dogs (Yoon et al. 2020; Spada et al. 2021). In particular, Yoon and colleagues described in an original study prostatic involution after castration in normal dogs and dogs affected by BPH (Yoon et al. 2020).
When the contrast is injected, the prostate gland is enhanced in 10 seconds, reaching a peak around 30 seconds, and having a homogeneous wash out phase. When evaluated in the longitudinal view, the contrast is firstly seen enhancing both prostatic cranial arteries and the entire capsule, then branching off homogeneously from the periphery to the centre of the gland, towards the urethra. During the wash out phase, the gland homogeneously loses enhancement. The urethra cannot be clearly distinguished until the wash out phase occurs, as the urethral wash out is longer than the prostatic parenchymal one (Russo et al. 2009). Prostatic enhancement after castration is similar to the one in intact dogs even though contrast parameters tend to change when compared to intact dogs (Yoon et al. 2020; Spada et al. 2021). Abnormal prostate glands in intact dogs have been described using CEUS. Benign lesions have a homogeneous enhancement similar normal prostate with an increased intensity of the contrast agent, due to the higher vascularization that can be observed in BPH (Angrimani et al. 2020) and prostatitis (Lea et al. 2022; Troisi et al. 2015). Both prostatitis and BPH may be characterized by the presence of avascular area representing cysts, and with an increased peripheral rim enhancement persisting in the wash out phase in case of abscesses (Troisi et al. 2015). Trends for prostatic tumours have been reported in dogs concerning the ultrasonographic appearance e using CEUS (Vignoli et al. 2011). Prostatic neoplasia may present as single nodule or diffuse prostatic pathology. The single nodule may be evaluated and compared to the surrounding parenchyma. The diffuse pattern is characterized by an inhomogeneous enhancement with abnormal vessel

diameter and orientation within the gland. Moroever, CEUS has been applied in human medicine to increase the precision in taking bioptic sample in targeted lesions, detected by using this technique. Nevertheless, the diffuse pattern requires that bioptic sample should collected randomly within the gland, increasing the possibility of false negative (Vignoli et al. 2011). Prostatic adenocarcinoma may present variable enhancement pattern, with an increased contrast intensity of the single nodule (Vignoli et al. 2011) or with hypoechoic lesions with potential anechoic areas representing necrotic tissue (Troisi et al. 2015). CEUS demonstrated to be useful to distinguish benign from malignant conditions, but the characterization of the single neoplastic type still need bioptic sampling. No studies have been reported to evaluate abnormal prostate in castrated dogs.

2.2.2 Contrast-enhanced ultrasound of the testes

B-mode and Pulsed wave doppler ultrasound are reliable methods to evaluate the testicles both in cats and dogs and have a high accuracy in the detection of testicular conditions (Orlandi et al. 2022; Bigliardi et al. 2019). However, besides the excellent application of these techniques, the differentiation between benign and malignant lesions remains challenging due to the lack of specific ultrasonographic signs. Moreover, Orlandi and colleagues found that the ultrasonographic appearance of testicular tumours may vary and the signs are not typical for a specific neoplasia (Orlandi et al. 2022).

Few reports are available in literature concerning the use of CEUS to assess testicles in dogs. In human, CEUS showed to be more accurate than standard two dimensional and Doppler ultrasound in acute scrotal disease, in particular infarction, trauma and torsion, as well as for detection of changes of microvascularization in cases of varicocele and for identifying testicular masses tumours (Caretta et al. 2010; Bertolotto et al. 2011; Lock et al. 2011; Valentino et al. 2011).

In dogs, CEUS showed promising results for detecting both benign and malignant testicular conditions. Once contrast agent is administered, in about 10 seconds the testicular artery, located cranially and within the pampiniform plexus is enhanced, followed by marginal testicular artery and intraparenchymal testicular arteries, having a homogeneous enhancement of the peripheral zone of the testis. After a few seconds, the parenchyma enhances homogeneously, with parenchymal arteries still visible. At the peak reached in about 20 seconds, the parenchyma is homogeneously

enhanced, and it is not possible to locate the intraprenchymal vessels anymore. During the wash out phase the parenchyma quickly and homogeneously loses enhancement (Volta et al. 2014).
Differences between benign and malignant lesions using CEUS were reported by Volta and colleagues, with non-neoplastic lesions showing a reduced peak intensity and homogeneous enhancement. The same study reported differences among tumour types, with a peculiar enhancement pattern with persistent inner vessels with a hypoisoechoic background associated with seminomas. These findings did not agree with the results reported by Orlandi and colleagues, that did not find any typical enhancement pattern associated with a specific tumour type. However, both studies found found that neoplastic lesions were mainly associated with a hyperenhancing pattern, an increase in peak intensity and a quicker wash in phase, when compared to the normal parenchyma (Orlandi et al. 2022).
CEUS showed to be a promising diagnostic tool to distinguish benign from malignant lesions (Volta et al. 2014), and to detect masses that were not revealed by other ultrasonographic techniques such as B-mode, Colour Doppler and B-flow (Orlandi et al. 2022). Besides the auspicious results concerning the use of this technique, its involvement in routine veterinary practice is still pending, due to the few information available in the literature.

2.3 Contrast-enhanced ultrasound in female reproduction

2.3.1 Contrast-enhanced ultrasound of the ovaries and uterus

Few studies have been conducted to assess the characteristics of ovaries and uterus using CEUS in dogs. Just one study, that is part of the present thesis, has been reported to evaluate canine ovaries during follicologenesis, ovulation and corpora lutea formation, and will be discussed furtherly in this manuscript (Nogueira Aires et al. 2022). Quartuccio and colleagues reported the use of CEUS to evaluate the uterus in dogs with cystic endometrial hyperplasia. From 6–8 s after contrast agent injection, the hyperplastic endometrium showed a homogeneous enhancement (wash-in phase), then the decrease in enhancement was slow during the wash-out phase, with evidence of contrast up to 2 min. The examination evidenced the opposition between the intense enhancement in the hyperplastic endometrium and the lack of signal inside the cysts (Quartuccio et al. 2020).

2.3.2 Contrast-enhanced ultrasound in the pregnant dog

Contrast-enhanced ultrasound has been applied to evaluate the normal canine pregnancy and it was demonstrated to be a safe method, with no adverse pregnancy outcomes (Orlandi et al., 2019, Silva et al., 2022). Enhancement can be detected initially in the uterine artery, followed by a rapid distribution to the parietal uterine vessels and a radial distribution to the placenta, which almost simultaneously is distributed homogenously in the embryonic vesicle or placenta. The wash-out is progressive and homogenous. No enhancement can be detected in the embryo/fetus, as the microbubbles do not cross the placental barrier. Quantitative assessment of placental enhancement demonstrates similar perfusion parameters in its dorsal and ventral regions.

2.4 References

Angrimani DSR, Francischini MCP, Brito MM, Vannucchi CI. Prostatic hyperplasia: Vascularization, hemodynamic and hormonal analysis of dogs treated with finasteride or orchiectomy. PLoS One. 2020 Jun 25;15(6):e0234714. doi: 10.1371/journal.pone.0234714. PMID: 32584842; PMCID: PMC7316311.

Appis A W, Tracy M J, Feinstein S B. Update on the safety and efficacy of commercial ultrasound contrast agents in cardiac applications. Echo Res Pract. 2015;2:R55–R62.

Bargellini P, Orlandi R, Paloni C, et al. Evaluation of contrast-enhanced ultrasonography as a method for detecting gallbladder necrosis or rupture in dogs. Vet Radiol Ultrasound. 2016;57(6):611-620. doi:10.1111/vru.12404

Bertolotto M, Derchi LE, Sidhu PS, Serafini G, Valentino M, Grenier N, Cova MA, 2011: Acute segmental testic- ular infarction at contrast-enhanced ultrasound: early features and changes during follow-up. Am J Roentgenol 196, 834–841.

Bigliardi, E.; Ferrari, L. Contrast-enhanced ultrasound of the normal canine prostate gland: Contrast-Enhanced Ultrasound of Prostate. Vet. Radiol. Ultrasound 2010, 52, 107–110.

Bigliardi E, Denti L, De Cesaris V, et al. Colour Doppler ultrasound imaging of blood flows variations in neoplastic and non-neoplastic testicular lesions in dogs. Reprod Domest Anim. 2019;54(1):63-71. doi:10.1111/rda.13310

Blohm KO, Tichy A, Nell B. Clinical utility, dose determination, and safety of ocular contrast-enhanced ultrasonography in horses: A pilot study. Vet Ophthalmol. 2020;23(2):331-340. doi:10.1111/vop.12730

Burns, P.N.; Wilson, S.R. Focal Liver Masses: Enhancement Patterns on Contrast-Enhanced Images—Concordance of US Scans with CT Scans and MR Images. Radiology 2007, 242, 162–174.

Burti S, Zotti A, Rubini G, et al. Contrast-enhanced ultrasound features of malignant focal liver masses in dogs. Sci Rep. 2020;10(1):6076. Published 2020 Apr 8. doi:10.1038/s41598-020-63220-3

Canejo-Teixeira R, Lima A, Santana A. Applications of Contrast-Enhanced Ultrasound in Splenic Studies of Dogs and Cats. Animals. 2022; 12(16):2104. https://doi.org/10.3390/ani12162104

Caretta N, Palego P, Schipilliti M, Torino M, Pati M, Ferlin A, Foresta C, 2010: Testicular contrast harmonic imaging to evaluate intratesticular

perfusion altera- tions in patients with varicocele. J Urol- ogy 183, 263–269.

Choi SY, Jeong WC, Lee YW, Choi HJ. Contrast enhanced ultrasonography of kidney in conscious and anesthetized beagle dogs. J Vet Med Sci. 2016 Feb;78(2):239-44. doi: 10.1292/jvms.15-0199. Epub 2015 Sep 28. PMID: 26412201; PMCID: PMC4785112.

Claudon M, Dietrich C F, Choi B I, Cosgrove D O, Kudo M, Nolsoe C P, Piscaglia F et al. Guidelines and good clinical practice recommendations for contrast enhanced ultrasound (CEUS) in the liver–update 2012: a WFUMB-EFSUMB initiative in cooperation with representatives of AFSUMB, AIUM, ASUM, FLAUS and ICUS. Ultraschall Med. 2013;34:11–29.

Dietrich C F, Ignee A, Greis C, Cui X W, Schreiber-Dietrich D G, Hocke M.Artifacts and pitfalls in contrast-enhanced ultrasound of the liver Ultraschall Med 2014. 35108–125.quiz 126-107

Dietrich CF, Averkiou M, Nielsen MB, et al. How to perform Contrast-Enhanced Ultrasound (CEUS). Ultrasound Int Open. 2018;4(1):E2-E15. doi:10.1055/s-0043-123931

Feinstein S. B., Cheirif J., Ten Cate F. J., Silverman P. R., Heidenreich P. A., Dick C., et al. (1990). Safety and efficacy of a new transpulmonary ultrasound contrast agent: initial multicenter clinical results. J. Am. Coll. Cardiol. 16 316–324. 10.1016/0735-1097(90)90580-I

Feng, C.; Hu, B.; Hu, B.; Chen, L.; Li, J.; Huang, J. Comparative Study of Conventional US, Contrast Enhanced US and Enhanced MR for the Follow-up of Prostatic Radiofrequency Ablation. Exp. Ther. Med. 2017, 13, 3535–3542.

Forsberg, F.; Johnson, D.K.; Merton, D.A.; Liu, J.-B.; Losco, P.E.; Hagen, E.K.; Goldberg, B.B. Contrast-Enhanced Transrectal Ultrasonography of a Novel Canine Prostate Cancer Model. J. Ultrasound Med. 2002, 21, 1003–1013.

Freccero, F.; Toaldo, M.B.; Castagnetti, C.; Cipone, M.; Diana, D. Contrast-Enhanced Ultrasonography of the Uterus During Normal Equine Pregnancy: Preliminary Report in Two Mares. J. Equine Vet. Sci. 2017, 54, 42–49.

Gramiak R., Shah P. M. (1968). Echocardiography of the Aortic Root. Invest. Radiol. 3 301–388. 10.1097/00004424-196809000-00011

Haers, H.; Saunders, J.H. Review of clinical characteristics and applications of contrast-enhanced ultrasonography in dogs. J. Am. Vet. Med. Assoc. 2009, 234, 460–470.

References

Hagen MW, Louey S, Alaniz SM, et al. Changes in microvascular perfusion of heart and skeletal muscle in sheep around the time of birth. Exp Physiol. 2023;108(1):135-145. doi:10.1113/EP090809

Henri M., Florence E., Aurore B., Denis H., Frederic P., Francois T., et al. (2014). Contribution of contrast-enhanced ultrasound with Sonovue to describe the microvascularization of uterine fibroid tumors before and after uterine artery embolization. Eur. J. Obstet. Gynecol. Reprod. Biol. 181 104–110. 10.1016/j.ejogrb.2014.07.030

Hwang J, Kang K, Kang J, et al. Effect of catheter diameter and injection rate of flush solution on renal contrast-enhanced ultrasonography with perfluorobutane in dogs. Am J Vet Res. 2019;80(9):825-831. doi:10.2460/ajvr.80.9.825

Ignee A, Schuessler G, Cui X W. Endocavernous Contrast-Enhanced Ultrasound – Different Applications, Literature Review and Future Perspectives. Ultraschall Med. 2013;34:2–26.

Jia, L.; Bin, H.; Bing, H.; Jin, H. CEUS Examination of the Outcome of Radiofrequency Ablation of Canine Prostate Lesions. Minim. Invasive Ther. Allied Technol. 2021, 30, 334–340.

Jiang N., Xie B., Zhang X., He M., Li K., Bai J., et al. (2014). Enhancing ablation effects of a microbubble-enhancing contrast agent (“sonovue”) in the treatment of uterine fibroids with high-intensity focused ultrasound: a randomized controlled trial. Cardiovasc. Intervent. Radiol. 37 1321–1328. 10.1007/s00270-013-0803-z

Kienle RD Thomas WP: Echocardiography. In: Nyland TG, Mattoon JS: Small Animal Diagnostic Ultrasound, 2nd ed. WB Saunders Company, Philadelphia, 2002, pp 354-423.

Kitano M., Kudo M., Yamao K., Takagi T., Sakamoto H., Komaki T., et al. (2012). Characterization of small solid tumors in the pancreas: the value of contrast-enhanced harmonic endoscopic ultrasonography. Am. J. Gastroenterol. 107 303–310. 10.1038/ajg.2011.354

Laluhová, D.; Ohlerth, S.; Wergin, M.; Melzer, K.; Roos, M.; Kaser-Hotz, B. Differentiation of spontaneous canine tumors with contrast-enhanced colour and power Doppler ultrasound. Vet. Radiol. Ultrasound 2004, 45, 590.

Larson AC, Didier R, Daszewska-Smith G, et al. The fetal lamb model of congenital diaphragmatic hernia shows altered cerebral perfusion using contrast enhanced ultrasound. J Pediatr Surg. 2022;57(6):991-998. doi:10.1016/j.jpedsurg.2022.02.006

References

Lea C, Walker D, Blazquez CA, Zaghloul O, Tappin S, Kelly D. Prostatitis and prostatic abscessation in dogs: retrospective study of 82 cases. Aust Vet J. 2022 Jun;100(6):223-229. doi: 10.1111/avj.13150. Epub 2022 Feb 17. PMID: 35176814.

Lock G, Schmidt C, Helmich F, Stolle E, Dieckmann KP, 2011: Early experience with contrast-enhanced ultrasound in the diagnosis of testicular masses: a feasibility study. J Urology 77, 1049–1053.

Mantziaras G, Vasileiou NG, Ioannidi KS, et al. Use of contrast-enhanced ultrasonographic examination to evaluate health status of mammary glands of ewes at the end of a lactation period. J Dairy Res. 2018;85(1):39-43. doi:10.1017/S002202991800002X

Mantziaras, G.; Luvoni, G.C. Advanced ultrasound techniques in small animal reproduction imaging. Rep. Dom. Anim. 2020, 55, 17–25.

Murotsuki, J. Contrast-Enhanced Ultrasound in Obstetrics and Gynecology. Donald Sch. J. Ultrasound Obstet. Gynecol. 2007, 1, 16–19

Nogueira Aires, L.P.; Gasser, B.; Silva, P.; Del'Aguila-Silva, P.; Yamada, D.I.; Carneiro, R.K.; Bressianini Lima, B.; Padilha-Nakaghi, L.C.; Ramirez Uscategui, R.A.; Spada, S.; et al. Ovarian Contrast-Enhanced Ultrasonography and Doppler Fluxometry in Bitches during the Postovulatory Estrus and Corpora Lutea Formation. Theriogenology 2022, 194, 162–170.

Nyman, H.T.; Kristensen, A.T.; Kjelgaard, M.; McEvoy, F.J. Contrast-enhanced ultrasonography in normal canine liver. Evaluation of imaging and safety parameters. Vet. Radiol. Ultrasound 2005, 46, 243–250.

Ogden NKE, Cullen MD, Stack JD. Assessment of intrasynovial injection in horses by contrast-enhanced ultrasonography using air bubbles created by agitation of solution. Equine Vet J. 2021;53(6):1159-1168. doi:10.1111/evj.13388

Ohlerth, S.; Rüefli, E.; Rohrer Bley, C.; Sieber-Ruckstuhl, N.; Melzer, K.; Kaser-Hotz, B. Assessment of tissue perfusion in the normal canine spleen with contrast harmonic imaging. Vet. Radiol. Ultrasound 2005, 47, 110.

Orlandi, R.; Vallesi, E.; Boiti, C.; Polisca, A.; Troisi, A.; Righi, C.; Bargellini, P. Contrast-Enhanced Ultrasonography of Maternal and Fetal Blood Flows in Pregnant Bitches. Theriogenology 2019, 125, 129–134.

Orlandi, R.; Vallesi, E.; Boiti, C.; Polisca, A.; Bargellini, P.; Troisi, A. Characterization of Testicular Tumor Lesions in Dogs by Different Ultrasound Techniques. Animals 2022, 12, 210.

References

Paefgen V, Doleschel D, Kiessling F. Evolution of contrast agents for ultrasound imaging and ultrasound-mediated drug delivery. Front Pharmacol. 2015;6:197. Published 2015 Sep 15. doi:10.3389/fphar.2015.00197

Piscaglia F, Nolsoe C, Dietrich C F, Cosgrove D O, Gilja O H, Bachmann N M, Albrecht T et al. The EFSUMB guidelines and recommendations on the clinical practice of contrast enhanced ultrasound (CEUS): Update 2011 on non-hepatic applications. Ultraschall Med. 2012;33:33–59.

Prada F., Perin A., Martegani A., Aiani L., Solbiati L., Lamperti M., et al. (2014). Intraoperative contrast-enhanced ultrasound for brain tumor surgery. Neurosurgery 74 542–552. 10.1227/NEU.0000000000000301

Quartuccio, M.; Liotta, L.; Cristarella, S.; Lanteri, G.; Ieni, A.; D'Arrigo, T.; De Majo, M. Contrast-Enhanced Ultrasound in Cystic Endometrial Hyperplasia–Pyometra Complex in the Bitch: A Preliminary Study. Animals 2020, 10, 1368.

Rademacher, N.; Ohlerth, S.; Scharf, G.; Laluhova, D.; Alt, N.; Sieber, N.; Roos, M.; Kaser-Hotz, B. Changes of the feline pancreatic architecture, vascularity and perfusion. Vet. Radiol. Ultrasound 2005, 47, 109.

Rick T, Kleiter M, Schwendenwein I, Ludewig E, Reifinger M, Hittmair KM. Contrast-enhanced ultrasonography characteristics of intrathoracic mass lesions in 36 dogs and 24 cats. Vet Radiol Ultrasound. 2019;60(1):56-64. doi:10.1111/vru.12698

Russo, M.; Vignoli, M.; Catone, G.; Rossi, F.; Attanasi, G.; England, G. Prostatic Perfusion in the Dog Using Contrast-Enhanced Doppler Ultrasound. Reprod. Domest. Anim. 2009, 44, 334–335.

Russo, M.; Vignoli, M.; England, G. B-Mode and Contrast-Enhanced Ultrasonographic Findings in Canine Prostatic Disorders. Reprod. Domest. Anim. 2012, 47, 238–242.

Salwei, R.M.; O'Brien, R.T.; Matheson, J.S. Use of contrast harmonic ultrasound for the diagnosis of congenital portosystemic shunts in three dogs. Vet. Radiol. Ultrasound 2003, 44, 301–305.

Salwei, R.M.; O'Brien, R.T.; Matheson, J.S. Characterization of lymphomatous lymph nodes in dogs using contrast harmonic and power Doppler ultrasound. Vet. Radiol. Ultrasound 2005, 46, 411–416.

Santos VJC, Del'Aguila-Silva P, Silva P, Gasser B, Estrada CRV, Carneiro RK, Pavan L, Aires LP, da Cruz ICK, Uscategui RAR, Vicente WRR, Silva LA, Feliciano MAR. Contrast-enhanced ultrasound evaluation of the utero-placental perfusion in ewes. Small Ruminant Research, Volume

References

228, 2023. 107113, ISSN 0921-4488, https://doi.org/10.1016/j.smallrumres.2023.107113.

Sboros V, Averkiou M, Lampaskis M, et al. Imaging of the ovine corpus luteum microcirculation with contrast ultrasound. Ultrasound Med Biol. 2011;37(1):59-68. doi:10.1016/j.ultrasmedbio.2010.10.013

Schwarz S, Clevert D-A, Ingrisch M, Geyer T, Schwarze V, Rübenthaler J, Armbruster M. Quantitative Analysis of the Time–Intensity Curve of Contrast-Enhanced Ultrasound of the Liver: Differentiation of Benign and Malignant Liver Lesions. Diagnostics. 2021; 11(7):1244. https://doi.org/10.3390/diagnostics11071244

Seiler, G.S.; Brown, J.C.; Reetz, J.A.; Taeymans, O.; Bucknoff, M.; Rossi, F.; Ohlerth, S.; Alder, D.; Gaschen, L. Safety of contrast-enhanced ultrasonography in dogs and cats: 488 cases (2002–2011). J. Am. Vet. Med. Assoc. 2013, 242, 1255–1259.

Seiler, G.S.; Campbell, N.; Nixon, B.; Tsuruta, J.K.; Dayton, P.A.; Jennings, S.R.; Redding, W.R.; Lustgarten, M. Feasibility and safety of contrast-enhanced ultrasound in the distal limb of six horses. Vet. Radiol. Ultrasound 2016, 57, 282–289.

Silva, P.; Maronezi, M.C.; Padilha-Nakaghi, L.C.; Gasser, B.; Pavan, L.; Nogueira Aires, L.P.; Russo, M.; Spada, S.; Ramirez Uscategui, R.A.; Moraes, P.C.; et al. Contrast-Enhanced Ultrasound Evaluation of Placental Perfusion in Brachicephalic Bitches. Theriogenology 2021, 173, 230–240.

Simeoni F, Terragni R, Rubini G, et al. B-Mode and Contrast Enhanced Ultrasonography Features of Gastric Inflammatory and Neoplastic Diseases in Cats. Animals (Basel). 2020;10(8):1444. Published 2020 Aug 18. doi:10.3390/ani10081444

Simeoni F, Del Signore F, Aste G, Bargellini P, Rubini G, Terragni R, Tamburro R, Falerno I, de Pasquale F, Russo M, et al. B-Mode and Contrast Enhanced Ultrasonography Features of Gastric Inflammatory and Neoplastic Diseases in Dogs. Animals. 2021; 11(3):670. https://doi.org/10.3390/ani11030670

Sinagra L, Orlandi R, Caspanello T, Troisi A, Iannelli NM, Vallesi E, Pettina G, Bargellini P, De Majo M, Boiti C, et al. Contrast-Enhanced Ultrasonography (CEUS) in Imaging of the Reproductive System in Dogs: A Literature Review. Animals. 2023; 13(10):1615. https://doi.org/10.3390/ani13101615

References

Spada, S.; England, G.C.W.; Vignoli, M.; Carluccio, A.; Russo, M. Contrast-Enhanced Ultrasound Imaging of Prostate Gland in Neutered Dogs. Animals 2021, 11, 559.

Stan F, Gudea A, Damian A, et al. Ultrasonographic Algorithm for the Assessment of Sentinel Lymph Nodes That Drain the Mammary Carcinomas in Female Dogs. Animals (Basel). 2020;10(12):2366. Published 2020 Dec 10. doi:10.3390/ani10122366

Stock E, Vanderperren K, Haers H, Duchateau L, Hesta M, Saunders JH. Quantitative Differences Between the First and Second Injection of Contrast Agent in Contrast-Enhanced Ultrasonography of Feline Kidneys and Spleen. Ultrasound Med Biol. 2017 Feb;43(2):500-504. doi: 10.1016/j.ultrasmedbio.2016.09.013. Epub 2016 Oct 14. PMID: 27746009.

Troisi, A.; Orlandi, R.; Bargellini, P.; Menchetti, L.; Borges, P.; Zelli, R.; Polisca, A. Contrast-Enhanced Ultrasonographic Characteristics of the Diseased Canine Prostate Gland. Theriogenology 2015, 84, 1423–1430.

Uemura H., Sano F., Nomiya A., Yamamoto T., Nakamura M., Miyoshi Y., et al. (2013). Usefulness of perflubutane microbubble-enhanced ultrasound in imaging and detection of prostate cancer: phase II multicenter clinical trial. World J. Urol. 31 1123–1128. 10.1007/s00345-012-0833-831

Valentino M, Bertolotto M, Derchi L, Bertaccini A, Pavlica P, Martorana G, Baro- zzi L, 2011: Role of contrast enhanced ultrasound in acute scrotal disease. Eur Radiol 21, 1831–1840.

Vanderperren K, Stock E, Pardon B, Saunders J. Contrast-enhanced ultrasound in sheep. Small Ruminant Research. Volume 152, 2017, pp 33-40, ISSN 0921-4488, https://doi.org/10.1016/j.smallrumres.2016.12.017.

Vignoli, M.; Russo, M.; Catone, G.; Rossi, F.; Attanasi, G.; Terragni, R.; Saunders, J.; England, G. Assessment of Vascular Perfusion Kinetics Using Contrast-Enhanced Ultrasound for the Diagnosis of Prostatic Disease in Dogs: Prostatic Perfusion Kinetics Assessed by CEUS. Reprod. Domest. Anim. 2011, 46, 209–213.

Volta, A.; Manfredi, S.; Vignoli, M.; Russo, M.; England, G.; Rossi, F.; Bigliardi, E.; Di Ianni, F.; Parmigiani, E.; Bresciani, C.; et al. Use of Contrast-Enhanced Ultrasonography in Chronic Pathologic Canine Testes. Reprod. Dom. Anim. 2014, 49, 202–209.

References

Waller, K.R.; O'Brien, R.T.; Zagzebski, J.A. Quantitative contrast ultrasound analysis of renal perfusion in normal dogs. Vet. Radiol. Ultrasound 2007, 48, 373–377.

Wdowiak M, Rychlik A, Nieradka R, Nowicki M. Contrast-enhanced ultrasonography (CEUS) in canine liver examination. Pol J Vet Sci. 2010;13(4):767-773. doi:10.2478/v10181-010-0007-2

Yoon, S.; Alfajaro, M.M.; Cho, K.-O.; Choi, U.-S.; Je, H.; Jung, J.; Jang, Y.; Choi, J. Perfusion Change in Benign Prostatic Hyperplasia before and after Castration in a Canine Model: Contrast Enhanced Ultrasonography and CT Perfusion Study. Theriogenology 2020, 156, 97–106.

Chapter 3

Contrast-enhanced ultrasound of the prostate gland in castrated dogs

Spada S, England GCW, Vignoli M, Carluccio A, Russo M. Contrast-Enhanced Ultrasound Imaging of Prostate Gland in Neutered Dogs. Animals. 2021; 11(2):559. https://doi.org/10.3390/ani11020559

3.1 Introduction

Prostate neoplasia (PN) is a rare disease (prevalence of 0.43%) in both intact and neutered dogs (Axiak & Bigio, 2012), with Shetland Sheepdogs and Scottish Terriers at increased risk (Bryan et al. 2007). The mean age of diagnosis is 10 years. Adenocarcinoma, transitional cell carcinoma, and undifferentiated carcinoma are the most frequently reported PN (Cornell et al. 2000; Leroy & Northurp, 2009; Smith, 2008; Teske et al. 2002).
A higher prevalence of PN is seen in neutered dogs; however, both neutered and intact animals develop it at the same age. This aspect suggests that neutering is not an initiator of cancer, but promotes tumor progression (Bryan et al. 2007; Teske et al. 2002), or at least does not protect against the development of neoplasia.
Neutering is a routine surgical procedure in dogs and results in a decrease in testosterone and its active metabolite DHT (dihydrotestosterone) in the general circulation. The reduction of these hormones leads to prostate shrinkage and a decrease in sexual behavior, resulting in infertility (Johnston et al. 2000; Romagnoli, 2008). In the last two decades, several studies have shown a statistically significant increased risk of diagnosis of various neoplastic diseases in neutered males and females compared to intact dogs, which has sparked an international debate on whether elective neutering is still a tool that should be routinely performed (Sorenmo et al. 2003; Mckenzie, 2010). However, a definitive explanation of how the absence of gonadal hormones may influence the development of neoplasia in reproductive or nonreproductive tissues is still pending (Schrank & Romagnoli, 2020).
Early diagnosis of PN in dogs remains challenging, because of the lack of specific tumor markers found in tissue, blood, bone marrow, or other body fluids; therefore, the true incidence of prostate cancer may be higher than currently thought (Teske et al. 2002).
The first step in a PN diagnosis is digital rectal examination, which may provide information about prostate disorders (Weaver, 1981; Hargis & Miller, 1983). When a prostate gland with PN is palpated, it may be felt as an oversized, irregular, immobile, asymmetric mass that may occasionally cause pain when touched (White, 2000). In normal dogs, surgical castration results in a 70% reduction in the size of the gland. Although this process begins as early as 7–14 days after neutering, complete regression of the gland can be expected by 4 months (Johnston et al. 2000). Nevertheless, the

assessment of prostate size may not be useful to differentiate between malignant and benign prostate conditions (Bradbury et al. 2009).

On B-mode ultrasound, the prostate may appear increased in dimension and asymmetrical, with irregular and poorly defined outlines. Focal or diffuse, hyperechoic, or mixed lesions may be found throughout the parenchyma. Hyperechoic foci with acoustic shadowing representing mineralization and cavitary, cyst-like lesions varying in size, shape, and number may also be present. Extension of pathologic changes to the urethra or bladder neck, enlargement of regional lymph nodes, and disruption of the capsule are threatening ultrasound signs suggestive of neoplasia (Smith, 2008; Matoon & Nyland, 2015; Russo et al. 2012). Interestingly, neutered dogs with prostatic mineralization are likely to have PN, unlike intact male dogs with prostatic mineralization, which may be affected by either neoplastic or non-neoplastic prostatic disease (Bradbury et al. 2009).

Histological evaluation by ultrasound-guided fine needle aspiration (FNA) has been shown to be the most accurate test for detecting PN. Nevertheless, due to the low contrast and specificity existing between malignant areas and normal tissues on ultrasound images, nontargeted 12-site systematic biopsies covering the whole prostate gland are often performed to detect neoplasia, causing unnecessary pain to the patient (Cunto et al. 2019; Thiemeyer et al. 2019; Liu et al. 2019). Therefore, due to the lack of specific tumor ultrasonographic patterns, it is of great importance to develop innovative imaging techniques to increase the sensitivity and specificity of prostate cancer screening at an early stage, which may become very helpful to collect fewer and targeted samples, thereby reducing pain and stress.

The staging of canine PN should include a computed tomography scan, which may potentially be performed before cytological or histological results are available (Liu et al. 2019; Ravicini et al. 2018). Magnetic resonance imaging and scintigraphy are rarely performed (Leroy & Northrurp, 2009; Levy et al. 2017).

In recent years, new advanced ultrasound techniques have been undertaken for the detection of prostate cancer in dogs, such as color and pulsed Doppler sonography, contrast-enhanced ultrasound (CEUS) (Vignoli et al. 2011), and elastography (Domoslowska et al. 2018).

In veterinary medicine, CEUS has been used successfully to accurately detect the perfusion patterns of the liver, spleen, and kidneys in healthy dogs (Ziegler et al. 2003) and showed some differences between malignant and benign hepatic, renal, and splenic nodules in dogs and cats as a function of perfusion patterns (Nakamura et al. 2009; O'Brien et al. 2004).

CEUS is a technique that uses a specific contrast agent injected into the vessels, to highlight the small vascular bed. The contrast agent mainly constitutes microbubbles consisting of a gas core and a stabilized biological shell (Hunt & Romero, 2017). Despite there being few studies about CEUS, this method may be performed to collect detailed information about lesions and to distinguish a benign lesion from a malignant one, by evaluating prostate gland vascularization (Hunt & Romero, 2017; Bennet et al. 2018). Unlike color Doppler sonography, CEUS allows measurement of tissue perfusion independently of vessel size and vascular flow velocity. Perfusion can be assessed quantitatively, using replenishment kinetics or derivates thereof. Tumor perfusion is a surrogate parameter for their viability and, moreover, the degree of vascularity of a tumor can express its aggressiveness and help to predict its response to treatment (Delorme & Krix, 2006).

Second-generation contrast agents, such as SonoVue® (Bracco Diagnostics, Inc., Milan, Italy) and Sonazoid® (Daiichi-Sankyo Co., Ltd., Tokyo, Japan), are now commercially available in North America, Europe, and Asia. SonoVue®, consisting of sulfur hexafluoride (SF6) within a phospholipid shell, allows visualization of small vessels and microvascular perfusion in capillary beds and tumors (Tamura et al. 2019).

Images can be directly observed and show vascular detail or may be subjected to quantitative analysis of specific regions of interest using commercial software, allowing assessment of perfusion peak intensity, time to peak, persistence within the vascular bed, and time for complete clearance of the contrast agent (de Souza et al. 2017).

In recent years, several European research groups have reported promising results of CEUS for the diagnosis of PN and for guiding biopsies both in human and veterinary medicine.

According to a human study by Halpern et al. (Halpern et al. 2012) in 2012, there are significant benefits of CEUS compared to a systematic biopsy in distinguishing aggressive PN.

Mitterberger and colleagues reported a higher detection rate of prostate cancer in humans using CEUS along with Doppler during systematic biopsy (Mitterberger et al. 2007).

In addition, Frauscher (Frauscher, 2007) reported a significant increase in the detection rate of human prostate cancer with CEUS, with a 2.6-fold higher probability than biopsy of detecting prostate cancer.

Considering the excellent results of CEUS in human medicine, its application has also recently increased in veterinary medicine.

The work by Russo et al. (Russo et al. 2009) described the normal perfusion pattern and perfusion dynamics of the dog prostate, using CEUS.
Interestingly, PN in intact dogs can indeed be detected with CEUS, and there are trends in perfusion parameters between tumor types. Peak intensity values of perfusion (PPI) and time to peak (TTP) values are higher in prostatic carcinoma than in leiomyosarcoma. In cases of prostatic carcinoma, there is hyper-perfusion of the tumor during the wash-in phase and hypo-echogenicity during the wash-out phase, when compared to normal dogs. Leiomyosarcoma can be characterized in all phases by a homogeneous anechoic nonperfused area with surrounding highly vascularized parenchyma (Vignoli et al. 2011; de Souza et al. 2017).
The purpose of the present study was to describe the normal perfusion pattern and perfusion dynamics of prostate gland in castrated dogs with contrast-enhanced ultrasound and to consider whether this technique might be applicable for the detection of PN in this group.

3.2 Materials and Methods

Sixty-four, clinically normal, adult male crossbreed dogs, neutered at least 6 months prior to the present study, with an average age of approximately 2 to 14 years old and weighing between 7 and 55 kg, were used in this work.
Consecutive patients were prospectively enrolled from the “Zia Giuseppina” kennel in Caivano (Naples, Italy), assisted by two veterinary officers, in charge of the health control of the kennel. All experimental protocols in accordance with the relevant guidelines and regulations were approved by the Ethics Committee of the Department of Veterinary Medicine and Animal Production of the University of Naples, Federico II (protocol code 2016/0090751).
The dogs recruited for the present study underwent a standardized protocol that included a clinical examination, serum chemistry profile, complete blood cell count, and urinalysis (data not shown), as well as B-mode and CEUS ultrasound examination of the prostate. A 20G intravenous, three-way valved catheter was placed in the cephalic vein to rapidly infuse the bolus dose of freshly prepared contrast agent. The dogs were positioned in right lateral recumbency and linear (4–18 MHz) and microconvex transducers (6.6–8.0 MHz - Esaote Mylab 30 gold, Genova, Italy) were used to obtain scans of the prostate gland. The prostate and iliac lymph nodes were evaluated on the basis of their size, shape, margins, echogenicity, echotexture, and capsular integrity.

All patients were cooperative and, thus, no sedative or anesthesia was needed.

The transducer was placed at the level of the bladder neck and then moved, caudally, to visualize the prostate, in the longitudinal plane until a detailed image of the gland was obtained. The image was then frozen, and the maximal length (L) from the cranial to the caudal pole of the prostate and the maximal depth (DL) from the dorsal to the ventral part of the prostate were measured. Then, the transducer was rotated through 90° to obtain a transverse section.

The maximum width (W) and depth (DT) were measured, using the Atalan formulas (Atalan et al. 1999).

The prostate volume (PV) and the prostate weight (PW) were also calculated using the Atalan formulas (Atalan et al. 1999).

$$PV = \frac{0.487 \times L \times W \times (DL + DT)}{2} + 6.38$$

Data were compared using linear regression analysis with other parameters including body weight, age, and age at castration, to establish potential relationships, as described by previous studies in intact dogs (Atalan et al. 1999; Ruel et al. 1998). Color Doppler examination was performed at a frame rate of 0.7–1.4 frames per second, to study the prostate gland vascularization. The probe was then moved dorsally and cranially, to evaluate medial iliac lymph nodes by B-mode ultrasound.

For the CEUS examination, a second-generation contrast agent SonoVue® (sulfur hexafluoride microbubbles; Bracco Imaging S.p.A., Milan, Italy) was used in combination with a 5–7.5 MHz linear transducer with coded harmonic capability and dedicated software for contrast-enhanced ultrasound analysis (Contrast Tuned Imaging (CnTI-TM), Contrast Tuned Imaging technology, Esaote, Genova, Italy).

To decrease the acoustic impact of the ultrasound waves on the microbubble contrast agent and to increase its persistence in the blood flow, the mechanical index was always less than 0.1 (range 0.05–0.1), corresponding to an acoustic pressure lower than 45 kPa. A single focal zone was placed in the deepest part of the prostate. The overall gain and time gain compensation were adjusted, so that no signal from the prostatic parenchyma was present and only a very low background signal from the prostatic capsule was retained, to have an anatomical reference in the image.

The contrast agent was injected into the cephalic vein at a dose of 0.03 mL/kg of prepared solution (5 mg/mL) followed by a rapid bolus of 5 mL of saline solution. The timer was activated at the moment of the start of the injection (T = 0), and the flow of the contrast agent into the prostate was observed in real time.

Care was taken to keep the probe in the same position for at least 60 s.

Difficulties occurred in the case of particularly obese dogs, with BCS (Body condition score) > 4, where the prostate was partly or entirely within the pelvic cavity, and the operator had to increase the probe pressure to clearly visualize the prostatic margins and keep the prostate still in the center of the ultrasound image, for the whole time of the examination (60 s).

The entire examination was digitally recorded, to be reviewed, so that the enhancement pattern could be analyzed.

A commercial software application, Qontrast® (EC mark nr.0051, class IIA, Bracco, Milan, Italy) was used to design time–intensity curves. To obtain information, one frame was selected every 1 s for the first 60 s of the videos. In each sampled frame, the entire prostate was used as a single region of interest (ROI), manually defined by drawing a line around the shape of the prostate. A contrast-enhanced time–intensity curve was calculated for the ROI. The software calculated time–intensity curves on a pixel-by-pixel basis, fitted them to parametric curves, and calculated the following parameters, starting from T0: PPI (perfusion peak intensity) expressed as a percentage, TTP (time to peak, starting from T = 0) expressed in seconds, MTT (medium transit time) expressed in seconds, RBV (regional blood volume) expressed in cm3, and RBF (regional blood flow) expressed in cm^3/s. Mean values and standard deviations of the previous parameters were then calculated.

Patients were monitored for 2 h after the contrast agent injection, to control and prevent any side-effects. The whole examination lasted at least 15 min in each dog. There were eight examinations per day, and they were performed once a week for 8 weeks, in a total of 64 patients.

Repeated-measures ANOVA was performed to understand whether there was a difference in PPI percentage values and TTP values at different time points (15 s, 30 s, and 45 s). Greenhouse–Geisser correction was used when Mauchly's test of sphericity was violated. When significant interaction effects were observed, post hoc pairwise comparisons with Bonferroni adjustment were applied to discover which specific means differed.

All analyses were performed using SPSS software version 17.1 for Windows (SPSS Inc., Chicago, IL, USA), and a p-value <0.05 was considered statistically significant.

3.3 Results

No physical, laboratory, or ultrasonographic abnormalities and no side-effects or anaphylactic reactions related to the contrast-enhanced ultrasound examination were found in any of the 64 examined dogs.
B-mode ultrasound revealed that all the prostate glands had an oval shape with clear and smooth margins, as well as homogeneous and hypoechoic parenchyma. The urethra was always visible as anechoic to hypoechoic linear (in longitudinal view) and rounded (in trasverse view) area, surrounded by a hyperechoic wall, which was not always visible (Figure 3.1).

a) 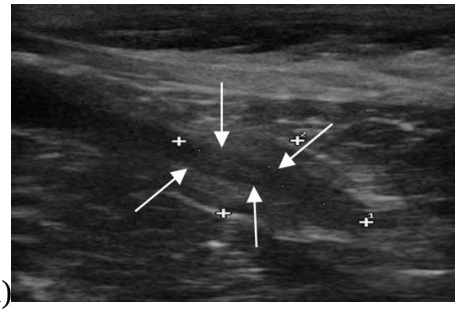 b) 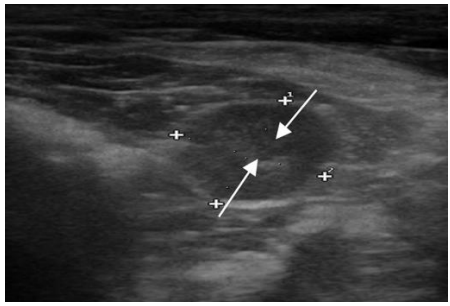

Fig. 3. 1 B-mode images of the prostate gland (case number 56). (a) Longitudinal view of the prostate gland, which appears pears oblong in shape, mildly echogenic, compared to the hypoechoic urethra (evidenced with arrows). (b) Transverse view of the same patient, in which the prostate appears ovoidal in shape and, in its center, the hypoechoic circular urethra (evidenced with arrows).

No focal lesions were discovered in the prostatic parenchyma, and the sizes of the iliac lymph nodes were within normal limits.
According to the measured parameters, the average prostate volume was 8.48 cm^3 ± 1.19 (± SD). Mean and standard deviation were calculated for the prostate volume, weight, age, and age at castration (Table 3.1). Scatter plots and linear regression analysis were performed to look for a possible correlation between the average values of the prostate volume, and the

weight, age, and age at castration (Figure 3.2). No obvious relationship between prostate volume and other parameters was found.

Tab. 3. 1 Mean and standard deviation of the reported parameters in the 64 dogs

	Weight (kg)	Age (months)	Age at castration (months)	Prostate volume (cm^3)
Mean	23.72	67.88	35.02	8.48
Standard deviation	10.69	35.60	28.55	1.19

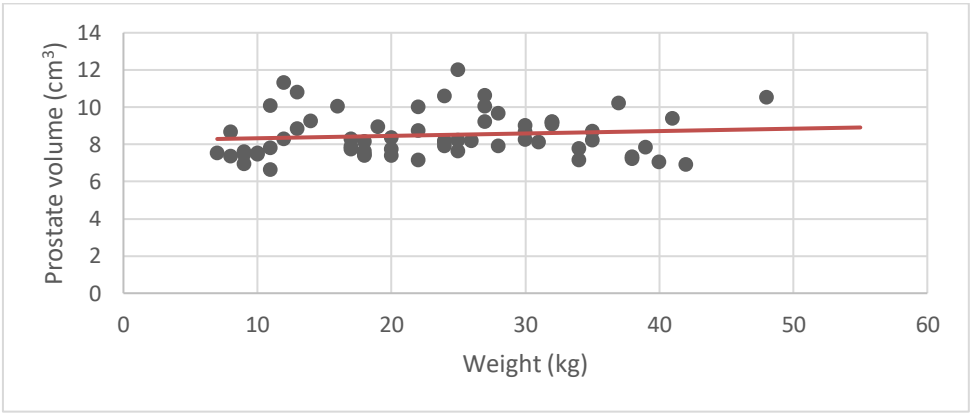

a)

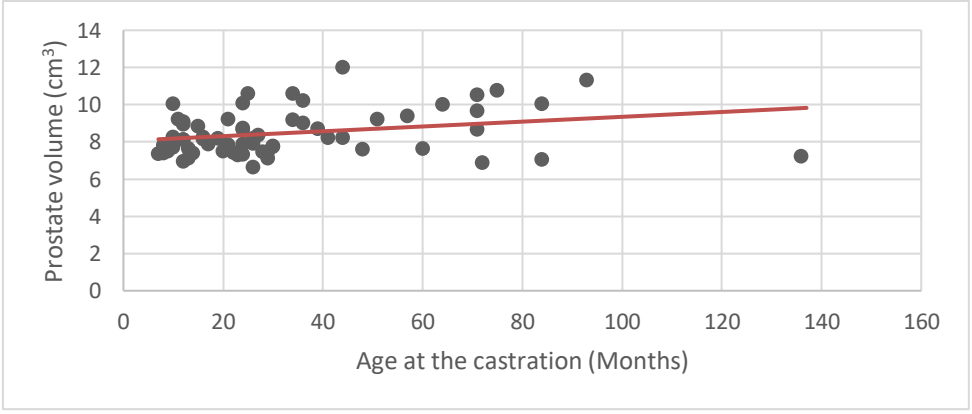

b)

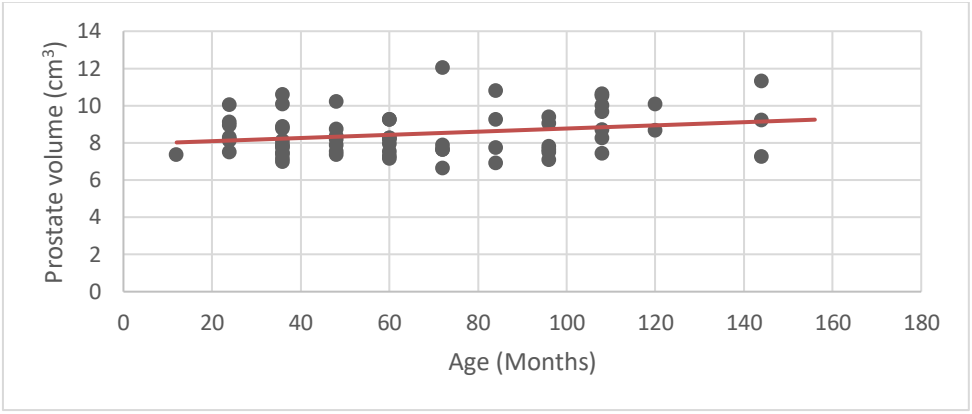

c)

Fig. 3. 2 Linear regression analysis has been performed to describe a hypothetical correlation between prostate volume and other parameters. None of the examined parameters seemed to influence the prostate volume in the 64 castrated dogs: (a) Relationship between Prostate volume and weight; (b) Relationship between Prostate volume and Age at castration; (c) Relationship between Prostate volume and Age.

For CEUS, the wash-in phase was visible after 15 s, when there was homogenous enhancement of the prostatic parenchyma. During the wash-out phase, a homogenous decrease in echogenicity was seen in all cases. The urethra was constantly seen as an echogenic linear (longitudinal view) or round (transverse view) area, more intense compared to the prostatic parenchyma (Figure 3.3).

The flow of the contrast agent was processed using the software (Q-contrast, Milan, Italy), to evaluate perfusion maps and times intensity curves and the results are shown in Table 3.2.

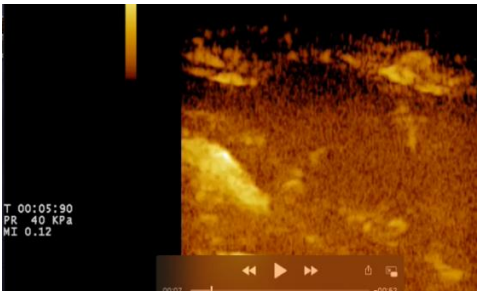

a)

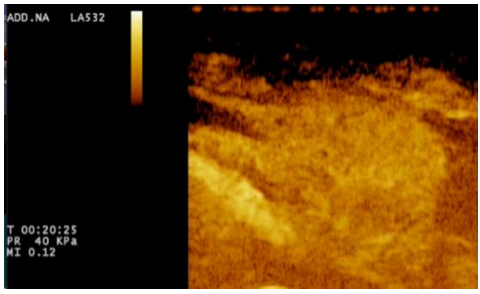

b)

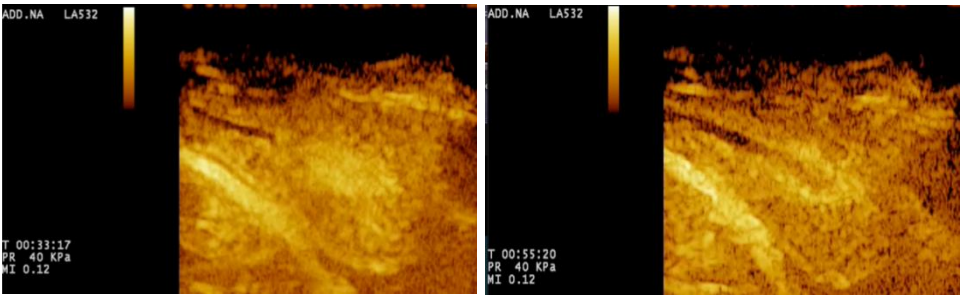

c) d)

Fig. 3. 3 Contrast-enhanced ultrasound examination: (a) Frame at 5 seconds from T0. The contrast agent has not reached the prostate yet. Therefore, the gland appears to be still hypo-enhanced; (b) Frame at 20 seconds from T0. The contrast agent is increasing the gland echogenicity; (c) Frame at 33 seconds from T0. The wash-in phase ends up with a peak enhancement. The prostate results to be hyper-enhanced; (d) Frame after 55 seconds from T0, which represents the wash-out phase. The prostate results to be hypo-enhanced, when compared to the one at 33 seconds.

Tab. 3. 2 Mean and standard deviation of the CEUS parameters calculated by the Qcontrast software in the prostates of the 64 examined dogs.

	PPI (%)	TTP (s)	RBV (cm^3)	RBF (cm^3/s)	MTT (s)
Mean	45.29	34.07	3192.62	56.19	54.26
Standard deviation	8.19	7.93	1723.20	13.78	21.35

A repeated measures ANOVA with a Greenhouse-Geisser correction determined that mean values of PPI percentages differed statistically significantly between time points ($F = 6.00$, $P < 0.01$). Post hoc tests using the Bonferroni correction revealed that there were no significant differences between the PPI average values described at 15 s and the ones at 45 s ($p=0.23$), and between the average PPI values at 30 s and the ones at 45 s ($p=0.51$).

However, at 30s average PPI values increased to 41.17 ± 9.53 %, which was statistically significantly different to 15s ($p < 0.001$). Therefore, we can conclude that a wait of 15 seconds from the first measurement resulted in an increase of PPI percentage (Figure 4).

The same statistical analysis has been performed in order to find significant dif-ferences in the three-time points for TTP mean values (Figure 5), but the TTP analysis did not result significant ($p=0.299$).

3.4 Discussion

Clinical assessment of prostate dysfunction in neutered dogs remains subjective and inaccurate. B-mode ultrasound results are particularly useful for assessing the size, shape, margins, echotexture, echogenicity, and position of the prostate gland, as well as for evaluating the draining reproductive lymph nodes. Assessment of prostate size is an important component in differentiating prostate disease in dogs and is usually performed by rectal palpation, abdominal radiographs, and ultrasound (Barsanti & Finco, 1995). Although it seems to be relatively easy to determine prostate size using linear measurements of prostate height, width, or length, or to estimate prostate volume (Barsanti & Finco, 1995; Juniewicz et al. 1989; Suzuki et al. 1998), there is still debate about the exact relationship between the prostate gland size and the canine body weight in intact dogs (Atalan et al. 1999; Ruel et al. 1998), possibly due to the potential complication of age-related changes in prostate volume (Komolpatana et al. 2000; Berry et al. 1986). In the work by Atalan et al. 1999, it was demonstrated that prostatic weight and volume were related to body weight and age in intact dogs but not in neutered dogs. However, since prostate volume was only measured in two neutered dogs in that study, no statistical analyses were performed on prostate volume and other parameters in this group.

Orchidectomy causes a significant reduction in the prostatic dimension, beginning soon after 7–14 days, and reaching 70% of the entire volume of the gland in 6 months (Johnston et al. 2000). Nonetheless, none of the previous studies provided a reference range for prostate volume in neutered dogs. In the present study, we found that prostate size did not appear to be related to body mass in neutered dogs, and the average of the prostatic volume was 8.48 cm^3 ± 1.19 (±SD).

To determine the normal range of prostatic volume found in healthy neutered dogs, it was important to examine a cohort of 64 adult castrated dogs (age 2 to 14 years and weight 7–55 kg) with no clinical signs of prostatic diseases. There was no apparent correlation between weight, age, and age at castration, and prostate volume, suggesting that, in neutered dogs, the prostate volume is not influenced by any of the previous parameters. Nonetheless, due to the low sample size, further studies are needed on a larger number of castrated dogs, to establish a recognized reference range.

The prostate may succumb to both focal and diffuse parenchyma changes, which may be hyperechoic, hypoechoic, or of mixed echogenicity. These

changes are also nonspecific and require further investigation, which may include Doppler or contrast-enhanced ultrasound imaging (de Souza et al. 2017). Color Doppler evaluation appears to be useful for the assessment of the vascularity in intact dogs, but it is unsuccessful in neutered dogs because of the reduced prostate vessel diameter. Flow within intratumoral neovessels (10–40 μm diameter) may also be below the resolution of conventional Doppler ultrasound. This hypothesis could be supported by our study, where, despite using low PRF (pulse repetition frequency), which increases the detection of slow vascular flow, the prostatic artery and its branches could not be seen.

CEUS, however, allows the visualization of microvascularization, making it an interesting and promising diagnostic tool for the evaluation of the prostate especially within the castrated dogs, where vessel size is smaller than that in intact ones. In human medicine, CEUS is a well-established technique for the diagnosis of PN. A study by Unal et al. (Unal et al. 2000) described that CEUS detected 68–79% of all tumor foci larger than 5 mm, leading the authors to conclude that CEUS was the best single diagnostic tool for prostate carcinoma detection. Our investigation produced detailed prostatic perfusion patterns, which can serve as a normal dataset of prostatic appearance in neutered dogs, and which can possibly be used as an early diagnostic method for detecting focal lesions related to PN.

Real-time contrast study allowed a better and detailed visualization of the prostatic gland vascularization than color Doppler examination. Nonetheless, since the qualitative analysis results are subjective, to perform an objective evaluation of the perfusion kinetics, collected data were standardized with a dedicated contrast-enhanced ultrasound analytical software (Q-contrast, Bracco, Italy), allowing the collection of all parameters obtained by perfusion maps and time–intensity curves. The most significant perfusion parameters were PPI (perfusion peak intensity) and TTP (time to peak). In particular, the PPI average was 45.2% (±8.2%), while TTP average was 34.1 s (±7.9 s). Intact dogs had a PPI average of 16.8% and a TTP average of 33.6 s (Russo et al. 2009). Vignoli et al. (Vignoli et al. 2011) evidenced that there were no significant differences in prostatic perfusion in dogs with benign prostatic pathology compared with normal dogs, while, in dogs affected by prostatic adenocarcinoma, the PPI average was 23.7% and the TTP average was 26.9 s, suggesting that intratumoral vessels resulted in an increased, faster enhancement of the contrast agent.

PPI calculated in neutered dogs was higher than that calculated in healthy intact dogs, while TTP values were quite similar. A possible explanation for

the higher PPI value could be related to the gradual parenchymal reduction, due to the previous castration, which does not change the vascularity of the prostate, thereby increasing the intensity of the ultrasound contrast agent.
To analyze the PPI and TTP variance trends in castrated dogs, means for PPI and TTP were further calculated at three different time points. Some necessary adjustments to the analysis models were included, to take into account specific features of the population. In particular, Greenhouse–Geisser correction (GGc) adjusts for the lack of sphericity in repeated-measures ANOVA. In this case, the p-value results were lower than 0.005. Taking multiple samples, then, the PPI in castrated dogs was coherent 99% of the time with the results found in our work, in contrast to TTP, whose p-value was 0.299, showing no significance of the coefficients. Further analysis was conducted to verify the existence of significant differences at the three time points. Results were significant when looking at the difference between 15 and 30 s. Interestingly, coefficients for PPI at 30 and 45 s were not statistically different. Lastly, TTP parameters showed no significant differences across all time sets. Further studies on a higher number of samples should be performed to standardize PPI and TTP parameters in the prostate of castrated dogs.
In the present study, none of the 64 examined dogs showed any focal or multifocal lesions related to PN, despite the literature reporting a higher incidence in neutered dogs. It has been reported that targeted biopsies during CEUS increase the detection rate of human prostate cancer (Vignoli, 2010). In neutered dogs, we believe that targeted biopsies during CEUS can be used to reduce the number of core biopsies and to establish clear diagnostic samples.

3.5 Conclusion

In conclusion, CEUS seems to be a sensitive diagnostic tool compared to B-mode ultrasound in the analysis of prostatic features in castrated dogs.
The continued advances made in diagnostic imaging technology have led to substantial improvement in disease investigation, and it appears that contrast-enhanced ultrasound imaging, in particular, will significantly improve our ability to diagnose prostatic pathology in neutered dogs

3.6 References

Atalan, G.; Holt, P.E.; Barr, F.J. Ultrasonographic estimation of prostate size in normal dogs and relationship to bodyweight and age. J. Small Anim. Pract. 1999, 40, 408–412. [Google Scholar] [CrossRef] [PubMed]

Axiak, S.M.; Bigio, A. Canine prostatic carcinoma. Compend. Contin. Educ. Vet. 2012, 34, E1–E5. [Google Scholar]

Barsanti, J.; Finco, D. Prostatic disease. In Textbook of Veterinary Internal Medicine: Diseases of the Dog and Cat, 4th ed.; Ettinger, S.J., Feldman, E.C., Eds.; WB Saunders Co.: Philadelphia, PA, USA, 1995; pp. 1662–1685. [Google Scholar]

Bennett, T.C.; Matz, B.M.; Henderson, R.A.; Straw, R.C.; Liptak, J.M.; Selmic, L.E.; Collivignarelli, F.; Buracco, P. Total prostatectomy as a treatment for prostatic carcinoma in 25 dogs. Vet. Surg. 2018, 47, 367–377. [Google Scholar] [CrossRef]

Berry, S.J.; Coffey, D.S.; Ewing, L.L. Effects of aging on prostate growth in beagles. Am. J. Physiol. Regul. Integr. Comp. Physiol. 1986, 250, 1039–1046. [Google Scholar] [CrossRef]

Bradbury, C.A.; Westropp, J.L.; Pollard, R.E. Relationship between prostatomegaly, prostatic mineralization, and cytologic diagnosis. Vet. Radiol. Ultrasound 2009, 50, 167–171. [Google Scholar] [CrossRef]

Bryan, J.N.; Keeler, M.R.; Henry, C.J.; Bryan, M.E.; Hahn, A.W.; Caldwell, C.W. A population study of neutering status as a risk factor for canine prostate cancer. Prostate 2007, 67, 1174–1181. [Google Scholar] [CrossRef]

Cornell, K.K.; Bostwick, D.G.; Cooley, D.M.; Hall, G.; Harvey, H.J.; Hendrick, M.J.; Pauli, B.U.; Render, J.A.; Stoica, G.; Sweet, D.C.; et al. Clinical and pathologic aspects of spontaneous canine prostate carcinoma: A retrospective analysis of 76 cases. Prostate 2000, 45, 173–183. [Google Scholar] [CrossRef]

Cunto, M.; Mariani, E.; Anicito Guido, E.; Ballotta, G.; Zambelli, D. Clinical approach to prostatic diseases in the dog. Reprod. Domest. Anim. 2019, 54, 815–822. [Google Scholar] [CrossRef]

de Souza, M.B.; da Silva, L.D.M.; Moxon, R.; Russo, M.; England, G.C.W. Ultrasonography of the prostate gland and testes in dogs. Practice 2017, 39, 21–32. [Google Scholar] [CrossRef]

Delorme, S.; Krix, M. Contrast-enhanced ultrasound for examining tumor biology. Cancer Imaging 2006, 6, 148–152. [Google Scholar] [CrossRef] [PubMed] [Green Version]

References

Domosławska, A.; Zduńczyk, S.; Jurczak, A.; Janowski, T. Elastography as a diagnostic tool in the prostate tumour detection in Labrador retriever. Andrologia 2018, 50, e13139. [Google Scholar] [CrossRef]

Frauscher, F. Contrast-enhanced Ultrasound in Prostate Cancer. Eur. Oncol. Haematol. 2007, 2. [Google Scholar] [CrossRef] [Green Version]

Halpern, E.J.; Gomella, L.G.; Forsberg, F.; McCue, P.A.; Trabulsi, E.J. Contrast enhanced transrectal ultrasound for the detection of prostate cancer: A randomized, double-blind trial of dutasteride pretreatment. J. Urol. 2012, 188, 1739–1745. [Google Scholar] [CrossRef]

Hargis, A.M.; Miller, L.M. Prostatic carcinoma in dogs. Compend. Contin. Educ. Pract. Vet. 1983, 5, 647–656. [Google Scholar]

Hunt, D.; Romero, J. Contrast-Enhanced Ultrasound. Magn. Reson. Imaging Clin. N. Am. 2017, 25, 725–736. [Google Scholar] [CrossRef]

Johnston, S.D.; Kamolpatana, K.; Root-Kustritz, M.V.; Johnston, G.R. Prostatic disorders in the dog. Anim. Reprod. Sci. 2000, 60–61, 405–415. [Google Scholar] [CrossRef]

Juniewicz, P.E.; Ewing, L.L.; Dahnert, W.F.; Hamper, U.M.; Dembeck, C.; Sanders, R.C.; Coffey, D.S. Determination of canine prostatic size in situ: Comparison of direct caliper measurement with radiologic and transrectal ultrasonographic measurements. Prostate 1989, 14, 55–64. [Google Scholar] [CrossRef]

Kamolpatana, K.; Johnston, G.R.; Johnston, S.D. Determination of canine prostatic volume using transabdominal ultrasonography. Vet. Radiol. Ultrasound 2000, 41, 73–77. [Google Scholar] [CrossRef]

LeRoy, B.E.; Northrup, N. Prostate cancer in dogs: Comparative and clinical aspects. Vet. J. 2009, 180, 149–162. [Google Scholar] [CrossRef]

Lévy, X.; Mimouni, P.; Loukeri, S.; Claret, E. Canine prostate specific esterase as a diagnostic marker for BPH: Validation study of the in-clinic test. In Proceedings of the Oral exposition in International Congress EVSSAR 2017, Vienna, Austria, 29 June–1 July 2017. [Google Scholar]

Liu, C.; Xing, M.; Cong, B.; Qiu, C.; He, D.; Wang, C.; Xiao, Y.; Yin, T.; Shao, M.; Qiu, W.; et al. In vivo transrectal imaging of canine prostate with a sensitive and compact handheld transrectal array photoacoustic probe for early diagnosis of prostate cancer. Biomed. Opt. Express 2019, 10, 1707. [Google Scholar] [CrossRef] [PubMed]

Mattoon, J.S.; Nyland, T.G. Prostate and Testes. In Small Animal Diagnostic Ultrasound, 3rd ed.; Mattoon, J.S., Nyland, T.G., Eds.; Saunders: St. Louis, MO, USA, 2015; Volume 1, pp. 608–633. [Google Scholar]

References

McKenzie, B. Evaluating the benefits and risks of neutering dogs and cats. Cab Rev. Perspect. Agric. Vet. Sci. Nutr. Nat. Resour. 2010, 5, 1–18. [Google Scholar] [CrossRef] [Green Version]

Mitterberger, M.; Pelzer, A.; Colleselli, D.; Bartsch, G.; Strasser, H.; Pallwein, L.; Aigner, F.; Gradl, J.; Frauscher, F. Contrast-enhanced ultrasound for diagnosis of prostate cancer and kidney lesions. Eur. J. Radiol. 2007, 64, 231–238. [Google Scholar] [CrossRef] [PubMed]

Nakamura, K.; Sasaki, N.; Yoshikawa, M.; Ohta, H.; Hwang, S.J.; Mimura, T.; Yamasaki, M.; Takiguchi, M. Quantitative contrast-enhanced ultrasonography of canine spleen. Vet. Radiol. Ultrasound 2009, 50, 104–108. [Google Scholar] [CrossRef] [PubMed]

O'Brien, R.T.; Iani, M.; Matheson, J.; Delaney, F.; Young, K. Contrast harmonic ultrasound of spontaneous liver nodules in 32 dogs. Vet. Radiol. Ultrasound 2004, 45, 547–553. [Google Scholar] [CrossRef] [PubMed]

Ravicini, S.; Baines, S.J.; Taylor, A.; Amores-Fuster, I.; Mason, S.L.; Treggiari, E. Outcome and prognostic factors in medically treated canine prostatic carcinomas: A multi-institutional study. Vet. Comp. Oncol. 2018, 16, 450–458. [Google Scholar] [CrossRef] [PubMed]

Romagnoli, S. Surgical gonadectomy in the bitch and queen: Should it be done and at what age. 2008. In Proceedings of the Southern European Veterinary Conference and Congreso Nacional AVEPA, Barcelona, Spain, 17–19 October 2008. [Google Scholar]

Ruel, Y.; Barthez, P.Y.; Mailles, A.; Begon, D. Ultrasonographic evaluation of the prostate in healthy intact dogs. Vet. Radiol. Ultrasound 1998, 39, 212–216. [Google Scholar] [CrossRef]

Russo, M.; Vignoli, M.; Catone, G.; Rossi, F.; Attanasi, G.; England, G.C.W. Prostatic perfusion in the dog using contrast-enhanced doppler ultrasound. Reprod. Domest. Anim. 2009, 44, 334–335. [Google Scholar] [CrossRef] [PubMed]

Russo, M.; Vignoli, M.; England, G.C.W. B-mode and contrast-enhanced ultrasonographic findings in canine prostatic disorders. Reprod. Domest. Anim. 2012, 47, 238–242. [Google Scholar] [CrossRef]

Schrank, M.; Romagnoli, S. Prostatic neoplasia in the intact and castrated dog: How dangerous is castration? Animals 2020, 10, 85. [Google Scholar] [CrossRef] [Green Version]

Smith, J. Canine prostatic disease: A review of anatomy, pathology, diagnosis, and treatment. Theriogenology 2008, 70, 375–383. [Google Scholar] [CrossRef] [PubMed]

References

Sorenmo, K.U.; Goldschmidt, M.; Shofer, F.; Goldkamp, C.; Ferracone, J. Immunohistochemical characterization of canine prostatic carcinoma and correlation with castration status and castration time. Vet. Comp. Oncol. 2003, 1, 48–56. [Google Scholar] [CrossRef]

Suzuki, K.; Ito, K.; Okazaki, H.; Ono, Y.; Kurokawa, K.; Suzuki, T.; Yamanaka, H. Estimation of canine prostatic volume: Nomogram based on prostatic cubic volume. Int. Urol. Nephrol. 1998, 30, 725–730. [Google Scholar] [CrossRef]

Tamura, M.; Nakamura, K.; Osuga, T.; Shimbo, G.; Sasaki, N.; Morishita, K.; Ohta, H.; Takiguchi, M. Findings of contrast-enhanced ultrasonography with sonazoid for cholangiocellular adenoma in three dogs. J. Vet. Med. Sci. 2019, 81, 1104–1108. [Google Scholar] [CrossRef] [PubMed] [Green Version]

Teske, E.; Naan, E.C.; van Dijk, E.M.; van Garderen, E.; Schalken, J.A. Canine prostate carcinoma: Epidemiological evidence of an increased risk in castrated dogs. Mol. Cell. Endocrinol. 2002, 197, 251–255. [Google Scholar] [CrossRef]

Thiemeyer, H.; Taher, L.; Schille, J.T.; Harder, L.; Hungerbuehler, S.O.; Mischke, R.; Hewicker-Trautwein, M.; Kiełbowicz, Z.; Brenig, B.; Schütz, E.; et al. Suitability of ultrasound-guided fine-needle aspiration biopsy for transcriptome sequencing of the canine prostate. Sci. Rep. 2019, 9, 1–14. [Google Scholar] [CrossRef] [PubMed]

Unal, D.; Sedelaar, J.P.; Aarnink, R.G.; Van Leenders, G.J.; Wijkstra, H.; Debruyne, F.M.; De La Rosette, J.J. Three-dimensional contrast-enhanced power Doppler ultrasonography and conventional examination methods: The value of diagnostic predictors of prostate cancer. BJU Int. 2000, 86, 56–64. [Google Scholar] [CrossRef] [PubMed] [Green Version]

Vignoli, M. Image-Guided Biopsy and Contrast-Enhanced Ultrasonography: Alternative Methods to Improve Imaging Diagnosis. Ph.D. Thesis, Faculty of Veterinary Medicine, Ghent University, Merelbeke, Belgium, 2010. Available online: http://hdl.handle.net/1854/LU-3239852 (accessed on 29 October 2010).

Vignoli, M.; Russo, M.; Catone, G.; Rossi, F.; Attanasi, G.; Terragni, R.; Saunders, J.H.; England, G.C. Assessment of Vascular Perfusion Kinetics Using Contrast-enhanced Ultrasound for the Diagnosis of Prostatic Disease in Dogs. Reprod. Domest. Anim. 2011, 46, 209–213. [Google Scholar] [CrossRef] [PubMed]

References

Weaver, A. Fifteen cases of prostatic carcinoma in the dog. Vet. Rec. 1981, 109, 74–75. [Google Scholar] [CrossRef]

White, R.A.S. Prostatic surgery in the dog. Clin. Tech. Small Anim. Pract. 2000, 15, 46–51. [Google Scholar] [CrossRef]

Ziegler, L.E.; O'Brien, R.T.; Waller, K.R.; Zagzebski, J.A. Quantitative contrast harmonic ultrasound imaging of normal canine liver. Vet. Radiol. Ultrasound 2003, 44, 451–454. [Google Scholar] [CrossRef]

Chapter 4

Digital post-processing analysis of prostatic perfusion in neutered dogs

Submitted and accepted by Veterinary radiology and ultrasound Journal

4.1 Introduction

The canine prostate gland can be affected by several pathological conditions, which often lead to similar clinical symptoms, making diagnostic process challenging (Smith, 2008). Although intact dogs represent most of the clinical cases, neutered dogs may also develop prostatic disorders such as prostatic tumours and prostatitis (Wilson, 2011). The role of neuter status has been the object of ongoing research and debate because gonadectomy may increase the incidence and/or hasten the progression of several pathological conditions both in female and male dogs. In particular, recent studies reported a higher prevalence of prostate neoplasia in neutered dogs (Bryan et al. 2007; Mckenzie et al. 2010; Teske et al. 2002; Schrank & Romagnoli, 2020) with two studies reporting an odds ratio of approximately 3.9 of prostatic neoplasia occurring in a neutered dog population compared to an intact population (Bryan et al. 2007; Sorenmo et al. 2003). However, it has been hypothesized that castration had no effect on the development of prostate neoplasia, but might play an influential role in the progression of the disease from an androgen-dependent to an androgen-independent state (Bryan et al. 2007; Cornell et al. 2000; Lai et al. 2008). Since castration may prevent unwanted sexual behaviour and reproduction, reduce straying, and prevent androgen-dependent diseases such as benign prostate hyperplasia, (Schrank & Romagnoli, 2020) it is commonly performed both in less and more developed countries. Nevertheless, before neutering pet animals, a comprehensive counselling of the owners regarding potential short and long-term advantages and disadvantages of the procedure is mandatory. In this context it is, therefore, imperative to understand the link between neuter status and the progression of prostatic neoplasia in dogs.

The diagnosis of prostatic neoplasia is challenging both in intact and neutered dogs, due to the lack of specific features or markers associated with the disease (Bradbury et al. 2009). Although B-mode ultrasound examination is a reliable and widely used method for detecting prostatic pathology there are no specific parameters associated with the detection of prostate neoplasia (Schrank & Romagnoli, 2020; Bradbury et al. 2009; Kuhnt et al. 2020). Contrast-enhanced ultrasound (CEUS) uses a specific ultrasonographic contrast agent injected intravenously to highlight the small vascular supply. CEUS has been used successfully to detect the prostate gland perfusion patterns in both intact and neutered dogs (Russo et al. 2009; Vignoli et al. 2011; de Souza et al. 2017; Spada et al. 2021; Troisi et al. 2015) and in detecting prostatic neoplasia. Vignoli and colleagues found

trends in perfusion parameters between prostatic tumour types in intact dogs, (Vignoli et al. 2011) nevertheless few information about perfusion patterns of the healthy prostate and prostatic neoplasia in neutered dogs have been reported (Spada et al. 2021). However, the assessment of CEUS images is still subjective in clinical practice, and objective measurements may be influenced by several factors, such as ROI tracing and size, machine settings and individual variability. Recently, the use of post-processing software to analyse images has been proposed as an additional technique to optimize the interpretation of ultrasonographic images in terms of echotexture and vascularization of the targeted tissues. Several softwares have been tested to analyse and objectivize B-mode and Colour Doppler images in animal reproduction (Siqueira et al. 2009; Salzano et al. 2020; Moxon et al. 2015; Tomlinson et al. 2017). Objective analysis of ultrasonographic images allows measurement of tissue characteristics (Pearson & Adams, 1995) and enables detection of changes in echogenicity or vascular blood supply which may not be distinguished by the human eye (Rivers et al. 1996; Arteaga et al. 2005). Our hypothesis is that the use of a free post-processing tool such as ImageJ could be of advantage in animal andrology for the quantitative assessment of perfusion patterns following CEUS. Moreover, we do believe that could be helpful in the identification of specific characteristics of prostate glands among specimens, since the high variability identified using CEUS in prostate (Spada et al. 2021).
The present study aims to evaluate the applicability of a post-processing digital analysis software ImageJ for the assessment of prostate perfusion obtained by contrast-enhanced ultrasonography in neutered dogs and to identify influence of weight, age and neutering timing on vascularization features of the prostate.

4.2 Materials and methods

4.2.1 Animal selection

The present study is an analytical and anatomic study as it aims to investigate the feasibility of a digital post-processing software in the analysis of contrast-enhanced ultrasound images of prostate glands in neutered dogs and to detect any correlation between prostate vascularization and individual characteristics. Twenty-three, adult, healthy, neutered male, crossbreed dogs with an average age of approximately 72 (IQR= 48-96)

months and weight 24 (IQR=12-32) kg, an average age at castration of approximately 36 (IQR= 24-60) months and an average time elapsed since castration of approximately 25 (IQR= 12-37) months, were randomly and consecutively enrolled from a private kennel in Caivano (Naples, Italy). Specific data concerning the specimen's characteristics are reported in Table 4.1.

Tab. 4. 1 Descriptive characteristics of the studied population.

	Age (months)	Weight (Kg)	Age at castration (months)	Time elapsed since castration (months)	Prostate volume (cm^3)
Dog 1	144	12	136	8	11.33
Dog 2	48	17	19	29	7.89
Dog 3	84	17	34	50	7.75
Dog 4	96	31	39	57	9.03
Dog 5	60	25	44	16	8.24
Dog 6	36	22	11	25	7.74
Dog 7	72	25	48	24	12.03
Dog 8	108	28	34	74	10.63
Dog 9	156	39	137	19	7.25
Dog 10	96	18	29	67	7.49
Dog 11	48	38	36	12	10.22
Dog 12	96	18	64	32	7.64
Dog 13	96	41	93	6	7.07
Dog 14	60	32	57	6	9.24
Dog 15	36	24	26	10	10.61
Dog 16	60	11	10	50	7.53
Dog 17	96	42	60	36	9.4
Dog 18	48	10	23	25	7.46
Dog 19	108	55	71	37	10.53
Dog 20	36	10	13	23	6.97
Dog 21	72	9	51	21	7.62
Dog 22	30	9	24	6	7.48
Dog 23	60	30	26	34	7.94

Inclusion criteria for the present study were established by a second year ECAR resident and an Animal Reproduction Full Professor and supervised by two ECAR board certified reproduction specialist and were as follows: castration should have been performed at least 6 months prior to the examination, after the time needed for the prostate to regress until 80% of the intact size, not depending on pre-neutering prostate conditions; 24 the medical history of the dog recorded no diseases related to the lower urogenital system; no dogs with suspicion of neoplasia based on clinical signs, blood analysis and andrological examination were enrolled; the recruited dogs had to be 12 months of age or older, with a body condition score of 3/5 and the prostatic gland appeared within normal limits in terms of shape, margins, echogenicity and echotexture, with no focal lesions detected during the B-mode ultrasonographic examination. None of the recruited animals was excluded from the study because of deviation from selection criteria.
All dogs were housed in the kennel since the moment of the castration, which was performed by public veterinary officers, as part of the public control of stray dogs. The reproductive history prior the castration was unknown. The study was part of a routine general examination performed at the kennel. Since all dogs were cooperative, no sedation was performed. All experimental protocols were in accordance with the relevant guidelines and regulations approved by the Ethics Committee of the Department of Veterinary Medicine and Animal Production of the University of Naples, Federico II (protocol 2016/0090751).

4.2.2 B-mode and CEUS examination

All dogs underwent a standardized andrological check-up prior to the B-mode and CEUS examination on the same day, consisting of a clinical examination including inspection and palpation of the remnants of the scrotum, penis, and prepuce, cytological examination of preputial smear, and serum chemistry profile and complete blood cell count. Dogs were considered healthy based on the absence of reproductive abnormalities, and blood analysis within normal ranges. The ultrasonographic procedure was performed by a single recognized experienced operator. The dogs were positioned in right lateral recumbency and microconvex (2–8.0 MHz - Esaote Mylab 30 gold, Genova, Italy) and linear transducers (4–9 MHz) were used to perform B-mode and Colour Doppler ultrasound of the prostate and iliac lymph nodes which were evaluated in terms of size, shape, margins,

echogenicity, echotexture, and capsular integrity. The prostate was visualized in longitudinal and transverse view by rotating the probe of 90°, and length (L), Depth in both views (DL, DT) and width (W) were measured to calculate prostate volume using the Atalan formula (Atalan et al. 1999).
For CEUS examination of the prostate gland, a 20G intravenous, three-way valved catheter (Smiths medical Jelco, Lower Pemberton, Ashford, Kant, UK) was placed in the non-dependant cephalic vein to allow rapid infusion of the bolus dose of freshly prepared contrast agent SonoVue® (sulfurhexafluoride microbubbles; Bracco Imaging S.p.A., Milan, Italy). A 5–7.5 MHz linear transducer with coded harmonic capability and dedicated software for CEUS analysis (Contrast Tuned Imaging (CnTI-TM), Contrast Tuned Imaging technology, Esaote, Genova, Italy) was placed at the level of the bladder neck and then moved caudally to visualize the prostate, in the longitudinal plane until a detailed image of the gland at its maximal dimension was obtained. The longitudinal view was chosen in order to have in the same scan both prostatic lobes and so both right and left cranial prostatic arteries. To decrease the acoustic impact of the ultrasound waves on the microbubble contrast agent and to increase its persistence in the blood flow, the mechanical index was always less than 0.1 (range 0.05–0.1), corresponding to an acoustic pressure lower than 45 kPa. A single focal zone was placed covering the whole image of the prostate. The overall gain and time gain compensation were adjusted, so that no signal from the prostatic parenchyma was present and only a very low background signal from the prostatic capsule was retained, to have an anatomical reference in the image.
A second-generation contrast agent SonoVue® (sulfurhexafluoride microbubbles; Bracco Imaging S.p.A., Milan, Italy) was injected into the cephalic vein at a dose of 0.03 mL/kg of solution (5 mg/mL) prepared according to the manufacturer's manual, directly followed by a rapid bolus of 5 mL of saline solution. The timer was activated at the moment of the injection beginning (T = 0), and the flow of the contrast agent into the prostate was observed in real time. Care was taken to keep the probe in the same position for at least 60 s. The whole examination was digitally recorded, to be reviewed, so that the enhancement pattern could be analysed.
A commercial software application, Qontrast® (EC mark nr.0051, class IIA, Bracco, Milan, Italy) was used to design time–intensity curves. The Qontrast programme was held on a dedicated image analysis computer to facilitate data evaluation. To obtain information, one frame was selected every 1 s for the first 60 s of the videos. In each sampled frame, the entire prostate was used as a single region of interest (ROI), manually defined by drawing a line

around the shape of the prostate. A contrast-enhanced time–intensity curve was calculated for the ROI. The software calculated time–intensity curves on a pixel-by-pixel basis, fitted them to parametric curves, and calculated the following parameters, starting from T0: PPI (perfusion peak intensity) expressed as a percentage and TTP (time to peak, starting from T = 0) expressed in seconds. Mean values and standard deviations of these parameters were then calculated.

4.2.3 ImageJ Post-Processing

Videoclips were transferred to a Laptop computer (Asus VivoBook 15, i5, 8th generation) and underwent semi-automated analysis using a macro developed with ImageJ software (National Institutes of Health, Bethesda, Mary-land; http:rsb.info.nih.gov/ij/). Videoclips were analysed at the moment of the peak (TTP) previously determined by Qontrast software. The clip was frozen, and the quantity of pixel/cm was measured using the scale provided by the ultrasound machine. Then, a plugin Contrast Limited Adaptive Histogram Equalization (CLAHE), included in the ImageJ software, was activated, to implement and enhance the local contrast between close pixels (Figure 4.1).

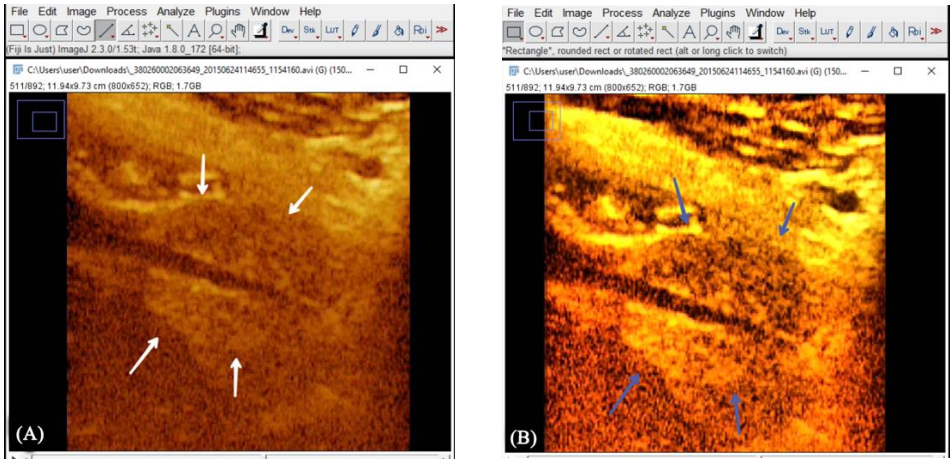

Fig. 4. 1 CLAHE filter is activated to improve image quality and increase the contrast between close structure. a) Contrast-enhanced ultrasound at the time of the peak of the prostate gland (white arrows). b) Activation of the CLAHE plugin to highlight the prostatic margins (blue arrows)

The prostate margins were manually drawn on the longitudinal axis as the maximum diameter of the gland, and the resulting prostate area (PA) was then selected and calculated. Colour threshold plugin was activated to detect more intense coloured areas, corresponding to the area of vascularization (AV), that was finally measured (Figure 4.2).

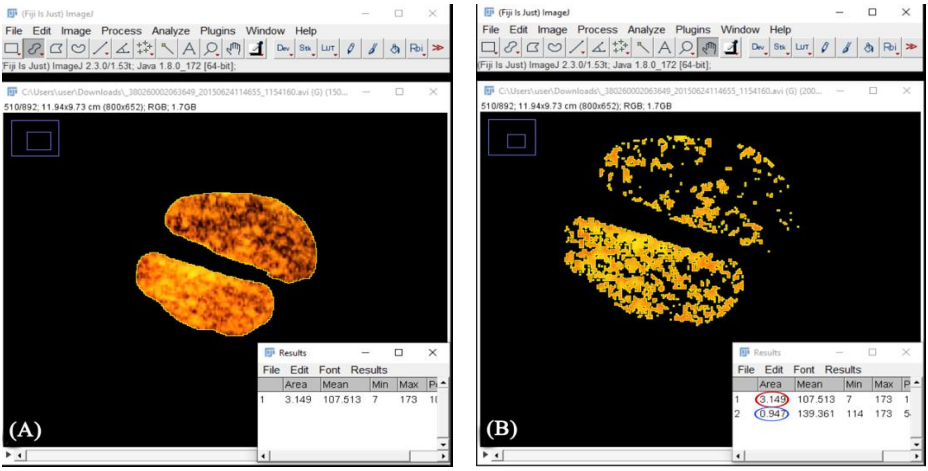

Fig. 4. 2 a) The prostate area is defined by tracing the margins and the periprostatic tissues and the urethra were removed. b) The area of the prostate previously measured (red circle) and the area of vascularization (blue circle) measured with Colour threshold were used to calculate VR.

Vascularization ratio (VR) was then calculated with the following formula:

$$VR = {}^{AV}/_{PA}$$

PPI and VR were calculated at 15s, 30s and 45s. All dogs were clinically monitored for two hours after the procedure by the kennel clinician in charge of the animal's health control and by kennel's operators for the subsequent 24 hours to detect any immediate or delayed side effect related to the injection of contrast agent, as reported by Seiler et al. 2013.

4.2.4 Statistical analysis

Data were first recorded using a computerized spreadsheet (Microsoft® Excel® 2021, Redmond, WA, USA) and then imported into Statistical Package for Social Sciences (SPSS IBM® Statistics version 27.0, IBM

Corporation, Armonk, NY, USA) for statistical analysis. Normality of data distribution was tested using Shapiro-Wilk test. Variables were normally distributed, and results were reported as mean and standard deviation. Repeated-measures ANOVA was performed to detect any significant difference at three different timepoints (15s, 30s, and 45s) within PPI and VR values, in order to describe the perfusion trends during the whole examination. Greenhouse–Geisser correction was used when Mauchly's test of sphericity was violated. When significant interaction effects were observed, post hoc pairwise comparisons with Bonferroni adjustment were applied to discover which specific means differed.
VR, PPI and TTP values were compared with body weight, age, age at castration, and time elapsed since castration using Pearson correlation tests to establish potential correlation. The correlation was considered weak, moderate, strong, or perfect respectively when the value of the correlation coefficient was 0.1–0.3, 0.4–0.6, 0.7–0.9, or 1, respectively. For all statistical tests, the level of significance was set at $P < 0.05$.

4.3 Results

No physical, laboratory, or ultrasonographic abnormalities and no side-effects or anaphylactic reactions related to the contrast agent injection were found in any of the dogs.
On B-mode ultrasound examination, the prostate glands appeared ovoidal in shape, with clear regular margins, homogeneous and diffusely hypoechoic in all dogs. Prostatic volume findings are reported in Table 1. Colour Doppler did not reveal any blood flow within the prostatic parenchyma, besides using a low PRF (pulse repetition frequency). Urinary bladder appeared regular, with wall thickness within normal ranges and anechoic endoluminal content. No evidence of iliac lymphadenopathy was observed, and the nodes appeared regular in dimensions according to Mayer and colleagues (Mayer et al. 2010) and Citi and colleagues (Citi et al. 2020).
CEUS revealed a typical prostate gland vascularization pattern. The contrast agent firstly enhanced in the right and left prostatic artery branches, which tunnelled into the prostatic capsule and branched homogeneously into many small parenchymal arteries directed medially towards the urethra. In the wash out phase, the parenchyma homogeneously lost enhancement. The urethral wash out appeared subjectively to be slower than the one of prostatic parenchyma in all dogs, maintaining a hyper-enhanced pattern after the peak of enhancement. For quantitative measurements, PPI, TTP and VR

values obtained by using CEUS and ImageJ software respectively are reported in Table 4.2.

Tab. 4. 2 Mean and standard deviation of the prostatic perfusion parameters calculated by Qontrast and ImageJ software of the 23 examined dogs.

	PPI (%)	TTP (s)	VR (%)
Mean	47.8	35.9	39.6
Standard Deviation	9.8	8.97	12.9

ImageJ was able to detect prostate perfusion in all videoclips analysed. The post-processing procedure performed with ImageJ took around 2 minutes per videoclip.
A repeated measures ANOVA with Greenhouse Geisser correction determined that mean values of PPI percentage and VR values differed statistically between time-points ($p< 0.001$). Post-hoc tests using the Bonferroni Correction revealed that there were significant differences between the PPI and VR average values described at 15s and those described at 30s, and the latter and the values described at 45s ($p < 0.001$). There was no statistical difference between values described at 45s and those described at 15s. However, VR and PPI tended to increase from 15s and 30s and decrease after 45s. Correlation tests were performed between the VR, PPI and TTP values and weight, age, age at castration and time elapsed since castration, and results are reported in Table 4.3

Tab. 4. 3 Pearson correlation coefficient between VR, PPI and TTP values and age, weight, age at castration and time elapsed since castration.

Vascularization parameters	Age (months)	Weight (kg)	Age at castration (months)	Time elapsed since castration (months)
VR (%)	-0.5*	-0.6**	-0.4	-0.08
TTP (s)	0.6**	0.4*	0.6**	-0.09
PPI (%)	-0.2	-0.4	0.07	0.3

* Indicates statistical significance ($p < 0.05$); ** Indicates statistical significance ($p < 0.01$)

A moderate negative correlation was found between VR and body weight ($p = 0.003$) and age ($p = 0.03$) (Figure 4.3), while a positive correlation was

found between TTP and weight (p = 0.048), age (p = 0.005) and age at castration (p = 0.002) (Figure 4.4). No correlation was found between PPI and the individual parameters.

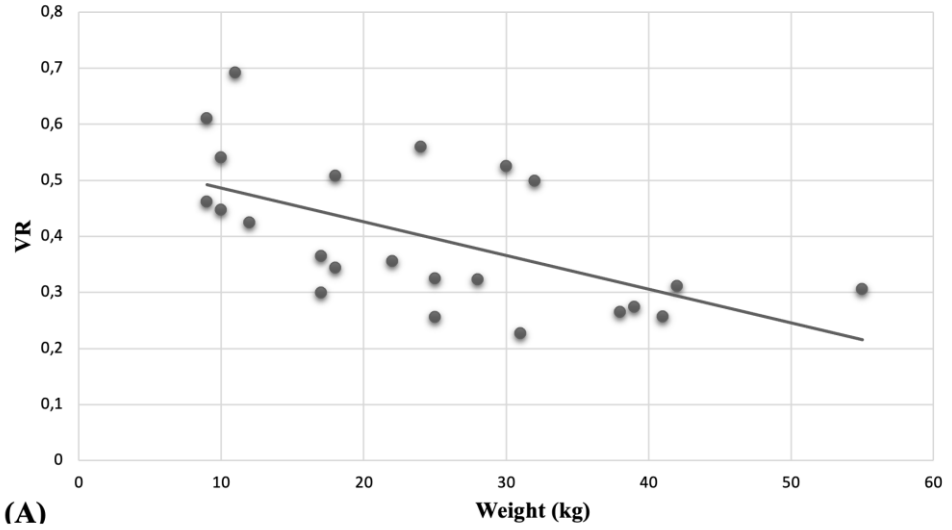

(A)

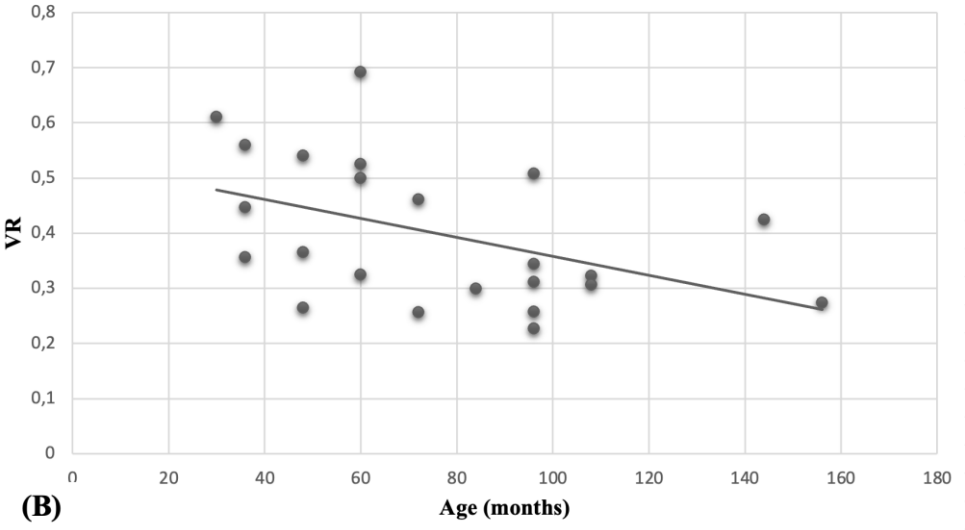

(B)

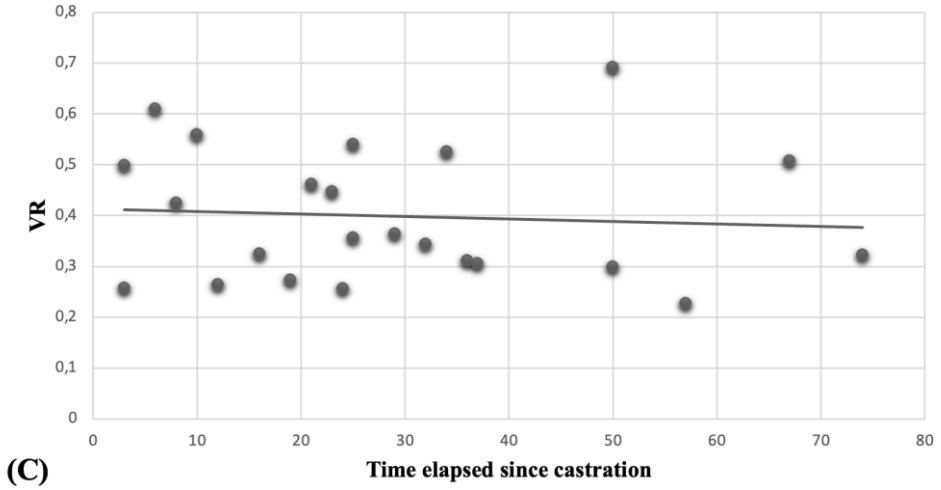

Fig. 4. 3 a) Moderate negative correlation was observed between VR and weight. b) Moderate negative correlation was observed between VR and age. c) No correlation was found between VR and time elapsed since castration.

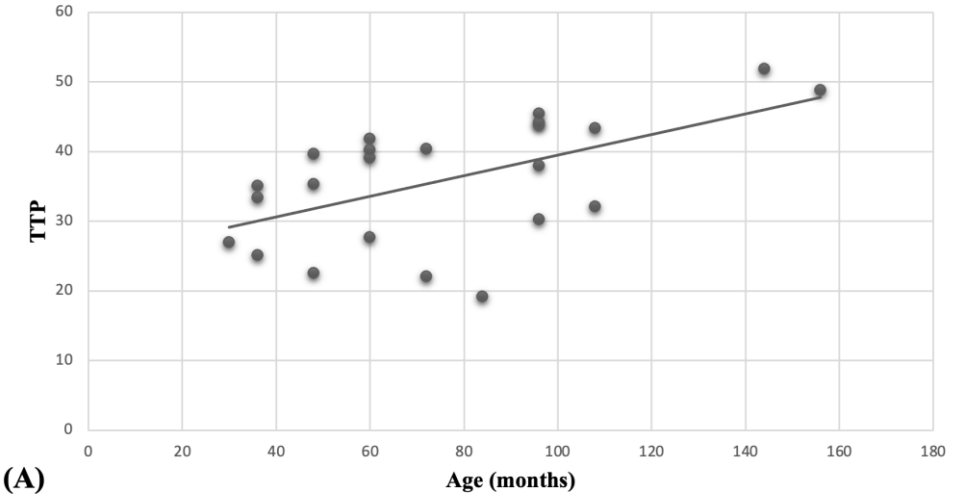

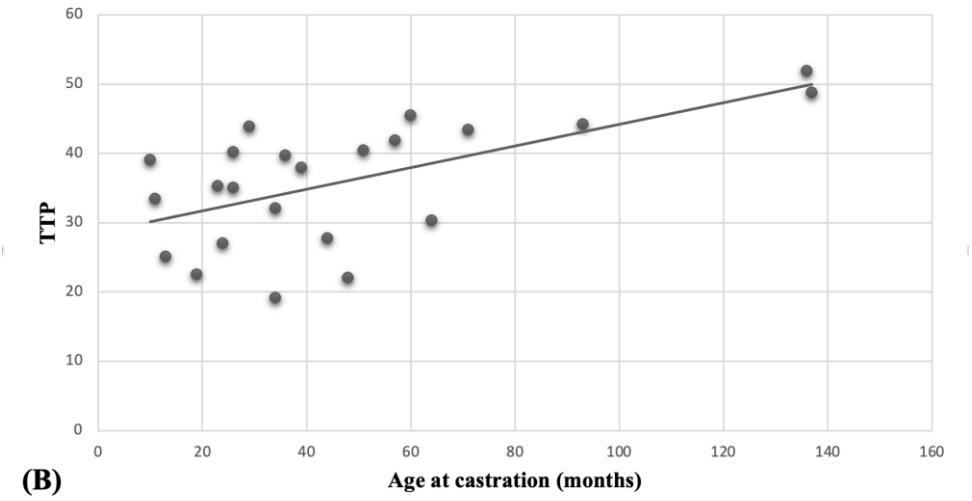

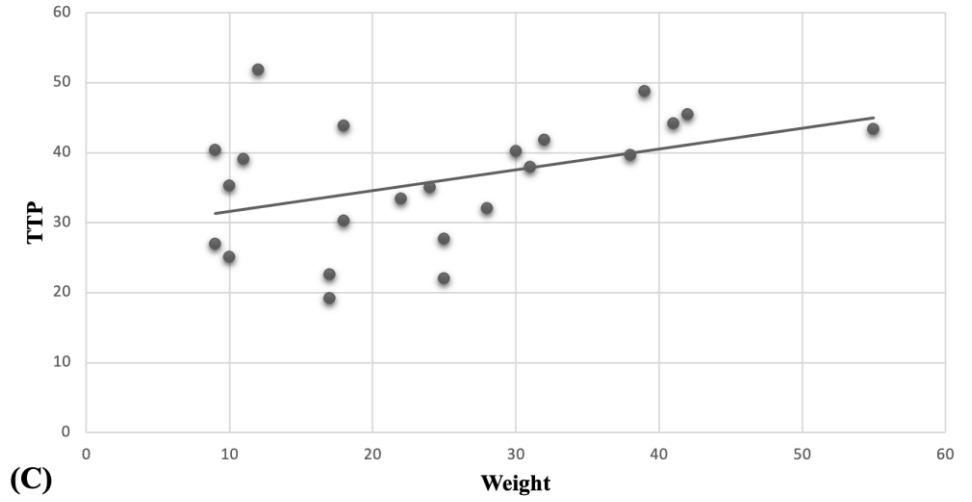

Fig. 4. 4 a) Moderate positive correlation between TTP and Age. b) Moderate positive correlation between TTP and Age at castration. c) Moderate positive correlation between TTP and weight.

4.4 Discussion

The present study provided and revealed new insights about the prostate gland changes after neutering and the ImageJ software potentials in quantifying prostatic vascularization in the post-processing evaluation of CEUS. Contrast-enhanced ultrasound confirmed to be a non-invasive method to quantify vascular blood supply of prostate glands in neutered dogs. No sedation was needed in the present study, in order to minimize perfusion changes due to the administration of anaesthetic drugs. However, patient restraint could be a stressful moment for the dog, which could affect heart rate or blood pressure during the procedure, influencing quantitative results especially for TTP. We could not exclude that our results were affected by the present parameters, since they were not measured during the examination. B-mode ultrasound is a reliable method for the detection of prostate diseases in neutered dogs, although identification and interpretation of specific pathologies remains subjective. The absence of specific clinical signs relating to individual diseases, and the high incidence of subclinical diseases makes it challenging to differentiate benign from malignant conditions in neutered dogs in many cases, so that fine needle aspiration and/or biopsy is often required (Bradbury et al. 2009; Troisi et al. 2015).
The development of prostatic pathology is often associated with changes in the vascular supply as well as changes in the prostatic parenchyma (Vignoli et al. 2011; Troisi et al. 2015). Nevertheless, as shown within the present study, Colour Doppler ultrasound may not be sensitive enough to detect blood flow within the prostatic parenchyma especially in neutered dogs due to the small vessels' size. CEUS has recently emerged as a highly sensitive technique for evaluating vascular perfusion, essentially by measuring peak flow and transit time within tissues using video-densitometric analysis of real-time images (Russo et al. 2012). Furthermore, this technique has provided promising results for the assessment of prostatic perfusion, both in intact and neutered dogs, being the only diagnostic tool in this group (Russo et al. 2009; Vignoli et al. 2011; Spada et al. 2021; Troisi et al. 2015). Despite the promising results, the interpretation of contrast enhancement using this technique remains still subjective (Egger et al. 2012), as more data and analysis are required to standardize the present method and analyse the sensitivity and specificity for the assessment of prostate diseases. A quantitative tool for evaluating prostatic perfusion might be useful for the early detection of prostate neoplasia in dogs. In a first step, this study aimed to evaluate post-processing digital analysis of prostatic perfusion in healthy

dogs. The ImageJ software has recently been shown to be a promising semi-automated analysis tool, useful for quantifying vascularization detected by using Colour Doppler ultrasound (Salzano et al. 2020; Orlandi et al. 2022). Egger and colleagues successfully evaluated the applicability of ImageJ in the analysis of contrast-enhanced ultrasound of liver lesions in humans (Egger et al. 2012). Stock and colleagues applied the software to measure the perfusion intensity of kidney and spleen in cats detected with CEUS (Stock et al. 2017). In the present study within ImageJ software, the use of CLAHE plugin allowed an improved visualization of the prostatic margins, increasing precision in tracing prostatic ROI, which enabled the exclusion of the prostatic urethral vascularization and surrounding periprostatic tissues. Moreover, with respect to findings in the cohort of neutered dogs examined, statistical analysis revealed similar trends between PPI measured by Qontrast software and VR values obtained by ImageJ post processing, as both increased in the first 15s, reaching a peak at 30s and decreasing at 45s. In this study a single infusion of contrast was used since the study was largely for screening. Previous works have shown that repeated doses of contrast may be required when multiple lesions are present, or when there is patient movement during the study (Stock et al.2017; Simeoni et al. 2020; Simeoni et al. 2021). Moreover, previous studies focused on contrast-enhanced ultrasound of the prostate gland reported the use of a single infusion of contrast agent, therefore we decided to apply the same methodology in order to standardize the results (Russo et al. 2009; Vignoli et al. 2011; Spada et al. 2021; Troisi et al. 2015; Russo et al. 2012). Both PPI and VR quantify changes of contrast agent during perfusion through the targeted tissue. However, VR analyses area of distribution of the blood flow, unlike PPI which measures the brilliance value in a single ROI, whose value may be influenced by the vessels and prostate size and so extremely variable among specimens. This hypothesis may be supported by the fact that VR values were coherent with TTP findings when looking at their association with specimens' parameters, unlike PPI results. Moreover, using a ratio helps in standardizing the values, as prostate dimensions and perfusion may vary widely among specimens, as it can be inferred by the large standard deviation of the perfusion parameters. We postulate that post-processing digital analysis of prostatic perfusion has merit for the quantification of vascular perfusion of the prostate gland of dogs. This methodology might, therefore, also be useful for the examination of other organs. Nevertheless, the reproducibility of the results was not tested by evaluating inter-operator variability. A limited margins of error could be due to ROI tracing, which

was manually drawn, and on the setting of the machine, influencing the quality of the images. However, the use of CLAHE plugin could reduce this limitation by increasing the pixel contrast, in order to be more precise in the definition of prostatic margins. Moreover, the level of saturation used with Colour Threshold was the same for all videoclips. Based on these assumptions, we could say that the technique has the potential to be highly reproducible, when using the same settings between specimens. Further studies should be performed in order to investigate the reproducibility of the technique. Nevertheless, the great standard deviation detected among PPI, VR and TTP values may reflect a variable morphological appearance of prostate gland in neutered dogs, which could explain the challenging nature of diagnostic procedures in regard to prostatic malignancies.

Several studies have examined the influence of body weight on prostatic parameters, especially the gland size (Kuhnt et al. 2020; Atalan et al. 1999; Ruel et al. 1998; Haverkamp et al. 2019; Delaude et al. 2021). Bosma and colleagues reported a significant correlation between body weight and single prostatic size parameters, such as length, height and depth in castrated dogs (Bosma et al. 2022), unlike our previous report which did not show any association between prostate volume and size of the dog (Spada et al. 2021). In the present study a negative moderate correlation between VR and both body weight and age was found, but no relation to the age at castration ($p = 0.056$) and time elapsed since castration ($p = 0.7$) was detected, whereas a positive moderate correlation was found between TTP values and weight, age and age at castration. To our knowledge there are no reports about vascularization differences between dogs of different sizes. The negative and positive correlation, respectively between VR and TTP with body weight suggests that prostate vascularization involution may be variable among dogs of different sizes, with vascular supply being reduced in large compared to small size breed dogs, in terms of vessels number and diameter, and quantity of vascular blood supply. It cannot be excluded that weight or body condition score may influence prostate vascular supply or impair its visualisation using the CEUS method, as the presence of obesity, fatty infiltration of the prostate, or metabolic conditions might play a role in the parenchymal appearance of the prostate. In the present study, all dogs had a body condition score of 3/5, therefore we do not believe that obesity could have influenced our evaluation and, moreover, very small size dogs were not involved, as the lowest weight recorded was 9 kg. Further studies should be performed on different groups of dogs based on their body size.

Concerning the negative and positive correlation registered between VR and TTP values, respectively with age, Kuhnt and colleagues reported differences in tissue structure among neutered dogs of different ages by using CT (Kuhnt et al. 2020). However, that study reported a difference in terms of heterogeneity between younger and older dogs, but no significant differentiation was found concerning vascular blood supply. The authors inferred that the homogenous pattern of prostate tissue observed in neutered dogs younger than 4 years of age might have been due to the absence of long-term influence of sex hormones on prostate tissue or to the low incidence of chronic diseases in this group. Our results suggest that age-related changes in the prostate gland may still occur even after neutering or may be seen as a result of pre-neutering processes, then affecting parenchymal vascularization, which can be visible even after prostate involution.

Furthermore, the present study found a positive correlation between age at castration and TTP, which may reflect an influence of the timing of exposure to gonadal hormones on prostate vascularization appearance after castration. In dogs, BPH affects (gross or microscopic evidence) the 80% of intact male dogs over 5 years old and more 95% of intact male dogs over 9 years old, (Sirinarumitr et al. 2001; Cunto et al. 2022) having an influence also on prostatic vascularization (Yoon et al. 2020; Angrimani et al. 2020). The positive correlation between age at castration and TTP observed in the present study may be due to the higher incidence of prostatic diseases or hormonal-related changes in older dogs, as suggested also by Kuhnt and colleagues (Kuhnt et al. 2020) that are likely to have modified vascular architecture of the prostate gland in the pre-neutering life. Nevertheless, the lack of correlation between age at castration with VR and PPI may indicate that after neutering the overall quantity of vascular blood supply is not or really affected by the moment of lifespan when surgical neutering is performed. Unfortunately, the medical and reproductive history before neutering of the recruited dogs was unknown. Interestingly, in the present study none of the prostate vascularization parameters was correlated with time elapsed since castration, indicating that prostatic parenchymal and vascular regression after neutering is a process influenced by individual characteristics, age at castration and eventually other parameters. However, none of the dogs enrolled in the present study was castrated very old or very early, so that no more precise evaluation is possible. In addition, the longest time elapsed since castration registered was 74 months. Further studies should be conducted with dogs neutered at more diverging age, so that the

effect of neutering of prepubertal, pubertal, adult and geriatric dogs may be assessed. Moreover, another step for future studies would be to describe anatomical and functional differences between dogs of different sizes and ages, and on the short- and long-term changes occurring in prostatic parenchyma and vascular supply after neutering.

4.5 Conclusion

The results of this study provide more details about the prostate vascularization in healthy neutered dogs. They may provide a baseline of information which may be useful for improving the differentiation between benign and malignant conditions of the prostate gland. CEUS and the post-processing analysis tool ImageJ allowed an objective analysis of vascular perfusion in all dogs and has the potential to improve the diagnostic possibilities for the examination of the male reproductive tract. In future studies, it should be assessed if specific diseases such as neoplasia may lead to specific vascularisation patterns which can be identified by CEUS. Eventually, the findings may be used for early detection, determination of the tumour type or malignancy of neoplasia.

4.6 References

Angrimani DSR, Francischini MCP, Brito MM, Vannucchi CI. Prostatic hyperplasia: Vascularization, hemodynamic and hormonal analysis of dogs treated with finasteride or orchiectomy. PLoS One. 2020 Jun 25;15:e0234714.

Arteaga AA, Barth AD, Brito LFC. Relationship between semen quality and pixel–intensity of testicular ultrasonograms after scrotal insulation in beef bulls. Theriogenology. 2005 Jul;64.

Atalan G, Holt PE, Barr FJ. Ultrasonographic estimation of prostate size in normal dogs and relationship to bodyweight and age. Journal of Small Animal Practice. 1999 Mar;40.

Bosma F, Wijsman S, Huygens S, Passon-Vastenburg M. Ultrasonographic measurements of the prostate gland in castrated adult dogs. Acta Vet Scand. 2022 Dec 8;64.

Bradbury CA, Westropp JL, Pollard RE. Relationship between prostatomegaly, prostatic mineralization, and cytologic diagnosis. Veterinary Radiology and Ultrasound. 2009 Mar;50:167–171.

Bryan JN, Keeler MR, Henry CJ, Bryan ME, Hahn AW, Caldwell CW. A population study of neutering status as a risk factor for canine prostate cancer. Prostate. 2007 Aug 1;67:1174–1181.

Cazzuli G, Damián JP, Molina E, Pessina P. Post-castration prostatic involution: A morphometric and endocrine study of healthy canines and those with benign prostatic hyperplasia. Reproduction in Domestic Animals. 2022 Feb 9;57.

Citi S, Oranges M, Arrighi E, Meucci V, Della Santa D, Tommaso M. Sonographic Evaluation of Medial Iliac Lymph Nodes-to-Aorta Ratio in Dogs. Vet Sci. 2020 Feb 11;7.

Cornell KK, Bostwick DG, Cooley DM, et al. Clinical and pathologic aspects of spontaneous canine prostate carcinoma: A retrospective analysis of 76 cases. Prostate. 2000 Oct 1;45.

Cunto M, Ballotta G, Zambelli D. Benign prostatic hyperplasia in the dog. Anim Reprod Sci. 2022 Dec;247.

de Souza MB, Silva LDM da, Moxon R, Russo M, England GCW. Ultrasonography of the prostate gland and testes in dogs. In Pract. 2017 Jan;39:21–32.

Delaude A, Broeckx BJG, Saunders JH, De Winter L, Hillaert A, Stock E. Intra- and Inter-observer Variability of Computed Tomographic

Measurements of the Prostate Gland in Neutered Dogs. Front Vet Sci. 2021 Jun 7;8.

Egger C, Goertz R, Strobel D, et al. Dynamic Contrast-Enhanced Ultrasound (DCE-US) for Easy and Rapid Evaluation of Hepatocellular Carcinoma Compared to Dynamic Contrast-Enhanced Computed Tomography (DCE-CT) – A Pilot Study. Ultraschall in der Medizin - European Journal of Ultrasound. 2012 Nov 15;33.

Haverkamp K, Harder LK, Kuhnt NSM, Lüpke M, Nolte I, Wefstaedt P. Validation of canine prostate volumetric measurements in computed tomography determined by the slice addition technique using the Amira program. BMC Vet Res. 2019 Dec 4;15.

Kuhnt N, Harder LK, Nolte I, Wefstaedt P. Computed tomographic features of the prostatic gland in neutered and intact dogs. BMC Vet Res. 2020 Dec 24;16.

Lai C-L, van den Ham R, van Leenders G, van der Lugt J, Mol JA, Teske E. Histopathological and immunohistochemical characterization of canine prostate cancer. Prostate. 2008 Apr 1;68.

Mayer MN, Lawson JA, Silver TI. Sonographic characteristics of presumptively normal canine medial iliac and superficial inguinal lymph nodes. Veterinary Radiology & Ultrasound. 2010 Nov;51.

McKenzie B. Evaluating the benefits and risks of neutering dogs and cats. CAB Reviews: Perspectives in Agriculture, Veterinary Science, Nutrition and Natural Resources. 2010.

Moxon R, Bright L, Pritchard B, et al. Digital image analysis of testicular and prostatic ultrasonographic echogencity and heterogeneity in dogs and the relation to semen quality. Anim Reprod Sci. 2015 Sep;160.

Orlandi R, Vallesi E, Boiti C, Polisca A, Bargellini P, Troisi A. Characterization of Testicular Tumor Lesions in Dogs by Different Ultrasound Techniques. Animals. 2022 Jan 17;12.

Pierson RA, Adams GP. Computer-assisted image analysis, diagnostic ultrasonography and ovulation induction: Strange bedfellows. Theriogenology. 1995 Jan;43.

Rivers BJ, Walter PA, Holm JC, et al. Gray-Scale Sonographic Characterization of Aminoglycoside-Induced Nephrotoxicosis in a Canine Model. Invest Radiol. 1996 Oct;31.

Ruel Y, Barthez PY, Mailles A, Begon D. Ultrasonographic evaluation of the prostate in healthy intact dogs. Veterinary Radiology & Ultrasound. 1998.

References

Russo M, Vignoli M, Catone G, Rossi F, Attanasi G, England GCW. Prostatic perfusion in the dog using contrast-enhanced doppler ultrasound. Reproduction in Domestic Animals. 2009;334–335.

Russo M, Vignoli M, England GCW. B-mode and contrast-enhanced ultrasonographic findings in canine prostatic disorders. Reproduction in Domestic Animals. 2012 Dec;47:238–242.

Salzano A, Russo M, Anglani G, et al. Early Prediction of Corpus Luteum Functionality Using an Imaging Software. Front Vet Sci. 2020 Jun 18;7.

Schrank M, Romagnoli S. Prostatic neoplasia in the intact and castrated dog: How dangerous is castration? Animals. MDPI AG; 2020.

Seiler GS, Brown JC, Reetz JA, et al. Safety of contrast-enhanced ultrasonography in dogs and cats: 488 cases (2002–2011). J Am Vet Med Assoc. 2013 May 1;242.

Simeoni F, Del Signore F, Aste G, et al. B-Mode and Contrast Enhanced Ultrasonography Features of Gastric Inflammatory and Neoplastic Diseases in Dogs. Animals. 2021 Mar 3;11:670.

Simeoni F, Terragni R, Rubini G, et al. B-Mode and Contrast Enhanced Ultrasonography Features of Gastric Inflammatory and Neoplastic Diseases in Cats. Animals. 2020 Aug 18;10:1444.

Siqueira LGB, Torres CAA, Souza ED, et al. Pregnancy rates and corpus luteum–related factors affecting pregnancy establishment in bovine recipients synchronized for fixed-time embryo transfer. Theriogenology. 2009 Oct;72.

Sirinarumitr K, Johnston SD, Kustritz MVR, Johnston GR, Sarkar DK, Memon MA. Effects of finasteride on size of the prostate gland and semen quality in dogs with benign prostatic hypertrophy. J Am Vet Med Assoc. 2001 Apr 15;218.

Smith J. Canine prostatic disease: A review of anatomy, pathology, diagnosis, and treatment. Theriogenology. 2008 Aug;70:375–383.

Sorenmo KU, Goldschmidt M, Shofer F, Goldkamp C, Ferracone J. Immunohistochemical characterization of canine prostatic carcinoma and correlation with castration status and castration time. Vet Comp Oncol. 2003 Mar;1.

Spada S, England GCW, Vignoli M, Carluccio A, Russo M. Contrast-Enhanced Ultrasound Imaging of Prostate Gland in Neutered Dogs. Animals. 2021 Feb 20;11.

Stock E, Vanderperren K, Haers H, Duchateau L, Hesta M, Saunders JH. Quantitative Differences Between the First and Second Injection of

References

Contrast Agent in Contrast-Enhanced Ultrasonography of Feline Kidneys and Spleen. Ultrasound Med Biol. 2017 Feb;43:500–504.

Teske E, Naan EC, van Dijk EM, Van Garderen E, Schalken JA. Canine prostate carcinoma: epidemiological evidence of an increased risk in castrated dogs. Mol Cell Endocrinol. 2002 Nov;197.

Tomlinson M, Jennings A, Macrae A, Truyers I. The value of trans-scrotal ultrasonography at bull breeding soundness evaluation (BBSE): The relationship between testicular parenchymal pixel intensity and semen quality. Theriogenology. 2017 Feb;89.

Troisi A, Orlandi R, Bargellini P, et al. Contrast-enhanced ultrasonographic characteristics of the diseased canine prostate gland. Theriogenology. 2015 Nov;84.

Vignoli M, Russo M, Catone G, et al. Assessment of Vascular Perfusion Kinetics Using Contrast-enhanced Ultrasound for the Diagnosis of Prostatic Disease in Dogs. Reproduction in Domestic Animals. 2011 Apr;46:209–213.

Wilson JD. The Critical Role of Androgens in Prostate Development. Endocrinol Metab Clin North Am. 2011 Sep;40.

Yoon S, Alfajaro MM, Cho K-O, et al. Perfusion change in benign prostatic hyperplasia before and after castration in a canine model: Contrast enhanced ultrasonography and CT perfusion study. Theriogenology. 202

Chapter 5

Long-term effect of orchiectomy on the ultrasonographic appearance of canine prostate gland: preliminary results

Submitted to Theriogenology journal

Long-term effect of orchiectomy on the ultrasonographic appearance of canine prostate gland: preliminary results

5.1 Introduction

Contraception by surgical sterilization including gonadectomy (ovariectomy or orchiectomy) is an irreversible procedure that results in permanent cessation of reproductive function. As gonadectomy is irreversible such surgical programs are widely accepted for population control (Reichler, 2009). Bilateral orchiectomy has a prophylactic and therapeutic effect on androgen-dependent diseases, such as benign prostatic hyperplasia (BPH), chronic and acute prostatitis and perineal hernias (Reichler, 2009; Smith, 2008; Cunto et al. 2022). In dogs, BPH may be diagnosed on 80% of intact male dogs over 5 years of age (Sirinarumitir et al. 2001) and more than 95% of intact male dogs over 9 years old (Cunto et al. 2022). The prostate gland is an androgen-dependent organ and orchiectomy results in regression of prostatic tissue in both normal dogs and dogs with BPH (Angrimani et al. 2020; Cazzuli et al. 2022). After removal of the testicles, androgen concentrations decline, leading to a rapid involution of the size of the gland, with an expected reduction of 80% within 90 days, thus affecting prostate features and function (Cazzuli et al. 2022; Johnston et al. 2000). Interestingly, whilst orchiectomy is an accepted and well-recognized method for the prevention and treatment of BPH (Cunto et al. 2022), recent studies reported a higher risk of prostatic neoplasia in neutered dogs increasing concern for choosing orchiectomy for the treatment of canine BPH. Nevertheless, it appears that orchiectomy does not initiate tumor development but may increase the incidence or hasten the progression of prostatic neoplasia (Teske et al. 2002; Bryan et al. 2007; Shidaifat et al. 2007; Schrank & Romagnoli, 2020). However, a definitive reason has not been identified yet, thus being imperative improving the knowledge of prostate physiology after gonadal hormone withdrawal and the changes that occur in the prostatic parenchyma. Unfortunately, data about the ultrasonographic changes that occur throughout the period of prostate gland involution after orchiectomy are scant (Angrimani et al. 2020; Cazzuli et al. 2022; Yoon et al. 2020). B-mode ultrasound is particularly useful for the assessment of size, shape, margins, echogenicity, echotexture and position of the prostate gland, as well as for evaluating the draining reproductive lymph nodes (Smith, 2008; Russo et al. 2012; Mayer et al. 2010; Citi et al. 2020). Despite the excellent application of ultrasound for imaging the prostate gland, the detection of prostate neoplasia can be challenging due to the lack of specific B-mode ultrasonographic features

both in intact and neutered dogs (Schrank & Romagnoli, 2020; Russo et al. 2012; Matton & Nyland, 2015; Bradbury et al. 2009). Prostatomegaly, dishomogeneous parenchyma and the presence of mineralization are common but not pathognomonic findings in prostatic neoplasia, highlighting the importance of establishing reference characteristics in castrated male dogs (Bradbury et al. 2009). Moreover, few studies have been conducted on the ultrasonographic appearance and features of the normal prostate gland in this group (Bosma et al. 2022; Spada et al. 2021). Innovative ultrasonographic techniques, such as contrast-enhanced ultrasound (CEUS), have been successfully used to improve the visualization and diagnosis of pathologic conditions of the prostate (Russo et al. 2012; Spada et al. 2021; Russo et al. 2009; Vignoli et al. 2011). CEUS involves the intravenous injection of gas-filled microbubbles which enhance the backscatter of ultrasound waves, resulting in the amplification of signals from blood flow (Dietrich et al. 2018; Nogueira et al. 2022). Prostate neoplasia, even in its early stages, usually exhibits increased blood flow due to neoangiogenesis. These features may be detected by using CEUS, including asymmetric rapid inflow, increased focal enhancement, and asymmetry of intraprostatic vessels which are beyond the resolution of conventional techniques including Color and Power Doppler (Russo et al. 2012; Vignoli et al. 2011; de Souza et al. 2017). Prostatic perfusion features in healthy neutered dogs have been described, whereas information about vascularization of prostatic neoplasia in this group is still under investigation (Spada et al. 2021). Despite the promising results obtained by performing CEUS for the characterization of prostatic perfusion in dogs, it is still not considered a widely reliable diagnostic tool since there few studies have been conducted in this species. Furthermore, vascularization regression analysis and description after castration has been poorly investigated. Angrimani and colleagues reported that orchiectomy induces morphological and vascular involution, in terms of Doppler ultrasound parameters and histological findings (Angrimani et al. 2020). Yoon and colleagues analyzed prostate perfusion changes using both CEUS and computerized tomography (CT) and confirmed the vascular regression occurring after castration (Yoon et al. 2020). Nevertheless, the focus of all the studies was to monitor regression of the prostate in the first 90 days after castration, and to our knowledge no information are available about changes occurring after this period of time.

The aim of the present preliminary study was to use B-mode and CEUS to monitor long-term prostate involution in a group of ten dogs after at least

three months elapsed since orchiectomy. We hypothesized that this would provide new and important information about the ultrasonographic features of the prostate gland in neutered dogs in order to facilitate diagnosis of malignancies.

5.2 Materials and methods

5.2.1 Animal Selection

A cohort of 11 adult, healthy, neutered male, crossbreed, kenneled dogs with a median age of approximately 42 (IQR= 30.27-56.12) months and a median weight of 23 (IQR= 13.68-27.91) kg, with a median age at castration of approximately 25.5 (IQR= 16.41-41.18) months and median time elapsed since castration of approximately 21.5 (IQR= 13.85-22.74) months, were selected from a private kennel in Caivano (Naples, Italy). The dogs were evaluated by using B-mode ultrasound and CEUS twice: the first evaluation was performed at the moment of the selection (T0) and the second one was performed six years later (T1). Inclusion criteria for the study were as follows: castration should have been performed at least 3 months prior the first examination (T0); the medical history of the dog recorded no diseases related to the lower urogenital system; no dogs with suspicion of neoplasia based on clinical signs, blood analysis and andrological examination were normal; the recruited dogs had to be 12 months of age or older and the prostatic gland should have appeared within normal limits in terms of shape, margins, echogenicity and echotexture, with no focal lesions, during the ultrasonographic examination. One dog had to be excluded from the present study for prostatic abnormalities detected at T1 correlated to a splenic mass with multiple metastasis including prostate gland. Descriptive features of the sample population eligible for further examination at T0 and T1 are reported in Table 5.1.

Tab. 5. 1 Descriptive features of the sample population.

	Age (months)		Weight (Kg)		Age at castration (months)	Time elapsed since castration (months)	
	T0	T1	T0	T1		T0	T1
Dog 1	15	17	24	96	11	13	85
Dog 2	10	10	36	108	13	23	95
Dog 3	24	22	60	132	44	16	88
Dog 4	23	25	36	108	11	25	97
Dog 5	24	24	36	108	14	22	94
Dog 6	24	23	48	120	26	22	94
Dog 7	38	42	48	120	25	23	95
Dog 8	32	29	63	135	60	3	75
Dog 9	9	9	72	144	51	21	93
Dog 10	9	9	36	108	12	24	96

All dogs were housed in the kennel since the time of the castration, which was performed by public veterinary officers, as part of the public control of stray dogs. The reproductive history prior the castration was unknown. The study enrollment was conducted in the context of a routine general examination performed at the kennel, together with two veterinary officers, in charge of the kennel's health control. No sedation was required as all dogs revealed to be cooperative, being not necessary to exclude any patient for aggressiveness. All experimental protocols were in accordance with the relevant guidelines and regulations approved by the Ethics Committee of the Department of Veterinary Medicine and Animal Production of the University of Naples, Federico II (protocol 2016/0090751). A standardized examination was performed for all dogs consisting of a recent and historical anamnesis of the patient, a general clinical examination followed by a breeding soundness examination, comprehensive of inspection and palpation of the prepuce, penis and scrotal remnants if present, digital rectal palpation and B-mode ultrasound and CEUS of the prostate gland.

5.2.2 B-mode ultrasound

For the ultrasound examination, dogs were positioned in right lateral recumbency, to the right of the operator and with the head parallel to the ultrasound machine. Prepubic hair were clipped, and alcohol and acoustic gel were applied to the skin to allow imaging. B mode and CEUS evaluations were performed with two different sets of equipment: a microconvex transducer (2-8 MHz) for B-mode ultrasound and a high frequency linear transducer (4–9 MHz - Esaote Mylab 30 gold, Genova, Italy) for CEUS at T0; a multifrequency microconvex transducer (3-11 MHz - Mindray, mQuadro, Vetus 7, Mindray Medical, Milan, Italy) for both B-mode and CEUS at T1. The ultrasonographic procedure was performed by a single operator (MR).
Image quality adjustments (gain, depth, focal zone, dynamic range) were made as necessary to obtain optimal quality images. For B-mode ultrasound, the microconvex transducer was placed on the skin and the urinary bladder was visualized. Then, the probe was moved caudally until a detailed image of a longitudinal bilobed prostate gland was acquired. In the longitudinal view, the maximum length (L – Cranio-caudal length) and the depth (DL – Dorso-ventral length) of the gland were measured and acquired. The probe was then rotated of 90° to obtain a transverse scan of the gland, and width (W – Latero-lateral length) and transverse depth (DT – Dorso-ventral length) of the prostate were measured. Prostate volume (PV) was then calculated by using the Atalan formula (Atalan et al. 1999):

$$PV = \frac{0.487 \times L \times W \times (DL + DT)}{2} + 6.38$$

The prostate was evaluated in terms of size, shape, margins, echogenicity, and echotexture in both views.

5.2.3 CEUS examination

For CEUS examination of the prostate gland, a 20G intravenous, three-way valved catheter (Smiths Medical Jelco, Lower Pemberton, Ashford, Kant, UK) was placed in the cephalic vein to allow rapid infusion of the bolus dose of a freshly prepared second-generation contrast agent SonoVue® (sulfurhexafluoride microbubbles; Bracco Imaging S.p.A., Milan, Italy).

Both the transducer used for CEUS examination were characterized by coded harmonic capability and equipped with a dedicated software for CEUS analysis (Contrast Tuned Imaging (CnTI-TM), Contrast Tuned Imaging Technology, Esaote, Genova, Italy at T0; UWN+ (Ultra-Wideband Non-linear Contrast Imaging Feature) Contrast ImagingTM at T1). For each examination the mechanical index was set lower than 0.1 (range 0.05 – 0.1), corresponding to an acoustic pressure of 45 kPa, to decrease the acoustic impact of the ultrasound waves on the microbubble contrast agent. The prostate gland was imaged, and a single focal zone was placed covering the whole prostate. Dual visualization at T1 allowed the creation of a reference B-mode image on the screen once the contrast software was activated. At T0, gain and time-gain compensation were adjusted to result in a reduced signal from the parenchyma. The contrast agent, prepared according to the manufacturer's manual, was injected into the cephalic vein at a dose of 0.03 mL/kg of solution (5 mg/mL), directly followed by a rapid bolus of 5 mL of saline solution. The timer was activated at the moment of the beginning of the injection (T = 0), and the flow of the contrast agent into the prostate was observed in real time. Care was taken to keep the probe in the same position for at least 60 s. The entire examination was digitally recorded, to be reviewed, so that the enhancement pattern could be systematically analyzed. For the advanced quantitative evaluation of the CEUS data, two commercial software programmes, Qontrast® (EC mark nr.0051, class IIA, Bracco, Milan, Italy) and Mindray machine software (UWN+Contrast ImagingTM Quantification Analysis Software) were used respectively at T0 and T1, to design time–intensity curves. In each frame, the entire prostate was used as a single region of interest (ROI), manually defined by drawing a line around the shape of the prostate. The software calculated time–intensity curves on a pixel-by-pixel basis, fitted them to parametric curves, and calculated the following parameters, starting from the moment of injection: perfusion peak intensity (PPI) expressed as a percentage, and Time to Peak (TTP, starting from T = 0) expressed in seconds. Median values and percentile quartiles of the perfusion parameters were then calculated.

The recruited dogs were monitored and observed for at least two hours after the procedure by the clinician in charge of the kennels, and during the following 24 hours by the kennel staff to detect any immediate or delayed reaction to the contrast agent injection (Seiler et al. 2013).

5.2.4 Statistical analysis

Data were recorded using a computerized spreadsheet (Microsoft® Excel® 2021, Redmond, WA, USA) and then imported into Statistical Package for Social Sciences (SPSS IBM® Statistics version 27.0, IBM Corporation, Armonk, NY, USA) for statistical analysis. Non-parametric tests were used for evaluation. Post hoc analysis with Wilcoxon's signed-rank test was conducted to compare individual changes in terms of prostate volume, PPI and TTP between the two timepoints. Differences were considered statistically significant when $p < 0.05$.

5.3 Results

No physical or ultrasonographic abnormalities and no side-effects or anaphylactic reactions related to the CEUS examination were found in any of the ten patients. All prostate glands appeared as an ellipsoid shaped gland, with smooth margins and a hypoechoic homogenous parenchyma. The urethra was visible as a linear or circular hypoechoic structure on longitudinal or transverse view, respectively, in all dogs (Figure 5.1).

a) 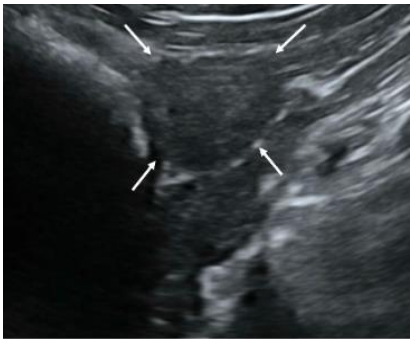 b) 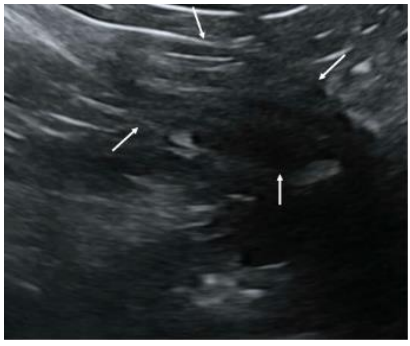

Fig. 5. 1 B-mode ultrasound of the prostate gland in transverse (a) and longitudinal view (b). The prostate gland appears as a hypoechoic spheroidal (a) or ellipsoid (b) structure, with smooth margins and homogeneous parenchyma.

No visible changes in the prostatic parenchyma were found in terms of echogenicity and echotexture between T0 and T1. A minimal prostate volume reduction was detected ($p = 0.005$), with a mean prostate volume at T1 of 7.52 cm^3 ± 0.44 and an average reduction in volume of 0.23 cm^3 (Figure 5.2).

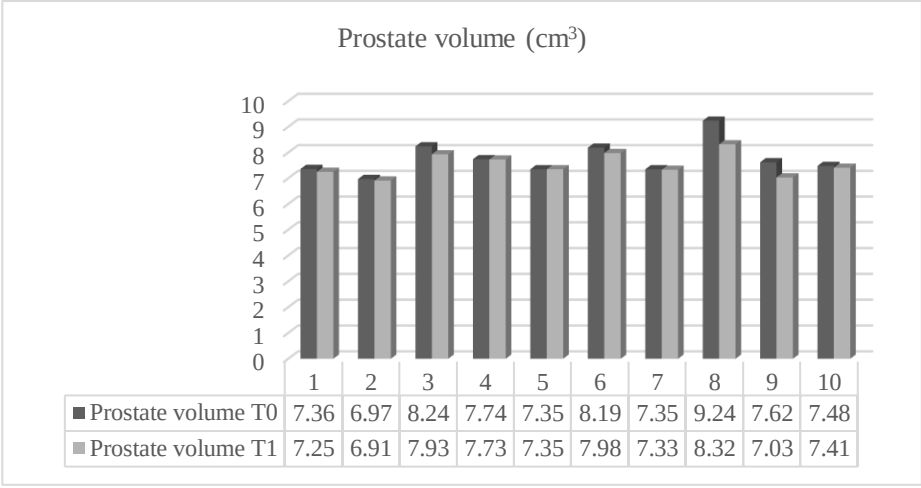

	1	2	3	4	5	6	7	8	9	10
Prostate volume T0	7.36	6.97	8.24	7.74	7.35	8.19	7.35	9.24	7.62	7.48
Prostate volume T1	7.25	6.91	7.93	7.73	7.35	7.98	7.33	8.32	7.03	7.41

Fig. 5. 2 Prostate volume comparison for 10 individual dogs imaged after at least 3 months elapsed since castration (T0) and six years later (T1).

Color doppler ultrasound did not allow the detection of prostatic vascular flow in any of the patients at T0 and T1. CEUS of the prostate was able to reveal the gland vascularization in all dogs. No differences were subjectively observed in the way the contrast agent enhanced the gland between the two timepoints. The contrast agent firstly enhanced the signal of prostatic artery branches, which advance into the prostatic capsule and branched homogeneously into many small parenchymal arteries directed medially towards the urethra. In the wash-out phase, the parenchyma lost the enhancement pattern homogeneously. At T1 the prostate appeared less enhanced and brilliant when compared to T0 and contrast agent perfusion resulted to be slower and less homogeneous (Figure 5.3).

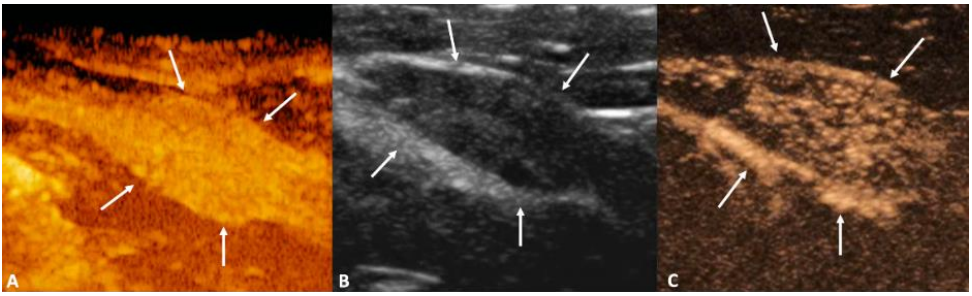

Fig. 5. 3 CEUS of the prostate gland (white arrows) at the peak enhancement performed at T0 (a) and T1 (b and c). At T1 the prostate gland resulted to be less homogeneous and characterized by a reduced contrast intensity when compared to T0 by using CEUS.

Quantitative analysis revealed that PPI significantly reduced (p=0.005), while TTP significantly increased (p=0.005) from T0 to T1 in all dogs. Contrast parameters comparisons are represented in the graphs (Figure 5.4).

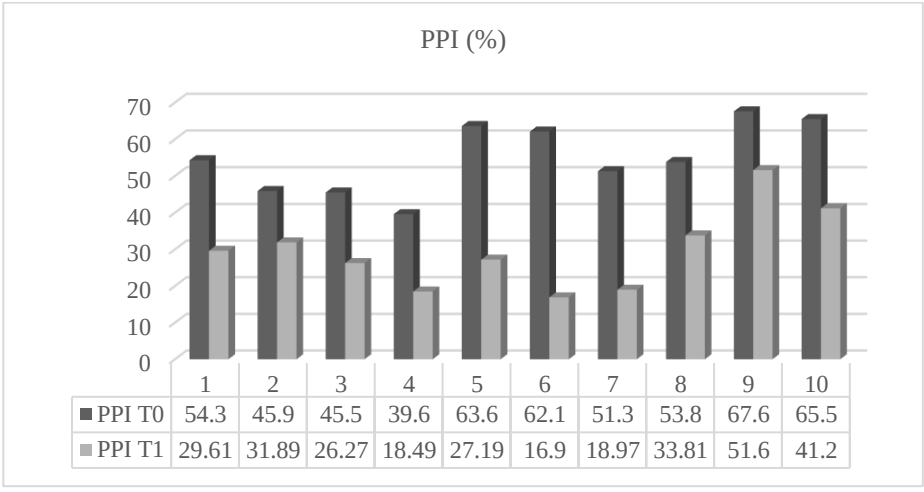

	1	2	3	4	5	6	7	8	9	10
PPI T0	54.3	45.9	45.5	39.6	63.6	62.1	51.3	53.8	67.6	65.5
PPI T1	29.61	31.89	26.27	18.49	27.19	16.9	18.97	33.81	51.6	41.2

a)

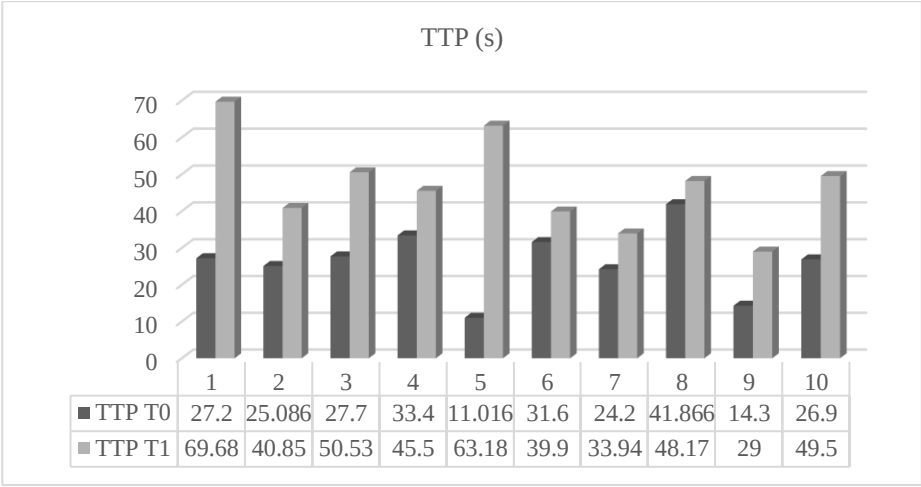

	1	2	3	4	5	6	7	8	9	10
TTP T0	27.2	25.086	27.7	33.4	11.016	31.6	24.2	41.866	14.3	26.9
TTP T1	69.68	40.85	50.53	45.5	63.18	39.9	33.94	48.17	29	49.5

b)

Fig. 5. 4 CEUS parameters of Perfusion Peak Intensity (PPI) (a) and Time to Peak (TTP) (b) for 10 individual dogs imaged after at least 3 months elapsed since castration (T0) and six years later (T1).

5.4 Discussion

The preliminary results of the present study suggest that prostatic involution is not a short-term process, and that the regression of prostate vascularization after orchiectomy occurs over a longer time period than expected until now, during which there was also a trend for prostate volume to reduce. To our knowledge this is the first study to analyze long-term prostatic involution using ultrasound in dogs, with previous work only examining the first 90 days after orchiectomy (Angrimani et al. 2020; Cazzuli et al. 2022; Yoon et al. 2020).

Prostatic involution in terms of a reduction in the size of the prostate gland has been described and appears to be triggered by a progressive shrinkage of the prostatic acini with a relative increase of the fibromuscular tissue until only low number of tubules with a single epithelial lining remains (Palmieri et al. 2022). These findings are in accordance with the observed higher collagen fiber density of periurethral and peripheral region of the prostate gland in neutered dogs (Ruetten et al. 2018).

Orchiectomy is considered to be the fastest treatment for benign prostate conditions in dogs with greater rate of involution expected within one week

after surgery (Cunto et al. 2022; Cazzuli et al. 2022). Although a significant reduction in prostate volume was detected in the present study, the average percentage of volume regression was only 2.8 %, which represents a minimal reduction in terms of gland size. However, dogs were an average of 21 months from surgery at the time of first examination and were then re-examined six years later. Interestingly, one dog did show almost no size reduction after the previous examination. The present results are not in contrast with the findings by Yoon and colleagues and Cazzulli and colleagues, on the timing of regression of the prostate gland, where a remarkable regression in the first 7-15 days after orchiectomy, followed by a decrease in the involution rate, with minimum percent volume loss recorded between 60 and 90 days was described (Cazzuli et al. 2022; Yoon et al. 2020). We hypothesize that prostate size involution slows remarkably after 3 months from the orchiectomy, until minimal percentage of volume reduction is reached. Since in our study examination at only two time points was possible and the time lapse between T0 and T1 was six years, we cannot outline further the regression during specific time intervals. In the present study, we decided to consider just prostate volume (rather than individual linear measurements of the prostate gland) as we believe that volume represents a good way to assess the overall dimensions of the prostate gland, even though many variables are considered within the calculation (Bosma et al. 2022; Atalan et al. 1999), because of the clinical relevance. The prostate volume results of 7.52 cm^3 ± 0.44 are in line with previous findings from other studies (Yoon et al. 2020; Spada et al. 2021).

Although recent studies have reported that prostatomegaly may not be the only parameter needed in the diagnosis of prostatic malignancies (Bradbury et al. 2009), a baseline for mean dimensions in neutered dogs remains important in terms for early detection of prostate changes.

Since parenchymal changes are considered not to be sensitive enough for the detection of prostatic neoplasia, the assessment of vascular blood supply abnormalities of the gland has the potential to be helpful for an early diagnosis (Russo et al. 2012; Vignoli et al. 2011). However, it has been taken into account that prostate gland vascularization is strongly influenced to neuter status and hormonal activity. Several studies have investigated vascular parenchymal changes during benign and malignant conditions in intact dogs (Angrimani et al. 2020; Vignoli et al. 2011; Troisi et al. 2015; Lima et al. 2021; Zelli et al. 2013) and after neutering (Angrimani et al. 2020; Yoon et al. 2020; Spada et al. 2021).

CEUS has been successfully applied to the prostate gland in neutered dogs to describe prostate enhancement and perfusion, reporting differences between intact and neutered dogs in a sample population (Spada et al. 2021). The present study showed similar perfusion characteristics detected in the previous studies conducted on prostate gland in castrated dogs (Yoon et al. 2020; Spada et al. 2021). CEUS was able to detect vascularization in the present groups unlike Color Doppler. However, it is still not known if this technique could be useful being used alone or with biopsy for the early detection of prostate malignancies, as evaluated in other studies in human medicine (Liu et al. 2020; Postema et al. 2017; Salib et al. 2022). A high variability in terms of perfusion measurements was detected within all studies focused on canine prostate evaluation using CEUS. Such variability may of course reflect procedural errors, or a divergence in terms of vascular blood supply among individuals which may vary at different times after orchiectomy, different age or breeds. Therefore, it is crucial to assess how prostate vascularization usually changes after castration. To the best of our knowledge, this is the first study to report long-term regression of prostatic vascularization in dogs, which appears to last longer than expected. Lower PPI values are associated with a decreased vessel number and to an overall reduction in blood perfusion. On the other hand, an increase in TTP may be related to reduced number of vessels branching off the prostate gland, which slow down blood flow and indirectly the contrast agent in enhancing the prostate gland. In the present study, marked PPI decrease and TTP increase was observed in all dogs. The results of the present study support the findings from Yoon and colleagues, who reported an evident decrease in vascular blood flow only 60 days after castration by using CEUS, way longer than the size involution process (Yoon et al. 2020). However, the difference in terms of regression rate between volume and vascular blood supply has not been clarified yet. Orchiectomy results in an abrupt decrease in testosterone and dihydrotestosterone serum concentration, which normally act as the main stimulus for prostate physiology and cell proliferation. Decreased hormone concentration is followed rapidly by a significant prostate volume loss (Shidaifat et al. 2007; Lima et al. 2021). However, a decrease in androgens may also be one of the most important causes for a reduction in blood perfusion, which is believed to be the main factor affecting cell proliferation after castration (Shidaifat et al. 2007). Recent studies reported that reduced dihydrotestosterone concentrations lead to lower VEGF-A (Vascular endothelial growth factor-A) expression

and thus definitely inhibiting neo-vascularization (Angrimani et al. 2020). However, the difference in timing between morphological and vascularization involution may suggest that apoptotic processes occurring to vascular endothelial cells after castration may not be the main cause for cell proliferation arrest (Yoon et al. 2020). Another reason could be that pre-acinar capillaries in the parenchymal zone may be the first vessels to involute, determining a severe reduction in terms of prostate epithelial cells nutrition and consequent apoptosis. The small size of the pre-acinar capillaries (with diameters of 5–7 µm and the endothelial layer thickness of 0.2 µm (Sun et al. 2017)) may explain why androgen deprivation effects on parenchymal perfusion enhancement may not be seen soon after orchiectomy and may need more time to be detected. It remains open, to which extent the changes documented in this study are caused by neutering and the loss of sexual steroids. Potentially, the regression of prostatic volume and vascularization may partly be dependent on age related changes. Therefore, further studies should investigate if similar changes may also be found in non-neutered male dogs. Even though a wide time lapse was considered for the present preliminary study, using just two moments and evaluations could have limited our information. Further studies involving more examinations, on a yearly basis, could be helpful to get more insights into the dynamics of prostate regression.

5.5 Conclusion

The present preliminary study provided new insights and information about prostate gland physiology and involution after orchiectomy. The present findings could be used as a baseline in clinical practice for the assessment and differentiation between normal and abnormal prostate parenchyma and vascularization in the surgically neutered dog.

5.6 References

Angrimani DSR, Francischini MCP, Brito MM, Vannucchi CI. Prostatic hyperplasia: Vascularization, hemodynamic and hormonal analysis of dogs treated with finasteride or orchiectomy. PLoS One 2020;15:e0234714. https://doi.org/10.1371/journal.pone.0234714.

Atalan G, Holt PE, Barr FJ. Ultrasonographic estimation of prostate size in normal dogs and relationship to bodyweight and age. Journal of Small Animal Practice 1999;40. https://doi.org/10.1111/j.1748-5827.1999.tb03052.x.

Bosma F, Wijsman S, Huygens S, Passon-Vastenburg M. Ultrasonographic measurements of the prostate gland in castrated adult dogs. Acta Vet Scand 2022;64. https://doi.org/10.1186/s13028-022-00634-1.

Bradbury CA, Westropp JL, Pollard RE. Relationship between prostatomegaly, prostatic mineralization, and cytologic diagnosis. Veterinary Radiology and Ultrasound 2009;50:167–71. https://doi.org/10.1111/j.1740-8261.2009.01510.x.

Bryan JN, Keeler MR, Henry CJ, Bryan ME, Hahn AW, Caldwell CW. A population study of neutering status as a risk factor for canine prostate cancer. Prostate 2007;67:1174–81. https://doi.org/10.1002/pros.20590.

Cazzuli G, Damián JP, Molina E, Pessina P. Post-castration prostatic involution: A morphometric and endocrine study of healthy canines and those with benign prostatic hyperplasia. Reproduction in Domestic Animals 2022;57. https://doi.org/10.1111/rda.14036.

Citi S, Oranges M, Arrighi E, Meucci V, Della Santa D, Tommaso M. Sonographic Evaluation of Medial Iliac Lymph Nodes-to-Aorta Ratio in Dogs. Vet Sci 2020;7. https://doi.org/10.3390/vetsci7010022.

Cunto M, Ballotta G, Zambelli D. Benign prostatic hyperplasia in the dog. Anim Reprod Sci 2022;247. https://doi.org/10.1016/j.anireprosci.2022.107096.

de Souza MB, Silva LDM da, Moxon R, Russo M, England GCW. Ultrasonography of the prostate gland and testes in dogs. In Pract 2017;39:21–32. https://doi.org/10.1136/inp.i6054.

Dietrich CF, Averkiou M, Nielsen MB, Barr RG, Burns PN, Calliada F, et al. How to perform Contrast-Enhanced Ultrasound (CEUS). Ultrasound Int Open 2018;4:E2–15. https://doi.org/10.1055/s-0043-123931.

Johnston SD, Kamolpatana K, Root-Kustritz MV, Johnston GR. Prostatic disorders in the dog. Anim Reprod Sci 2000;60–61. https://doi.org/10.1016/S0378-4320(00)00101-9.

References

Lima CB, Angrimani DSR, Flores RB, Vannucchi CI. Endocrine, prostatic vascular, and proapoptotic changes in dogs with benign prostatic hyperplasia treated medically or surgically. Domest Anim Endocrinol 2021;75:106601. https://doi.org/10.1016/j.domaniend.2020.106601.

Liu G, Wu S, Huang L. Contrast-enhanced ultrasound evaluation of the prostate before transrectal ultrasound-guided biopsy can improve diagnostic sensitivity. Medicine 2020;99:e19946. https://doi.org/10.1097/MD.0000000000019946.

Mattoon JS, Nyland TG. Prostate and Testes. In: Mattoon JS, Nyland TG, editors. Small animal diagnostic ultrasound . 3rd ed., St. Louis, MO, USA: Saunders; 2015, p. 608–33.

Mayer MN, Lawson JA, Silver TI. Sonographic characteristics of presumptively normal canine medial iliac and superficial inguinal lymph nodes. Veterinary Radiology & Ultrasound 2010;51. https://doi.org/10.1111/j.1740-8261.2010.01710.x.

Nogueira Aires LP, Gasser B, Silva P, Del'Aguila-Silva P, Yamada DI, Carneiro RK, et al. Ovarian contrast-enhanced ultrasonography and Doppler fluxometry in bitches during the postovulatory estrus and corpora lutea formation. Theriogenology 2022;194:162–70. https://doi.org/10.1016/j.theriogenology.2022.10.009.

Palmieri C, Fonseca-Alves CE, Laufer-Amorim R. A Review on Canine and Feline Prostate Pathology. Front Vet Sci 2022;9. https://doi.org/10.3389/fvets.2022.881232.

Postema AW, Scheltema MJ V., Mannaerts CK, Van Sloun RJG, Idzenga T, Mischi M, et al. The prostate cancer detection rates of CEUS-targeted versus MRI-targeted versus systematic TRUS-guided biopsies in biopsy-naïve men: a prospective, comparative clinical trial using the same patients. BMC Urol 2017;17:27. https://doi.org/10.1186/s12894-017-0213-7.

Reichler I. Gonadectomy in Cats and Dogs: A Review of Risks and Benefits. Reproduction in Domestic Animals 2009;44:29–35. https://doi.org/10.1111/j.1439-0531.2009.01437.x.

Ruetten H, Wegner KA, Romero MF, Wood MW, Marker PC, Strand D, et al. Prostatic collagen architecture in neutered and intact canines. Prostate 2018;78:839–48. https://doi.org/10.1002/pros.23641.

Russo M, Vignoli M, Catone G, Rossi F, Attanasi G, England GCW. Prostatic perfusion in the dog using contrast-enhanced doppler ultrasound. Reproduction in Domestic Animals, vol. 44, 2009, p. 334–5. https://doi.org/10.1111/j.1439-0531.2009.01442.x.

References

Russo M, Vignoli M, England GCW. B-mode and contrast-enhanced ultrasonographic findings in canine prostatic disorders. Reproduction in Domestic Animals 2012;47:238–42. https://doi.org/10.1111/rda.12059.

Salib A, Halpern E, Eisenbrey J, Chandrasekar T, Chung PH, Forsberg F, et al. The evolving role of contrast-enhanced ultrasound in urology: a review. World J Urol 2022;41:673–8. https://doi.org/10.1007/s00345-022-04088-y.

Schrank M, Romagnoli S. Prostatic neoplasia in the intact and castrated dog: How dangerous is castration? Animals 2020;10. https://doi.org/10.3390/ani10010085.

Seiler GS, Brown JC, Reetz JA, Taeymans O, Bucknoff M, Rossi F, et al. Safety of contrast-enhanced ultrasonography in dogs and cats: 488 cases (2002–2011). J Am Vet Med Assoc 2013;242. https://doi.org/10.2460/javma.242.9.1255.

Shidaifat F, Gharaibeh M, Bani-Ismail Z. Effect of Castration on Extracellular Matrix Remodeling and Angiogenesis of the Prostate Gland. Endocr J 2007;54:521–9. https://doi.org/10.1507/endocrj.K07-009.

Sirinarumitr K, Johnston SD, Kustritz MVR, Johnston GR, Sarkar DK, Memon MA. Effects of finasteride on size of the prostate gland and semen quality in dogs with benign prostatic hypertrophy. J Am Vet Med Assoc 2001;218. https://doi.org/10.2460/javma.2001.218.1275.

Smith J. Canine prostatic disease: A review of anatomy, pathology, diagnosis, and treatment. Theriogenology 2008;70:375–83. https://doi.org/10.1016/j.theriogenology.2008.04.039.

Spada S, England GCW, Vignoli M, Carluccio A, Russo M. Contrast-Enhanced Ultrasound Imaging of Prostate Gland in Neutered Dogs. Animals 2021;11. https://doi.org/10.3390/ani11020559.

Sun F, Báez-Díaz C, Sánchez-Margallo FM. Canine prostate models in preclinical studies of minimally invasive interventions: part I, canine prostate anatomy and prostate cancer models. Transl Androl Urol 2017;6:538–46. https://doi.org/10.21037/tau.2017.03.61.

Teske E, Naan EC, van Dijk EM, Van Garderen E, Schalken JA. Canine prostate carcinoma: epidemiological evidence of an increased risk in castrated dogs. Mol Cell Endocrinol 2002;197. https://doi.org/10.1016/S0303-7207(02)00261-7.

Troisi A, Orlandi R, Bargellini P, Menchetti L, Borges P, Zelli R, et al. Contrast-enhanced ultrasonographic characteristics of the diseased

References

canine prostate gland. Theriogenology 2015;84. https://doi.org/10.1016/j.theriogenology.2015.07.029.

Vignoli M, Russo M, Catone G, Rossi F, Attanasi G, Terragni R, et al. Assessment of Vascular Perfusion Kinetics Using Contrast-enhanced Ultrasound for the Diagnosis of Prostatic Disease in Dogs. Reproduction in Domestic Animals 2011;46:209–13. https://doi.org/10.1111/j.1439-0531.2010.01629.x.

Yoon S, Alfajaro MM, Cho K-O, Choi U-S, Je H, Jung J, et al. Perfusion change in benign prostatic hyperplasia before and after castration in a canine model: Contrast enhanced ultrasonography and CT perfusion study. Theriogenology 2020;156:97–106. https://doi.org/10.1016/j.theriogenology.2020.06.026.

Zelli R, Orlandi R, Troisi A, Cardinali L, Polisca A. Power and Pulsed Doppler Evaluation of Prostatic Artery Blood Flow in Normal and Benign Prostatic Hyperplasia-Affected Dogs. Reproduction in Domestic Animals 2013;48:768–73. https://doi.org/10.1111/rda.12159.

Chapter 6

Contrast-enhanced ultrasound evaluation of placental perfusion in brachicephalic bitches

Silva P, Maronezi MC, Padilha-Nakaghi LC, Gasser B, Pavan L, Nogueira Aires LP, Russo M, Spada S, Ramirez Uscategui RA, Moraes PC, Rossi Feliciano MA. Contrast-enhanced ultrasound evaluation of placental perfusion in brachicephalic bitches. Theriogenology. 2021 Oct 1;173:230-240. doi: 10.1016/j.theriogenology.2021.08.010. Epub 2021 Aug 10. PMID: 34399387.

6.1 Introduction

One of the primary stages of canine pregnancy is implantation, during which the blastocyst attaches to the uterine wall and the trophoblastic cells migrate inside the endometrium, allowing the development of embryonic tissues and a vascular suply (Paulson & Comizzoli, 2021). The thinning of the muscle layer makes the vessels more developed, creating connections with low vascular resistance (Lin et al. 1995), and consequently, low pressure (Longo, 1983). This generates an established placental uterine vascular bed which gradually grows during pregnancy (Nautrup, 1998; Di Salvo et al. 2006; Blanco et al. 2009).

The structural changes and biochemical alterations that occur during the gestational period trigger a morphophysiological modification of the cardiovascular system with a progressive increase in cardiac output to meet the growing metabolic demands of the maternal-embryonic/fetal unit (Almeida et al. 2017). The association of hemodynamic changes leads to adequate perfusion through the vascular uteroplacental interphase, consisting of the spiral arteries, which spread according to the gestational development but progressively reduce their vascular resistance to conform to the growth of the embryonic and fetal tissues (Di Salvo et al. 2006).

Doppler is an ultrasound imaging technique that favors the identification of most of the hemodynamic changes in pregnant bitches (Di Salvo et al. 2006; Blanco et al. 2009; Almeida et al. 2017). Estimation of dopplerfluxometric indices of the placental vessels allows non-invasive assessment of arterial blood flow and peripheral vascular resistance. The calculated parameters may indicate a progressive increase in placental blood flow resulting from vessel diameter development and reduction in their resistance and permit a correlation with the histopathological examination of the spiral arteries (Di Salvo et al. 2006). With these precepts, dopplerfluxometric assessment of placental and/or fetal structures allows monitoring of gestational process development, helping to predict the timing of delivery, infer fetal distress, identify fetal development abnormalities, and provide tools for more accurate clinical pregnancy monitoring (Divon & Ferber, 2001; Harman & Baschat, 2003; Giannico et al. 2016).

Despite the excellent applicability of Doppler ultrasound, innovative ultrasonographic techniques have been used in the study of tissue vascularization such as contrast-enhanced ultrasound (CEUS). CEUS allows a more accurate examination of tissue hemodynamics, improving the

visualization of microcirculation and qualitative and quantitative assessment of perfusion (Cosgrove, 2006; Bargellini et al. 2018). This technique has been shown to be safe for the hemodynamic evaluation of the maternal-fetal binome in primates, horses, rodents, and canines (Zhou et al. 2013; Roberts et al. 2016; Freccero et al. 2017; Orlandi et al. 2019), considering that pregnant animals were enrolled as experimental models appropriate for future application in pregnant women (Roberts & Frias, 2020).

In particular, a recent study investigated CEUS application for the evaluation of placental perfusion dynamics in the first and second third of physiological pregnancy in nine bitches (Orlandi et al. 2019). In addition to ascertaining the apparent safety of the technique, the authors identified placental perfusion without diffusion of contrast agent into the embryonic or fetal tissues and detected no significant changes in quantitative variables of perfusion during the first 45 days of gestation but recommended further studies with a larger number of bitches at different pregnancy stages.

Recent studies in non-human primates have demonstrated the importance of CEUS in the in vivo detection of placental dysfunction associated with protein restriction in the diet (Roberts et al. 2018), chronic intake of high-fat diets (Kuo et al. 2019; Salati et al. 2019), and in Zika-virus-infected non-human primates (Hirsch et al. 2018) as confirmed by reduction of placental blood perfusion rates. This potential of CEUS in detecting abnormalities in placental function may allow for early medical intervention to improve prenatal management and obtain healthy offspring, thus promoting the creation of more complete studies on placental dysfunction in various species. To our knowledge, no studies have described the applicability of CEUS for placental assessment of hydrops or abnormalities in bitches, mainly in brachycephalics, which are animals with a high prevalence of gestational abnormalities (Hopper et al. 2004).

It is possible to infer that physiological changes in vascular resistance play a crucial role in providing adequate placental blood flow in pregnancy and that Doppler imaging is an efficient ultrasonographic technique for the evaluation of these hemodynamic changes. However, there is insufficient evidence of the ability of CEUS examination to distinguish pregnancy-related changes in placental blood flow and the to detect gestational abnormalities in bitches. Therefore, the study of physiological and pathological pregnancy hemodynamics in brachycephalic bitches using Doppler and CEUS techniques at different stages of this process can be considered relevant. The aim of the study was to assess qualitative and

quantitative perfusion parameters for fetuses of healthy brachycephalic bitches as well as evaluate placental vascularization and perfusion in bitches with fetal abnormalities identified shortly before birth. The goal is to provide data to allow early detection of gestational anomalies related to placental dysfunction as well as promote studies on perfusion and kinetics during pregnancy in other species.

6.2 Materials and methods

This study was conducted with the approval of the Ethics Committee on the Use of Animals (CEUA) of the Faculty of Agricultural and Veterinary Sciences, Unesp/Jaboticabal (003074/19). Twenty two females of brachycephalic breeds, weighing 11.3 ± 1.6 kg, with an average age of 2.7 ± 1.0 years were enrolled in the study as healthy canine females, without gestational changes (n = 22,which, 19 French Bulldogs and 3 Pugs), considered healthy, based on the absence of physical, hematological, blood biochemical, and ultrasonographic abnormalities during pregnancy; and eighth brachycephalic patients presenting gestational abnormalities detected in the last gestational week and belonging to the routine patient group of the Veterinary Hospital (n = 8, which, 1 French Bulldog and 7 English Bulldogs, weighed 24.4 ± 2.4 (18.8–32.2) kg).

The owners of the animals, who are professional breeders with whom cooperation agreements are in place, allowed their bitches to participate in this study by signing a consent form. The breeder's staff had been previously trained to recognize signs of proestrus, such as edema and vulvar bleeding. Once bitches exhibited these signs, vaginal cytology was performed daily until 80% of the anucleated superficial cells were found, which is indicative of estrus (Christie et al. 1972; Socha et al. 2012). After this confirmation, serum progesterone concentration (P4) was measured daily using the chemiluminescence immunoassay (CLIA) until detection of ovulation, in which bitches were inseminated using fresh semen. Ovulation was established based in previous studies regarding CLIA and prediction of parturition date (Gloria et al. 2018; Kutzler et al. 2003; Kim et al. 2007), in which, day 0 of gestation was established as the day in that P4 concentration was ≥1.5 ng/mL and on the next day was ≥3.0 ng/mL, whereas ovulation day was considered the day 2 of gestation, in which P4 concentration was ≥4.0 ng/mL. With these precepts, the ultrasound diagnosis of the pregnancy was performed on d ay 25 of gestation since the estimated LH peak using an

ACUSON S2000® device (Siemens, Munich, Germany) and a 9.0 MHz linear probe according to the parameters defined in the literature (Lopate, 2008). With this confirmation, the females were subjected to subsequent examinations.

6.2.1 B-mode and Doppler ultrasound examinations

Ultrasound examination was performed in lateral or dorsal recumbency. However, prior to the beginning of the performance, hair in the abdominal region was clipped and ultrasound gel was applied on the skin. The transducer was placed on the abdominal area and ultrasonographic device parameters (depth, gain, mechanical index, and focus) were adjusted to ensure good image quality. The examinations were performed by a single experienced operator to reduce evaluation time, minimize the stress experienced by the animals, and consistently verify the exams and development of gestation (Socha et al. 2012; Yeager et al. 1992; Simoes et al. 2018; England et al. 1990). During the ultrasonographic evaluation, gestational age was confirmed using the following formulas: less than 40 days: (6 x Gestational Sac Diameter) + 20; more than 40 days: (15 x Biparietal Diameter) + 20) (Yeager et al. 1992; England et al. 1990).
In the group of healthy animals, data were collected on days 25 (M1 - post-implantation), 45 (M2 - fetogenesis), and 58 (M3 - end of pregnancy) of gestation to cover each third of the pregnancy. During the ultrasound evaluations, a complete scan of the pregnancy was performed, but in the two fetuses closest to the ovaries, objective variables of this study were collected, in order to reduce the examination time, perform an evaluation of intrafetal variation and keep the same specimens in each examination. At M3, the litter was more deeply evaluated to detect eventual morphophysiological abnormalities. On the other hand, patients with gestational abnormalities were evaluated only at M3, when were taken for obstetric care.
B-mode ultrasonography was performed to assess fetal development and viability, detect developmental changes, and measure biparietal and abdominal diameters (Feliciano et al. 2015). The pulsed Doppler mode was also used to measure heart rate.
Once the previous evaluations were completed, color Doppler mode was used to locate the umbilical artery (Giannico et al. 2016). After its identification, the spectral Doppler mode was activated. The vascular

sampling cursor was fixed between 2 and 3 mm and placed in the center of the umbilical artery, with care taken to keep the angle between the cursor and the vessel axis greater than 60°.
Flow spectral tracings were evaluated and recorded until quality waves were achieved with as few artifacts as possible. Three flow waves were selected for the electronic measurement of the dopplerfluxometric variables: systolic velocity (SV), diastolic velocity (DV), mean time-averaged minimum velocity (TaMin), mean time-averaged maximum velocity (TaMax), pulsatility index (PI), and resistance index (RI) (Gasser et al. 2020). These evaluations, as well as heart rate measurement, were performed before and immediately after CEUS evaluations described below to detect possible effects of the contrast agent on placental and fetal hemodynamics (Freccero et al. 2017).

6.2.2 Contrast-enhanced ultrasound (CEUS)

After the B-mode and Doppler examinations, CEUS was performed using harmonic imaging software (CADENCE - contrast pulse sequencing technology, Siemens, Munich, Germany) with a mechanical index fixed at 0.09 and a dynamic range of 90. The sonographer framed the placenta and its vasculature of one of two fetuses previously evaluated (whichever is easier to place in the center of the screen) in the center of the screen and manually fixed the transducer to keep it still, in order to carry out only a contrasted study and reduce the chances of complications that this technique could cause. An intravenous bolus of 0.01 mL/kg of contrast medium (sulfur hexafluoride) was administered (SonoVue®, Bracco, São Paulo, Brazil) using a 20-gauge catheter placed in the cephalic vein followed by 5 mL of saline solution (NaCl 0.9%). At the time of injection (T0), the video recording lasted 120 s for further analysis, as described and validated by previous studies (Gasser et al. 2020; Waller et al. 2007; Dong et al. 2013; Choi et al. 2016). During CEUS examination, qualitative evaluation of the images was performed in order to identify uniform filling of placental regions (homogeneous and heterogeneous), hypoperfusion of the areas, and possible changes in pattern enhancement occurring throughout the gestational period. The recorded videos were transferred to an offline analysis module (DICOM® Digital Imaging and Communications in Medicine, Rosslyn, VA, USA) in which two trained and blind evaluators for gestation time initially defined areas of interest, including the largest portion

of the placentation area. The areas were subdivided into five sub-regions of interest (ROI) of approximately 1 mm2 each (Figure 6.1), avoiding the inclusion of large blood vessels identified by the greenish colors in the image.

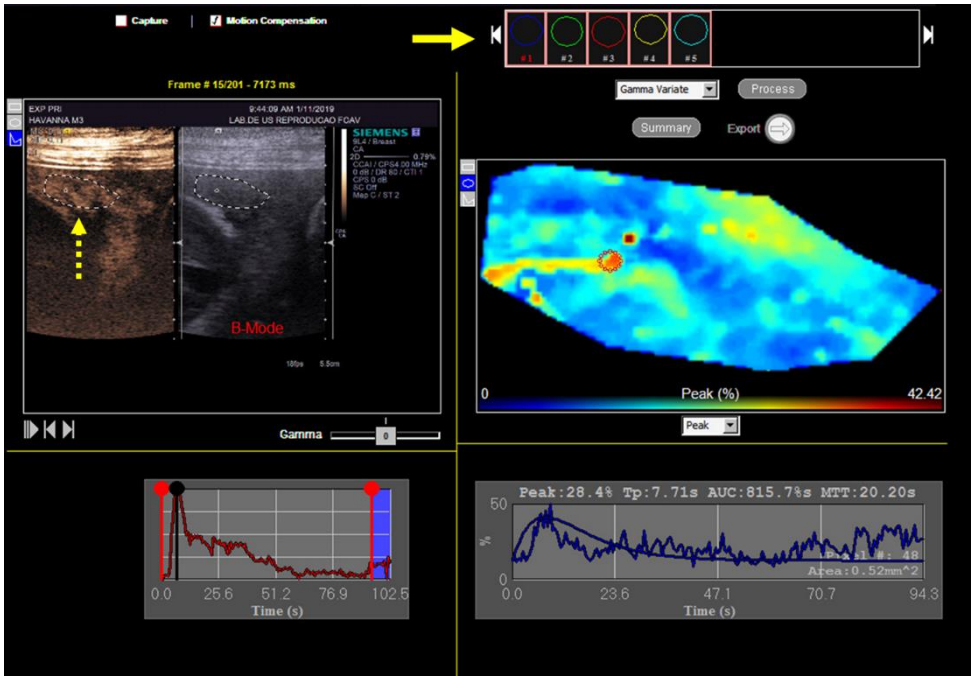

Fig. 6. 1 CEUS examination image of healthy brachycephalic bitch's placental area with quantitative evaluation and regions of interest (ROIS) (continuous arrow) determination already selected in the region of interest of the placenta (dashed arrow) in CADENCE software.

These ROIs were selected randomly to avoid methodological bias. Once the ROIs were defined, the processing software (CADENCE) designed time-intensity curves (TIC) and automatically calculated perfusion parameters: peak contrast intensity (peak in % of pixels), time to peak (Tpeak in s), average transmission time (TmT in s), area under the curve (AUC), and the average number of pixels (pixels) (Figure 6.2).

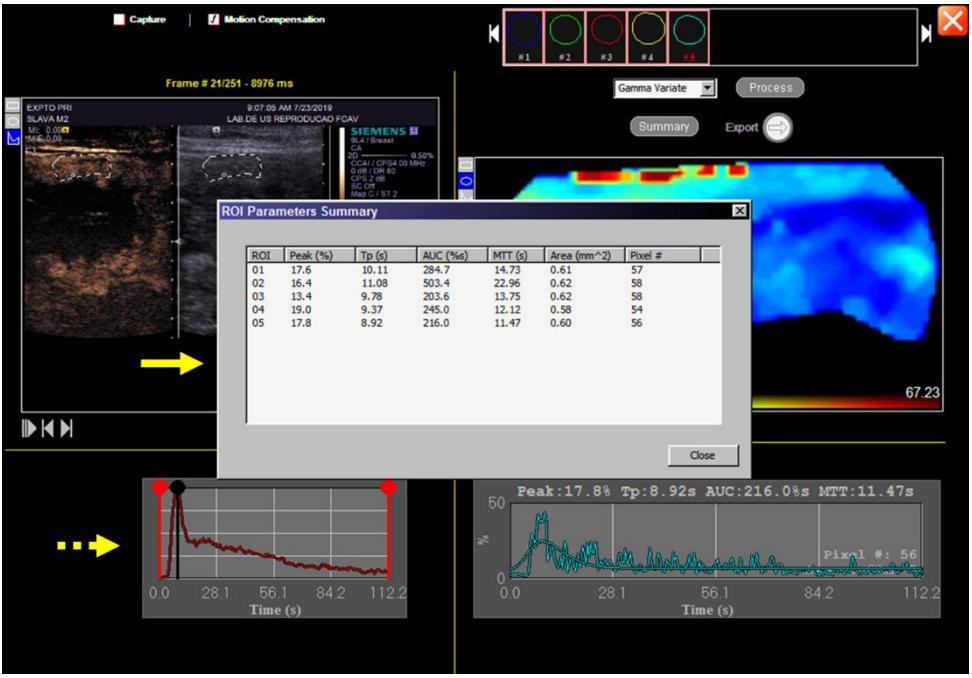

Fig. 6. 2 CEUS examination image of healthy brachycephalic bitch's placental area, with quantitative evaluation of data obtained by graphic microbubbles (continuous arrow) representing contrast input (peak) and output (dashed arrow) in CADENCE software.

6.2.3 Statistical analysis

The results were analyzed using R software (version 3.3.0; R Foundation for Statistical Computing, Austria). The normality of the variables was evaluated by the Shapiro-Wilk test and the homoscedasticity of the variances using the Bartlett test. After proving the supposed mathematics, the variables collected from each structure were compared between the evaluators in the case of CEUS and between the different observations (measured in B-mode in triplicate, the results of the three waves analyzed in Doppler mode, and the five ROIs of CEUS) by the ANOVA test. The difference between them were estimated by the Bland-Altman test, the results obtained in the two fetuses evaluated by the Student's t-test, and the difference between them as estimated by the Bland-Altman test compared. Once the similarities among the observers, observations, and fetuses were proven, the general means of each of the studied variables were calculated

and used for further analysis. Subsequently, these variables were compared among the days of gestation by an analysis of variance (ANOVA) in an entirely randomized and post-test Tukey model. If sufficient data were collected from days 25, 45, and 58, they were also correlated with the days of gestation by a Spearman's test. The resulting data are presented as means ± standard deviations (SD) as well as 95% confidence interval calculations. When fetal/neonatal abnormalities were identified at the time of the M3/process evaluation, the data resulting from the evaluation of these fetuses were identified as abnormal and compared with the data of normal fetuses at the time of M3 using the Mann-Whitney test. If this test was significant, a discriminatory power analysis was performed to identify abnormalities using the ROC curves, the cohort value (CV), sensitivity, specificity, positive predictor value (PPV), negative predictor value (NPV), and accuracy using the logistic regression model.
The significance level was set at 95% ($p < 0.05$) for all tests. For fetuses with abnormalities, the values were arranged in tables, including the means and standard deviation values, and the qualitative findings were described. Due to the limited number of abnormalities, the results were compared descriptively with the normality findings.

6.3 Results

Ultrasound evaluations in B-mode, Doppler, and CEUS were easily performed, and the use of contrast apparently did not cause any intercurrence or detectable side effects in the clinical evaluation of females and neonates delivered through elective cesarean section surgery. Of the 30 animals included in this study, 22 had normal gestational processes, adequate gestational development, and no evident abnormalities. This resulted in 108 healthy puppies, of which 44 were evaluated in this study. Eight of the 30 bitches evaluated presented with fetal abnormalities: six females with fetuses presenting with anasarca and two with hydrocephalus. In the case of fetuses affected by anasarca, thickening of the subcutaneous region due to the accumulation of anechoic content could be detected at the 58th day of pregnancy. Fetuses affected by hydrocephalus were characterized by ventriculomegaly imaged as ventricles full of anechoic content, in addition to the retraction and hyperechogenicity of brain tissue.

6.3.1 Physiological gestation

Regarding the parameters determined by B-mode ultrasound, the AD (abdominal diameter) increased as gestation progressed. At M1, it was 1.13 ± 0.34 cm; at M2, 2.66 ± 0.38 cm; and at M3, 3.72 ± 0.45 cm (P < 0.0001). On the other hand, BPD increased (P < 0.024) from M1 (0.76 ± 0.25 cm) to M2 (2.45 ± 2.21 cm) and remained similar (P>0.05) at M3 (2.48 ± 0.16 cm). The fetal heart rate was similar (P > 0.05) at M1 (226 ± 14 bpm) and M2 (231 ± 10 bpm), decreasing thereafter (P = 0.01) at M3 (218 ± 17 bpm).
The values of the variables evaluated by Doppler fluxometry of the fetal umbilical artery are presented in Table 6.1. These variables were measurable only at moments M2 and M3. The variables SV, DV, TaMax, and TaMin showed a significant increase from M2 to M3 (P > 0.05), while the PI and RI values decreased from M2 to M3 (P > 0.05).

Tab. 6. 1 Mean ± SD of quantitative variables evaluated in the umbilical cord by pulsed Doppler mode in 44 fetuses in different thirds of the gestation of 22 brachycephalic bitches.

Variable	Moment (days)	Average ± SD	P-value	CI 95%
SV (cm/s)	45	61.7 ± 20.3	0.0332*	53-71
	58	77.6 ± 26.9		66-90
DV (cm/s)	45	10.2 ± 4.28	0.0010*	8-12
	58	17.1 ± 8.21		14-21
TaMAX (cm/s)	45	27.9 ± 8.70	0.0142*	24-32
	58	36.7 ± 13.1		31-42
TaMIN (cm/s)	45	13.4 ± 4.59	0.0056*	11-15
	58	18.7 ± 6.84		16-22
	58	1.73 ± 0.25		1.6-1.8
RI	45	0.841 ± 0.41	0.0014*	0.82-0.86
	58	0.79 ± 0.34		0.78-0.81

cm/s, centimeters/second; SD, standard deviation; SV, systolic velocity; DV, diastolic velocity; TaMin, time-averaged minimum velocity; TaMax, time-averaged maximum velocity; PI, pulsatility index; RI, vascular resistance index. ∗Considered statistically significant by Student's t-test ($p \leq 0.05$).

Table 6.2 describes the values of the dopplerfluxometric variables evaluated before and after the application of the contrast medium. When comparing these two moments, no significant changes were observed in M2 or M3 (P>0.05), except for PI, which showed a higher value after contrast administration (P < 0.01; Figure 6.3).

Tab. 6. 2 Mean ± SD of quantitative variables evaluated in the umbilical cord by pulsed Doppler mode before and after the use of microbubble contrast in 44 fetuses evaluated at 45 and 58 days of gestation of 22 brachycephalic bitches.

Variable	Before Average ± SD	After Average ± SD	Bias	SD-Bias
SV (cm/s)	70.1 ± 25.3	73.0 ± 22.1	2.43	13.07
DV (cm/s)	14.0 ± 7.31	13.4 ± 5.32	-0.84	5.39
TaMAX (cm/s)	32.3 ± 12.0	33.1 ± 10.0	0.06	6.80
TaMIN (cm/s)	16.2 ± 6.30	16.1 ± 5.21	0.02	3.55
PI	1.83 ± 0.24	1.92 ± 0.31	0.11	0.28
RI	1.10 ± 1.80	0.83 ± 0.06	-0.01	0.05

cm/s, centimeters/second; SD, standard deviation; SV, systolic velocity; DV, diastolic velocity; TaMin, time-averaged minimum velocity; TaMax, time-averaged maximum velocity; PI, pulsatility index; RI, vascular resistance index. Bias: systematic deviation from the actual value ∗Statistically significant by Student's t-test ($p \leq 0.05$).

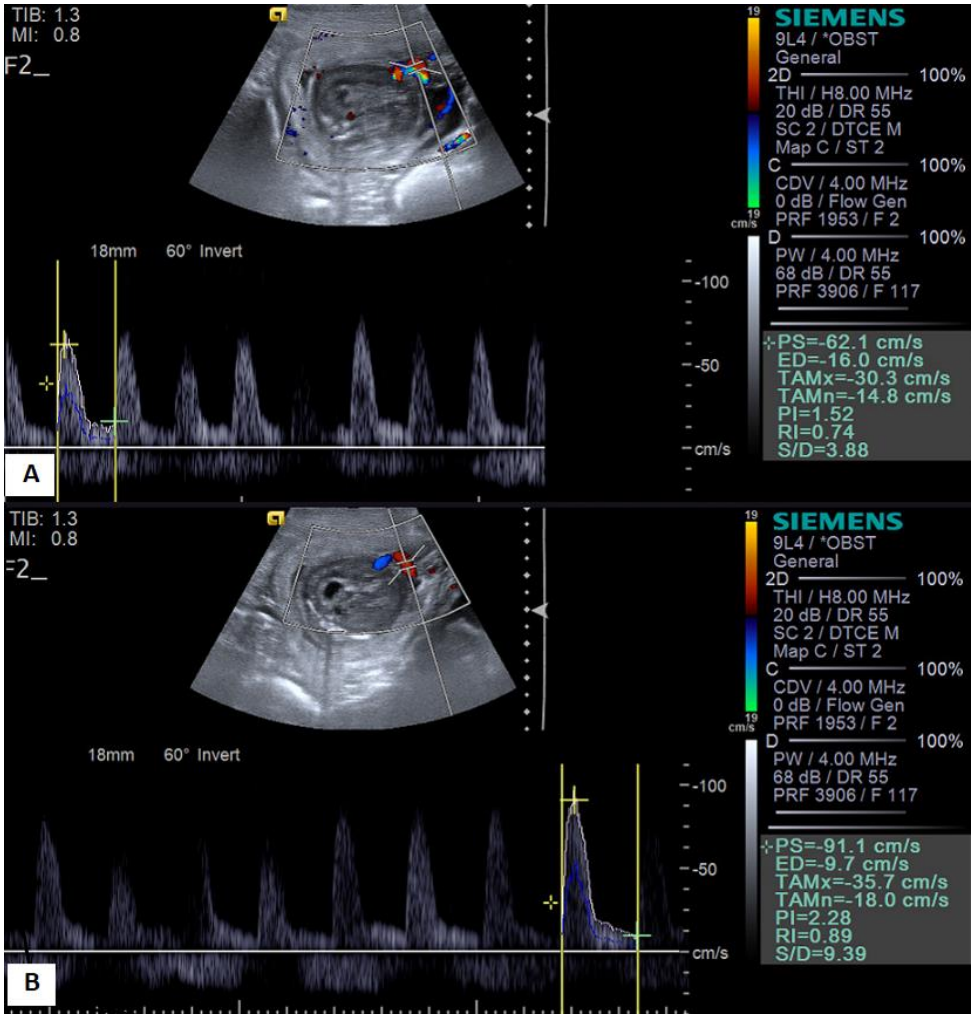

Fig. 6. 3 Pulsed Doppler ultrasound image, showing the dopplerfluxometric indices of the fetal umbilical cord at 45 days of gestation (M2) in a brachycephalic bitch, before (a) and after (b) the use of CEUS contrast. It is possible to observe an increase in the pulsatility index (PI).

The variables evaluated at CEUS always remained constant, that is, there was no significant variation in the values of Peak, Tpeak, TmT, and AUC in Pixels at moments M1, M2, and M3 ($P < 0.05$) as shown in Table 3. Qualitative evaluation showed centripetal perfusion of the placenta, with contrast agent enhancing the uterine vessels during the wash-in phase and

spreading from the periphery to the center of the organ then decreasing during the wash-out phase in a consistently homogeneous manner. Regardless of the gestational period, the contrast agent was distributed homogeneously around the embryonic vesicle wall and in the placenta but did not enhance the embryonic/fetal tissues (Fig. 4). The number of fetuses at the moment of the evaluation did not seem to influence the enhancement pattern of the contrast agent (Fig. 5).

Tab. 6. 3 Average ± SD of quantitative variables evaluated by the contrast-enhanced ultrasonography (CEUS) software in a fetus of each pregnant brachycephalic bitch in different thirds of gestation (n).

Variable	Moment (days)	N	Average ± SD	P-value
SV (cm/s)	25	20	20.7 ± 6.97	0.3210
	45	18	21.7 ± 5.83	
	58	16	23.8 ± 5.64	
DV (cm/s)	25	20	17.0 ± 5.51	0.4622
	45	21	14.5 ± 5.13	
	58	21	15.1 ± 8.52	
TaMAX (cm/s)	25	20	30.3 ± 9.46	0.7444
	45	21	32.9 ± 15.1	
	58	21	32.9 ± 11.9	
TaMIN (cm/s)	25	20	813 ± 500	0.9276
	45	18	840 ± 416	
	58	16	872 ± 422	
RI	25	20	78.5 ± 24.8	0.7651
	45	18	72.2 ± 43.6	
	58	16	71.5 ± 23.5	

%: percentage, s: seconds, %s: percentage per second, SD: standard deviation, F: fetus, Fpeak: intensity peak in pixels, Ftp: time to intensity peak in seconds, Fmtt: average transmission time, AUC: area under the curve, Fpixels: inclination of the input curve in pixels. *Considered statistically significant by the t-Student test, ($P \leq 0.05$).

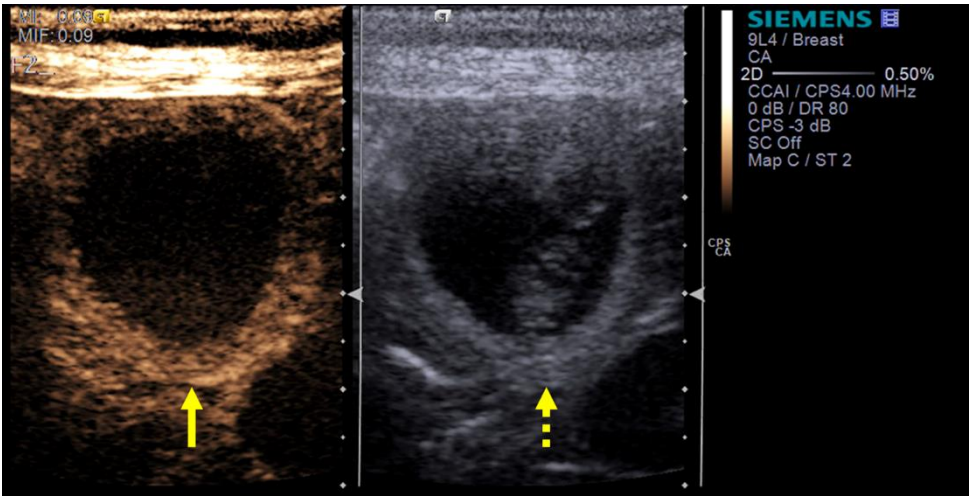

Fig. 6. 4 Ultrasound image demonstrating the application of contrast microbubbles in a highlighted region (arrow) on a 25-day old brachycephalic bitch, while it is possible to visualize the largest placental area (continuous arrow) specific Cadence mode for performing contrast microbubble ultrasonography (dashed arrow) B-mode to facilitate the visualization of the evaluated area.

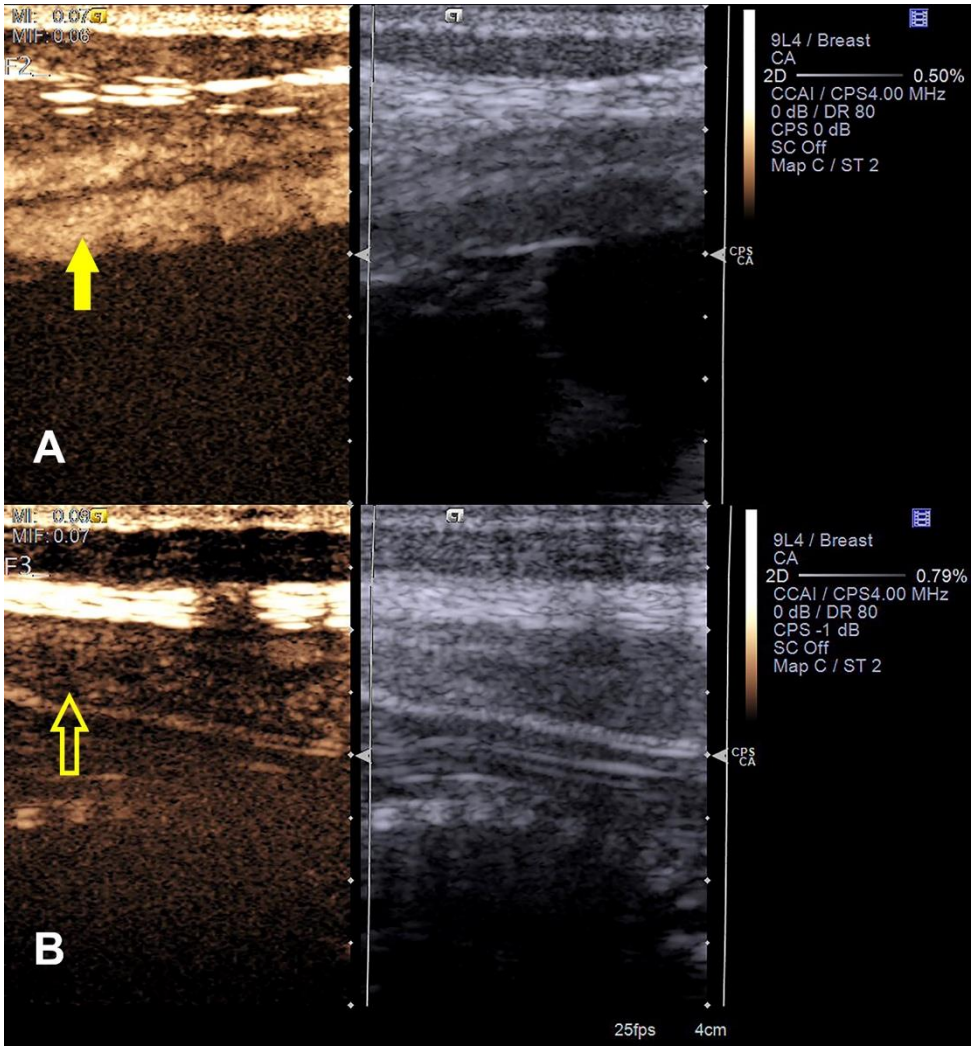

Fig. 6. 5 Ultrasound image demonstrating the peak contrast enhancement of microbubbles in the placental region (arrows) of brachycephalic bitches at 58 days of gestation. In A, a homogeneous and intense filling of the placental tissue (filled arrow) of fetuses without developmental changes is observed. In B, a heterogeneous filling of the tissue is observed with less intensity, with the presence of hypo-echoic areas (empty arrow) in the placental parenchyma of the fetus with developmental alterations.

7.3.2 Gestational abnormalities

Table 4 compares the variables evaluated at M3 in fetuses of physiological pregnancies (n = 44) and in fetuses whose abnormalities were detected near birth, such as hydrocephalus and anasarca (n = 8). In fetuses with abnormalities, contrast filling in the placenta was heterogeneous and with less apparent enhancement, indicating tissue perfusion failure and consequent placental dysfunction. None of the quantitative variables evaluated by B-mode and Doppler showed significant differences (P > 0.05) between normal and abnormal fetus. However, on CEUS evaluation, Tpeak, TmT, and AUC were higher (P < 0.05) in abnormal fetuses when compared to normal fetuses, while Peak and Pixels were similar (P > 0.05). Thus, a Tpeak >14.2 s (CV) indicates fetal abnormalities (anasarca or hydrocephaly) with a sensitivity of 83.3%, a specificity of 71.4%, a PPV of 45.5%, an NPV 93.8%, and an accuracy of 74.1%. A TmT >35.8 s (CV) indicates fetal abnormalities (anasarca or hydrocephalus) with a sensitivity of 83.3%, a specificity of 66.7%, a PPV of 41.7%, an NPV of 93.3%, and an accuracy of 70.4%. An AUC >1099 indicates fetal abnormalities (anasarca or hydrocephalus) with a sensitivity of 83.3%, a specificity of 75.0%, a PPV of 55.6%, an NPV of 92.3%, and an accuracy of 77.3%.

Tab. 6. 4 Median ± IQR (interquartile range) of quantitative variables evaluated by B-mode, Doppler, and Contrast-enhanced (CEUS) ultrasound techniques in fetuses resulting from abnormality-free pregnancies (NF, n = 44) and in fetuses in which abnormalities (hydrocephalus and anasarca) were detected near birth (AF, n = 8), at 58 days of gestation (M3).

Variable	NF	AF	P-Value
AD (cm)	3.76 ± 0.62	3.84 ± 2.36	0.5937
BPD (cm)	2.49 ± 0.58	2.69 ± 0.61	0.4399
HR (bpm)	216 ± 29.0	222 ± 93.0	0.9375
SV (cm/s)	83.4 ± 28.2	69.3 ± 39.4	0.2602
DV (cm/s)	16.1 ± 6.79	14.1 ± 4.47	0.1514
TaMAX (cm/s)	36.6 ± 15.8	32.4 ± 23.1	0.4168
TaMIN (cm/s)	18.1 ± 8.14	17.3 ± 11.8	0.3875
PI	1.80 ± 0.45	1.68 ± 0.29	0.2043

RI	0.80 ± 0.06	0.81 ± 0.08	0.9266
Peak (%)	23.9 ± 6.68	21.8 ± 10.2	0.7114
Tpeak (s)	13.1 ± 6.74	22.0 ± 25.8	0.0181*
TmT (s)	33.0 ± 14.9	40.6 ± 28.5	0.0488
AUC	783 ± 630	1236 ± 342	0.0113*
Pixels	72.0 ± 30.0	91.7 ± 37.8	0.0528

cm/s: centimeters/second, SD: standard deviation, AD: abdominal diameter, HR: heart rate, SV: systolic velocity, DV: diastolic velocity, TaMin: time-averaged minimum velocity, TaMax: time-averaged maximum velocity, PI: pulsatility index, RI: vascular resistance index. %: percentage, s: seconds, %s: percentage per second, SD: standard deviation, F: fetus, Fpeak: peak intensity in pixels, Ftp: time to peak intensity in seconds, Fmtt: average transmission time, AUC: area under the curve, Fpixels: inclination of the input curve in pixels.
*Considered to be statistically significant ($P \leq 0.05$). significant by the t-Student test, ($P \leq 0.05$).

6.4 Discussion

The present study evaluated placental perfusion and umbilical cord blood flow in 44 healthy fetuses and 8 abnormal fetuses, providing specific information for brachycephalic bitches, which present high rates of gestational complications (Pereira et al. 2019). To date, there is only one study in which CEUS was performed for placental evaluation in bitches of different breeds with physiological gestation (Orlandi et al. 2019). Nevertheless, the cited study did not describe patterns involving placentas at the end of pregnancy nor any gestational abnormalities. The present study brings information about hemodynamics throughout pregnancy, standardize perfusion parameters in healthy brachycephalic bitches and evaluated the diagnostic accuracy of Doppler and contrast-enhanced ultrasound for the detection of fetal abnormalities, such as anasarca and hydrocephalus.
A healthy and functional placenta-concept binomial is important for the development of the fetus and for the gestational process especially when considering the placental features and fetal demands during intrauterine life. Thus, the evaluation of different time points of the pregnancy process is crucial in the study of embryonic, fetal, and placental vascular adaptation. Therefore, in the present study, the evaluations covered all thirds of the pregnancy, thus allowing for correlation between specific hemodynamic aspects and gestational development of the maternal fetal binomial. Breeding standardization is also important for defining normal and specific

values for a given group of animals since studies involving the use of echo-Doppler indicate that animal weights influence blood flow. In fact, different values of uterine and umbilical vessel flow can occur during the gestation of bitches with different weights (Blanco et al. 2020; Gaikwad et al. 2020); a variation that may also be seen using the CEUS technique. The choice of brachycephalic bitches for this study was based on the fact that these breeds have a higher incidence of congenital malformations (Pereira et al. 2019), making the hemodynamic evaluation an interesting alternative for possible identification of alterations during prenatal check-ups in pregnant dogs.

Due to the importance of CEUS in the obstetric evaluation of the functional status of the placenta (Poret-Bazin et al. 1987), it should be noted that no side effects were observed for mothers and fetuses, with the latter developing normally and having heart rates and appropriate biometric measurements for the species in accordance with reports from previous studies (Giannico et al. 2016; Feliciano et al. 2015). There were no changes in gestational hemodynamics evaluated by Doppler before and after the CEUS exam. The use of contrast in the post-implantation period and fetogenesis and at the end of pregnancy did not cause any visible ultrasound changes in the maternal-fetal binomial nor promoted changes in the neonates of females belonging to group 1.

Additionally, CEUS has been considered a safe method for the evaluation of uteroplacental blood perfusion as the microbubbles do not cross the placenta, that is, there is no enhancement of the embryonic or fetal structures as observed in the present study. This observation makes it unlikely that CEUS would cause side effects in the fetus (Roberts et al. 2016; Freccero et al. 2017; Orlandi et al. 2019; Murotsuki, 2007). The use of contrast agent was safe even in the first third of pregnancy, which is a critical period of fetal development. This confirms previous findings in primates (Keator et al. 2011) and in bitches (Orlandi et al. 2019), where contrast administration did not cause any damage to the mother nor the fetus.

Dopplerfluxometric wave shape analysis of the umbilical artery has been increasingly used to evaluate fetal well-being. This results in the detection of flow velocities and vascular indices in the different branches of the uterine and fetal circulations (Jaffe et al. 1997) and is also recommended as a diagnostic tool for the monitoring of high-risk pregnancies in bitches after 40 days of gestation (Gaikwad et al. 2020). Literature states the umbilical cord cannot be detected by ultrasound before 40 days of gestation (Johnston et al. 2001), thus confirming the findings of our study where it could be

visualized just after 45 days of gestation. In this dopplerfluxometric analysis of the umbilical cord, a significant increase in blood flow from M2 to M3 was verified with a decrease in RI and PI. Similar changes in blood flow and vascular resistance in the uterine artery of healthy bitches from 40 days until the end of gestation were observed in a previous study (Blanco et al. 2020). Other studies in bitches also found a linear increase in blood flow and a decrease in RI and PI as gestation progressed (Nautrup, 1998; Di Salvo et al. 2006; Gaikwad et al. 2020). An explanation for these findings could be related to the adaptive changes in circulation throughout pregnancy (Poston et al. 1995), such as an increase in blood volume. Decreased vascular resistance seems to assist in increasing placental blood flow, which is important for fetal development (Rennie et al. 2007; Yadav et al. 2016). Abnormal remodeling of the spiral arteries in the placental bed leads to a reduced blood supply to the organ as in pathological conditions, such as pre-eclampsia and fetal growth restriction (Prosens et al. 1972; Yagel et al. 1999).

Umbilical artery pulsatility rates suggest that adaptive changes to increase fetal-placental blood flow did not occur in the first trimester of pregnancy in humans (Den Ouden et al. 1990). From the second to third trimester, the decrease in vascular resistance is reflected in the analysis of the umbilical waveform (McParland & Pearce, 1998), with a progressive decrease in resistance over time. To maintain uteroplacental blood flow under normal conditions, obliteration of 50% of the terminal placental vessels should occur before circulation is compromised, as observed in previous studies evaluating the PI of the umbilical artery (Trudinger, 1991).

Comparing the dopplerfluxometric parameters before and after inoculation of the contrast medium, no changes in the clinical value of the dopplerfluxometric variables were detected. However, an increase in emphasis was noted after the use of the contrast agent. Our findings show that the increase in Doppler signal was similar to that described in primates, horses, rats, women, and bitches (Freccero et al. 2017; Orlandi et al. 2019; Poret-Bazin et al. 2013; Keator et al. 2011; Hua et al. 2009). The CEUS technique has been widely used in veterinary medicine to increase enhancement of the perfusion and vascularization of different organs beyond the placenta, thus allowing identification of small lesions with much better accuracy than could be achieved with conventional ultrasonography (Cosgrove et al. 2003).

The quantitative parameters measured during placental CEUS of brachycephalic bitches remained constant throughout pregnancy, that is, placental perfusion did not change despite the significant increase in umbilical blood flow. When using CEUS, maintenance of quantitative perfusion parameters in the proximal and distal placenta of bitches at 23, 30, and 45 days of gestation has been observed (Orlandi et al. 2019). As already described, the resistance rates of the uteroplacental and umbilical arteries decrease progressively during gestation in healthy bitches, generating adequate perfusion of the placenta and fetal viscera (Gaikwad et al. 2020). An absolute increase in blood flow was observed in fetal sheep, which could be due to a relative decrease in peripheral resistance in other parts of the fetus and the creation of new vascular tunnels in the placenta (Rudolf & Heyman, 1970; Trudinger et al. 1987). The establishment of a high-flow and low-resistance circulation on both sides of the placenta is mainly a result of increased vessel cross-section due to villous angiogenesis on the fetal side, remodeling of the spiral arteries, and vasodilatation on the maternal side (Flo et al. 2010). This could be explained by the adaptation of the placental vascular network in bitches to maintain adequate blood perfusion for fetal development [58], resulting in a compensatory method similar to what occurs in humans to prevent pressure changes in healthy pregnancies (Blanco et al. 2011; Vallance et al. 1989; Blanco et al. 2012).

As pregnancy progresses, plasticity in the developing placenta promotes development of vascular adaptations to ensure proper fetal growth and meet the increasing metabolic demands of the fetus through the structural, morphological, and functional changes dependent on pregnancy (Roberts et al. 2016; Yadav et al. 2016; Kowalewski et al. 2020). The vascular network of the placenta undergoes extensive and continuous remodeling during pregnancy. Therefore, angiogenesis is of great importance in placental development and must be properly regulated. Failure to do so may lead to intrauterine fetal growth restriction and unsatisfactory obstetric outcomes (Burton et al. 2009). In addition, the balance between the fetal umbilical circulation and maternal uterine placenta is important for oxygen transfer through the placenta. It has been found that there is continuous placental growth throughout pregnancy, as demonstrated by an increase in weight and size of the organ, in the number of villi in the tertiary trunk, and in the total number of small arterial channels, which results in the continuous expansion of the placental vascular tree and a decrease in vascular resistance (Trudinger & Giles, 1989; Tesi et al. 2020).

Furthermore, the capillary walls of the placenta have elastic properties because they can spread and compress themselves in response to the pressure differential between maternal and fetal circulations (Karimu & Burton, 1994). The pressure differential tends to increase during pregnancy as the fetal heart matures; therefore, we can imagine a continually increasing force of distension being applied (Burton et al. 2009). The importance of evaluating placental function makes CEUS a tool that can be used in addition to visualizing and quantifying placental perfusion in different species because it can provide information to assist in the identification of altered blood flow (Roberts et al. 2016). Therefore, the evaluation of placental blood perfusion is one of the central indicators of placental function, and the description of patterns of placental perfusion in healthy pregnancies by means of CEUS allows for the early identification of abnormalities, which is not yet found in veterinary medical literature.

Qualitatively, it was possible to confirm homogeneous placental perfusion from the first evaluation at 25 days in the embryonic vesicles and placental tissue until the last moment at 58 days without noting any differences in enhancement patterns. Similarly, another study also found homogeneous contrast perfusion patterns during the stage of the first two-thirds of gestation in the placentas of healthy bitches using the same technique (Orlandi et al. 2019). The canine placenta starts showing branches of umbilical cord blood vessels that irrigate both the yolk sac and the placental waist between and 25–30 days of gestation (Miglino et al. 2006). In the present study, it was possible to continue evaluation during pregnancy and verify the maintenance of this homogeneous placental perfusion until the end of the bitch gestation. In horses, a homogeneous pattern of placental perfusion was also verified (Freccero et al. 2017). However, in humans, the data revealed regional differences in the intervillous space perfusion within an individual placenta (Roberts et al. 2016). The structural differences between the placentas, mainly between the endotheliochorial and canine annular zonary areas and the human hemochorial and discoidal areas, are responsible for the observed differences.

At the beginning of pregnancy, we obtained images of the entire placenta in the field of vision (Fig. 3), which became unfeasible later in pregnancy since only part of the placenta could be visualized. The same occurred in another study on bitches, where it was possible to evaluate the entire placenta at 25 days but no longer during pregnancy (Orlandi et al. 2019). This limitation was also reported in other studies regarding CEUS evaluation throughout

the pregnancy of rodents (Arthuis et al. 2013), mares (Freccero et al. 2017), humans and primates (Roberts et al. 2016), where it was only possible to obtain a complete placental image or a larger area at the beginning of pregnancy.

The similarities in the values obtained by Doppler fluxometry of the umbilical artery of normal and abnormal canine fetuses has also been described in the literature (Freitas et al. 2016), demonstrating that in cases of hydropsy there may be no changes in the umbilical vascularization of the abnormal maternal-fetal binomial. Nonetheless, when evaluating placental vascularization, increased RI (3rd week) and PI (6th week) in the uteroplacental arteries of congenital abnormal fetuses (among them, three with hydropsy) was also observed by the same study.

This increase in uteroplacental vascular resistance in the 3rd week of canine fetuses with congenital abnormalities is directly related to placental dysfunction (contrast filling failure) observed in our study using CEUS, which seems to be the result of limited vascular development and incomplete trophoblastic invasion of the placental bed (Reynolds et al. 2006). It is possible that earlier evaluations of abnormal brachycephalic fetuses could have detected the placental dysfunction process early by CEUS.

In cases of hydropsy, the placenta usually presents with swelling and late tissue maturation from a histopathological point of view (Parks, 2015), confirming the findings described in this study in fetuses with anasarca and hydrocephalus. Late maturation or failure in placental development seems to be directly related to the delay in contrast filling, as verified by CEUS in canine fetuses with these abnormalities.

It should be considered that few abnormal canine fetuses (eight individuals) and types of gestational changes (anasarca and hydrocephaly) were evaluated in this study. These aspects could be viewed as limitations of this study. However, the results are extremely promising with respect to the use of CEUS, demonstrating safe application of this technique in individuals with abnormal pregnancies and indicating great potential for experimental use (with research using a greater number of abnormal fetuses, different gestational events, various types of abnormalities, and histopathological evaluation of placental tissues). Its applicability to the obstetric routine to detect gestational processes which would put canine females and other species at risk of developing placental dysfunction must be further evaluated.

It is important to comment on two points of our research: 1) had no limitations regarding the application of the CEUS technique in the evaluation of our animals, at all times of evaluation, we were able to perform the CEUS exam of the placenta, however, we lost the quantitative evaluation of 4 samples averaged due to a problem with the offline perfusion assessment software during the pandemic (Table 3); 2) the presence of two different races in the healthy group (French Bulldogs and Pugs) is not a bias to consider, because the two races are considered brachycephalic, medium-sized, with similar weights and we made a non-parametric comparison of the most important values with non-significant result. We also know that size or racial factor has no significant interference in the characteristic of placental and umbilical blood perfusion, since these characteristics of placentation are the same in any canine specimen.

6.5 Conclusion

The association of dopplerfluxometric techniques and CEUS allowed the establishment of qualitative and quantitative parameters of gestational hemodynamics at all stages of pregnancy in healthy brachycephalic bitches without causing gestational changes in the fetal maternal binomial. It was possible to follow the maternal-fetal vascular adaptations according to gestation progression; determine the vascular dynamics of the fetal umbilical artery by Doppler (homogeneous during the evaluated periods), possibly correlating with the development and showed decreased rates of pulsatility and resistance in the final third; as well as analyze the qualitative and quantitative features of placental perfusion by CEUS, which proved to be constant throughout the whole gestational process in healthy bitches. It is important to emphasize that these techniques are safe for both the pregnant female dog and the fetus, making the use of both techniques even more interesting. Finally, CEUS has detected placental dysfunction in female dog with abnormal pregnancies, with fetuses presenting with anasarca and hydrocephaly as verified by heterogenicity in tissue perfusion, lower intensity of placental tissue filling, and delay in perfusion times, with a diagnostic accuracy close to 75%.

6.6 References

Almeida VT, Uscategui RAR, Silva PDA da, Avante ML, Simo~es APR, Vicente WRR. Hemodynamic gestational adaptation in bitches. Cie^ncia Rural 2017;47:e20160758. https://doi.org/10.1590/0103-8478cr20160758.

Arthuis CJ, Novell A, Escoffre JM, Patat F, Bouakaz A, Perrotin F. New insights into uteroplacental perfusion: quantitative analysis using Doppler and contrast-enhanced ultrasound imaging. Placenta 2013;34:424e31. https:// doi.org/10.1016/j.placenta.2013.01.019.

Bargellini P, Orlandi R, Paloni C, Rubini G, Fonti P, Righi C, et al. Contrast-enhanced ultrasound complements two-dimensional ultrasonography in diagnosing gallbladder diseases in dogs. Vet Radiol Ultrasound 2018;345e356. https://doi.org/10.1111/vru.12601.

Blanco PG, Arias D, Rube A, Barrena JP, Corrada Y, Gobello C. An experimental model to study resistance index and systolic/diastolic ratio of uterine arteries in adverse canine pregnancy outcome. Reprod Domest Anim 2009;44:162e6. https://doi.org/10.1111/j.1439-0531.2009.01369.x.

Blanco PG, Batista PR, Re NE, Mattioli GA, Arias DO, Gobello C. Electrocardiographic changes in normal and abnormal canine pregnancy. Reprod Domest Anim 2012;47:252e6. https://doi.org/10.1111/j.1439-0531.2011.01846.x.

Blanco PG, Huk M, Lapuente C, Tortora M, Rodríguez R, Arias DO, et al. Uterine and umbilical resistance index and fetal heart rate in pregnant bitches of different body weight. Anim Reprod Sci 2020;212:106255. https://doi.org/ 10.1016/j.anireprosci.2019.106255.

Blanco PG, Rodríguez R, Rube A, Arias DO, Tortora M, Díaz JD, et al. Doppler ultrasonographic assessment of maternal and fetal blood flow in abnormal canine pregnancy. Anim Reprod Sci 2011;126:130e5. https://doi.org/10.1016/j.anireprosci.2011.04.016.

Brosens IA, Robertson WB, Dixon HG. The role of the spiral arteries in the pathogenesis of preeclampsia. Obstet Gynecol Annu 1972;1:177e91.

Burton GJ, Charnock-Jones DS, Jauniaux E. Regulation of vascular growth and function in the human placenta. Reproduction 2009;138:895e902. https:// doi.org/10.1530/REP-09-0092.

Choi SY, Jeong WC, Lee YW, Choi HJ. Contrast enhanced ultrasonography of kidney in conscious and anesthetized beagle dogs. J Vet Med Sci 2016;78: 239e44. https://doi.org/10.1292/jvms.15-0199.

References

Christie DW, Bailey JB, Bell ET. Classification of cell types in vaginal smears during the canine oestrous cycle. Br Vet J 1972;128:301e10. https://doi.org/ 10.1016/S0007-1935(17)36935-X.

Cosgrove D. Angiogenesis imaging - ultrasound. Br J Radiol 2003;76:S43e9. https://doi.org/10.1259/bjr/86364648.

Cosgrove D. Ultrasound contrast agents: an overview. Eur J Radiol 2006;60: 324e30. https://doi.org/10.1016/j.ejrad.2006.06.022.

Den Ouden M, Cohen-Overbeek TE, Wladimiroff JW. Uterine and fetal umbilical artery flow velocity waveforms in normal first trimester pregnancies. BJOG 1990;97:716e9. https://doi.org/10.1111/j.1471-0528.1990.tb16245.x.

Di Salvo P, Bocci F, Zelli R, Polisca A. Doppler evaluation of maternal and fetal vessels during normal gestation in the bitch. Res Vet Sci 2006;81:382e8. https://doi.org/10.1016/j.rvsc.2006.03.004.

Divon MY, Ferber A. Umbilical artery Doppler velocimetry - an update. Semin Perinatol 2001;25:44e7. https://doi.org/10.1053/sper.2001.22892.

Dong Y, Wang W, Cao J, Fan P, Lin X. Quantitative evaluation of contrast-enhanced ultrasonography in the diagnosis of chronic ischemic renal disease in a dog model. PloS One 2013;8:e70337. https://doi.org/10.1371/ journal.pone.0070337.

England GCW, Allen WE, Porter DJ. Studies on canine pregnancy using b-mode ultrasound: development of the conceptus and determination of gestational age. J Small Anim Pract 1990;31:324e9. https://doi.org/10.1111/j.1748- 5827.1990.tb00821.x.

Feliciano MAR, Maciel GS, Coutinho LN, Almeida VT, Uscategui RR, Vicente WRR. Gestational echo biometry in brachycephalic pregnant bitches. Ciencia Anim Bras 2015;16:419e27. https://doi.org/10.1590/1089- 6891v16i327069.

Flo K, Wilsgaard T, Acharya G. Relation between utero-placental and feto-placental circulations: a longitudinal study. Acta Obstet Gynecol Scand 2010;89:1270e5. https://doi.org/10.3109/00016349.2010.512069.

Freccero F, Toaldo MB, Castagnetti C, Cipone M, Diana A. Contrast-enhanced ultrasonography of the uterus during normal equine pregnancy: preliminary report in two mares. J Equine Vet Sci 2017;54:42e9. https://doi.org/10.1016/ j.jevs.2017.02.011.

Freitas LA, Mota GL, Silva HVR, Carvalho CF, Silva LDM. Can maternal-fetal hemodynamics influence prenatal development in dogs? Anim Reprod Sci 2016;172:83e93. https://doi.org/10.1016/j.anireprosci.2016.07.005.

References

Gaikwad SM, Gulavane SU, Kumbhar UB, Shelar RR, Chaudhari RJ, Ribeiro RA. Doppler evaluation of maternal vessels in normal gestation and threatened abortion in canines. Ir Vet J 2020;73:1e9. https://doi.org/10.1186/s13620- 020-00169-9.

Gasser B, Uscategui RAR, Maronezi MC, Pavan L, Simo~es APR, Martinato F, et al. Clinical and ultrasound variables for early diagnosis of septic acute kidney injury in bitches with pyometra. Sci Rep 2020;10:1e12. https:// doi.org/10.1038/s41598-020-65902-4.

Giannico AT, Garcia DAA, Gil EMU, Sousa MG, Froes TR. Assessment of um- bilical artery flow and fetal heart rate to predict delivery time in bitches. Theriogenology 2016;86:1654e61. https://doi.org/10.1016/ j.theriogenology.2016.03.042.

Gloria A, Contri A, Carluccio A, Robbe D. Blood periovulatory progesterone quantification using different techniques in the dog. Anim Reprod Sci 2018;192:179e84. https://doi.org/10.1016/j.anireprosci.2018.03.006.

Harman CR, Baschat AA. Comprehensive assessment of fetal wellbeing: which Doppler tests should be performed? Curr Opin Obstet Gynecol 2003;15: 147e57. https://doi.org/10.1097/00001703-200304000-00010.

Hirsch AJ, Roberts VHJ, Grigsby PL, Haese N, Schabel MC, Wang X, et al. Zika virus infection in pregnant rhesus macaques causes placental dysfunction and immunopathology. Nat Commun 2018;9:1e15. https://doi.org/10.1038/ s41467-017-02499-9.

Hopper BJ, Richardson JL, Lester N v. Spontaneous antenatal resolution of canine hydrops fetalis diagnosed by ultrasound. J Small Anim Pract 2004;45: 2e8. https://doi.org/10.1111/j.1748-5827.2004.tb00187.x.

Hua X, Zhu LP, Li R, Zhong H, Xue YF, Chen ZH. Effects of diagnostic contrast- enhanced ultrasound on permeability of placental barrier: a primary study. Placenta 2009;30:780e4. https://doi.org/10.1016/j.placenta.2009.06.009.

Jaffe R, Jauniaux E, Hustin J. Maternal circulation in the first-trimester human placenta - myth or reality? Am J Obstet Gynecol 1997;176:695e705. https:// doi.org/10.1016/S0002-9378(97)70572-6.

Johnston SD, Root Kustritz M v, Olson PNS. Canine and feline theriogenology. 2001.

Karimu AL, Burton GJ. The effects of maternal vascular pressure on the di- mensions of the placental capillaries. BJOG 1994;101:57e63. https://doi.org/ 10.1111/j.1471-0528.1994.tb13011.x.

References

Keator CS, Lindner JR, Belcik JT, Bishop Cv, Slayden OD. Contrast-enhanced ultrasound reveals real-time spatial changes in vascular perfusion during early implantation in the macaque uterus. Fertil Steril 2011;95:1316e21. https://doi.org/10.1016/j.fertnstert.2011.01.040.

Kim YH, Travis AJ, Meyers-Wallen VN. Parturition prediction and timing of canine pregnancy. Theriogenology 2007;68:1177e82. https://doi.org/10.1016/j.theriogenology.2007.08.018.

Kowalewski MP, Tavares Pereira M, Kazemian A. Canine conceptus-maternal communication during maintenance and termination of pregnancy, including the role of species-specific decidualization. Theriogenology 2020;150:329e38. https://doi.org/10.1016/j.theriogenology.2020.01.082.

Kuo K, Roberts VHJ, Gaffney J, Takahashi DL, Morgan T, Lo JO, et al. Maternal high-fat diet consumption and chronic hyperandrogenemia are associated with placental dysfunction in female rhesus macaques. Endocrinology 2019;160:1937e49. https://doi.org/10.1210/en.2019-00149.

Kutzler MA, Mohammed HO, Lamb Sv, Meyers-Wallen VN. Accuracy of canine parturition date prediction from the initial rise in preovulatory progesterone concentration. Theriogenology 2003;60:1187e96. https://doi.org/10.1016/ S0093-691X(03)00109-2.

Lin S, Shimizu I, Suehara N, Nakayama M, Aono T. Uterine artery Doppler velocimetry in relation to trophoblast migration into the myometrium of the placental bed. Obstet Gynecol 1995;85:760e5. https://doi.org/10.1016/0029- 7844(95)00020-R.

Longo LD. Maternal blood volume and cardiac output during pregnancy: a hypothesis of endocrinologic control. Am J Physiol Regul Integr Comp Physiol 1983;245:R720e9. https://doi.org/10.1152/ajpregu.1983.245.5.r720.

Lopate C. Estimation of gestational age and assessment of canine fetal maturation using radiology and ultrasonography: a review. Theriogenology 2008;70:397e402. https://doi.org/10.1016/j.theriogenology.2008.05.034.

McParland P, Pearce JM. Review article: Doppler blood flow in pregnancy. Placenta 1988;9:427e50. https://doi.org/10.1016/0143-4004(88)90055-0.

Miglino MA, Ambrosio CE, Martins D dos S, Wenceslau CV, Pfarrer C, Leiser R. The carnivore pregnancy: the development of the embryo and

fetal mem- branes. Theriogenology 2006;66:1699e702. https://doi.org/10.1016/ j.theriogenology.2006.02.027.

Murotsuki J. Contrast-enhanced ultrasound in obstetrics and gynecology. Donald Sch J Ultrasound Obstet Gynecol 2007;1:16e9. https://doi.org/ 10.5005/jp-journals-10009-1094.

Nautrup CP. Doppler ultrasonography of canine maternal and fetal arteries during normal gestation. J Reprod Fertil 1998;112:301e14. https://doi.org/ 10.1530/jrf.0.1120301.

Orlandi R, Vallesi E, Boiti C, Polisca A, Troisi A, Righi C, et al. Contrast-enhanced ultrasonography of maternal and fetal blood flows in pregnant bitches. Theriogenology 2019;125:129e34. https://doi.org/10.1016/j.theriogenology.2018.10.027.

Parks WT. A Pathologist's approach to nonimmune hydrops. J Fetal Med 2015;2:143e9. https://doi.org/10.1007/s40556-015-0055-x.

Paulson EE, Comizzoli P. Endometrial receptivity and embryo implantation in carnivoresdcommonalities and differences with other mammalian species. Biol Reprod 2021;104:771e83. https://doi.org/10.1093/biolre/ioab001.

Pereira KHNP, Correia LECS, Oliveira ELR, Bernardo RB, Jorge MLN, Gobato MLM, et al. Incidence of congenital malformations and impact on the mortality of neonatal canines. Theriogenology 2019;140:52e7. https:// doi.org/10.1016/j.theriogenology.2019.07.027.

Poret-Bazin H, Simon EG, Bleuzen A, Dujardin PA, Patat F, Perrotin F. Decrease of uteroplacental blood flow after feticide during second-trimester pregnancy termination with complete placenta previa: quantitative analysis using contrast-enhanced ultrasound imaging. Placenta 2013;34:1113e5. https:// doi.org/10.1016/j.placenta.2013.08.002.

Poston L, McCarthy AL, Ritter JM. Control of vascular resistance in the maternal and feto-placental arterial beds. Pharmacol Ther 1995;65:215e39. https://doi.org/10.1016/0163-7258(94)00064-A.

Rennie MY, Whiteley KJ, Kulandavelu S, Adamson SL, Sled JG. 3D visualisation and quantification by microcomputed tomography of late gestational changes in the arterial and venous feto-placental vasculature of the mouse. Placenta 2007;28:833e40. https://doi.org/10.1016/j.placenta.2006.12.005.

Reynolds LP, Caton JS, Redmer DA, Grazul-Bilska AT, Vonnahme KA, Borowicz PP, et al. Evidence for altered placental blood flow and

vascularity in compromised pregnancies. J. Physiol 2006;572:51e8. https://doi.org/10.1113/ jphysiol.2005.104430.

Roberts VHJ, Frias AE. Contrast-enhanced ultrasound for the assessment of placental development and function. Biotechniques 2020;69:392e9. https://doi.org/10.2144/btn-2020-0069.

Roberts VHJ, Lo JO, Lewandowski KS, Blundell P, Grove KL, Kroenke CD, et al. Adverse placental perfusion and pregnancy outcomes in a new nonhuman primate model of gestational protein restriction. Reprod Sci 2018;25:110e9. https://doi.org/10.1177/1933719117704907.

Roberts VHJ, Lo JO, Salati JA, Lewandowski KS, Lindner JR, Morgan TK, et al. Quantitative assessment of placental perfusion by contrast-enhanced ultra- sound in macaques and human subjects. Am J Obstet Gynecol 2016;214:369. https://doi.org/10.1016/j.ajog.2016.01.001. e1-e8.

Rudolph AM, Heymann MA. Circulatory changes during growth in the fetal lamb. Circ Res 1970;26:289e99. https://doi.org/10.1161/01.RES.26.3.289.

Salati JA, Roberts VHJ, Schabel MC, Lo JO, Kroenke CD, Lewandowski KS, et al. Maternal high-fat diet reversal improves placental hemodynamics in a nonhuman primate model of diet-induced obesity. Int J Obes 2019;43: 906e16. https://doi.org/10.1038/s41366-018-0145-7.

Simo~es APR, Feliciano MAR, Maronezi MC, Uscategui RAR, Bartlewski PM, de Almeida VT, et al. Elastographic and echotextural characteristics of foetal lungs and liver during the final 5 days of intrauterine development in dogs. Anim Reprod Sci 2018;197:170e6. https://doi.org/10.1016/ j.anireprosci.2018.08.025.

Socha P, Rudowska M, Janowski T. Effectiveness of determining the parturi- tion date in bitches using the ultrasonographic fetometry as compared to hormonal and cytological methods. Pol J Vet Sci 2012;15:447e53. https:// doi.org/10.2478/v10181-012-0069-4.

Tesi M, Miragliotta V, Scala L, Aronica E, Lazzarini G, Fanelli D, et al. Rela- tionship between placental characteristics and puppies' birth weight in toy and small sized dog breeds. Theriogenology 2020;141:49e57. https://doi.org/ 10.1016/j.theriogenology.2019.08.017.

Trudinger BJ, Giles WB. Clinical and pathologic correlations of umbilical and uterine artery waveforms. Clin Obstet Gynecol 1989;32:669e78. https:// doi.org/10.1097/00003081-198912000-00007.

Trudinger BJ, Stevens D, Connelly A, Hales JRS, Alexander G, Bradley L, et al. Umbilical artery flow velocity waveforms and placental resistance:

the effects of embolization of the umbilical circulation. Am J Obstet Gynecol 1987;157: 1443e8. https://doi.org/10.1016/S0002-9378(87)80241-7.

Trudinger BJ. Doppler ultrasound studies and fetal abnormality. In: Drife JO, Donnai D, editors. Antenatal diagnosis of fetal abnormalities; 1991. p. 113e25. https://doi.org/10.1007/978-1-4471-1854-1_9.

Vallance P, Collier J, Moncada S. Effects of endothelium-derived nitric oxide on peripheral arteriolar tone in man. Lancet 1989;334:997e1000. https://doi.org/10.1016/S0140-6736(89)91013-1.

Waller KR, O'Brien RT, Zagzebski JA. Quantitative contrast ultrasound analysis of renal perfusion in normal dogs. Vet Radiol Ultrasound 2007;48:373e7. https://doi.org/10.1111/j.1740-8261.2007.00259.x.

Yadav BK, Neelavalli J, Krishnamurthy U, Szalai G, Shen Y, Nayak NR, et al. A longitudinal study of placental perfusion using dynamic contrast enhanced magnetic resonance imaging in murine pregnancy. Placenta 2016;43:90e7. https://doi.org/10.1016/j.placenta.2015.12.019.

Yagel S, Anteby EY, Shen O, Cohen SM, Friedman Z, Achiron R. Placental blood flow measured by simultaneous multigate spectral Doppler imaging in pregnancies complicated by placental vascular abnormalities. Ultrasound Obstet Gynecol 1999;14:262e6. https://doi.org/10.1046/j.1469- 0705.1999.14040262.x.

Yeager AE, Mohammed HO, Meyers-Wallen V, Vannerson L, Concannon PW. Ultrasonographic appearance of the uterus, placenta, fetus, and fetal mem- branes throughout accurately timed pregnancy in beagles. Am J Vet Res 1992;53:342e51.

Zhou YJ, Yuan ML, Li R, Zhu LP, Chen ZH. Real-time placental perfusion on contrast-enhanced ultrasound and parametric imaging analysis in rats at different gestation time and different portions of placenta. PloS One 2013;8: e58986. https://doi.org/10.1371/journal.pone.0058986.

Chapter 7

High-definition ultrasonography in the evaluation of the reproductive tract of bitches during the follicular phase of the estrous cycle

Aires LPN, Gasser B, Silva P, Del Aguila Da Silva P, Silveira MV, Carneiro RK, IwaoYamada D, Padilha-Nakaghi LC, Uscategui RAR, Spada S, Russo M, Feliciano MAR. High-definition ultrasonography in the evaluation of the reproductive tract of bitches during the follicular phase of the estrous cycle. Anim Reprod Sci. 2021 Nov;234:106870. doi: 10.1016/j.anireprosci.2021.106870. Epub 2021 Oct 14. PMID: 34673364

High-definition ultrasonography in the evaluation of the reproductive tract of bitches during the follicular phase of the estrous cycle

7.1 Introduction

The complexity of the bitch's reproductive physiology is a great challenge for appropriate breeding management, because correct identification of the periovulatory changes is one of the determining factors for a successful determination of the physiological state of bitches (Groppetti et al., 2015). Monitoring the changes in reproductive tract structures related to the periovulatory period of bitches can be performed in many ways, such as observing clinical symptoms, vaginal cytology, vaginoscopy, hormonal assays and ultrasonography (Lindsay, 1983, Silva et al., 1996, England and Concannon, 2002, Moxon et al., 2012, Lévy, 2016). Due to physiological variations and individual characteristics of each bitch, however, such as differences in clinical manifestations among bitches, duration of each phase of the estrous cycle, interval between estrous cycles and findings as a result of conducting each of these examinations, such as correlation between vaginal cytology and blood progesterone concentrations, knowledge and experience is required, as well as cautious interpretations (Wilborn and Maxwell, 2012).

The utility of ultrasonography in small animal reproduction has evolved from safe and early pregnancy diagnosis to applications in reproductive management, allowing for obstetric evaluations, diagnosis of urogenital disorders and visualization of ovarian and uterine changes related to the female reproductive status (Davidson and Baker, 2009, Barbosa et al., 2013), however, to properly apply and interpret this imaging modality for evaluation of reproductive processes, the sonographer must have adequate knowledge regarding the reproductive physiology of the bitch, as well as extensive training and ability to properly conduct the procedures (Wilborn et al., 2012).

The development of new technologies for ultrasonic imaging has allowed acquisition of images with more precise resolution of the reproductive tract, fetal development and organogenesis (Davidson and Baker, 2009). Several studies have been conducted to elucidate the changes in the sonographic aspects of reproductive tract of bitches throughout the estrous cycle (Boyd et al., 1993, England and Allen, 1989, Renton et al., 1992, Wallace et al., 1992, Lévy and Fontbonne, 2007, England et al., 2009, Kim et al., 2009, Freitas et al., 2017). Nevertheless, with the advances in ultrasonic imaging quality, there is a need to evaluate the usefulness of these new technologies in reproductive evaluation, to study the reproductive system and correlate

findings with physiological processes to improve breeding management procedures.

A new technology termed HD (High Density) ultrasonography, also known as high-definition ultrasonography, has gained interest and applicability for diagnostic imaging and has been determined to be effective for human medicine peripheral nerves (Karmakar et al., 2013) and carpal tunnel evaluations (Tan et al., 2011). In veterinary medicine, there has been results from only one study reported regarding applicability of this technique in gestational ultrasonography and fetal organogenesis in brachycephalic breeds (Maronezi et al., 2021), but there are no reports regarding the usefulness of this technique in the evaluation of the reproductive tract and about changes occurring throughout the estrous cycle in non-pregnant bitches.

The HD technique is based on the use of transducers with a large number of piezoeletric elements (which can reach up to 4096 elements), separated by a small pitch, differing from conventional transducers (which normally contain around 128 elements), resulting in sound-waves with smaller width, thus proportioning greater axial, lateral and elevational spatial resolution, besides providing for a more precise contrast and more detailed images due to the larger number of pixels, generating images with greater quality than those resulting with use of conventional transducers (Lieu, 2010, Szabo, 2014, Merritt, 2018).

The aim of the present study was to sonographically evaluate the dog uterus and ovaries during the follicular phase of the estrous cycle using B mode HD technologies and to standardize findings with blood progesterone concentrations. The hypothesis is that the high-definition images resulting with the use of the HD transducer will allow for more precise evaluation of the reproductive tract, especially the ovaries and ovarian structures throughout the estrous cycle, providing further information regarding the physiological changes of utero-ovarian structures.

7.2 Materials and methods

7.2.1 Animal selection

This study was approved by the Ethics Committee on the Use of Animals (CEUA) of the host institution (protocol No. 003074/19). The animals were from an experimental kennel of the Institution or from external tutors. All

details of the experiment were explained and permission for participating in the study was obtained by means of a consent form.
All patient data and history were obtained, and physical examinations were performed to evaluate each female, as established in the literature (Johnston et al., 2001, Grundy et al., 2002). Inclusion criteria were: patients of reproductive age (peripubertal to 6 years of age), no history of reproductive disease, no gestational anomalies, no changes at the time of physical and obstetric examinations, no sonographic evidence of morphological abnormalities of the reproductive tract. Animals that did not meet the criteria were not included.
Seven Beagle bitches (87.5%) and one (12.5%) mongrel (totaling eight animals) were evaluated, weighing between 7.4 and 11.3 kg. Age ranged from 9 months to 5 years, but the majority of bitches (seven) were 9–11 months old. All bitches were considered healthy based on criteria previously established. Of the eight bitches, seven were nulliparous and pubescent, with expression of the first estrous cycle subsequent to puberty. The oldest bitch (5 years) was primiparous, with history of a previous pregnancy, normal parturition with no complications and no fetal nor neonatal abnormalities.

7.2.2 Timepoints of evaluations

All bitches were sonographically evaluated at five different timepoints. The first timepoint (M1) was established as the time of onset of proestrus (vulvar swelling and bloody discharge), with confirmation occurring based on vaginal cytology and serum progesterone concentration. After this period, all bitches were monitored by observation of clinical symptoms, behavior changes and findings using serial vaginal cytology examinations (2-day intervals or when considered necessary based on clinical symptoms or findings in vaginal smears). Vaginal smears were assessed and when it was determined the bitches were in transition from proestrus to estrus as confirmed by serum progesterone concentration, the second timepoint of evaluations was established (M2).
Two days after the M2 timepoint, all bitches were evaluated at three additional timepoints (M3, M4 and M5), with there being 2-day intervals between evaluations of vaginal cytology and quantifications of serum progesterone concentrations.

7.2.3 Vaginal cytology and hormonal concentrations

All bitches were monitored for onset of vulvar swelling and bloody discharge. The first day there were detections of these marker characteristics was considered as the first day of proestrus. From that timepoint, vaginal cytology was performed every 2 days to monitor the progression of the phase and to identify changes related to the transition of the estrous cycle phases. Samples obtained using vaginal cytology techniques were placed on microscope slides and stained using rapid panoptic stain. Evaluation of vaginal smears was made using a microscope (Nikon Eclipse E200) at 100x magnification and interpreted according to the percentage of superficial cornified cells. When 80–90% of the cells present were detected to be superficial cornified cells, this was defined as the timepoint when there was onset of estrus and when there was an abrupt decrease of cornified cells, associated with an increase in parabasal, intermediate cells, as well as neutrophils, this was defined as the timepoint when there was onset of diestrus based on findings in a previous study (Johnston et al., 2001).
Blood progesterone concentrations were quantified to confirm each reproductive phase at the timepoints previously described. To quantify the progesterone concentration (P4), blood samples were obtained by venipuncture of the jugular or cephalic veins. Blood samples were subsequently transferred to a vacuum tube with no anticoagulant for subsequent centrifugation to obtain the serum, which was used for quantification of serum progesterone concentration using Chemiluminescence procedures (Immulite® 1000 Progesterone - SIEMENS). The results were interpreted according to data established in the literature for this technique (Gloria et al., 2018): proestrus: 0.09–1.04 ng/mL; preovulatory period: 1.29–2.7 ng/mL; ovulatory period: 3.18–12.28 ng/mL; oocyte maturation period (post ovulatory period): 17.17–24.7 ng/mL.

7.2.4 Ultrasonographic evaluation

For ultrasonographic assessment, abdominal hair was clipped and bitches were transferred to the examination room. All patients were fasted for 6 h prior to the evaluation. Bitches were positioned in dorsal or lateral recumbency, parallel to the equipment, with their heads towards the

monitor. Acoustic gel was applied to allow evaluation of the structures in the abdominal area.

Ultrasonic evaluations were performed using an ACUSON S2000/SIEMENS, equipped with a linear multifrequency transducer (5.5–18 MHz) utilizing the HD technology, associated with tissue harmonic imaging. Frequency was standardized from 12 to 16 MHz to allow adjustments for complete visualization of the reproductive tract, as necessary. All evaluations were performed by a single operator.

The evaluation was initiated in the caudal abdomen area, identifying the uterine body between the urinary bladder and the descending colon in a sagittal view. Technical adjustments, such as gain, dynamic range, focal zone and frequency were performed as needed to maximize image quality. Qualitative (echogenicity and echotexture) and values for quantitative (uterine body thickness in sagittal view) variables were assessed.

Ovarian evaluations were performed caudal to the ipsilateral kidney in sagittal and transverse views, subtly positioning the transducer lateromedially and craniocaudally and using a fanning motion to assess the organ and evaluate the parenchymal structures (follicles and corpus luteum). Technical adjustments regarding image quality were performed as needed. Qualitative (echogenicity, echotexture, presence or absence of fluid around the ovary) and quantitative (height and length in sagittal view) variables were evaluated. Cine-loop clips of the ovarian images were stored in DICOM format for subsequent analysis using medical image visualization software (RadiAnt DICOM Viewer 2020.1.1 Version 64bits).

Frames that allowed complete analyses of the ovarian parenchymal structures were selected to determine the diameter of each structure. These numbers of these structures were determined and categorized into one of four groups based on size in mm of structures: G1 $\leq$ 1; G2: from 1.01 to 3.5; G3: from 3.51 to 5.5; G4: from 5.51 to 10. To determine wall thickness of each structure, the thickest portion of the wall was identified and the width was determined. The values of wall thickness of each structure were then used to calculate mean wall thickness for structures in each ovary.

7.2.5 Statistical analysis

Statistical analysis was performed using the R® software (R Foundation for Statistical Computing; Vienna, Austria). Initially, the Bartlett test of homogeneity of variances and Shapiro-Wilk test for normality of residuals

were performed on the data for quantitative evaluations. The values for real or transformed data obtained by conducting ultrasonographic evaluations were compared at all timepoints using the ANOVA test and correlations were determined using the Spearman test. There were considered to be mean differences when there was a $P < 0.05$.

7.3 Results

There was a difference in blood progesterone concentrations for each timepoint ($P < 0.05$). Mean values of blood progesterone concentrations at each timepoint are provided in Table 7.1.

Tab. 7. 1 Mean ± SD of serum progesterone concentration, uterine thickness and ovarian dimensions (height and length in sagittal view) obtained using HD ultrasonography procedures of bitches at each timepoint of evaluation.

	Progesterone (ng/mL)	Uterine thickness (mm)	Height (mm)		Length (mm)	
			Left Ovary		Right Ovary	
M1	0.756 ± 0.904^{a}	10.495 ± 1.479^{a}	7.413 ± 0.546^{a}	8.2 ± 1.948^{a}	11.563 ± 2.243^{a}	13.762 ± 1.545^{a}
M2	6.03 ± 4.32^{ab}	12.35 ± 1.269^{b}	8.588 ± 1.502^{ab}	9.425 ± 1.35^{ab}	14.725 ± 1.1^{b}	16.512 ± 1.716^{ab}
M3	10.81 ± 6.23^{bc}	12.21 ± 1.371^{b}	10.475 ± 1.724^{bc}	10.475 ± 2.491^{ab}	15.6 ± 1.546^{b}	19.037 ± 2.385^{b}
M4	16.96 ± 6.29 ^{cd}	12.875 ± 1.314^{b}	10.475 ± 1.861^{bc}	11.463 ± 2.326^{b}	15.1 ± 1.552^{b}	19.325 ± 1.952^{b}
M5	20.69 ± 5.12^{d}	13.163 ± 0.944^{b}	10.563 ± 1.115^{c}	10.721 ± 1.654^{ab}	16.563 ± 2.467^{b}	19.2 ± 2.368^{b}

Different letters in the same column indicate differences ($P < 0.05$).

Serum progesterone concentrations at each timepoint, associated with vaginal cytology indicated that at the M1 timepoint encompassed the early to mid-proestrus period. Concentrations of progesterone at the M2 timepoint were those during the preovulatory and ovulatory periods. Concentrations of progesterone at the M3 timepoint were those during a portion of the ovulatory and postovulatory periods. The concentrations of progesterone at subsequent timepoints (M4 and M5) represented those during the postovulatory period, as established by Gloria et al. (2018) based on progesterone concentrations that were quantified using the

Chemiluminescence technique. In two bitches, the concentrations at the M5 timepoint were those collected during diestrus based on cytological evaluations.

7.3.1 Uterine ultrasonography

It was possible to identify the uterine body and the ovaries of all patients during the sonographic evaluation relatively easily (eight uteri, 16 ovaries). The uterine horns were partially identified due to the position of these structures in the abdomen and overlapping of the intestinal loops. Images of the cervix, uterine body, uterine bifurcation and uterine horn are included in Figure 7.1.

Fig. 7. 1 Sonographic aspects of the uterus using HD ultrasonography. A. Longitudinal view of the cervix (between white arrows) and the uterine body (between hollow arrows). B. Longitudinal view of the uterine body, where the region of the uterine bifurcation (*) is identified and two tubular structures can be detected cranially, one dorsally and the other ventrally, corresponding to the uterine horns. C. Longitudinal view of the left uterine horn (between electronic calipers) identified as a tubular structure with differentiation of the uterine layers and sublayers due to hormonal functions.

The uterus had a homogenous echotexture but portions of distinct echogenicity of the uterine walls were observed at all timepoints in all bitches, resulting in a "multilayer" aspect. These areas were more prominent in the uterine horns as compared with the uterine body. In total, six areas were distinguished in the uterine walls of all bitches.
Starting from the lumen (fine echogenic line at the center) to the serous surface, a hypoechoic layer was identified, closely related to the next layer, a fine hyperechoic image. The next layer external from the lumen was a small hypoechoic zone and lying next to this zone was a well-defined hyperechoic layer. There was another hypoechoic region lying outside to the

hyperechoic layer, and the outer layer was a fine echogenic layer (Figure 7.2). There was no anechoic fluid detected in the uterine lumen at any timepoint when evaluations were conducted.

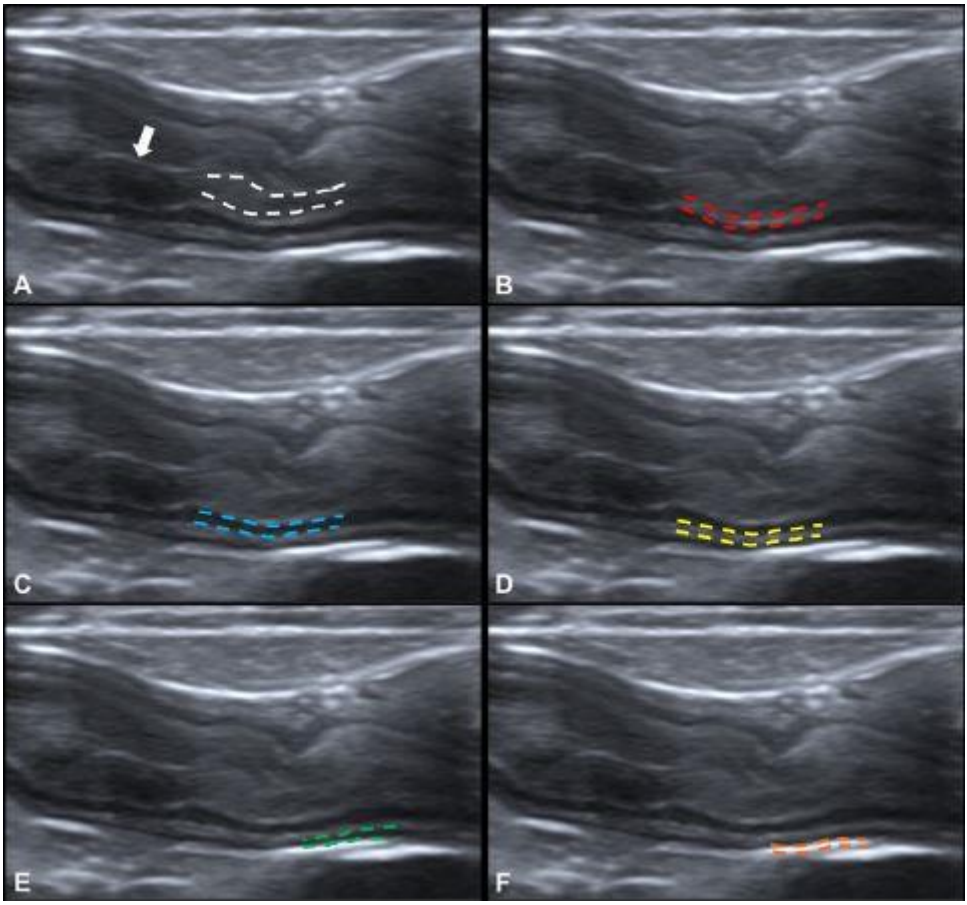

Fig. 7. 2 Longitudinal ultrasonographic view of the left uterine horn of a bitch during estrus (P4 = 8.9 ng/mL), demonstrating a "multilayer" aspect of the uterine walls. A. A relatively hypoechoic layer (between the white dashes) was detected, close to the luminal interface (white arrow). B. A hyperechoic region is visible (between the red dashes) right next to the previous layer. C. Hypoechoic portion (between the blue dashes). D. Linear hyperechoic area (between the yellow dashes). E. Hypoechoic region delimitated by the green dashes. F. Fine echogenic region between the orange dashes. (For interpretation of the references to colour in this figure legend, the reader is referred to the web version of this article).

The uterine body lining was thicker at the M1 and M2 timepoints. The uterine body was of similar thickness at subsequent timepoints as the M1 and M2 timepoints when evaluations were conducted (Table 7.1).

7.3.2 Ovarian ultrasonography

The sonographic appearance of the ovaries was markedly different at the different timepoints (Figure 7.3).

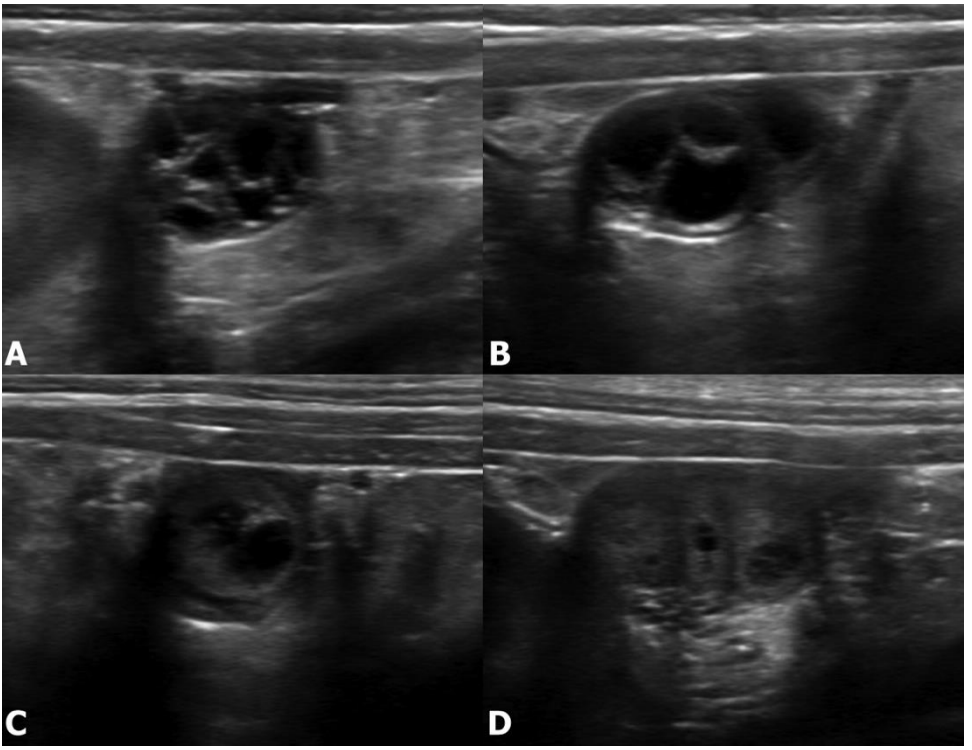

Fig. 7. 3 Sonographic images of the ovaries and the modifications throughout the follicular phase. A. Longitudinal view of the left ovary of a bitch during early proestrus, where several cavitary thin-walled and fluid-filled structures are observed in the ovarian parenchyma. B. Longitudinal view of the left ovary of a bitch during early estrus, before ovulation. It was possible to observe that follicular structures with greater dimensions compared to early proestrus and follicular walls became slightly thickened. C. Longitudinal view of the left ovary of a bitch during the postovulatory period. One ovarian structure with markedly irregular internal margins is identified, corresponding to a corpus hemmoraghicum. D. Longitudinal view of the right ovary of

a bitch during early diestrus. Ovarian contours are slightly irregular in shape with three almost completely solid ovarian structures, with very small cavitary areas and markedly thickened regular walls, corresponding to corpora lutea.

At the M1 timepoint, ovaries were oval-shaped with well-defined and regular contours and was hypoechoic compared to the adjacent tissue and predominantly homogenous parenchyma, with the presence of small thin-walled ovarian structures filled with anechoic content. After the M2 timepoint, ovarian qualitative characteristics were markedly different (Table 7.2).

Tab. 7. 2 Percentage of qualitative findings observed in the ovaries of eight bitches (16 ovaries) using HD ultrasonography.

	Ovarian structures' content			Fluid in ovarian bursa		Focal Reactivity		Contours		Echogenicity		Echotexture	
	An (%)	Mix (%)	Ec (%)	Pr (%)	Ab (%)	Pr (%)	Ab (%)	Re (%)	Ir (%)	Hypo (%)	Hyper (%)	Ho (%)	Co (%)
M1	100	0	0	0	100	75	25	81.25	18.75	100	0	100	0
M2	50	50	0	75	25	100	0	43.75	56.25	100	0	6.25	93.75
M3	0	87.5	12.5	50	50	87.5	12.5	18.75	81.25	68.75	31.25	0	100
M4	0	50	50	31.25	68.75	81.25	18.75	31.25	68.75	37.5	62.5	0	100
M5	0	31.25	68.75	0	100	25	75	37.5	62.5	0	100	0	100

Legends: An: anechoic; Mix: mixed echogenicity; Ec: echogenic. Pr: present; Ab: absent; Re: regular; Ir: irregular; Hypo: hypoechoic; Hyper: hyperechoic; Ho: homogenous; Co: coarse

Furthermore, there was a difference in ovarian height and length at the timepoints when evaluations occurred ($P < 0.05$), as indicated by information included in Table 7.1. Ovarian dimensions were positively correlated with serum progesterone concentration (height: $r = 0.775$; length: $r = 0.624$) and uterine thickness (height: $r = 0.411$; length: 0.384).
At the M1 timepoint, there was no fluid around the ovaries in any patient. At the subsequent timepoint (M2), there was fluid accumulation around 12 ovaries (75%; Figure 7.4). After the M2 timepoint, there was lesser fluid

quantities than at the M1 timepoint with there being fluid detected around 50% (8) of the ovaries. At the M3 timepoint there fluid around 31.3% (5) of the ovaries at the M4 and M5 timepoints there was no fluid around the ovaries of any bitches (Table 7.2).

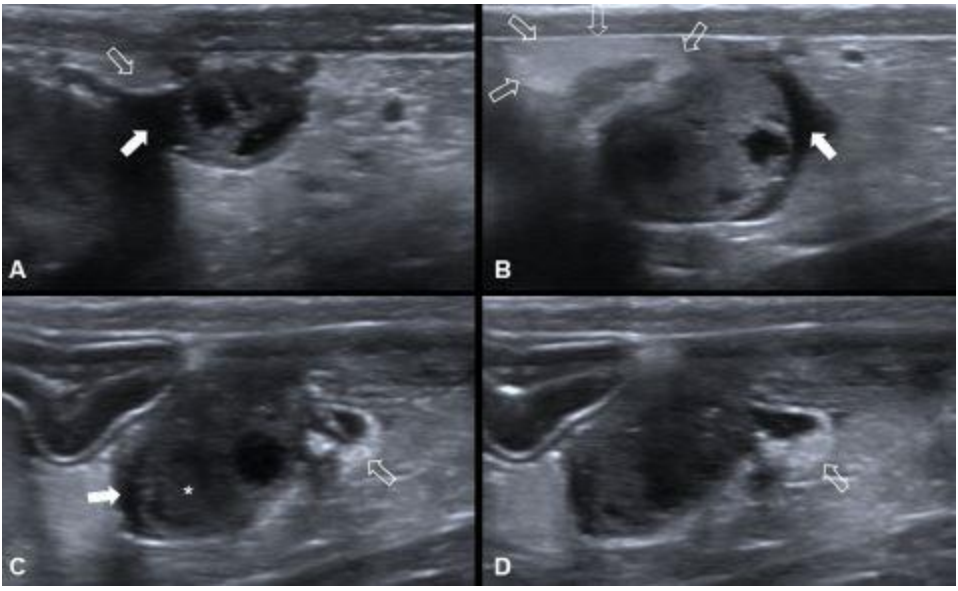

Fig. 7. 4 Sagittal ultrasonographic view of ovarian structures and modifications of the ovaries and adjacent tissue throughout the evaluations. Presence of fluid around the ovary (white arrow) located in the ovarian bursa, as detected in A, B and C was more commonly observed at the M2 timepoint, but was also present at the M3 and M4 timepoints. Tissue reactivity (hollow arrows in A, B, C and D was present at all timepoints of evaluation. There was greater echogenicity of the cavitary ovarian structure content (asterisk) as noted in C.

Another qualitative finding was a characteristic increase in fat tissue echogenicity adjacent to the ovaries at all timepoints when there were evaluations (Figure 7.4), with a varied occurrence at each timepoint. There were these findings in 75% (12) of the ovaries evaluated at the M1 timepoint. At the M2 timepoint, there was this characteristic echogenicity for all ovaries (100%). At the M3 timepoint, the tissue characteristic echogenicity was visualized at 87.5% (14 ovaries) evaluations. At M4, there was this characteristic in 81.3% (13 ovaries) and at the M5 timepoint, this occurred with only 25% (four ovaries) of the evaluations. When present, this

characteristic echogenicity was observed bilaterally in all bitches, except at the M4 timepoint, where a mongrel bitch had this characteristic echogenicity only around the left ovary.

7.3.3 Ovarian structure

At all timepoints, it was possible to note that subtle movements in a fanning motion of the transducer were required for proper evaluation of the ovaries, allowing for identification of the ovarian structures. Because ovaries and the parenchymal structures increased in size, it was more difficult to select a single frame in which it was possible to visualize the entire organ at its maximum height and length and identify all ovarian structures. Several frames were selected for complete identification of the ovaries at the maximum dimension in the sagittal view and to localize ovarian structures at the maximum diameter.

At the M1 timepoint, all bitches had small thin-walled cavitary rounded structures filled with anechoic content, indicative of ovarian follicles. At this timepoint, bitches had a mean of five follicles per ovary (mean of 4.5 on the left ovary and 5.5 on the right ovary). The number of follicles per ovary at this timepoint differed in five bitches (62.5%).

At the M2 timepoint, in seven bitches (87.5%), there was a smaller number of ovarian structures when compared to the M1 timepoint and, among these, in five (74.43%) bitches there were fewer ovarian structures in both ovaries. In only one bitch (12.5%), was there a subsequent detection of fewer structures at the subsequent timepoint (M3). The other patients (87.5%) had a consistent number of structures per ovary after the M2 timepoint.

Only one structure smaller than 1 mm was detected in all bitches. The number of ovarian structures as compared with the number at the previous timepoint differed when there were some evaluations. Among these, the number of G2 structures differed in both ovaries ($P < 0.05$). The number of G4 structures was different only in the right ovary ($P < 0.05$; Table 7.3).

Tab. 7. 3 Mean ± SD number of ovarian structures from each group, diameter of the greatest ovarian structure and wall thickness at each timepoint when there were evaluations as assessed by HD ultrasonography in bitches.

	G1 (≤ 1 mm)		G2 (1.01 -3.5 mm)		G3 (3.51-5.5 mm)		G4 (5.51-10 mm)		Greatest structure diameter		Mean wall thickness (mm)	
	E	D	E	D	E	D	E	D	E	D	E	D
M1	0[a]	0.125 ± 0.354[a]	3.375 ± 2.387[a]	3.25 ± 3.2[a]	1 ± 1.069[a]	2.125 ± 2.357[a]	0.125 ± 0.354[a]	0[a]	3.85 ± 1.291[a]	3.812 ± 0.583[a]	0.6112 ± 0.1222[a]	0.5513 ± 0.1343[a]
M2	0[a]	0.125 ± 0.354[a]	1 ± 1.309[b]	1.5 ± 0.756[b]	2 ± 1.69[a]	1.625 ± 1.188[a]	0.5 ± 0.535[a]	0.875 ± 0.835[ab]	5.919 ± 1.646[a][b]	5.944 ± 1.376[a][b]	1.241 ± 0.404[a]	1.466 ± 0.523[b]
M3	0[a]	0.125 ± 0.354[a]	0.75 ± 1.035[b]	0.125 ± 1.246[b]	1.5 ± 1.512[a]	1.625 ± 1.188[a]	0.75 ± 0.886[a]	1.5 ± 1.195[b]	5.944 ± 2.157[a][b]	6.75 ± 2.108[b]	2.356 ± 0.496[b]	2.199 ± 0.695[bc]
M4	0[a]	0[a]	0.75 ± 1.035[b]	1 ± 0.756[b]	1.25 ± 1.165[a]	2.125 ± 0.835[a]	0.875 ± 0.835[a]	1.125 ± 0.835[ab]	6.519 ± 1.915[b]	7.169 ± 1.997[b]	2.574 ± 0.697[b]	2.446 ± 0.847[c]
M5	0[a]	0[a]	1.375 ± 1.188[ab]	0.875 ± 1.126[b]	0.75 ± 0.886[a]	2.25 ± 1.488[a]	0.625 ± 0.744[a]	1.125 ± 0.641[ab]	5.681 ± 2.1[ab]	7.431 ± 1.415[b]	2.976 ± 0.998[b]	2.753 ± 0.591[c]

Different letters in the same column indicate differences ($P < 0.05$).

Although the number of G4 structures were different only in the right ovary, the number of G4 structures was positively correlated with serum progesterone concentration (left ovary: r = 0.451; right ovary: r = 0.647) and uterine thickness (left ovary: r = 0.368; right ovary: r = 0.281).

There was a difference in size of the largest ovarian structure at the different timepoints of evaluations ($P < 0.05$; Table 3). In the left ovary, the size of the largest structure was positively correlated with serum progesterone concentration (r = 0.505), height (r = 0.664), length (r = 0.386) and number of G4 structures (r = 0.726) but was negatively correlated with size of G2 structures (r = 0.386). In the right ovary, there was positive correlation with serum progesterone concentration (r = 0.784), uterine thickness (r = 0.34), height (r = 0.742) and length (r = 0.765).

Mean ovarian structure wall thickness could also be easily assessed. There was a difference ($P < 0.05$) in mean wall thickness at the timepoints evaluated (Table 7.3). The values for this variable in both ovaries were positively correlated with serum progesterone concentration (left ovary: $r = 0.749$; right ovary: $r = 0.633$).

The sonographic identification that ovulation had occurred was based on the presence of fluid around the ovaries and/or decrease in the number of follicular structures when compared to the values at the M1 timepoint, as well as values for cytological and hormonal correlations. In six bitches (75%), the first detection of fluid around the ovary occurred at the M2 timepoint, and in the other two bitches this was detected for the first time at the M3 timepoint. There was a marked reduction of the cavitary ovarian structures after ovulation, being almost completely non-detectable subsequent to when ovulations occurred (Figure 7.5).

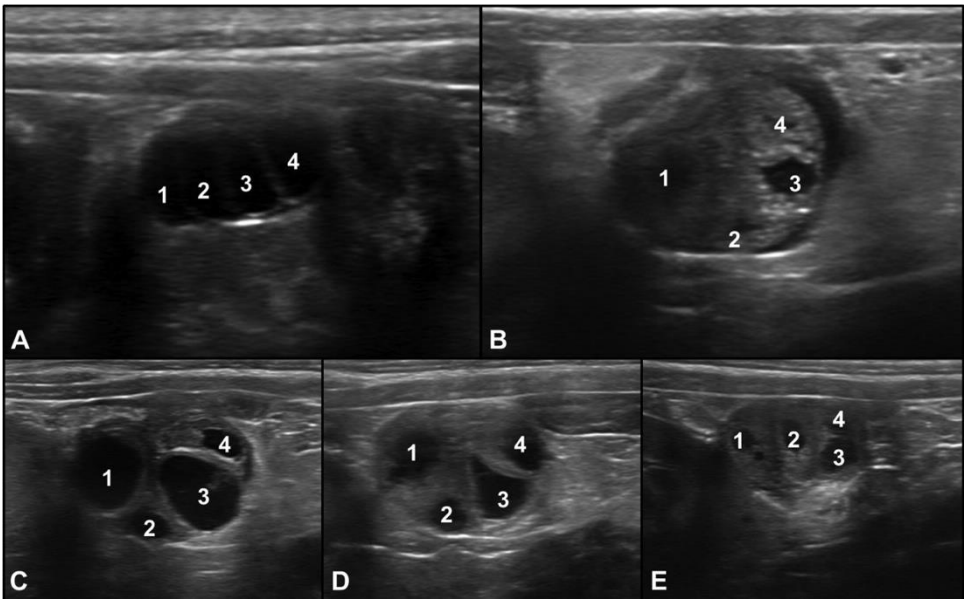

Fig. 7. 5 Sagittal view of the ovarian structures and modifications of the right ovary of a bitch (Beagle, nulliparous, 10 months-old) at the different timepoints of evaluation. A. At the M1 timepoint, the ovary was oval-shaped, with regular contours, hypoechoic parenchyma and presented four thin-walled cavitary structures (1, 2, 3 and 4), filled with homogenous anechoic fluid (P4 = 0.56 ng/mL). B. At the M2 timepoint, it is possible to observe that the ovarian parenchyma has a coarse echotexture, and the content of the ovarian structures has greater echogenicity. Each structure had thickened walls and the

cavitary area was smaller, especially structures 2 and 4, even though there was a small amount of fluid in the ovarian bursa and adjacent tissue reactivity (P4 = 8.9 ng/mL). C. At the M3 timepoint, there is an increase in the structure's dimensions, with hyperechoic walls and are filled with homogenous anechoic fluid (P4 = 14.6 ng/mL). D. At the M4 timepoint, there was a thickening of the walls of each structure, which had some irregular internal margins, and the ovary had a slight increase in echogenicity of the parenchyma. The contents of structures are still predominantly anechoic, but a small amount of debris can be identified in structure 1 (P4 = 22.6 ng/mL). E. At the M5 timepoint, the walls of the structures were thicker than at earlier timepoints and the cavitary areas were smaller with a nearly solid appearance to each structure. Vaginal cytology assessments indicated bitches were in cytological diestrus at this timepoint (P4 = 23.3 ng/mL).

8.4 Discussion

To the best of our knowledge, this is the first study regarding the application of HD ultrasonography for reproductive assessment of bitches during the follicular phase of the estrous cycle. Ultrasonography is the imaging method of choice for reproductive evaluation in small animals because it is non-invasive and allows for characterization of the changes of follicular and luteal structures (England et al., 2009). Results from the present study are indicative of the potential of the HD technology in complementing findings obtained with conventional B mode ultrasonography evaluations as evidenced by the greater definition of resolution in the images obtained, facilitating the understanding of the morphophysiological changes that occur during the estrous cycle of bitches.

While the first manifestation of proestrus generally occurs at puberty, many bitches may express behavioral estrus without there being occurrence of ovulation during the peripubertal period (Johnston et al., 2001). Gobello (2014) reported puberty in the bitch was a complex process and that the first manifestation of a typical follicular phase, evidence of ovulation and normal luteal phase could be a more precise estimate of sexual maturity. Considering that all seven pubescent bitches had regular proestrus and estrous occurrences, as evidenced by vaginal cytology and serum progesterone concentrations, as well as expected physical characteristics, behavior changes and evidence of ovulation, the bitches in the present study met the criteria for methodological bias regarding experimentation with pubescent bitches. More studies, however, are warranted with different age groups for further assessment of the changes in the reproductive system of bitches during the follicular phase of estrous cycles.

The uterine body could be identified in sagittal view in all patients. There have been no previous studies where there was identification of six distinct portions of the uterine wall of the bitch, therefore, this is an unprecedented finding. The "multilayer" aspect of the uterus when there is hormonal stimulation has already been described in bitches (England and Allen, 1989, Davidson and Baker, 2009, Kim et al., 2009, Freitas et al., 2017) and queens (Gatel et al., 2016), however, in the present study there was identification of a larger number of distinct regions of the uterine lining wall than previously reported.

Histologically, the uterus of the bitch is composed of three distinct layers, the outermost is the serous layer (perimetrium), overlying the muscular layer (myometrium) and inner region nearest to the uterine lumen, the mucosa/submucosa layer (endometrium), all of which have sublayers (Augsburger and Kürzi, 2004, Priedkalns and Leiser, 2006). The uterine tissue changes with fluctuations in hormonal concentrations and in some studies, this has been reported to occur in the edematous aspect of the endometrium, sublayer thickening, as well as there being distinct proliferative phases occurring (Galabova et al., 2003, Van Cruchten et al., 2004). The findings in the present study are directly related to image quality that could be obtained using the equipment and transducer due to improvement in axial, lateral and spatial resolutions resulting from utilization of the HD transducers (Lieu, 2010, Szabo, 2014, Merritt, 2018).

In the present study, the luminal interface was observed as a fine hyperechoic region, followed by a relatively hypoechoic layer and a fine echogenic region immediately below the luminal surface (Figure 7.2). In women, during the late proliferative period of the menstrual cycle, with transvaginal ultrasonography evaluations, the endometrium is detected as a "trilaminar" structure, where the fine echogenic luminal interface is centrally located, followed by the hypoechoic functional layer of the endometrium and the echogenic basal layer of the endometrium (Forrest et al., 1988, Lenz and Lindenberg, 1990, Bakos et al., 1993, Tetlow et al., 1999, Nalaboff et al., 2001), similar to findings in the present study.

Due to the similarity of findings in the present study with those in women, as well as the previous identification of the central hyperechoic region as the luminal interface, it is hypothesized that the bitch endometrium also has a "trilaminar" aspect during the follicular phase of the estrous cycle, the central portion corresponding to the lumen, the hypoechoic layer corresponding to the functional layer of the endometrium and the fine echoic

region corresponding to the basal layer of the endometrium. Further studies are, however, necessary to determine if there is verification of these uterine tissue characteristics using the techniques utilized in the present study.

Next to this "trilaminar" aspect, there was a hypoechoic layer detected in all patients. In women, a hypoechoic layer between the myometrium and the endometrium was identified using transvaginal ultrasonography and was described as the "sub-endometrial halo" or "junctional zone" (Fleischer et al., 1988, Tetlow et al., 1999). Histologically, however, this layer corresponds to a highly vascularized distinct myometrium portion, in which muscle cells are more compact, being consistent with hypoechoic characteristics (Tetlow et al., 1999).

This hypoechoic layer observed in all bitches also had similarities to the findings observed in women, thus, it is hypothesized that this "junctional zone" observed in the uterus of the bitch during the follicular phase of the estrous cycle corresponds to the inner circular layer of the myometrium. The hyperechoic region might correspond to the vascular layer of the myometrium and the next hypoechoic might correspond to the outer longitudinal layer of the myometrium. The outermost hyperechoic layer corresponds to the serous layer. During the follicular phase, hormones promote endometrium and myometrial thickening due to edema, development of the uterine glands, blood vessel enlargements and increased blood flow (Groppetti et al., 2010). The findings in the present study are possibly due to changes occurring during the estrous cycle, as well as the greater extent of resolution resulting from use of HD ultrasonography, considering there are no previous reports using conventional B mode ultrasonography.

With the progression of the estrous cycle, there was an increase in uterine thickness between early proestrus (M1) and estrus (M2), and after these timepoints, there were no changes in uterine thickness. Uterine thickening is related to the estrogenic functions during proestrus (England and Allen, 1989), which was also observed in the present study. After ovulation, however, followed by the decrease in concentrations of estrogens, the uterus begins to respond to progesterone which gradually increases during the luteal phase of the estrous cycle and there were no differences in the uterine characteristics during the postovulatory period, as evidenced in the present study which corroborates results of Kim et al. (2009), who performed conventional B-mode assessments in bitches to evaluate the sonographic aspect of the uterus during the different hormonal phases.

The sonographic identification of distinct uterine wall tissues during the follicular phase of the estrous cycle might provide for a greater understanding of physiological changes during the estrous cycle of bitches, as well as provide important information for reproductive assessment, provide for a means for early detection of uterine pathologies and correct identification of the affected region. Further studies are warranted to explore the capacity of this technology for these purposes.

During the preovulatory and ovulatory periods, all bitches had focal reactivity around the ovaries as evidenced by the increase in echogenicity of the adjacent fat tissues. Different from the present study, a hypoechoic "halo" surrounding the ovaries has been described at some timepoints during the periovulatory period using conventional B mode ultrasonography (Bergeron et al., 2013), which was considered to correspond to the ovarian bursa. There are no previous reports regarding the observation of tissue reactivity around the ovary similar to that detected in the present study.

The ovulatory process has already been compared to the inflammatory process, because angiogenic activity, increased vascular permeability, vasodilation and edema are essential characteristics of both processes (Duffy et al., 2019). In one study conducted with human ovaries, it was possible to observe that ovulation involves a cytokine signaling pathway, where the gonadotropin surge release initiates an inflammatory process in the granulosa cells (Poulsen et al., 2019). Considering that these tissue characteristics were more frequently observed during the preovulatory and ovulatory periods, it is hypothesized that this reactivity might be secondary to the inflammatory process in the ovaries around the time of ovulation.

The presence of fluid around the ovaries in this study has already been described and attributed as the accumulation of intra follicular fluid in the ovarian bursa after follicular rupture and ovulation (Lévy and Fontbonne, 2007). In a study conducted by Lévy and Fontbonne (2007), 39.6% of bitches had this fluid accumulation after ovulation, whereas in a study conducted by Barbosa et al. (2013), all bitches had this fluid accumulation 3 days after ovulation. In the present study, this fluid accumulation was detected at the M2 to M4 timepoints. Because of the anechoic fluid can remain for a few days, this finding should be interpreted cautiously when determining the time when ovulation occurs. Daily evaluations, as well as correlation with other values for variables (clinical manifestation, vaginal cytology and hormone concentrations) are required to confirm the day of ovulation.

In the present study, there was identification of an increase in follicular dimensions from early proestrus (M1) to estrus (M2), corroborating England et al. (2009), therefore, the capacity to detect follicular population dynamics. There is no definitive information regarding the chronology of processes in bitches regarding follicular recruitment, dominance, atresia or even if follicular growth is continuous or in waves (Evans, 2003). Due to the considerable preciseness of determinations using HD technology, it is believed that further studies with this technique could aid in allowing for a more precise understanding of the mechanisms related to the ovarian follicular dynamics in bitches.

In the present study, there was determination of when there was an increase in the wall thickness of the ovarian structures as the duration of the follicular phase of the estrous cycle advanced, where structures with wall thickness greater than 1 mm were observed during the preovulatory period. Wall thickening of ovarian structures has already been attributed to preovulatory luteinization of follicles (Lévy and Fontbonne, 2007) and to the initial formation of corpus luteum (England et al., 2009), where structures with wall thickness of 1 mm are considered preovulatory follicles and those greater than 1 mm are considered to be a corpus luteum. Due to the fluid-filled cavitary of the corpus luteum during the initial developmental stages, it might be difficult to sonographically differentiate this structure from preovulatory follicles or a corpus hemorrhagicum (Bergeron et al., 2013, Hollinshead and Hanlon, 2019). Considering that, in the present study, some ovarian structures that corresponded to preovulatory follicles had a wall thickness greater than 1 mm, it was possible to realize that measurements alone cannot be used to differentiate preovulatory follicles from the early developing corpus luteum, thus, differing from the study conducted by England et al. (2009).

Groppetti et al. (2015) conducted a histological analysis of the ovary of the bitch and there were early indications of luteinization of the large follicles during proestrus, characterized by cumulus mucification in the granulosa cells and that, in the ovulatory period, large follicles can coexist with corpus hemorrhagicum, the latter persisting until the end of the fertile period, developing into corpus luteum at the onset of diestrus. The findings of the present study indicated wall thickening after the M2 timepoint and these structures had changes in echogenicity of the content inside the antrum.

This indicates that the thick-walled ovarian structures during the postovulatory period might correspond to corpora hemorrhagica,

considering that, histologically, corpora lutea are only present with the onset of diestrus (Groppetti et al., 2015). In this context, HD ultrasonography provides for the capacity to have greater resolution for enhancing the understanding the ovarian changes during the postovulatory period. It, however, is noteworthy that daily evaluations were not performed in the present study, thus, limiting the comprehension of the changes regarding corpora hemorrhagica formation and the modification into corpora lutea. Further studies with HD ultrasonography, therefore, might be necessary for gaining a greater understanding of the sonographic aspect or the ovaries during the postovulatory period and diestrus.

7.5 Conclusion

The results of the present study provide unprecedented information regarding qualitative findings of the reproductive system of the bitch, where it was possible to detect distinct regions of the uterine wall during the follicular phase, as well as ovarian modifications in the follicular and periovulatory phases using high-definition ultrasonography, providing a new perspective in small animal reproductive ultrasonography. The technological advances in ultrasonography have allowed for great image resolution, consequently providing for a greater understanding of the sonographic anatomy and new applicability of this imaging technique, providing basic knowledge for further identification of physiological changes during different reproductive states. With the use of the HD technology, there were superb images obtained, allowing for more accurate assessment of the reproductive tract, which might aid in breeding management of dogs. Additionally, these findings provide opportunities for future studies utilizing the HD technique for improving reproductive management, as well as the application of this technique for early detection of morphophysiological changes that can lead to abnormalities of the estrous cycle.

7.6 References

Augsburger, H.R., Kürzi, M., 2004. Histomorphologic and morphometric evaluation of the uterine horns in nulliparous and multiparous Beagles. Am. J. Vet. Res. 65, 552–558. https://doi.org/10.2460/ajvr.2004.65.552.

Bakos,O.,Lundkvist,O¨.,Bergh,T.,1993.Transvaginalsonographicevaluation ofendometrialgrowthandtextureinspontaneousovulatorycycles-adescriptivestudy. Hum. Reprod. 8, 799–806. https://doi.org/10.1093/oxfordjournals.humrep.a138145.

Barbosa, C.C., Souza, M.B., Scalercio, S.R.R.A., Silva, T.F.P., Domingues, S.F.S., Silva, L.D.M., 2013. Ovarian and uterine periovulatory doppler ultrasonography in bitches. Pesq. Vet. Bras. 33, 1144–1150. https://doi.org/10.1590/S0100-736X2013000900016.

Bergeron, L.H., Nykamp, S.G., Brisson, B.A., Madan, P., Gartley, C.J., 2013. An evaluation of B-mode and color Doppler ultrasonography for detecting periovulatory events in the bitch. Theriogenology 79, 274–283. https://doi.org/10.1016/j.theriogenology.2012.08.016.

Boyd, J.S., Renton, J.P., Harvey, M.J., Nickson, D.A., Eckersall, P.D., Ferguson, J.M., 1993. Problems associated with ultrasonography of the canine ovary around the time of ovulation. J. Reprod. Fertil. Suppl. 47, 101–105.

Davidson, A.P., Baker, T.W., 2009. Reproductive ultrasound of the bitch and queen. Top. Companion Anim. Med. 24, 55–63. https://doi.org/10.1053/j. tcam.2008.11.002.

Duffy, D.M., Ko, C., Jo, M., Brannstrom, M., Curry, T.E., 2019. Ovulation: parallels with inflammatory processes. Endocr. Rev. 40, 369–416. https://doi.org/10.1210/ er.2018-00075.

England, G., Concannon, P.W., 2002. Determination of the optimal breeding time in the bitch: basic considerations. In: Concannon, P.W., England, G., Verstegen III, J., Linde Forsberg, C. (Eds.), Recent Advances in Small Animal Reproduction. International Veterinary Information Service, Ithaca.

England, G.C., Allen, W.E., 1989. Real-time ultrasonic imaging of the ovary and uterus of the dog. J. Reprod. Fertil. Suppl. 39, 91–100.

England, G.C.W., Russo, M., Freeman, S.L., 2009. Follicular dynamics, ovulation and conception rates in bitches. Reprod. Domest. Anim. 44, 53–58. https://doi.org/10.1111/j.1439-0531.2009.01416.x.

References

Evans, A., 2003. Characteristics of ovarian follicle development in domestic animals. Reprod. Domest. Anim. 38, 240–246. https://doi.org/10.1046/j.1439-0531.2003.00439.x.

Fleischer, A.C., Mendelson, E.B., Bohm-Velez, M., Entman, S.S., 1988. Transvaginal and transabdominal sonography of the endometrium. Semin. Ultrasound CT MR 81, 81–101.

Forrest, T.S., Elyaderani, M.K., Muilenburg, M.I., Bewtra, C., Kable, W.T., Sullivan, P., 1988. Cyclic endometrial changes: US assessment with histologic correlation. Radiology 167, 233–237. https://doi.org/10.1148/radiology.167.1.3279455.

Freitas, L.A., Mota, G.L., Silva, H.V.R., Silva, L.D.M., 2017. Two-dimensional sonographic and Doppler changes in the uteri of bitches according to breed, estrus cycle phase, parity, and fertility. Theriogenology 95, 171–177. https://doi.org/10.1016/j.theriogenology.2017.03.012.

Galabova, G., Egerbacher, M., Aurich, J.E., Leitner, M., Walter, I., 2003. Morphological changes of the endometrial epithelium in the bitch during metoestrus and anoestrus. Reprod. Domest. Anim. 38, 415–420. https://doi.org/10.1046/j.1439-0531.2003.00459.x.

Gatel, L., Gory, G., Chalvet-Monfray, K., Saunders, J.H., Rault, D.N., 2016. Intra- and inter-observer variability in ultrasonographical measurements of the uterus and ovaries in healthy, non-pregnant queens. J. Feline Med. Surg. 18, 110–117. https://doi.org/10.1177/1098612×15574317.

Gloria, A., Contri, A., Carluccio, A., Robbe, D., 2018. Blood periovulatory progesterone quantification using different techniques in the dog. Anim. Reprod. Sci. 192, 179–184. https://doi.org/10.1016/j.anireprosci.2018.03.006.

Gobello, C., 2014. Prepubertal and pubertal canine reproductive studies: conflicting aspects. Reprod. Domest. Anim. 49, 70–73. https://doi.org/10.1111/rda.12414. Groppetti, D., Aralla, M., Bronzo, V., Bosi, G., Pecile, A., Arrighi, S., 2015. Periovulatory time in the bitch: what's new to know? Comparison between ovarian histology and clinical features. Anim. Reprod. Sci. 152, 108–116. https://doi.org/10.1016/j.anireprosci.2014.11.008.

Groppetti, D., Pecile, A., Arrighi, S., Di Giancamillo, A., Cremonesi, F., 2010. Endometrial cytology and computerized morphometric analysis of epithelial nuclei: a useful tool for reproductive diagnosis in the bitch. Theriogenology 73, 927–941. https://doi.org/10.1016/j.theriogenology.2009.11.019.

References

Grundy, S.A., Feldman, E., Davidson, A., 2002. Evaluation of infertility in the bitch. Clin. Tech. Small Anim. Pract. 17, 108–115. https://doi.org/10.1053/svms.2002.36601.

Hollinshead, F., Hanlon, D., 2019. Normal progesterone profiles during estrus in the bitch: a prospective analysis of 1420 estrous cycles. Theriogenology 125, 37–42. https://doi.org/10.1016/j.theriogenology.2018.10.018.

S.D. Johnston, S.D., Root, M.V., Kustritz, Olson, P.N.S.,. 2001. Canine Feline Theriogenology, WB Saunders.

Karmakar, M.K., Shariat, A.N., Pangthipampai, P., Chen, J., 2013. High-definition ultrasound imaging defines the paraneural sheath and the fascial compartments surrounding the sciatic nerve at the popliteal fossa. Reg. Anesth. Pain Med. 38, 447–451. https://doi.org/10.1097/AAP.0b013e31829ffcb4.

Kim, J.-H., Mun, B.-G., Kim, B.-S., Park, I.-C., Suh, G.-H., Son, C.-H., 2009. Serial ultrasonographic appearance of normal uterus during estrous cycle in miniature schnauzer dogs. J. Embryo Transf. 24, 109–113.

Lenz, S., Lindenberg, S., 1990. Ultrasonic evaluation of endometrial growth in women with normal cycles during spontaneous and stimulated cycles. Hum. Reprod. 5, 377–381. https://doi.org/10.1093/oxfordjournals.humrep.a137106.

Levy, X., 2016. Videovaginoscopy of the canine vagina. Reprod. Domest. Anim. 51, 31–36. https://doi.org/10.1111/rda.12785.

Levy, X., Fontbonne, A., 2007. Determining the optimal time of mating in bitches: particularities. Rev. Bras. Reprod. Anim. 31, 128–134.

Lieu, D., 2010. Ultrasound physics and instrumentation for pathologists. Arch. Pathol. Lab. Med. 134, 1541–1556. https://doi.org/10.1043/2009-0730-RA.1. Lindsay, F.E.F., 1983. The normal endoscopic appearance of the caudal reproductive tract of the cyclic and non-cyclic bitch: post-uterine endoscopy. J. Small Anim. Pract. 24, 1–15. https://doi.org/10.1111/j.1748-5827.1983.tb00407.x.

Maronezi, M.C., Simo˜es, A.P.R., Uscategui, R.A.R., Pavan, L., Rodrigues, M.G.K., Mariano, R.S.G., Santos, V.J.C., Feliciano, M.A.R., 2021. Gestational echobiometry in brachycephalic bitches using high-definition ultrasonography. Pesq. Vet. Bras. 41, e06650 https://doi.org/10.1590/1678-5150-PVB-6650.

Merritt, C.R.B., 2018. Physics of ultrasound. In: Rumack, C.M., Levine, D. (Eds.), Diagnostic Ultrasound. Elsevier, Philadelphia, pp. 1–34.

References

Moxon, R., Batty, H., Irons, G., England, G.C.W., 2012. Periovulatory changes in the endoscopic appearance of the reproductive tract and teasing behavior in the bitch.Theriogenology 78, 1907–1916. https://doi.org/10.1016/j.theriogenology.2012.07.002.

Nalaboff, K.M., Pellerito, J.S., Ben-Levi, E., 2001. Imaging the endometrium: disease and normal variants. Radiographics 21, 1409–1424. https://doi.org/10.1148/radiographics.21.6.g01nv211409.

Poulsen, L., la, C., Englund, A.L.M., Wissing, M.L.M., Yding Andersen, C., Borup, R., Grøndahl, M.L., 2019. Human granulosa cells function as innate immune cells executing an inflammatory reaction during ovulation: a microarray analysis. Mol. Cell. Endocrinol. 486, 34–46. https://doi.org/10.1016/j.mce.2019.02.014.

Priedkalns, J., Leiser, R., 2006. Female reproductive system. In: Eurell, J.A., Frappier, B.L. (Eds.), Dellmann's Textbook of Veterinary Histology. Blackwell, pp. 256–278.

Renton, J.P., Boyd, J.S., Harvey, M.J.A., Ferguson, J.M., Nickson, D.A., Eckersall, P.D., 1992. Comparison of endocrine changes and ultrasound as means of identifying ovulation in the bitch. Res. Vet. Sci. 53, 74–79. https://doi.org/10.1016/0034-5288(92)90088-J.

Silva, L.D.M., Onclin, K., Verstegen, J.P., 1996. Assessment of ovarian changes around ovulation in bitches by ultrasonography, laparoscopy and hormonal assays. Vet. Radiol. Ultrasound 37, 313–320. https://doi.org/10.1111/j.1740-8261.1996.tb01236.x.

Szabo, T.L., 2014. Diagnostic Ultrasound Imaging: Inside Out, second ed. Elsevier.

Tan, T.C., Yeo, C.J., Smith, E.W., 2011. High definition ultrasound as diagnostic adjunct for incomplete carpal tunnel release. Hand Surg. 16, 289–294. https://doi.org/10.1142/S0218810411005564.

Tetlow, R.L., Richmond, I., Manton, D.J., Greenman, J., Turnbull, L.W., Killick, S.R., 1999. Histological analysis of the uterine junctional zone as seen by transvaginal ultrasound. Ultrasound Obstet. Gynecol. 14, 188–193. https://doi.org/10.1046/j.1469-0705.1999.14030188.x.

Van Cruchten, S., van den Broeck, W., D'Haeseleer, M., Simoens, P., 2004. Proliferation patterns in the canine endometrium during the estrous cycle. Theriogenology 62, 631–641. https://doi.org/10.1016/j.theriogenology.2003.11.015.

Wallace, S.S., Mahaffey, M.B., Miller, D.M., Thompson, F.N., Chakraborty, P.K., 1992. Ultrasonographic appearance of the ovaries of

dogs during the follicular and luteal phases of the estrous cycle. Am. J. Vet. Res. 53, 209–215.

Wilborn, R.R., Maxwell, H.S., 2012. Clinical approaches to infertility in the bitch. Vet. Clin. North Am. Small Anim. Pract. 42, 457–468. https://doi.org/10.1016/j.cvsm.2012.01.016.

Chapter 8

Ovarian contrast-enhanced ultrasonography and Doppler fluxometry in bitches during the postovulatory estrus and corpora lutea formation

Nogueira Aires LP, Gasser B, Silva P, Del'Aguila-Silva P, Yamada DI, Carneiro RK, Bressianini Lima B, Padilha-Nakaghi LC, Ramirez Uscategui RA, Spada S, Russo M, Rossi Feliciano MA. Ovarian contrast-enhanced ultrasonography and Doppler fluxometry in bitches during the postovulatory estrus and corpora lutea formation. Theriogenology. 2022 Dec;194:162-170. doi: 10.1016/j.theriogenology.2022.10.009. Epub 2022 Oct 13. PMID: 3626533

Ovarian contrast-enhanced ultrasonography and Doppler fluxometry in bitches during the postovulatory estrus and corpora lutea formation

8.1 Introduction

Ultrasonography is the imaging method of choice for the assessment of the bitch's reproductive tract, allowing the diagnosis of urogenital disorders, the evaluation of the morphological changes of the uterus and ovaries throughout the estrous cycle and providing early pregnancy detection (Davidson & Baker, 2009). Ultrasound can greatly improve breeding management, especially when combined with other methods, such as vaginal cytology, vaginoscopy and hormonal assays (England & Concannon, 2002; England et al. 2009; Aires et al. 2021; Levy & Fontbonne, 2007; Willborn & Maxwell, 2012).

The ovarian endocrine function depends on its active angiogenesis mechanisms, characterized by endothelial cell proliferation, which is highly dependent on the bitch's cyclic activity, reflecting the blood supply adaptation required for adequate gonadal function (Fraser & Wulff, 2003; Koster et al. 2001; Reynolds et al. 1992).

Doppler ultrasonography is a technique based on the interaction of soundwaves with moving blood cells, resulting in a frequency shift of the received echoes (Boote, 2003). Combined with the two-dimensional mode (B-mode), the technique itself provides important information regarding vascular architecture, presence of blood flow and its direction, as well as hemodynamic properties of the examined vessel (Carvalho et al. 2008). Extensive studies have been performed to evaluate the ovarian hemodynamic features of the bitch using Doppler ultrasound during different hormonal phases (Koster et al. 2001; Barbosa et al. 2013; Vermelen, 2009; Bicudo et al. 2010; Jurczak & Janowski, 2018; Polisca et al. 2013; Mansour et al. 2020). However, although Doppler ultrasonography can detect signals from small vessels, it cannot evaluate the microcirculation itself (Cosgrove, 2003).

Contrast-enhanced ultrasonography (CEUS) is a novel technique in which a contrast agent, that mainly constitutes microbubbles, consisting of a gas core and a stabilized, highly reflective biological shell, is administered intravenously, allowing the detection of the microvasculature for both qualitative and quantitative assessment of tissue perfusion (Tang et al. 2011; Wilson & Burns, 2010; Cosgrove, 2006).

Recent studies have evaluated the applicability of the CEUS technique in small animal reproduction. Studies available have been conducted for the assessment of placental perfusion in normal and abnormal canine pregnancy

(Silva et al. 2021; Orlandi et al. 2019), uterine perfusion in bitches with cystic endometrial hyperplasia-pyometra complex (Quartuccio et al. 2020), normal and abnormal canine testis and prostate (Orlandi et al. 2022; Spada et al. 2021; Troisi et al. 2015; Russo et al. 2012; Volta et al. 2014) and in mammary tumours (Feliciano et al. 2017; Feliciano et al. 2018; Gasser et al. 2018; Abma et al. 2019), demonstrating the feasibility of the technique and improving the diagnostic process in clinical and surgical management in various occasions.

Despite the growing interest in studying reproductive tissue perfusion, little is known about ovarian microcirculation and its detection using CEUS technology. Studies concerning CEUS evaluation of the ovaries have been conducted in sheep (Marret et al. 2006) and primates (Bishop et al. 2014; Hastings et al. 2012), demonstrating its applicability in evaluating vascular modification of the ovaries according to the cyclic activity. To our knowledge, there are no studies describing qualitative and quantitative findings of the ovarian perfusion in bitches using CEUS.

Therefore, CEUS evaluation may be a valuable tool for understanding the physiological changes of the canine ovary, particularly during the intense vascular modifications during the follicular phase of the estrous cycle and the formation of corpora lutea, aiming to provide better understanding of the physiological features during these periods improving reproductive management. Thus, the purpose of the present study was to perform Doppler and CEUS evaluations of the canine ovary during the follicular phase of the estrous cycle to detect perfusion changes associated with the endocrine events of this period, thus providing information that could contribute to better understanding the reproductive physiology of the bitch and provide a new method for evaluating bitches of great zootechnical value.

8.2 Materials and methods

This study is a continuation of the work previously published by the authors (Aires et al. 2021). Therefore, the methodology regarding animal inclusion, assessment timepoints, vaginal cytology and serum progesterone concentration for the present study is the same as that previously published by the authors.

8.2.1 Animals

This pilot study was approved by the Ethics Committee on Animal Use of the Home Institution (protocol No. 003074/19). All recruited patients were either from an experimental kennel of the Institution or from external tutors. Tutors were informed about the experiment methodologies and a consent form was filled to allow participation in the study.
Each patient underwent a thorough physical examination and reproductive history information, and pertinent patient data were obtained. Patients of reproductive age (pubertal to 6 years old) with no history of reproductive diseases, no gestational disorders, and no abnormalities detected in physical, gynecological, and sonographic examination were included.
A total of eight healthy bitches were evaluated, of which seven were Beagle (87,5%) and one was a mix-breed (12,5%). Age ranged from 9 months to 5 years and weight ranged from 7.4 to 11.3 kg. Moreover, seven bitches were nulliparous and pubescent (9–11 months old) at their first estrous cycle. The oldest patient was a 5 years-old primiparous bitch with history of a normal pregnancy and parturition without complications.

8.2.2 Timepoints of evaluation

Five different assessment timepoints were established corresponding to the periods of the estrous cycle. The first timepoint (T1) was established as the first day of proestrus, characterized by the onset of vulvar swelling and bloody discharge, confirmed by vaginal cytology and serum progesterone concentration. From this timepoint on, all bitches were monitored by serial clinical evaluations and vaginal cytology (2-day intervals or as needed based on symptoms and vaginal smears findings).
The second assessment timepoint (T2) was established as the period when vaginal smears and serum progesterone concentrations were indicative of the transition from proestrus to estrus.
After T2, three additional timepoints were established (T3, T4 and T5), each 2-days apart, at which vaginal cytology and serum progesterone quantification were also performed.

8.2.3 Vaginal citology and serum progesterone concentration

The owners were instructed to monitor the bitches in order to detect the onset of vulvar swelling and bloody discharge. The first day these signs were observed was considered as the first day of proestrus. Vaginal cytology was performed every 2 days to detect cytological changes to monitor the progression of the cycle and the transition from proestrus to estrus. Vaginal smear samples were placed on microscope slides, coloured with rapid panoptic stain (Laborclin, Pinhais, Brazil) and evaluated using a microscope (Nikon Eclipse E200) at 100x magnification, where interpretation was made considering the percentage of cornified cells. The onset of estrus was established as the moment 80–90% of the cells in the slide were cornified, whereas their abrupt decrease associated with an increase in parabasal and intermediate cells, as well as the presence of neutrophils was established as the onset of diestrus phase (Johnston et al. 2001).
For serum progesterone concentration, blood samples were obtained by either the jugular or cephalic veins. After collection, samples were transferred to a vacuum tube without anticoagulant and centrifuged to obtain the serum, which was used for quantification of serum progesterone concentration using a chemiluminescence technique (Immulite® 1000 Progesterone – SIEMENS). Interpretation of the results were based on the information present in the literature for this technique (Gloria et al. 2018) and were assessed as follows: proestrus: 0.09–1.04 ng/mL; preovulatory period: 1.29–2.7 ng/mL; ovulatory period: 3.18–12.28 ng/mL; oocyte maturation period (post ovulatory period): 17.17–24.7 ng/ml.

8.2.4 Ultrasonographic evaluation

Ultrasound examinations were performed by a single operator using an ACUSON S2000/SIEMENS machine, equipped with a linear multifrequency transducer (9.0 MHz) at all timepoints of evaluation established previously. All bitches fasted for at least 6 h before the examination. Patients underwent abdominal hair clipping before being transferred to the examination room, where a 20G catheter was placed in the cephalic vein. The bitches were placed in dorsal or lateral recumbency, parallel to the equipment, with their heads facing the monitor. Acoustic gel was applied on the skin to provide acoustic coupling. Technical adjustments (gain, depth, focal zone, dynamic range) were performed as needed for

optimal visualization. The ovaries were identified using conventional B-mode assessment, caudal to the ipsilateral kidney in sagittal view.

After the identification of the ovaries, Doppler assessment of the ovaries was performed as reported previously by Koster et al., 2001. Intraovarian vascularization was visualized using the Color-coded Doppler mode and the sample size was adjusted and limited to the ovarian area for optimal signal capture. Technical adjustments (gain, scale, filter) were performed as needed to obtain adequate visualization and to eliminate or reduce any ultrasound artifacts.

Once the intraovarian vasculature was identified, quantitative analyses were performed using the Pulsed-wave Doppler technique to obtain a velocity spectrum and calculate doppler-velocimetric parameters. The sample volume was adjusted to evaluate the entire lumen of the vessel and care was taken to evaluate just the intraovarian branches of the ovarian artery, rather than the ovarian artery itself. The insonation angle was manually corrected when needed but was always kept lower than 60°. Pulsed-wave Doppler was then activated, and a velocity spectrum was obtained. Quantitative analyses were performed, once three similar arterial waveforms were obtained. Velocimetric parameters obtained were systolic peak velocity (SPV) and end-diastolic velocity (EDV). Blood flow impedance was estimated by the resistivity index (RI) and the pulsatility index (PI), which were calculated automatically by the machine when a complete analysis of an entire cardiac cycle was selected. This procedure was performed in both ovaries.

For CEUS evaluation, a second-generation contrast agent (SonoVue®, Bracco, São Paulo, Brazil) was used, combined with a high frequency (9.0 MHz) linear transducer with harmonic capability and a dedicated software for CEUS examination and analysis (CADENCE™ contrast pulse sequencing (CPS) technology).

The Mechanical Index was always lower than 0.1, and a single focal zone was placed around the centre of the ovary. The contrast agent was injected via venous catheter (0.01 ml/kg), followed by the administration of 5 mL of saline solution (NaCl 0.9%). At the moment of the injection (T = 0), a timer was activated, and a video was recorded for 120 s. Care was taken to keep the transducer in the same position throughout recording time. This procedure was performed for both the left and right ovary.

A dedicated software (Contrast Dynamics™, Siemens, Germany) was then used to process the recorded videos and perform quantitative analysis to obtain time-intensity curves, showing the changes in enhancement over time

within a specific region of interest (ROI) allowing quantification of perfusion parameters.
A single ROI was drawn randomly in the ovarian parenchyma and a time-intensity curve was calculated by the equipment. A gamma variate map was also obtained from the selected ROI, for which five additional ROIs of approximately 1 mm^2 each were randomly selected (to avoid methodological bias). Once these ROIs were defined, the software designed time-intensity curves and automatically calculated perfusion parameters: peak contrast intensity (PPI peak in % of pixels), time to peak (TTP in s), mean transit time (MTT in s), area under the curve (AUC in %) and the average number of pixels (pixels).

8.2.5 Statistical analysis

The statistical analysis was performed using the R® software (R Foundation for Statistical Computing; Vienna, Austria). The Bartlett test for homogeneity of variances and the Shapiro-Wilk test for normality of residuals were performed on the data obtained by quantitative analysis. Values for real or transformed data obtained by performing ultrasonographic evaluations were compared at all timepoints using the ANOVA test and correlations were determined using the Spearman test and Bonferroni post-hoc. Mean differences were assumed to exist with a $P < 0.05$. The GraphPad Prism software (version 8.0) was used for the construction of the graphics.

8.3 Results

A significant difference was found when looking at serum progesterone concentration for each timepoint ($P < 0.05$) (Figure 8.1). Based on the study published by Gloria et al., 2018 and the similar methodology previously performed by the authors (Aires et al. 2021) where serum progesterone concentration was correlated with clinical and cytological findings, it was possible to determine that: T1 included early to mid-proestrus period, T2 corresponded to the preovulatory and ovulatory periods, T3 corresponded to the ovulatory and postovulatory periods, whereas both T4 and T5 corresponded to the postovulatory period. Two bitches exhibited a cytological diestrus during the T5 timepoint.

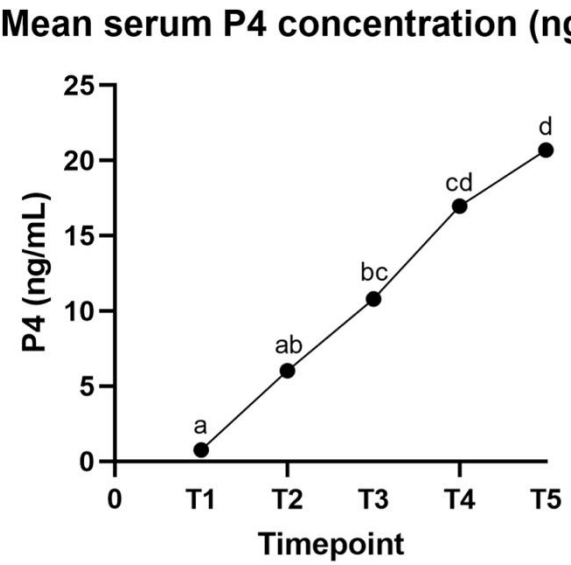

Fig. 8. 1 Graphic representation of the mean values of serum progesterone concentration (ng/mL) of bitches (n = 8) at each timepoint of evaluation. Different letters indicate statistical difference (P = 0,0001).

8.3.1 Doppler findings

Doppler evaluation was feasible and tolerated by most bitches. Some bitches became restless, and it made both the Coloured-coded and Pulsed-wave assessments challenging. In those cases, bitches were allowed to rest and walk for a while, before continuing the examination.

The subjective assessment of the Colour-coded Doppler evaluation can be seen in Figure 8.2. The vascularization patterns were similar in all bitches. It was possible to observe a discrete vascularization at T1. Ovarian vascularization markedly increased when progressing to T2, especially on the ventral surface of the ovary. After ovulation, vascularization was evident on the ventral surface, spreading to the central region of the ovary and started presenting a circular-like pattern surrounding the corpora haemorrhagica until the formation of the corpus luteum.

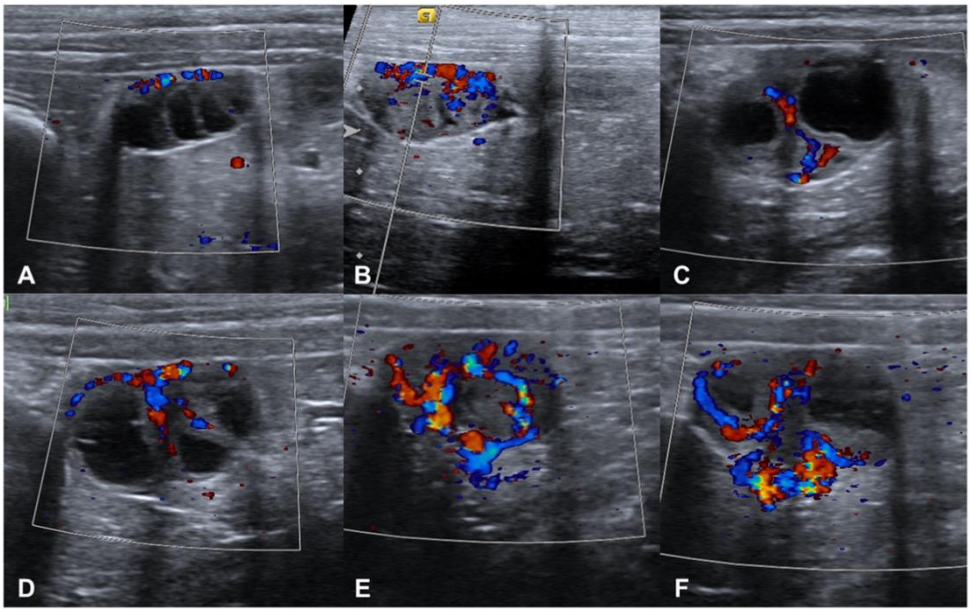

Fig. 8. 2 Color-coded Doppler evaluation of the right ovary of the bitch. A) early proestrus (P4 = 0.56 ng/mL). Vascularization is discreet and present only in the ventral surface of the ovary. B) postovulatory estrus (P4 = 8.9 ng/mL). It is possible to observe an increase in the number of coloured pixels present in the ventral surface. C) postovulatory estrus (P4 = 14.6 ng/mL), where vasculature is starting to present a semi-circular pattern, surrounding the ovarian structures present (corpora hemorrhagica). D) Postovulatory estrus (P4 = 22.6 ng/mL), where vasculature present is surrounding the ventral surface of the ovarian structures present. E) and F) early diestrus (based on cytological findings, P4 = 23.3 ng/mL). Markedly evident vasculature in a circular pattern, surrounding the cavitary corpora lutea. (For interpretation of the references to colour in this figure legend, the reader is referred to the Web version of this article).

In two bitches (25.0%), it was not possible to perform Pulsed-wave Doppler evaluations at T1. The waveform morphology of the intraovarian artery was similar in all bitches and was characterized by a low resistance spectral pattern, with a small systolic peak, followed by continuous diastolic flow, in which an early diastolic peak was observed (Figure 8.3). There was no difference between doppler velocimetric parameters of the left and right ovaries, therefore, only the results obtained from the left ovary were used for statistical analysis. Mean doppler-velocimetric parameters are found in Table 8.1.

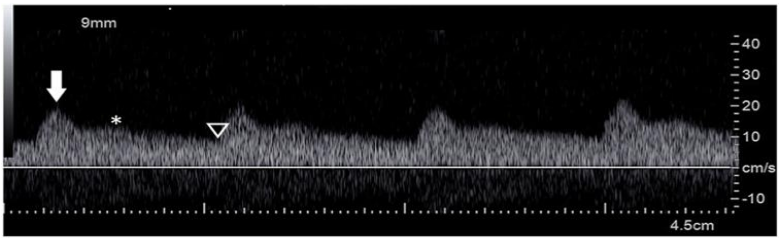

Fig. 8. 3 Pulsed-wave Doppler of the intraovarian artery, evidencing the waveform morphology characterized in four consecutive cardiac cycles. A small systolic peak (white arrow) is observed, followed by a continuous diastolic flow, in which a small diastolic peak (asterisk) is noted in the early diastolic phase. A low end-diastolic velocity is observed (hollow arrowhead).

Tab. 8. 1 Mean ± SD number of ovarian structures from each group, diameter of the greatest ovarian structure and wall thickness at each timepoint when there were evaluations as assessed by HD ultrasonography in bitches.

Timepoint	SPV (cm/s)	EDV (cm/s)	RI	PI
T1	10.93 ± 2.18^{A}	3.78 ± 2.41^{A}	0.66 ± 0.14^{A}	1.33 ± 0.55^{A}
T2	15.31 ± 5.05^{A}	6.61 ± 3.07^{AB}	0.59 ± 0.05^{A}	1.05 ± 0.13^{A}
T3	17.04 ± 3.5^{AB}	6.80 ± 1.90^{AB}	0.59 ± 0.07^{A}	1.02 ± 0.25^{A}
T4	25.96 ± 10.57^{B}	10.05 ± 4.4^{B}	0.61 ± 0.06^{A}	1.02 ± 0.2^{A}
T5	19.12 ± 7.03^{AB}	8.11 ± 4.29^{AB}	0.58 ± 0.09^{A}	1.09 ± 0.37^{A}

Different letters in the same column indicate differences ($P < 0.05$).

A numeric trend was observed for SPV and EDV values and a slight statistical difference was observed (P = 0.003 for SPV; P = 0.028 for EDV), as shown in Figure 8.4 and Table 8.1. Mean SPV and EDV showed a tendency to increase over time and at T4 there was a marked value increase for both parameters compared to the other timepoints. At T5, both parameters decreased. Furthermore, mean SPV and EDV values demonstrated a strong positive correlation with P4 concentration (r = 0.586 for SPV; r = 0; 569 for EDV). As with RI and PI, no statistical difference was found at any of the assessment timepoints (Figure 8.5).

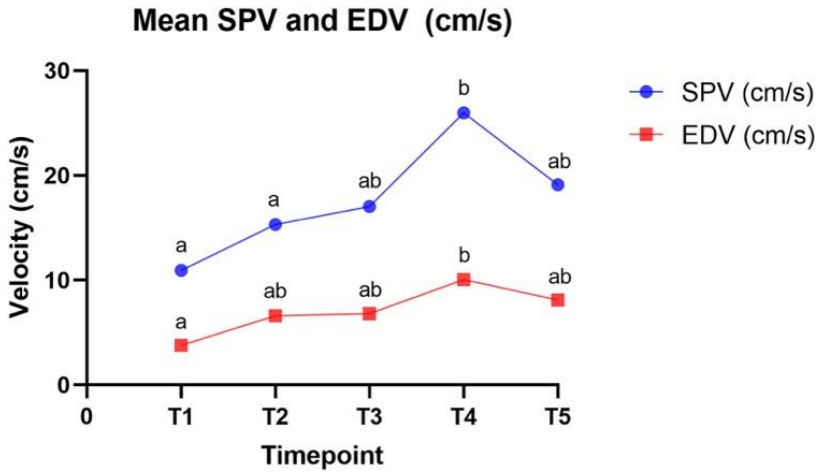

Fig. 8. 4 Graphic representation of the mean values of Systolic Peak Velocity (blue line and dot) and End-diastolic Velocity (red line and square) (cm/s) of the left ovary of bitches (n = 8) throughout the timepoints of evaluation. Different letters indicate statistical difference. (For interpretation of the references to colour in this figure legend, the reader is referred to the Web version of this article.)

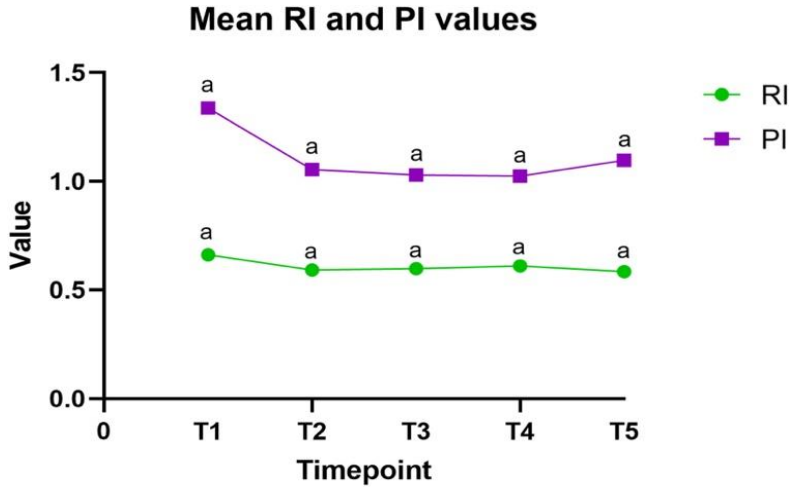

Fig. 8. 5 Graphic representation of the mean values of Resistivity Index (green line and dot) and Pulsatility Index (purple line and square) of the left ovary of bitches (n = 8) throughout the timepoints of evaluation. No difference was noted. (For interpretation of the references to colour in this figure legend, the reader is referred to the Web version of this article).

8.3.2 CEUS findings

All bitches tolerated the evaluation, although sudden moves or respiratory movements were present in some cases and hindered the assessment. Subjectively, little enhancement was present during the early proestrus, but as time progressed, peak intensity markedly increased. Despite the differences in enhancement intensity at each timepoint, all bitches showed homogenous enhancement throughout the evaluations (Figure 8.6).

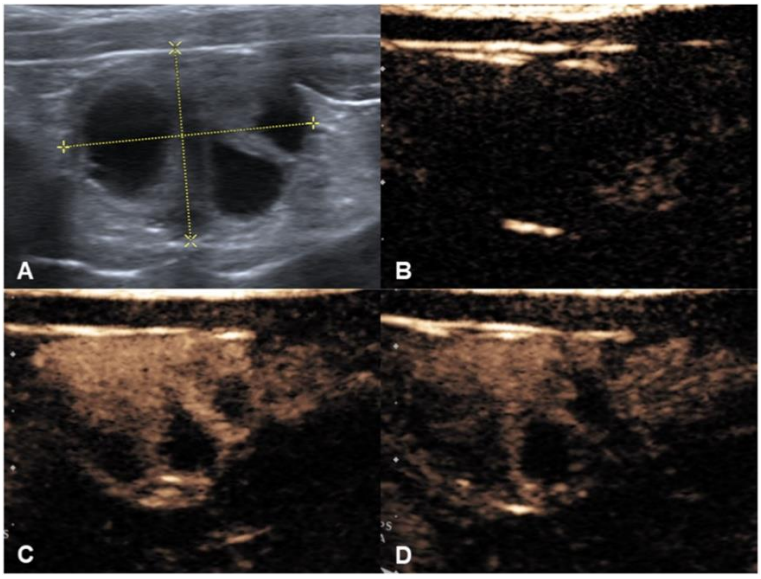

Fig. 8. 6 Contrast-enhanced ultrasonography (CEUS) of the right ovary of a bitch. A) B-mode image of the right ovary of a bitch at T4. B) Right after administration of the contrast medium (T = 0s), no enhancement is noted. C) Peak enhancement (T = 9s) is then observed with maximum pixel intensity enhancing the ovarian parenchyma, which is hyperintense compared to the adjacent tissue. Corpora hemorrhagica present have hyperintense walls and no enhancement is detected inside. D) At the end of the evaluation (T = 120s) discreet enhancement is still present.

The quantitative analysis of the CEUS study revealed that the perfusion parameters between the left and right ovary are similar, therefore, mean values of the contrast-enhanced study of the left ovary were used for statistical analysis. (Figure 8.7).

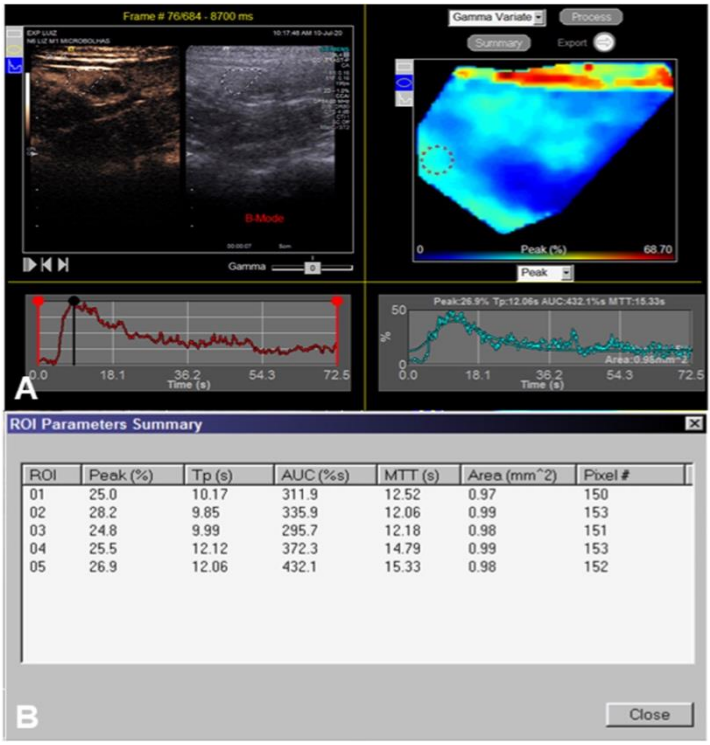

Fig. 8. 7 Quantitative CEUS evaluation using a dedicated software. A) A ROI is drawn over the contrast study and a time-intensity curve and a gamma variate map is obtained. B) Quantitative parameters are acquired from the time-intensity curve generated from the selected ROIs in the gamma variate map.

TTP (s) and Pixel variables were constant across the timepoints of evaluation ($P > 0.05$; Table 8.1), while Peak PPI (%), AUC (%) and MTT (s) were significantly higher at T5 ($P < 0.05$; Table 8.2), demonstrating a progressive increase from T1 on, similar to what was observed to P4 concentration. However, these parameters showed no correlation with P4 concentration.

Tab. 8. 2 Mean and Standard Deviation (SD) values of the perfusion variables evaluated by Contrast-enhanced ultrasonography of the bitches (n = 8) throughout the timepoints of evaluation.

Variable	Timepoint	Mean value	S.D.	P value
Peak (%)	T1	19.55^{AB}	5.05	0.037
	T2	18.70^{A}	8.06	
	T3	23.54^{ABC}	7.69	
	T4	26.67^{BC}	7.45	
	T5	29.85^{C}	8.75	
TTP (s)	T1	17.31^{A}	9.13	0.599
	T2	15.25^{A}	6.76	
	T3	16.73^{A}	2.83	
	T4	17.23^{A}	4.67	
	T5	20.31^{A}	4.96	
AUC (%/s)	T1	516.9^{A}	207.10	0.011
	T2	628.0^{A}	320.00	
	T3	801.0^{AB}	578.00	
	T4	889.0^{AB}	445.00	
	T5	1623^{B}	1052.00	
MTT (s)	T1	25.22^{A}	12.86	0.037
	T2	25.06^{A}	9.04	
	T3	27.43^{AB}	6.80	
	T4	28.76^{AB}	9.61	
	T5	38.04^{B}	15.50	
Pixels	T1	233.4^{A}	49.90	0.229
	T2	270.8^{A}	88.80	
	T3	216.9^{A}	25.04	
	T4	212.7^{A}	33.40	
	T5	236.5^{A}	42.50	

Peak (%): Peak intensity in % of pixels; TTp(s): Time to peak intensity in seconds; AUC: Area under the curve in % per second; MTT: Mean transit time in seconds.
Different letters in the same column indicate difference (Bonferroni $P < 0.05$).

8.4 Discussion

In the present study, ovarian vascularization and microcirculation were examined in eight bitches, providing information regarding ovarian perfusion at specific timepoints of the reproductive cycle. Adequate ovarian function is provided by the remodelling and angiogenic capability of the gonad's tissue and is considered a critically regulated process for ovulation and corpus luteum development and function (Reynolds et al. 1992; Adulafia & Sherer, 2000; Plendl, 2000; Devesa & Caicedo, 2019). To our knowledge, this is the first study focused on the evaluation of ovarian perfusion in the canine species using CEUS, providing unprecedented information on ovarian perfusion and hemodynamic throughout specific moments of the follicular phase of the estrous cycle.

In our study, seven bitches were pubescent, nevertheless all patients showed the expected physical and behavioural changes and regular proestrus and estrous phases and signs of ovulation, as detected by vaginal cytology findings and serum progesterone concentration. Puberty in the bitch is a complex process and Gobello (Gobello et al. 2014) stated that the first manifestation of a typical follicular phase, followed by evidence of ovulation and a normal luteal phase, are representative of sexual maturity. The fact that the majority of bitches in this study were pubescent could represent a methodological bias. However, considering that all of the pubescent bitches had a regular estrous cycle progression, we believe methodological bias was reduced. Nevertheless, further studies with bitches from different ages are required to investigate the vascular perfusion changes in canine ovaries during the follicular phase of the estrous cycle.

When using Colour-coded Doppler, an increase in the number of coloured pixels and their intensity, as well as a vascularization pattern with the progression of the evaluation period was identified. At T1, the cortical vascularization was more evident, whereas as the follicular phase progressed, the central region of the ovaries became more vascularized. The ovarian vascularization in the dog is complex. The ovarian artery branches in two little arterioles respectively cranially and caudally to the ovary, which cross the ovarian parenchyma dividing in intraovarian branches and arterioles, some of which penetrate the hilum and others lead to the cortex of the ovary (Esperança-Pina & Reis, 1984). Our findings suggest that as the follicular phase progresses over time, there is an increase in blood flow to

the cortical vessels with the hilar and medullary regions becoming more pronounced.

In the ovulatory phase, vascularization surrounding the preovulatory follicles and corpora hemorrhagica became evident. Considering that preovulatory follicles and corpora lutea are responsible for the production of angiogenic factors that are necessary for ovulation and maintenance of the luteal phase (Devesa & Caicedo, 2019), this is an expected finding consistent with other studies conducted in dogs (Vermeulen, 2009; Mansour et al. 2020). However, in the present study daily evaluations were not performed, which may limit the understanding of the changes in perfusion that can be detected by Doppler ultrasonography, as well as changes related to the upcoming ovulation.

In our study, Doppler evaluations only showed a slight statistical difference for SPV and EDV, while RI and PI did not differ across evaluation timepoints. Conversely, previous studies demonstrated an increase in SPV and EDV just before ovulation and, consequently, a decrease in RI (Koster et al. 2001; Barbosa et al. 2013), differing from our results. Considering that a numerical trend was observed for the Doppler velocimetric values and despite the slight statistical significance, we believe that our results are influenced by the small number of bitches evaluated, as well as the interval between evaluations. It is also prudent to consider technical factors regarding the acquisition of Doppler studies and the influence of the angle of the insonation. Despite the efforts to maintain angle correction as minimal as possible, differences of SPV and EDV values due to the variations of the angle of insonation cannot be completely ruled out if not accompanied by RI and PI changes, thus limiting the interpretation of the modification of these parameters. Nevertheless, we hypothesise that Doppler evaluations could be more sensitive to detect vascular modifications of the ovarian tissue if evaluations are performed more frequently.

CEUS evaluation proved to be feasible both qualitative and quantitative analysis. Subjective assessment of the ovarian perfusion demonstrated an increase in the enhancement intensity as the follicular phase progressed in all bitches, considering that the ovaries were markedly enhanced during the ovulatory and postovulatory estrus when compared to early proestrus. This can be explained by the necessity for angiogenesis for the development of follicles and ovulation, as well as for the development of corpora hemorraghica and, later, corpora lutea (Reynolds et al. 1992; Abulafia & Sherer, 2000). However, it is important to point out that, due to the fact that

daily evaluations were not performed in the present study, specific enhancement patterns could not be completely described during each day of the follicular phase to correlate them to the endocrine events that lead to ovulation. Therefore, further studies could be performed to investigate if CEUS could detect specific enhancement patterns that could be used to closely monitor physiological modifications and detect ovulation.
Quantitatively, PPI (%), AUC (%) and mTT (s) tended to increase over time, presenting a significant difference at T5. During the postovulatory period, marked tissue remodelling occurs in the ovary, where the ruptured follicles are transformed into corpora hemorraghica, which then become corpora lutea, highly vascularized ovarian structures responsible for producing and maintenance of the high levels of progesterone throughout both pregnancy and non-pregnancy diestrus in dogs (Abulafia & Sherer, 2000; Plendl, 2000; Concannon et al. 2011). CEUS resulted an interesting and a useful technique for the detection of vascularization in the ovary and gave the opportunity to detect perfusion increase during the progression of the estrous cycle, demonstrating that the important angiogenic remodelling related to the corpora lutea formation during this period could be detected by CEUS. Further CEUS studies could be useful to standardize quantitative perfusion parameters regarding the normal ovarian function and to evaluate if any abnormalities during corpora lutea formation or luteal insufficiency could lead to their modification. This perspective demonstrates that CEUS is a promising evaluation method that could be applied in the assessment of the ovarian function in women, as well as farm animals.

8.5 Conclusion

This study brings unprecedented findings regarding perfusion parameters of the ovaries of bitches during the follicular phase of the estrous cycle. Doppler evaluations only demonstrated a slight significance, however, the interval between the timepoints of evaluation could potentially limit the detection of vascular modifications of the ovaries by this technique, as well as technical factors regarding the insonation angle. CEUS evaluation demonstrated a subjective increase in the ovarian enhancement with the progression of the follicular phase, as well as quantitative perfusion differences during the postovulatory estrus, revealing that this technique could be applied for better understanding of the microvascular modifications required for the formation of corpora lutea. Additionally, further studies are

warranted to evaluate if this technique could detect abnormal ovarian perfusion that could represent abnormal corpora lutea formation and early luteal insufficiency, which, hopefully, could lead to better reproductive assessment and obstetric management in the future for veterinary patients, as well as for women.

8.6 References

Abma E, Stock E, de Spiegelaere W, van Brantegem L, Vanderperren K, Ni Y, et al. Power Doppler ultrasound and contrast-enhanced ultrasound demon- strate non-invasive tumour vascular response to anti-vascular therapy in canine cancer patients. Sci Rep 2019;9:1e12. https://doi.org/10.1038/s41598- 019-45682-2.

Abulafia O, Sherer DM. Angiogenesis of the ovary. Am J Obstet Gynecol 2000;182:240e6. https://doi.org/10.1016/S0002-9378(00)70519-9.

Aires LPN, Gasser B, Silva P, del Aguila Da Silva P, Silveira MV, Carneiro RK, et al. High-definition ultrasonography in the evaluation of the reproductive tract of bitches during the follicular phase of the estrous cycle. Anim Reprod Sci 2021;234. https://doi.org/10.1016/j.anireprosci.2021.106870.

Barbosa CC, Souza MB, Scalercio SRRA, Silva TFP, Domingues SFS, Silva LDM. Ovarian and uterine periovulatory Doppler ultrasonography in bitches. Pesqui Vet Bras 2013;33:1144e50. https://doi.org/10.1590/S0100- 736X2013000900016.

Bicudo ALC, Mamprim MJ, Lopes MD, Vulcano LC, Derussi AAP. [Conventional ultrasound examination and dopplerfluxometry of ovarian of bitch during the follicular phase of the oestral cycle]. Vet Zootec 2010;17:507e18 [Portuguese].

Bishop Cv, Molskness TA, Xu F, Belcik JT, Lindner JR, Slayden OD, et al. Quantification of dynamic changes to blood volume and vascular flow in the primate corpus luteum during the menstrual cycle. J Med Primatol 2014;43: 445e54. https://doi.org/10.1111/jmp.12132.

Boote EJ. AAPM/RSNA Physics Tutorial for Residents: topics in US: Doppler US techniques: concepts of blood flow detection and flow dynamics. Radio- graphics 2003;23:1315e27. https://doi.org/10.1148/rg.235035080.

Carvalho CF, Chammas MC, Cerri GG. Princípios físicos do Doppler em ultra-sonografia. Cie^ncia Rural 2008;38:872e9. https://doi.org/10.1590/s0103- 84782008000300047.

Concannon PW. Reproductive cycles of the domestic bitch. Anim Reprod Sci 2011;124:3e4. https://doi.org/10.1016/j.anireprosci.2010.08.028.

Cosgrove D. Angiogenesis imaging - ultrasound. Br J Radiol 2003;76:S43e9. https://doi.org/10.1259/bjr/86364648.

Cosgrove D. Ultrasound contrast agents: an overview. Eur J Radiol 2006;60: 324e30. https://doi.org/10.1016/j.ejrad.2006.06.022.

References

Davidson AP, Baker TW. Reproductive ultrasound of the bitch and queen. Top Companion Anim Med 2009;24:55e63. https://doi.org/10.1053/j.tcam.2008.11.002.

Devesa J, Caicedo D. The role of growth hormone on ovarian functioning and ovarian angiogenesis. Front Endocrinol 2019;10:450. https://doi.org/10.3389/fendo.2019.00450.

England G, Concannon PW. Determination of the optimal breeding time in the bitch: basic considerations. In: Concannon PW, England GCW, Verstegen III J, editors. Recent advances in small animal reproduction. Ithaca: International Veterinary Information Service; 2002.

England GCW, Russo M, Freeman SL. Follicular dynamics, ovulation and conception rates in bitches. Reprod Domest Anim 2009;44:53e8. https://doi.org/10.1111/j.1439-0531.2009.01416.x.

Esperança-Pina JA, Reis AM. Arterial component of the angioarchitecture of the canine ovary. Cells Tissues Organs 1984;120:112e6. https://doi.org/10.1159/000145903.

Feliciano MAR, Ramirez RAU, Maronezi MC, Maciel GS, Avante ML, Senhorello ILS, et al. Accuracy of four ultrasonography techniques in pre- dicting histopathological classification of canine mammary carcinomas. Vet Radiol Ultrasound 2018;59:444e52. https://doi.org/10.1111/vru.12606.

Feliciano MAR, Uscategui RAR, Maronezi MC, Simo~es APR, Silva P, Gasser B, et al. Ultrasonography methods for predicting malignancy in canine mammary tumors. PLoS One 2017;12:1e14. https://doi.org/10.1371/ journal.pone.0178143.

Fraser HM, Wulff C. Angiogenesis in the corpus luteum. Reprod Biol Endocrinol 2003;1:1e8. https://doi.org/10.1186/1477-7827-1-88.

Gasser B, Rodriguez MGK, Uscategui RAR, Silva PA, Maronezi MC, Pavan L, et al. Ultrasonographic characteristics of benign mammary lesions in bitches. Vet Med 2018;63:216e24. https://doi.org/10.17221/87/2017-VETMED.

Gloria A, Contri A, Carluccio A, Robbe D. Blood periovulatory progesterone quantification using different techniques in the dog. Anim Reprod Sci 2018;192:179e84. https://doi.org/10.1016/j.anireprosci.2018.03.006.

Gobello C. Prepubertal and pubertal canine reproductive studies: conflicting aspects. Reprod Domest Anim 2014;49:e70e3. https://doi.org/10.1111/rda.12414.

References

Hastings JM, Morris KD, Allan D, Wilson H, Millar RP, Fraser HM, et al. Contrast imaging ultrasound detects abnormalities in the marmoset ovary. Am J Primatol 2012;74:1088e96. https://doi.org/10.1002/ajp.22063.

Johnston SD, Root Kustritz M v, Olson PNS. Canine and feline theriogenology. 2001.

Jurczak A, Janowski T. Arterial ovarian blood flow in the periovulatory period of GnRH-induced and spontaneous estrous cycles of bitches. Theriogenology 2018;119:131e6. https://doi.org/10.1016/j.theriogenology.2018.06.014.

Koster K, Poulsen Nautrup C, Gunzel-Apel A. A Doppler ultrasonographic study of cyclic changes of ovarian perfusion in the Beagle bitch. Reproduction 2001;122:453e61. https://doi.org/10.1530/rep.0.1220453.

Lévy X, Fontbonne A. Determining the optimal time of mating in bitches: particularities. Rev Bras Reprod Anim 2007;31:128e34.

Mansour A, Abdeldjelil MC, Bougherara H, Khellaf D, Aissi A. Color-Doppler ultrasonography to predict the moment of ovulation in the bitch. Adv Anim Vet Sci 2020;8. https://doi.org/10.17582/journal.aavs/2020/8.7.782.787.

Marret H, Brewer M, Giraudeau B, Tranquart F, Satterfield W. Assessment of cyclic changes of microvessels in ovine ovaries using Sonovue® contrast- enhanced ultrasound. Ultrasound Med Biol 2006;32:163e9. https://doi.org/ 10.1016/j.ultrasmedbio.2005.10.004.

Orlandi R, Vallesi E, Boiti C, Polisca A, Troisi A, Righi C, et al. Contrast-enhanced ultrasonography of maternal and fetal blood flows in pregnant bitches. Theriogenology 2019;125:129e34. https://doi.org/10.1016/ j.theriogenology.2018.10.027.

OrlandiR,VallesiE,BoitiC,PoliscaA,BargelliniP,TroisiA.Characterizationof testicular tumor lesions in dogs by different ultrasound techniques. Animals 2022;12:210. https://doi.org/10.3390/ani12020210.

Plendl J. Angiogenesis and vascular regression in the ovary. Anat Histol Embryol 2000;29:257e66. https://doi.org/10.1046/j.1439-0264.2000.00265.x.

Polisca A, Zelli R, Troisi A, Orlandi R, Brecchia G, Boiti C. Power and pulsed Doppler evaluation of ovarian hemodynamic changes during diestrus in pregnant and nonpregnant bitches. Theriogenology 2013;79:219e24. https:// doi.org/10.1016/j.theriogenology.2012.08.005.

QuartuccioM,LiottaL,CristarellaS,LanteriG,IeniA,D'arrigoT,etal.Contrast-enhanced ultrasound in cystic endometrial hyperplasiaepyometra

complex in the bitch: a preliminary study. Animals 2020;10:1368. https://doi.org/ 10.3390/ani10081368.

Reynolds LP, Killilea SD, Redmer DA. Angiogenesis in the female reproductive system. Faseb J 1992;6:886e92. https://doi.org/10.1096/FASEBJ.6.3.1371260.

Russo M, Vignoli M, England GCW. B-mode and contrast-enhanced ultraso- nographic findings in canine prostatic disorders. Reprod Domest Anim 2012;47:238e42. https://doi.org/10.1111/rda.12059.

Silva P, Maronezi MC, Padilha-Nakaghi LC, Gasser B, Pavan L, Aires LPN, et al. Contrast-enhanced ultrasound evaluation of placental perfusion in brachice- phalic bitches. Theriogenology 2021;173:230e40. https://doi.org/10.1016/ j.theriogenology.2021.08.010.

Spada S, England GCW, Vignoli M, Carluccio A, Russo M. Contrast-enhanced ultrasound imaging of prostate gland in neutered dogs. Animals 2021;11:559. https://doi.org/10.3390/ani11020559.

Tang MX, Mulvana H, Gauthier T, Lim AKP, Cosgrove DO, Eckersley RJ, et al. Quantitative contrast-enhanced ultrasound imaging: a review of sources of variability. Interface Focus 2011;1:520e39. https://doi.org/10.1098/ rsfs.2011.0026.

Troisi A, Orlandi R, Bargellini P, Menchetti L, Borges P, Zelli R, et al. Contrast- enhanced ultrasonographic characteristics of the diseased canine prostate gland. Theriogenology 2015;84:1423e30. https://doi.org/10.1016/ j.theriogenology.2015.07.029.

Vermeulen MaE. Ovarian color-Doppler ultrasonography to predict ovulation in the bitch [master thesis, veterinary medicine Louisiana state university]. Utrecht University Repository; 2009.

Volta A, Manfredi S, Vignoli M, Russo M, England GCW, Rossi F, et al. Use of contrast-enhanced ultrasonography in chronic pathologic canine testes. Reprod Domest Anim 2014;49:202e9. https://doi.org/10.1111/rda.12250.

Wilborn RR, Maxwell HS. Clinical approaches to infertility in the bitch. Vet Clin North Am Small Anim Pract 2012;42:457e68. https://doi.org/10.1016/ j.cvsm.2012.01.016.

Wilson SR, Burns PN. Microbubble-enhanced US in body imaging: what role? Radiology 2010;257:24e39. https://doi.org/10.1148/radiol.10091210.

Chapter 9

Effect of Maca aqueous extract addition to a freezing extender for canine semen

Cocchia N, Merlo B, Calabria A, Spada S, Iacono E, Ciarcia R, Damiano S, Giordano E, Laperuta F, Gasparrini B, Del Prete C. Effect of Maca aqueous extract addition to a freezing extender for canine semen. Vet Res Commun. 2023 Sep 7. doi: 10.1007/s11259-023-10163-5. Epub ahead of print. PMID: 37676460.

Effect of Maca aqueous extract addition to a freezing extender for canine semen

9.1 Introduction

Cryopreservation of canine semen has become an increasingly popular technology. The outcome of artificial insemination with frozen semen is dictated by the quality of semen after thawing. Cryopreservation determines extensive oxidative damage to all cellular components resulting in a decreased semen quality, indicated by reduced viability, motility, and DNA integrity, and increased acrosome damage, and apoptosis, interfering with the fertilization capability (Kim et al. 2010).
In order to reduce cryopreservation-induced oxidative stress, extender supplementation with antioxidants has been proposed (Mahiddine and Kim 2021). Lepidium meyenii (Maca) is an Andean plant of the Brassicaceae family native of Peru, known for its antioxidant properties (Fu et al. 2021). Oral administration of Maca improves semen quality and hence sperm cryotolerance in bulls and stallions (Clément et al. 2010; Del Prete et al. 2018). A beneficial effect of Maca extract on in vitro fertilization outcome, associated to increased acrosome reaction and sperm motility, was also observed in mice (Aoki et al. 2019). It was recently demonstrated that the addition of Maca extract to the extender improves the quality of canine semen stored at 4 °C (Del Prete et al. 2022).
The aim of this study was to evaluate the effect of the addition of aqueous extract of Maca in the extender prior freezing on the post-thaw quality of dog spermatozoa.

9.2 Material and Methods

One ejaculate was collected by artificial vagina from each of ten dogs (n = 10) of different breeds (Rottweiler, English Setter, Shih Tzu, English Pointer, Miniature poodle), rang- ing between 2 and 8 (median of 5.5) years of age, housed in the FOOF breeder center (Caserta, Italy), where semen is routinely collected twice a week for inseminations purpose. Sperm rich fractions were examined for volume (mL) by aspiration into a 5-mL pipette, concentration using a Bürker counting chamber and for motility by Sperm Class Analyzer (SCA) system (Microptic SL, Veterinary Edition, Barce- lona, Spain).
A single-layer centrifugation (600 x g for 10 min) of raw semen with a cushion (Glucose 59.95 g, Sodium citrate tribasic dihydrate 3.7 g, Disodium EDTA 3.7 g, Sodium bicar- bonate 1.2 g, in 1 L of deionized water) was

used to partial eliminate seminal plasma as good as possible. After removal of supernatant, a two-step freezing protocol was performed. Semen was first diluted at room temperature (RT: 20–25 °C) with TCG (Tris 2.4 g, Citric Acid 1.4 g, Glucose 0.8 g, Penicillin G Sodium Salt 0.06 g, Streptomycin 0.1 g and distilled water to 100 ml) with 20% egg yolk and 3% glycerol to reach a concentration of 400×106 sperm/mL, and cooled over 30 min to 4 °C. Samples were then diluted 1:1 (v/v) to 200×106 sperm/mL with either TCG with 20% egg yolk, 7% glycerol and 1% Equex STM without (Ctrl) or with the addition of 10 µl/mL of aqueous extract of Maca (Maca) and equilibrated for additional 5 min at 4 °C.

Raw semen was centrifuged on a cushion at 600 x g for 10 min to partial eliminate the seminal plasma. After removal of supernatant, a two-step freezing protocol was performed. Semen was first diluted at room temperature (RT: 20–25 °C) with TCG (Tris 2.4 g, Citric Acid 1.4 g, Glucose 0.8 g, Penicillin G Sodium Salt 0.06 g, Streptomycin 0.1 g and distilled water to 100 ml) with 20% egg yolk and 3% glycerol to reach a concentration of 400×106 sperm/mL, and cooled over 30 min to 4 °C. Samples were then diluted 1:1 (v/v) to 200×106 sperm/mL with either TCG with 20% egg yolk, 7% glycerol and 1% Equex STM without (Ctrl) or with the addition of 10 µl/mL of aqueous extract of Maca (Maca) and equilibrated for additional 5 min at 4 °C. The preparation and composition of the aqueous extract of Maca were previously described (Del Prete et al. 2022). Diluted semen was frozen on liquid nitrogen (LN2) after 10 min suspension on vapor and stored for 4 weeks. Two straws per sample were thawed in a 37 °C water bath for 30 s.

Motility, kinetics, membrane integrity and mitochondrial membrane potential (MMP), as well as the levels of malondialdehyde (MDA), indicator of lipid peroxidation, were evaluated before freezing (fresh semen) and immediately post-thaw (T0). To evaluate post-thaw sperm longevity, x thermal-resistance test was conducted, evaluating samples at 1 (T1) and 2 h (T2) of incubation at 37 °C for motility and kinetics, sperm membrane integrity and mitochondrial membrane potential.

9.2.1 Semen collection and processing

Motility was assessed using Sperm Class Analyzer (SCA) system (Microptic SL, Veterinary Edition, Barcelona, Spain) installed on a camera-equipped light microscope system (Eclipse E200, Nikon, Japan). The

parameters included were: total motility (%), progressive motility (%), the percentage of sperm subpopulations (rapid, medium and slow), average path velocity (VAP; µm/s), straight-line velocity (VSL; µm/s), curvilinear velocity (VCL; µm/s), straightness (STR; %) and linearity (LIN; %), amplitude of lateral head (of lateral H; µm), wobble (WOB = VAP/VCL; %), beat cross frequency (BCF; beats/s). All particles sized between 10 and 80 µm2 were considered spermatozoa and classified as progressive motile in case of STR > 75%. SCA system setup was described in a previous study (Del Prete et al. 2018). For the evaluation, three µl of semen were placed in a 20 µm chamber (Leja, Nieuw-Vannep, Netherlands) pre-warmed at 37 °C. The evaluation was carried out at 100X magnification on a pre-warmed microscope stage and at least 500 spermatozoa in five randomly selected fields were assessed.

Mitochondrial transmembrane potential and membrane integrity were assessed by triple fluorescent labelling with propidium iodide (PI; InvitrogenTM, Eugene, Oregon, USA), SYBR green-14, and 5,5′,6,6′-tetrachloro-1,1′,3,3′- tetraethylbenzimi-dazolylcarbocyanine iodide (JC-1; Molecular Probes, Eugene, OR, USA) (Figure 9.1).

Thirty µL of each sample were incubated with 3 µl of SYBR green solution (5 µl SYBR-14 a10x + 15 µl PBS), 2 µl of PI solution (10 mg/ml) and 2 µl JC-1 solution (1 mg/ ml) at 37 °C in the dark for 15 min. At least 200 cells per sample were evaluated using confocal microscopy (Leica DM6B; Leica Microsystems, Wetzlar, German). Three sperm populations were identified: dead sperm (PI+), viable sperm with high MMP (HMMP) and viable sperm with low MMP (LMMP).

Sperm concentration of malondialdehyde (MDA) was measured using the thiobarbituric acid (TBA) procedure as previously described (Esterbauer and Cheeseman 1990). Concentrations of MDA were calculated using a calibration curve ranged between 0.5 and 2 pmoles/mL. The results were expressed as nmol/L of proteins.

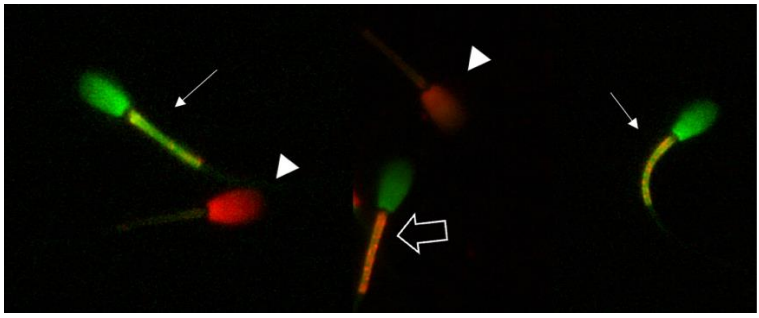

Fig. 9. 1 Example of canine sperm cells stained by SYBR-14/PI/JC-1: dead sperm (PI+; head arrow), viable sperm with high mitochondrial membrane potential (HMMP; SYBR-14+/PI-/JC-1+; big arrow) and viable sperm with low mitochondrial membrane potential (LMMP; SYBR-14+/PI-/JC-1-; small arrows).

9.2.6 Statistical analysis

Data were analyzed with Statistical Package for Social Sciences (SPSS IBM® Statistics version 27.0, IBM Corporation, Armonk, NY, USA). Because of non-normal distribution (Shapiro-Wilk test), results were expressed as median and interquartile range (IQR) and Wilcoxon non-parametric test was used to compare groups at each time point (Fresh semen, Post-thaw, T1, T2). The effect of storage time on semen parameters in each group (Ctrl or Maca) was evaluated Friedman test, post hoc analysis with Wilcoxon's signed-rank test was used to compare individual storage times.

9.3 Results

Fresh semen volume ranged between 0.4 and 12 mL (median of 2.4 mL), with a median concentration of 312.5×106 sperm/ml (IQR: 269,5- 462 sperm/mL). Fresh semen pre- sented a viability of 84 (79.3–85) % and HMMP of 38.5 (36-44.8) %.

Sperm motility and kinetic parameters of fresh semen and ctrl and Maca-treated semen post-thaw (T0, T1 and T2) are shown in Table 9.1. As expected, a reduction ($p \leq 0.05$) in total motility in both groups was observed post-thaw at T0 and T1 compared to fresh semen. Furthermore, total motility decreased ($p \leq 0.05$) at T1 and T2 compared to T0 (Table 9.1). Progressive motility decreased ($p \leq 0.05$) at increasing post-thawing times in the ctrl group, whereas it was not affected in the Maca-treated group. The

percentage of hyperactivated spermatozoa remained constant during the four time points in the ctrl, while increased ($p \leq 0.05$) in the Maca-treated semen at T1 and T2.

Tab. 9. 1 Total and progressive motility and the percentages of hyperactivated, rapid, medium and slow-moving spermatozoa assessed using Sperm Class Analyzer (SCA) in Control and Maca-treated (10 µL/mL of aqueous extract of Maca) dog semen (n = 10) before freezing (Pre), immediately after thawing and after 1 (T1) and 2 h (T2) of incubation at 37°C. All values are expressed as median and interquartile range (IQR); asterisk indicates statistical difference between groups at p≤ 0.05; the letters indicate statistically differences at at p≤ 0.05 between time points within each group.

	Total motility (%)		Progressive motility (%)		Hyperactive (%)	
	Control	*Maca*	*Control*	*Maca*	*Control*	*Maca*
Pre	86.4 (79.8-93)[a]	-	25.8 (20-39.7)[a]	-	2.8 (0.5-4.1)[a]	-
Post	31.2 (25.6-60.1)[b]	40.4 (28.5-58)[b]	7.4 (1.5-14.9)[a]	9.3 (0.6-23)[a]	0.5 (0-2.9)[a]	1.8 (0-6.7)[a]
T1	23.8 (15.9-36.3)[c]	33.1 (18-40.1)[*, c]	4.7 (0-7.9)[b]	5.5 (0.4-12.1)[a]	1.9 (0-11.1)[a]	6.8 (1.7-16.9)[b]
T2	25.6 (12.7-32.8)[c]	26.8 (10.5-42)[c]	0.5 (0-7.1)[b]	3.6 (0.4-9.6)[a]	4.3 (0-12.3)[a]	10 (0.7-17.9)[b]
	Rapid (%)		Medium (%)		Slow (%)	
	Control	*Maca*	*Control*	*Maca*	*Control*	*Maca*
Pre	16.4 (4.6-32)[a]	-	26.2 (23.2-29.8)[a]	-	35.8 (32.1-45.4)[a]	-
Post	5.7 (0-16.1)[a]	8.5 (1.7-20.7)[a]	2.1 (1.6-6.5)[b]	4.1 (2.6-6.9)[b]	25.5(19.4-32.2)[a]	26.9 (21.3-29.1)[a]
T1	4.7 (0-10.6)[a]	4.5 (1.4-16.1)[a]	1.4 (0.4- 2.8)[b]	2.3 (0.7-4)[*, b]	17.7 (12.2-22.1)[b]	19.2 (13-25.5)[b]
T2	1.1(0-10)[a]	4.6 (0.4-15.8)[a]	0.9 (0-2.1)[b]	2.1 (0.2-3.7)[b]	19.5 (11.9-22.3)[b]	21 (9.8-23.8)[b]

The pattern of the motile-sperm subpopulations (rapid, medium, slow) during thermal stress was similar in the two groups. Most of the sperm kinetic parameter followed the same pattern in the two groups over time (Table 9.2). However, in the ctrl group VSL decreased ($p \leq 0.05$) at T2, whereas in the maca-treated group remained at values similar to fresh semen at T0, T1 and T2. The LIN decreased ($p \leq 0.05$) in the ctrl group at T0, with a further reduction ($p \leq 0.05$) detected at T1 and T2; in contrast, in maca-treated group no decrease was observed after freezing and post-thaw incubation times.

Total motility and the percentage of sperm with medium velocity were higher ($p \leq 0.05$) in Maca-treated semen than in the ctrl after 1 h of incubation at 37 °C (T1; Table 9.1). At the same time point, WOB was

remarkably higher ($p \leq 0.05$) in Maca-treated group than in the ctrl (Table 9.2). There were no other differences in semen kinetic parameters between the two groups, as shown in Table 9.2.

Tab. 9. 2 Sperm velocities in control and Maca-treated (10 µL/mL of aqueous extract of Maca) canine semen (n=10) at different time points, before freezing (Pre), immediately after thawing (Post) and after 1 (T1) and 2 h (T2) of incubation at 37°C. All values are expressed as median and interquartile range (IQR). Significant differences between groups are indicated by an asterisk with $p \leq 0.05$; within each group (column), means with different letters (a–c) differed between time points ($p \leq 0.05$).

	VCL (µm/s)		VSL(µm/s)		VAP(µm/s)	
	Control	*Maca*	*Control*	*Maca*	*Control*	*Maca*
Pre	70.8 (57.5-82.9) [a]	-	40.1 (33.4-46.6)[a]	-	50.5 (45.8-60.9)[a]	-
Post	51.4 (28.7-71.8) [a]	59.9 (39.7-81.5) [a]	26.9 (15.8-33.7)[a]	34.7 (15.4-44.4) [a]	34.2(20.1-40.9)[b]	40.1 (24-52.7) [b]
T1	49.9 (25.2-77.6) [a]	57.7(37.1-80) [a]	21.1 (5.9-31)[ab]	23.2 (8.8-38.1) [a]	28 (10.5-42.1)[b]	31.7 (15.7-50.3) [b]
T2	33.5 (24-79.7) [a]	52.8 (25.9-88.9) [a]	9.3 (4.3-34.1) [b]	21.2 (7.1-29.3) [a]	15.3 (8.9-46.1)[b]	29.5 (11.7-48.6) [b]
	LIN (%)		STR(%)		WOB(%)	
	Control	*Maca*	*Control*	*Maca*	*Control*	*Maca*
Pre	51.5 (49.9-53.6) [a]	-	70.1 (66.9-73.7) [a]	-	70.7 (66.5-72.4)[a]	-
Post	37.2 (33.1-46.2) [b]	46 (23.1-51.7) [a]	64.1 (57-67) [a]	70.2 (52.5-71.9) [a]	55.2 (50.3-63.2) [b]	62.9 (41.8-66.9) [b]
T1	27.2 (17.7-32.4) [c]	30.8 (16.8-34.4) [a]	57.1 (48.1-59.8) [a]	59 (38.5-62.9) [a]	43.4 (36.9-51.4) [c]	48.4 (44.6 -53.1)*[b]
T2	24.8 (9.9-33.3) [c]	23.1 (15.1-34.4) [a]	55 (35.8-61.6) [a]	53.9 (47.8-64.3) [a]	46 (31.4-51.1) [c]	43.5 (31.3-51.5) [b]
	ALH (µm)		BCF (beat/s)			
	Control	*Maca*	*Control*	*Maca*		
Pre	1.7 (1.3-1.9) [a]	-	11.4 (9.1-12.7) [a]	-		
Post	1.3 (0.9-1.7) [a]	1.5 (1.1-1.8) [a]	6.1 (4.6-8.9) [a]	7.9 (4.6-11.5) [a]		
T1	1.4 (0.9-1.9) [a]	1.4 (1.2-2) [a]	5 (2-7.6) [a]	5.8 (3-8.7) [a]		
T2	1.1 (0.9-2) [a]	1.4 (0.9-2.3) [a]	3.4 (0.9-7.6) [a]	5.2 (2-7.7) [a]		

VCL: curvilinear velocity; VSL: straight-line velocity; VAP: average path velocity; LIN: linearity; STR: straightness; ALH: amplitude of lateral head; WOB: wobble (VAP/VCL); BCF: beat cross frequency.

As shown in Figure 9.2A, the percentage of viable sperm with HMMP decreased at post-thaw (T0) and at T1 compared to fresh semen, with a further decrease recorded at T2 in both groups ($P < 0.05$). Viable sperm with LMMP did not differ between fresh and post-thaw (T0) semen in both groups. However, a decrease of viable sperm with LMMP was observed in ctrl group between T0 and T1 and in Maca group between T1 and T2 (Figure 9.2B). No differences were found between Maca and ctrl groups at any time points.

As shown in Figure 9.3, lipid peroxidation did not differ between fresh and post-thaw (T0) semen in both groups; however, the MDA concentration at T0 was lower in Maca-treated semen than in the ctrl ($p < 0.05$).

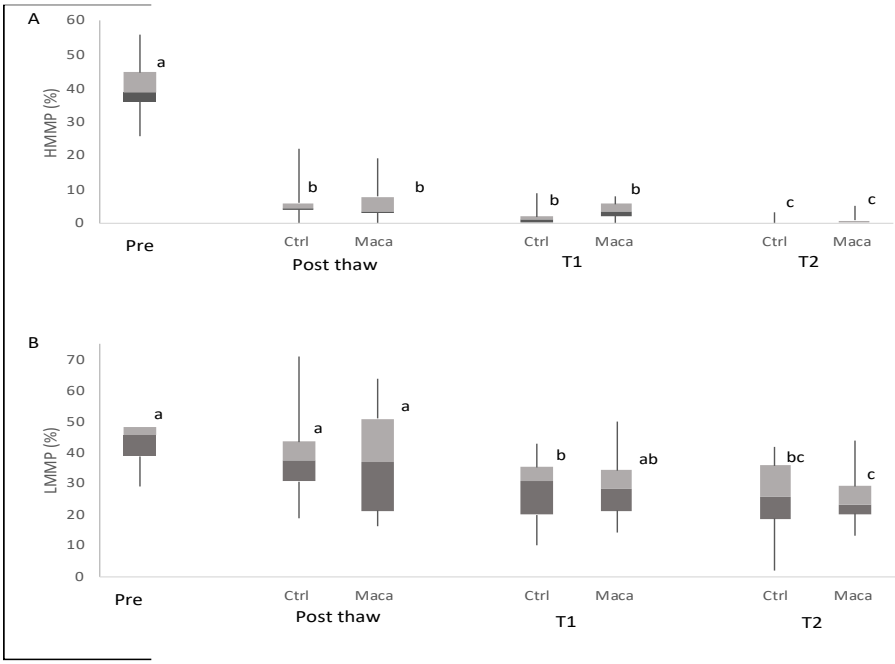

Fig. 9. 2 The percentage of viable sperm with high mitochondrial potential (HMMP: SYBR-14+/PI-/JC-1+) (a) and with low mitochondrial membrane potential (LMMP; SYBR-14+/ PI-/JC-1-) (b) in ctrl and Maca- treated dog semen (n = 10) at dif- ferent time points, before freezing (fresh semen), immediately after thawing (T0) and after 1 (T1) and 2 h (T2) of incubation at 37 °C. For each box, the central line represents the median, the edges represent the IQR (25th and 75th percentiles), the whiskers represent the extreme points; the letters (a-c) indicate significant differences at $p \leq 0.05$ between time points and groups.

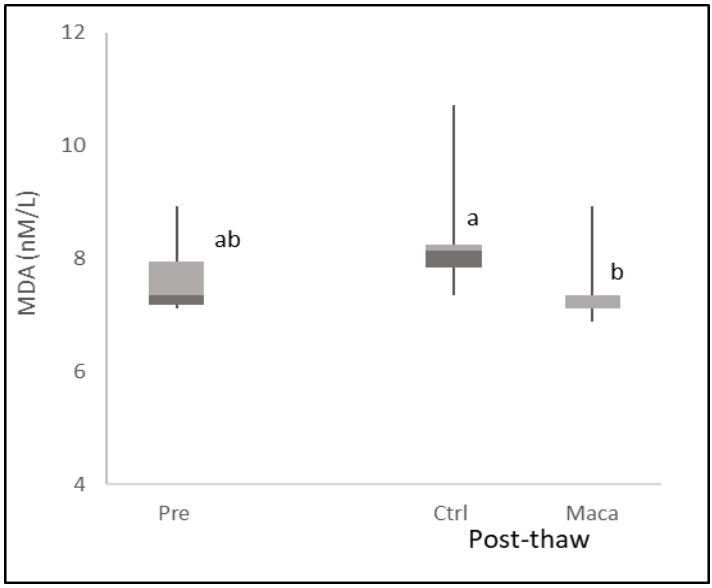

Fig. 9. 3 Lipid peroxidation before freezing (Fresh semen) and immediately post-thaw (T0) in Control (Ctrl) and Maca-treated (Maca) dog semen (n = 10). For each box, the central line represents the median, the edges represent the IQR (25th and 75th percentiles), the whiskers represent the extreme points; the letters (a,b) indicate significant differences at p ≤ 0.05 between time points and groups.

9.4 Discussion

This study showed a potential beneficial effect of Maca on sperm cryotolerance, indicated by reduced post-thaw lipid peroxidation, increased total motility, medium velocity and WOB after 1 h post-thawing incubation, as well as by the pattern of temporal decrease of other quality-related parameters.

Sperm motility is the most commonly used indicator of semen quality before and after freezing-thawing process (Martìnez 2004). Motility is expression of structural and functional competence of spermatozoa, and it is necessary to reach and colonize the oviduct (Scott 2000). A beneficial effect of Maca on sperm motility of refrigerated canine semen was previously recorded (Del Prete et al. 2022). Likewise, it was reported that Maca improves motility of human sperm (Leiva-Revilla et al. 2022) and frozen-thawed bovine sperm (Aoki et al. 2019).

An interesting finding was the increase in hyperactivation and WOB of canine frozen-thawed sperm after 1 h incubation at 37 °C when Maca was used. It has been suggested that hyperactivated bovine sperm with high WOB are able to efficiently progress in a fluid similar to cervical and oviductal mucus, reaching the oocyte more quickly (Hyakutake et al. 2018). Therefore, we speculate that the use of a Maca-supplemented extender for canine semen cryopreservation, due to the increased hyperactivated spermatozoa, may improve fertilization rates. Meanwhile, if the hyperactivation is acquired too early, the sperm cells drain their energy and risk not reaching the oocyte, reducing the efficiency of in vivo fertilization. Improved sperm hyperactivation was already reported 3 h after the addition of the same aqueous extract of Maca in cooled semen (Del Prete et al. 2022). This effect may be due to the presence of alkaloids in Maca known to increase cyclic adenosine monophosphate and intracellular calcium, important for the regulation of sperm movement (Wang et al. 2009).

Sperm motility depends on the energy supply provided by either oxidative phosphorylation or glycolysis and is correlated to inner mitochondrial potential in stallions and humans (Love et al. 2003). A decrease of mitochondrial membrane potential has been considered an early sign of apoptosis (Martin et al. 2004). In the present study freezing decreased sperm motility, that was associated with a decreased proportion of viable sperm with high mitochondrial membrane potential (HMMP). This is in contrast with an earlier study, in which low sperm motility was found to be unexpectedly associated with a high proportion of sperm with HMMP (Volpe et al. 2009).

Another interesting result of this study is the protective role of Maca against lipid membrane peroxidation of canine spermatozoa. Lipid peroxidation is caused by an increased production of ROS during the cryopreservation procedure (Lucio et al. 2016) and is a known marker of oxidative stress. Due to the high content of polyunsaturated fatty acids in the membrane, dog spermatozoa are highly sensitive to lipid peroxidation and less resistant to cooling (Bencharif et al. 2008). Our results agree with those of a previous study reporting the beneficial effects of Maca on the plasma membrane of canine cooled sperm (Del Prete et al. 2022). This effect may be due to the antioxidant activity of phenolic compounds and specific alkamides contained in Maca (Tafuri et al. 2019). Phenols act as effective inhibitors of peroxidation, by chelating redox-active metal ions and inhibiting free-radical mediated events (Rice-Evans 2001). Maca-specific alkamides called

‘Macamides’ scavenge free radicals and thus protect sperm cells from oxidative damage (Tafuri et al. 2019).

In conclusion, the supplementation of the extender with 10 µl/mL of aqueous extract of Maca prior freezing could ameliorate the cold shock resistance of spermatozoa, improving the fertility of frozen-thawed canine sperm, but further studies are indeed required to investigate the effects on post-thaw quality and fertilizing ability.

9.6 References

Aoki Y, Tsujimura A, Nagashima Y, Hiramatsu I, Uesaka Y, Nozaki T, Ogishima T, Shirai M, Shoyama Y, Tanaka H, Horie S (2019) Effect of Lepidium meyenii on in vitro fertilization via improve- ment in acrosome reaction and motility of mouse and human sperm. Reprod Med Biol 18:57–64. https://doi.org/10.1002/ rmb2.12251

Bencharif D, Amirat L, Anton M, Schmitt E, Desherces S, Delhomme G, Langlois ML, Barrière P, Larrat M, Tainturier D (2008) The advantages of LDL (low density lipoproteins) in the cryopreser- vation of canine semen. Theriogenology 70:1478–1488. https:// doi.org/10.1016/j.theriogenology.2008.06.095

Clément C, Kneubühler J, Urwyler A, Witschi U, Kreuzer M (2010) Effect of maca supplementation on bovine sperm quan- tity and quality followed over two spermatogenic cycles. Theriogenology 74:173–183. https://doi.org/10.1016/j. theriogenology.2010.01.028

Del Prete C, Tafuri S, Ciani F, Pasolini MP, Ciotola F, Albarella S, Carotenuto D, Peretti V, Cocchia N (2018) Influences of dietary supplementation with Lepidium meyenii (Maca) on stallion sperm production and on preservation of sperm quality during storage at 5° C. Andrology 6(2):351–361. https://doi.org/10.1111/ andr.12463

Del Prete C, Calabria A, Longobardi V, Palumbo V, Merlo B, Iacono E, Tafuri S, Carotenuto D, Ciani F, Damiano S, Ciarcia R (2022) Effect of Aqueous Extract of Maca Addition to an Extender for Chilled Canine Semen. Animals 12:1638. https://doi.org/10.3390/ ani12131638

Esterbauer H, Cheeseman KH (1990) Determination of aldehydic lipid peroxidation products: malonaldehyde and 4-hydroxynonenal. Methods Enzymol 186:407–421. https://doi. org/10.1016/0076-6879(90)86134-h

Fu L, Wei J, Gao Y, Chen R (2021) Antioxidant and antitumoral activities of isolated macamide and macaene fractions from Lepidium meyenii (Maca). Talanta 221:121635. https://doi.org/10.1016/j. talanta.2020.121635

Hyakutake T, Mori K, Sato K (2018) Effects of surrounding fluid on motility of hyperactivated bovine sperm. J Biomech 71:183–189. https://doi.org/10.1016/j.jbiomech.2018.02.009

Kim SH, Yu DH, Kim YJ (2010) Effects of cryopreservation on phosphatidylserine translocation, intracellular hydrogen peroxide, and DNA integrity in canine sperm. Theriogenology 73:282–292. https://doi.org/10.1016/j.theriogenology.2009.09.011

References

Leiva-Revilla J, Rolón M, Siyadatpanah A, de Lourdes Pereira M, Nissapatorn V (2022) First study of in vitro protective effect of Lepidium meyenii (Maca) on frozen–thawed bovine sper- matozoa. Vet World 15:1481–1488. https://doi.org/10.14202/ vetworld.2022.1481-1488

Love CC, Thompson JA, Brinsko SP, Rigby SL, Blanchard TL, Lowry VK, Varner DD (2003) Relationship between stallion sperm motility and viability as detected by two fluorescence staining techniques using flow cytometry. Theriogenology 60:1127–1138. https://doi.org/10.1016/S0093-691X(03)00122-5

Lucio CDF, Regazzi FM, Silva LCG, Angrimani DDSR, Nichi M, Vannucchi CI (2016) Oxidative stress at different stages of two-step semen cryopreservation procedures in dogs. Theriogenology 85:1568–1575. https://doi.org/10.1016/j. theriogenology.2016.01.016

Mahiddine FY, Kim MJ (2021) Overview on the antioxidants, egg yolk alternatives, and mesenchymal stem cells and derivatives used in canine sperm cryopreservation. Animals 11:1930. https://doi. org/10.3390/ani11071930

Martin G, Sabido O, Durand P, Levy R (2004) Cryopreservation induces an apoptosis-like mechanism in bull sperm. Biol Reprod 71:28–37. https://doi.org/10.1095/biolreprod.103.024281

Martìnez AP (2004) Canine fresh and cryopreserved semen evaluation. Anim Reprod Sci 82:209–224. https://doi.org/10.1016/j.anireprosci.2004.04.024

Rice-Evans C (2001) Flavonoid antioxidants. Curr Med Chem 8:797–807. https://doi.org/10.2174/0929867013373011

Scott MA (2000) A glimpse at sperm function in vivo: sperm trans- port and epithelial interaction in the female reproductive tract. Anim Reprod Sci 60:337–348. https://doi.org/10.1016/S0378-4320(00)00130-5

Tafuri S, Cocchia N, Carotenuto D, Vassetti A, Staropoli A, Mastel- lone V, Peretti V, Ciotola F, Albarella S, Del Prete C, Palumbo V, Esposito L, Vinale F, Ciani F (2019) Chemical analysis of Lepidium meyenii (Maca) and its effects on redox status and on reproductive biology in stallions. Molecules 24:1981. https://doi.org/10.3390/molecules24101981

Volpe S, Leoci R, Aiudi G, Lacalandra GM (2009) Relationship between motility and mitochondrial functional status in canine spermatozoa. Reprod Domest Anim 44:275–278. https://doi.org/10.1111/j.1439-0531.2009.01457.x

Wang H, Looper ML, Johnson ZB, Rorie RW, Rosenkrans CF (2009) Involvement of signaling pathways in bovine sperm motility, and effect

of ergot alkaloids. In Vitro Cell Dev Biol 45:483–489. http://www.jstor.org/stable/20616579

Chapter 10

Effect of crocin supplementation in the extender on the quality of chilled canine semen

Calabria A, Del Prete C, Roberto C, Longobardi V, Spada S, Alfano MT, De Felice D, Gasparrini B, Cocchia N. Effect of crocin supplementation in the extender on the quality of chilled canine semen. Anim Reprod Sci. 2023 Dec;259:107374. doi: 10.1016/j.anireprosci.2023.107374. Epub 2023 Nov 8. PMID: 37984312.

Effect of crocin supplementation in the extender on the quality of chilled canine semen

10.1 Introduction

n the last decades, there has been an increasing interest in artificial insemination (AI) in dogs, to overcome mating inability and improve breeding programs. Regarding the latter, the shipment of chilled or frozen semen allows the movement of semen from genetically superior dogs across countries, avoiding the risks of animal transportation and improving genetic variability. Both processing and shipping procedures are easier and cheaper with chilled compared to frozen semen whose transport requires expensive equipment (Verstegen et al., 2005). Moreover, vaginal insemination with chilled semen results in higher pregnancy rates and larger litter sizes compared to frozen semen, which requires intrauterine deposition (Linde-Forsberg, 2001, Pinto et al., 1999, Rota et al., 1995).

A major limiting factor of chilled semen is the limited lifespan of spermatozoa after prolonged storage, as quality deteriorates at increasing times, imposing the use of chilled semen within 4.9 days (England and Ponzio, 1996). It follows the importance of developing strategies to extend the lifespan of sperm during storage at 4 °C. It is known that the reduced sperm longevity is due to oxidative stress, resulting from increased production of reactive oxygen species (ROS) and reduced antioxidants (Aitken, 2017, Henkel, 2005, Silvestre et al., 2021). The presence of unsaturated fatty acid in the plasma membrane increases its elasticity but makes spermatozoa highly sensitive to the attack of free radicals during cooling (Tapia et al., 2012). Oxidative stress (OS) affects sperm motility, membrane fluidity, and DNA integrity, due to ROS-induced lipid peroxidation (Verstegen et al., 2005), and hence enrichment of the semen extender with antioxidants has been proposed to prevent OS during prolonged storage at 4 °C.

The spice saffron (Crocus sativum) has anti-inflammatory, anti-proliferative, and anti-apoptotic properties (Hashemzaei et al., 2020), mainly due to its known antioxidant function (Assimopoulou et al., 2005). Crocin, one of the carotenoids responsible for the antioxidant capacity of saffron, is known to protect cells from oxidative damage by scavenging ROS (Rahaiee et al., 2015). It has been reported that crocin protects spermatozoa from OS and consequent DNA damage in deer, ram and goat (Domínguez-Rebolledo et al., 2010, Longobardi et al., 2002; Mata-Campuzano et al., 2015). Furthermore, sperm incubation with crocin improved motility,

viability, and membrane integrity, as well as blastocyst yields in cattle (Sapanidou et al., 2015).
To the best of our knowledge, the effects of crocin on dog semen have not yet been investigated. We hypothesized that the enrichment of semen extender with crocin could improve dog sperm quality during storage at 4 °C, through its antioxidant action. The aim of this study was to evaluate the effects of crocin on sperm quality parameters, such as motility, kinetics, and membrane functionality, as well as on sperm intracellular ROS levels, lipid peroxidation, and DNA fragmentation during prolonged storage at 4 °C.

10.2 Materials and Methods

10.2.1 Experimental design

In Experiment 1, ejaculates from 10 dogs were split into four aliquots that were diluted in a TRIS-egg yolk extender supplemented with 0 (control group), 0.5, 1, and 2 mM crocin (C0.5, C1, and C2 groups) and stored at 4 °C. The concentrations were chosen according to previous studies (Longobardi et al., 2020, Longobardi et al., 2021, Sapanidou et al., 2022). Sperm membrane functionality, motility, and kinetics were assessed after 3 h, 24 h, 4 days, and 7 days (4 d and 7 d) of storage.
Based on the results, in Experiment 2 the more efficient concentration of crocin (0.5 mM) was chosen to evaluate sperm intracellular ROS levels, lipid peroxidation, and DNA fragmentation compared to the control. To do so, 10 ejaculates from the same dogs were diluted in the absence (control) and presence of 0.5 mM crocin and stored for up to 4 d. The analyses were carried out at 3 h, 24 h, and 4 d.The experiment was conducted in accordance with the code of ethics (D.lgs. 26—04/03/2014), and it was approved by the Ethics Committee of the Department of Veterinary Medicine and Animal Productions at the University of Naples Federico II, Italy (prot. no. PG/2021/0057934 of 07/06/2021).

10.2.2 Animals

Semen samples were collected from 10 dogs of the “FOOF” breeder center located in the province of Caserta (Italy) through their routine practice in the framework of breeding programs. The study included 9 small breed dogs (2 French bulldogs, 1 Jack Russel, 1 Pug, 1 Shih Tzu, 1 Poodle, and 1 Cavalier King Charles Spaniel) and 1 large breed dog (Golden Retriever), with ages

ranging from 1.5 to 8 years (median age was 6). Dogs received a standard commercial dog food twice daily and water ad libitum. All dogs received routine deworming treatments and vaccinations and shared the same environment for at least six months before the study.

10.2.3 Semen Collection and Processing

In both experiments, semen collection (n = 10 per each experiment) was performed with an artificial vagina. All ejaculates collected were white and milky in consistency. Raw semen was evaluated for volume, color, and concentration using a Burker's counting chamber. The volume of sperm-rich fraction was 3.1 ± 1.2 (mean ± SD) mL and sperm concentration was 211 ± 56 × 106 sperm/mL. Only ejaculates with ≥ 70% motility and ≥ 70% morphologically normal spermatozoa were included.
Each ejaculate was split into aliquots that were diluted to reach a final concentration of 100 × 106 sperm/mL respectively in egg-yolk TRIS-citrate glucose (EYT-G: Tris 2.4 g, Citric Acid 1.4 g, Glucose 0.8 g, Penicillin G Sodium Salt 0.06 g, Streptomycin 0.1 g, 20 mL of egg yolk and distilled water to 100 mL), i.e., the control group, and in EYT-G supplemented with different concentrations of crocin according to the experimental design. All aliquots were placed in a syringe without air, transported to the laboratory at 4 °C within 3 h, stored at 4 °C and analyzed at different time points according to the experimental design.

10.2.4 Membrane Integrity (Hypo-Osmotic Swelling Test)

The hyposmotic swelling test (HOST) was carried out at each time point to assess the functionality of the sperm plasma membrane in control and treated groups. Twenty microliters of semen were incubated at 37 °C for 45 min with 80 µL of pre-warmed HOST solution (0.73 g sodium citrate and 1.35 g fructose in 100 mL of distilled water, 150 mOsm). After incubation, a volume of 10 µL was placed on a glass slide and covered with a coverslip. Evaluations were conducted under phase-contrast microscopy (40 ×; Eclipse E200, Nikon, Tokyo, Japan) by operators unaware of the experimental design. The cells were classified as positive (damaged membrane) or negative (intact membrane) according to the presence or absence of coiled tails, respectively. A total of 200 spermatozoa were counted.

10.2.5 Motility Assessment

Sperm motility parameters (total and progressive motility, sperm subpopulations, and semen kinetic parameters) were assessed by a Sperm Class Analyzer (SCA) system (Microptic SL, Veterinary Edition, Barcelona, Spain) installed on a camera-equipped light microscope system (Eclipse E200, Nikon, Tokyo, Japan). The following parameters were considered for the assessment: total motility (%), progressive motility (%), the percentage of sperm subpopulations (rapid and medium progressive), average path velocity (VAP; µm/s), straight-line velocity (VSL; µm/s), curvilinear velocity (VCL; µm/s), straightness (STR; %), linearity (LIN; %), amplitude of lateral head displacement (ALH; beats/s) and beat cross frequency (beats/s).
SCA system settings for dog semen classified as spermatozoa, all the particles sized between 10 and 80 µm2, and as progressively motile spermatozoa those with 75% STR. The minimum velocity values considered for slow-medium and rapid spermatozoa subpopulations were 50 and 100 µm/s; spermatozoa with VCL below 10 µm/s were considered static and spermatozoa with VCL > 150 µm/s and ALH > 3.5 µm as hyperactive. Sixty frames per second with a minimum contrast of 35 were acquired.
For the evaluation, an aliquot of control or treated (C0.5, C1, and C2) semen at each time point was diluted 1:3 with TRIS-glucose-citrate in order to reach a concentration of 30 × 106 sperm/mL, as required by SCA system and incubated at 37 °C for 10 min before evaluation. Then, 5 µL were spotted onto a pre-warmed glass microscope slide, covered with a glass coverslip (22 mm × 22 mm). A minimum of five randomly selected microscopic fields with at least 100 sperm cells were evaluated in each sample, for a total of 500.

10.2.6 Intracellular ROS level

Sperm intracellular H2O2 levels were assessed with the fluorescent probe 2′,7′-Dichlorofluorescein diacetate (DCHF-DA) as previously described (Benedetti et al., 2022). The sperm (control and 0.5 mM Crocin groups) were incubated with 10 µM DCFH-DA for 30 min in the dark at 37 °C. After the incubation, 200 µL aliquots of these solutions were added to wells of a black-sided, clear-bottomed 96-well plate in replicates of three. The conversion of DCHF to the fluorescent product DCF was measured using a fluorescence spectrophotometer (GloMax®-Multi Detection System, Promega, Madison, WI) with excitation at 485 nm and emission at 535 nm.

ROS production was quantified from a DCHF standard curve and results were expressed as the intensity of DCHF fluorescence (Arbitrary Units, A.U.).

10.2.7 Lipid Peroxidation

Sperm lipid peroxidation of control and 0.5 mM crocin-treated samples was determined by assaying the Malondialdehyde (MDA) concentration using the thiobarbituric acid (TBA) test (Esterbauer and Cheeseman, 1990). To precipitate proteins, 100 µL of each sample was treated with 0.5 mL of cold 30% (w/v) trichloroacetic acid and centrifugated. One millimeter of supernatant was reacted with 1.3 mL of 0.5% (w/v) TBA at 85 °C for 40 min. In the TBA test reaction, each molecule of MDA reacts with two molecules of TBA with the production of a pink pigment having maximal absorbance at 532–535 nm. After cooling, the fluorescence was read at wavelengths of 536 nm for excitation and 557 nm for emission using a SPEX Fluoromax spectrophotofluorimeter (GloMax®-Multi Detection System, Promega, Madison, WI, USA). Concentrations of MDA were calculated using a calibration curve ranging between 0.5 and 2 pmol/mL and were expressed as nmol/L of proteins.

10.2.8 DNA fragmentation

The Terminal Deoxynucleotidyl Transferase (TdT)-Mediated dUTP Nick-End Labeling (TUNEL) assay was performed using the In Situ Cell Death Detection Kit (Roche Diagnostic, Mannheim, Germany) following the protocol previously described (Longobardi et al., 2020). Briefly, after fixation, cooled sperm (control and 0.5 mM Crocin groups) were permeabilized with 0.1% Triton X-100 containing 0.1% (w/v) sodium citrate for 10 min. Samples were then incubated with 50 µL TdT enzyme for 1 h at 37 °C in a dark and humidified atmosphere. After incubation, sperm were stained with bisbenzimide (Hoechst 33342; 1 mg/mL) for 30 min. Sperm cells were examined using a fluorescent microscope (Eclipse E-600; Nikon, Japan). The total sperm population was determined under blue fluorescence (DAPI filter, ex 330–380) revealing the nuclei of living or dead cells. Sperm with intense green fluorescence (FITC filter, ex 465–495) represent TUNEL-positive cells with DNA strand breaks in their nuclei. At least 200 spermatozoa of each sample were analyzed randomly to evaluate the percentage of TUNEL-positive sperm cells.

10.2.9 Statistical Analysis

Data were first recorded using a computerized spreadsheet (Microsoft® Excel® 2021, Redmond, WA, USA) and then imported into Statistical Package for Social Sciences (SPSS IBM® Statistics version 27.0, IBM Corporation, Armonk, NY, USA) for statistical analysis. The normality of the data and the homogeneity of variances were assessed using the Shapiro-Wilk and Levene tests, respectively. Accordingly, parametric and non-parametric tests were used in Experiment 1 and 2, respectively. Data are expressed as mean ± Standard Error when normally distributed, and as median and interquartile ranges (IQR) when not normally distributed. For Experiment 1, the Wilcoxon signed-rank test was used for comparisons among groups (control, C0.5, C1, and C2) at each time point and among storage time points within each group. In experiment 2, data on sperm intracellular ROS levels, lipid peroxidation, and DNA fragmentation were analyzed by a multivariate ANOVA (general linear model) with time points and groups as fixed factors and post hoc comparisons were carried out by Least Square Difference (LSD). Differences were considered statistically significant when $P \leq 0.05$.

10.3 Results

10.3.1 Membrane functionality (HOST)

The results of sperm membrane functionality during storage time are shown in Figure 10.1. A decrease ($P \leq 0.05$) of membrane functional integrity was observed at 7 days in all groups. Moreover, in the semen treated with 2 mM crocin (C2) a decrease ($P \leq 0.05$) was already recorded at 4 days. About the treatment effect, sperm membrane functionality was higher ($P \leq 0.05$) in C0.5 compared to both control and C1 groups at 4 days of storage. Furthermore, a higher ($P \leq 0.05$) proportion of sperm with functional intact membranes was recorded in the C0.5 and C1 groups compared to the control group after 7 days of storage. At any timepoint, no differences were detected between C2 and the other groups.

Effect of crocin supplementation in the extender on the quality of chilled canine semen

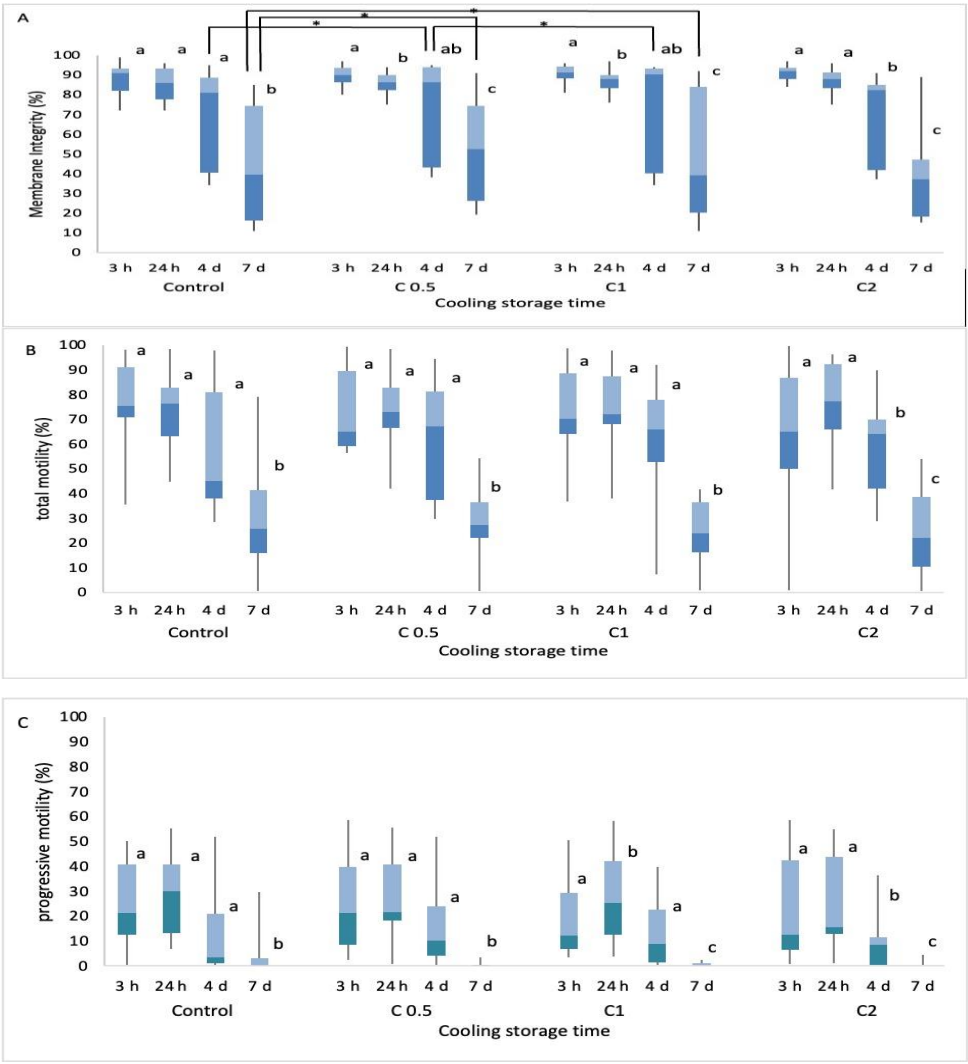

Fig. 10. 1 Membrane functionality (A), total (B) and progressive motility (C) of canine semen (N = 10) diluted with egg-yolk tris-citrate glucose (YET-G; control) or with YET-G supplemented with 0.5, 1, and 2 mM of crocin (C0.5, C1 and C2) after storage at 4 °C for 3 h, 24 h, 4, and 7 days (4 d and 7 d). For each box, the central line represents the median, the edges represent the IQR (25th and 75th percentiles), the whiskers represent the extreme points. Asterisks indicate significant difference at P ≤ 0.05 among groups within each time point. a,b,c Different letters indicate significant differences among time points within each group (P < 0.05).

10.3.2 Sperm kinematics

Results of total and progressive motility are depicted in Figure 10.1. No differences were observed in total and progressive motility among groups at any time point. During storage at 4 °C, total and progressive sperm motility decreased ($P \leq 0.05$) at 7 days in the control, C0.5 and C1 groups, while a reduction ($P \leq 0.05$) was already observed at 4 days in C2 group. Within the C1 group, progressive motility was higher ($P \leq 0.05$) after 24 h compared to the other times.
The results of kinetic parameters are shown in Table 10.1 The percentage of hyperactivated spermatozoa was similar among groups at all time points. This parameter decreased at 7 d of storage in all groups even if the difference was not statistically different in the control group. No differences in VCL were detected between the control and treated groups. After 4 days of storage, the VCL was higher in C0.5 than in C1 ($P \leq 0.05$) and the control group but in the latter case, the difference was not significant ($P > 0.07$). In all groups, VCL dropped ($P < 0.05$) only after 7 days of storage. The semen treated with 0.5 mM crocin (C0.5) exhibited higher ($P < 0.05$) VSL and VAP than the control group ($P \leq 0.05$) at 4 d of storage at 4 °C. Extending storage to 7 d resulted in a decrease of VAP in all groups; all treated groups, however, had lower ($P < 0.05$) values than the control.

Tab. 10. 1 Trends of hyperactivated spermatozoa (%) and semen kinetic parameters of canine (n=10) semen of control (CTRL) and Crocina groups (C0.5, C1 and C2) during storage at 4°C for 7 days.

	Storage time			
Hyper (%)	3h	24h	4d	7d
CTRL	2.9 (0-8) [a]	2.5 (0-8.2) [a]	0.3 (0-4.1) [a]	0 (0-1.1) [a]
C0.5	1.6 (0.2-11.4) [a]	1.9 (0.6-4.1) [a]	0.5 (0-4.3) [a]	0 (0-0) [b]
C1	2.5 (0.2-7.8) [a]	3.5 (0-7.3) [a]	0.9 (0-3.4) [ab]	0 (0-0) [b]
C2	2.2 (0.7-7.8) [a]	2.6 (1.2-9.8) [a]	0 (0-2.7) [a]	0 (0-0.4) [b]
VCL				
CTRL	73 (56.4-91.4)[a,xy]	77.7 (55.4-128.6)[a,xyz]	34.2 (19.3-91.2) [ab,xy]	24.1 (17.3-73.2)[b]

Effect of crocin supplementation in the extender on the quality of chilled canine semen

C0.5	84.2 (54.3-104.3)[a,x]	70.5 (49.5-107.1) [a,x]	65.5 (27.1-91.6) [a,x]	19.8 (16.2-30.3)[b]
C1	64.2 (40.7-95.2) [a,y]	83 (63.3-122.7) [b,y]	48.1 (26.9-71.8) [a,y]	19.8 (17.4-42.2)[c]
C2	68.7 (37.7-118.6) [a,xy]	81.6 (48.3-116.8) [b,xz]	44.4 (19.4-73.7) [a,xy]	17.5 (10.3-21.6)[c]
VSL				
CTRL	37.1 (26.4-49) [a]	39.3 (34-73.8) [a,xy]	13.7 (2.3-40.5)[b,x]	6.4 (3.2-24.3) [b,x]
C0.5	38 (20.2-57.5) [a]	39.2 (24.8-57.3) [a,xy]	26.8 (7.3-52.8) [a,y]	2.2 (1.3-7.4) [b,y]
C1	27.4 (21.5-43-1) [a]	39.9 (29.3-57.6) [b,x]	20.7 (8.4-29.3) [a,xy]	3.3 (1.5-13.6) [c,xy]
C2	34 (14.8-46) [ab]	35.5 (24.7-46.2) [a,y]	19.7 (3.4-29.7) [b,xy]	1.7 (0.7-4.8) [c,y]
VAP				
CTRL	49.2 (42.2-63.2) [a]	50.9 (40-92.7) [a,xy]	19.8 (5.7-52) [b,x]	11.2 (6.9-41.2) [b,x]
C0.5	53.2 (40.4-74.4) [a]	48 (32-75.7) [a,x]	36.6 (12.5-61.4) [a,y]	6.2 (5.1-14.2) [b,y]
C1	44.3 (28.2-61.2) [a]	56.7 (43-84.5) [b,y]	31.7 (13.8-41.8) [a,xy]	6.8 (3.4-23.7) [c,y]
C2	44.8 (24-81.2) [a]	53 (33.2-75.9) [a,x]	28.4 (6.7-44.9) [b,xy]	6.3 (3.4-10.3) [c,y]
LIN				
CTRL	47.6 (40-54.7) [a]	46.7 (41.4-55.4) [a]	29.8 (14.9-41.5) [b]	26.4 (17.3-33.2) [b,x]
C0.5	47 (40-48.7) [a]	41.8 (35.3-52.2) [a]	35.8 (27.4-44.8) [a]	14.2 (8.3 -24) [b,y]
C1	42.2 (40.1-52.5) [a]	46.3 (40.5-51.7) [a]	33 (31.1-40.5) [b]	17.3 (10-24.9) [c,xy]
C2	39.8 (35.1-45.1) [a]	41.5 (35.7-46.4) [a]	26.4 (17.3-33.2) [a]	9.9 (4.5-22.2) [b,y]
STR				
CTRL	66.4 (60-74) [a]	70.1 (65.2-73.1) [a]	53.8 (44.2-70.9) [b]	48.6 (42.3-62.5) [b,x]
C0.5	66.9 (61.2-71.2) [a]	64.1 (55.5-72.1) [a]	62.2 (49.8 -71.4) [a]	48.6 (36.4-54.5)[b,xy]
C1	65.4 (61-69.4) [a]	68 (60-71) [a]	60.2 (53.2-68.5) [ab]	59.3 (44.3-57.1) [b,x]
C2	63.4 (55.2-69.4) [a]	65.9 (57.7-71.3) [a]	60 (46.4-68.2) [a]	33.4 (11.8-50.7)[b,y]
BCF				

CTRL	8.8 (5.5-13.4) [a,x]	10.8 (6.4-13.7) [a]	3.8 (0.7-10.6) [b,x]	2 (1-8.2) [b,x]
C0.5	9.1 (4.9-12.9) [a,xy]	7.5 (5.6-13.2) [a]	6.9 (2.2-11.2) [a,y]	0.9 (0.6-2.5) [b,xy]
C1	6.8 (4.2-12) [a,y]	9.9 (6.8-14) [b]	5.5 (2.6-10.4) [a,xy]	0.9 (0.4-5) [c,xy]
C2	7.8 (4-14.2) [a,xy]	7.5 (4.7-13.6) [a]	6 (0.8-11) [b,xy]	0.8 (0.4-1.5) [c,y]

a, b, c Values with different superscripts within rows are significantly different; $P < 0.05$;
x,y Values with different superscripts within columns are significantly different; $P < 0.05$.
Abbreviations: VCL, curvilinear velocity; VSL, straight-line velocity; VAP, average path velocity; LIN, linearity; STR, straightness; BCF, beat cross frequency; ALH, amplitude of lateral head displacement.

No differences in LIN and STR were observed among groups at 3 h, 24 h, and 4 d of storage, whereas differences ($P < 0.05$) were detected at 7 d, with values tendentially higher in the control, as shown in Table 10.1. In relation to storage time, however, both parameters decreased ($P < 0.05$) in the control group at 4 d compared to earlier times, whereas this decrease ($P < 0.05$) was only detected in the C0.5 group at 7 d. BCF was higher ($P < 0.05$) in C0.5 group compared to the control at 4 d, with intermediate values in the other treated groups. The temporal pattern of BCF was similar to that of LIN and STR, with high values preserved up to 4 d and 7 d, respectively in the C0.5 and the control groups. Finally, ALH was higher ($P < 0.05$) in C0.5 compared to C1 and C2 groups at 4 d.

10.3.3 ROS levels, lipid peroxidation, and DNA fragmentation

As shown in Table 10.2, 0.5 mM crocin decreased ($P < 0.05$) the sperm intracellular ROS levels after 3 and 24 h storage compared to the control, while no differences were detected after 4 d. In the control group, ROS levels did not change at increasing storage times, while in the C0.5 group an increase ($P < 0.05$) was registered at 4 d. No differences in lipid peroxidation, indicated by the MDA concentrations, were recorded between the control and C0.5 groups at any time points, and unexpectedly no increase in lipid peroxidation was observed at prolonged storage times.

Tab. 10. 2 Sperm lipid peroxidation, measured as malondialdehyde (MDA) concentration, intracellular reactive oxygen species (ROS) levels and DNA fragmentation (TUNEL+ sperm), of canine semen (n = 10) during storage at 4 °C in the absence (control) and presence of 0.5 mM crocin for 4 days. Data are expressed as mean ± Standard Error (SE).

	Storage time		
ROS (A.U.)	3h	24h	4d
CTRL	903.5 ± 116.5^{x}	967.0 ± 176.8^{x}	933.2 ± 100.0
C0.5	$613.6 \pm 42.8^{y, a}$	578.0 ± 29.2^{ya}	1130.0 ± 133.8^{b}
MDA (mM)			
Ctrl	5.2 ± 0.5	5.4 ± 0.4	5.1 ± 0.3
C0.5	5.5 ± 0.4	5.2 ± 0.4	4.9 ± 0.4
TUNEL + (%)			
Ctrl	2.9 ± 0.6^{a}	6.9 ± 1.4^{a}	19.1 ± 1.7^{b}
C.05	3.7 ± 0.5^{a}	6.0 ± 2.0^{a}	18.3 ± 2.5^{b}

s, b Values with different superscripts within rows are significantly different; $P < 0.05$
x,y Values with different superscripts within columns are significantly different; $P < 0.05$

Finally, the percentages of sperm with fragmented DNA, i.e. TUNEL+, were similar in the control and C0.5 groups and increased ($P < 0.05$). only after 4 days.

10.4 Discussion

This study hypothesized that supplementation of the extender with crocin, an active constituent of saffron with antioxidant properties, would improve the quality of canine semen stored at 4 °C. The rationale behind this work originates from the evidence of OS occurring after prolonged refrigeration and of beneficial effects of crocin on sperm quality parameters reported in cattle, goats and buffalo (Longobardi et al., 2020, Longobardi et al., 2021, Sapanidou et al., 2022). To the best of our knowledge, this is the first study to assess the effects of crocin on chilled canine semen.

Effect of crocin supplementation in the extender on the quality of chilled canine semen

In order to evaluate the effects of crocin on sperm quality a dose-response trial was carried out, using concentrations (0, 0.5, 1 and 2 mM) previously tested (Longobardi et al., 2020, Longobardi et al., 2021, Sapanidou et al., 2022), showing that the most effective concentration for canine chilled semen was the lowest tested (0.5 mM), while the highest (2 mM) exerted in part a deleterious effect. The effects of the treatment were assessed at different times, such as 3 h, 24 h, 4 days, and 7 d. A deterioration of semen quality was recorded after 7 d of storage, the time at which sperm membrane functionality, total and progressive motility, as well as kinetic parameters, were significantly reduced in all groups. Meanwhile, the addition of the highest concentration of crocin (2 mM) to the extender caused a decrease of membrane functionality, total motility, and progressive motility earlier, i.e., at 4 d storage, indicating a potential toxic effect. The worsening of semen quality at prolonged storage time at 4 °C agrees with a previous study suggesting that chilled canine semen should be used for AI within 4.9 days (England and Ponzio, 1996). It has been previously shown that over extended storage at 4 °C spermatozoa switch from aerobic to anaerobic metabolism, due to oxygen consumption, and that the activation of glycolysis results in lactate production and hence reduced pH of the medium, leading in turn to decreased metabolism, ATP production and motility (Mann, 1964).

The most interesting findings of Experiment 1 regard the improvement of semen quality obtained with 0.5 mM crocin. Indeed, the addition of 0.5 mM crocin in the extender significantly increased sperm membrane functionality at both 4 and 7 d compared to the control group. Moreover, despite similar values of total motility and progressive motility, after 4 d of storage, most of the sperm kinetic parameters improved in the C0.5 group, compared to the control. Furthermore, in the C0.5 group, most of the kinetic parameters were preserved up to 4 d, whereas a decrease was already observed at this time in the control group. Motility is one of the most important indicators of the potential fertilizing ability of spermatozoa (Vijayaraghavan, 2003) and sperm kinetics is associated with fertility in various species (Broekhuijse et al., 2012, Marshburn et al., 1992).

It is known that sperm quality deteriorates at increasing storage times due to the occurrence of OS, resulting from an unbalance between ROS production and antioxidant systems (Silvestre et al., 2021). A correlation between OS and semen quality parameters has been demonstrated in dogs (Del Prete et al., 2018). Indeed, an improved semen quality of chilled canine semen has

been previously obtained by supplementing extender with several antioxidants such as maca, lycopene, cysteamine, and vitamins (Del Prete et al., 2022, Michael et al., 2009, Sheikholeslami et al., 2020).

In this study, the enrichment of the extender with 0.5 mM crocin improved sperm membrane functionality and sperm kinetics after 4 d of storage at 4 °C. To evaluate whether the beneficial effect of crocin was related to its antioxidant properties, this concentration was used in Experiment 2 to assess intracellular ROS levels, lipid peroxidation, and DNA fragmentation up to 4 d of storage. The reduced intracellular ROS levels, detected in the C0.5 group after 3 and 24 h storage of cooled canine semen, are in line with the known ROS scavenger function of crocin (Singla and Bhat, 2011, Sapanidou et al., 2015). This effect was unexpectedly lost after 4 d of storage, when the improvement of semen quality traits was more evident. Furthermore, he reduced intracellular ROS levels detected at 3 and 24 h in the C0.5 group were not associated with either increased lipid peroxidation or decreased DNA fragmentation. Regardless of the treatment, prolonged cooling of canine semen to 4 d was associated with increased DNA fragmentation, while lipid peroxidation was not affected by storage time. It is worth noting that the MDA levels in spermatozoa were relatively low in all groups and hence, due to the limitation of the assay and the high variability, small differences among groups could not be detected.

There are several reports on the beneficial effects of crocin on semen quality in different domestic species, in most of which, though crocin was added to the semen extender before freezing rather than chilling, and hence, results cannot be compared. In the goat supplementation of crocin in the extender decreased OS, improving sperm motility and DNA integrity of frozen-thawed sperm (Longobardi et al., 2020). In cattle, crocin improved sperm viability, motility, and kinetic parameters after thawing but a reduction of lipid peroxidation was only observed after 2 h post-thawing incubation (Sapanidou et al., 2022). In another study the incubation of frozen-thawed buffalo semen with crocin improved sperm membrane integrity and decreased DNA fragmentation and ROS levels (Longobardi et al., 2021). Undoubtedly, OS is more severe after freezing-thawing than cooling processes (Chatterjee and Gagnon, 2001). Moreover, there are fundamental differences between those two processes: during cryopreservation, OS increases the rigidity in the hydrophobic portion of the sperm membrane and consequently the susceptibility to lipid peroxidation (Chatterjee and Gagnon, 2001). Beneficial effects of the antioxidant supplementation in

semen extenders were observed during long storage periods, when the concentration of ROS dramatically increases (Silvestre et al., 2021). Based on our results, the improvement of membrane functionality and sperm kinetics observed in the C0.5 group after 4 d of storage is not associated with lower ROS levels, which decreased though during short-term storage; it is speculated that the antioxidant effect is lost over time due to reduced crocin bioavailability. Nevertheless, the improved protection from OS at early storage times seems to make spermatozoa more resistant during prolonged storage. Indeed, spermatozoa in the C0.5 group are exposed to high ROS levels for a shorter time. It would be interesting to evaluate whether re-exposing sperm to crocin during cooling would extend the beneficial effect on sperm quality beyond 4 d. The beneficial effects may also be related to other functions of crocin, such as the capability to increase intracellular detoxifying enzymes and to modulate membrane fluidity, leading to changes in its permeability to oxygen and other molecules (Assimopoulou et al., 2005).

10.5 Conclusion

In conclusion, we demonstrated that the enrichment of extender with crocin improves to a certain extent canine semen quality, particularly after 4 d of storage at 4 °C. At this time point crocin increased the percentage of sperm with intact membrane and most of the kinetic parameters. The treatment was not effective at further extending the lifespan of spermatozoa under chilling conditions, as shown by the deterioration of semen quality observed at 7 d. It was also demonstrated that crocin decreased sperm intracellular ROS levels at 3 and 24 h cooling, without affecting lipid peroxidation and DNA fragmentation. Further studies are required to further elucidate the mechanism of action of the compound, and validate these results, by assessing other fertility-associated parameters including fertilizing ability. Finally, from a future perspective, it would be interesting to assess the effect of crocin on the quality of frozen semen.

10.6 References

Aitken, R.J., 2017. Reactive oxygen species as mediators of sperm capacitation and pathological damage. Mol. Reprod. Dev. 84 (10), 1039–1052. https://doi.org/ 10.1002/mrd.22871.

Assimopoulou, A.N., Sinakos, Z., Papageorgiou, V., 2005. Radical scavenging activity of Crocus sativus L. extract and its bioactive constituents. Phytother. Res. 19 (11), 997–1000. https://doi.org/10.1002/ptr.1749.

Benedetti, S., Catalani, S., De Stefani, S., Primiterra, M., Fraternale, A., Palma, F., Palini, S., 2022. A microplate-based DCFH-DA assay for the evaluation of oxidative stress in whole semen. Heliyon 8 (9), e10642. https://doi.org/10.1016/j.heliyon.2022.e10642.

Broekhuijse, M.L.W.J., Sˇoˇstari´c, E., Feitsma, H., Gadella, B.M., 2012. Application of computer-assisted semen analysis to explain variations in pig fertility. J. Anim. Sci. 90 (3), 779–789. https://doi.org/10.2527/jas.2011-4311.

Chatterjee, S., Gagnon, C., 2001. Production of reactive oxygen species by spermatozoa undergoing cooling, freezing, and thawing. Mol. Reprod. Dev.: Inc. Gamete Res. 59 (4), 451–458. https://doi.org/10.1002/mrd.1052.

Del Prete, C., Ciani, F., Tafuri, S., Pasolini, M.P., Della Valle, G., Palumbo, V., Abbondante, L., Calamo, A., Barbato, V., Gualtieri, R., Talevi, R., 2018. Effect of superoxide dismutase, catalase, and glutathione peroxidase supplementation in the extender on chilled semen of fertile and hypofertile dogs. J. Vet. Sci. 19 (5), 667–675. https://doi.org/10.4142/jvs.2018.19.5.667.

Del Prete, C., Calabria, A., Longobardi, V., Palumbo, V., Merlo, B., Iacono, E., Tafuri, S., Carotenuto, D., Ciani, F., Damiano, S., Ciarcia, R., Cocchia, N., 2022. Effect of aqueous extract of maca addition to an extender for chilled canine semen. Animals 12 (13), 1638. https://doi.org/10.3390/ani12131638.

Domínguez-Rebolledo, A´.E., Ferna´ndez-Santos, M.R., Bisbal, A., Ros-Santaella, J.L., Ramo´n, M., Carmona, M., Martínez-Pastor, F., Garde, J.J., 2010. Improving the effect of incubation and oxidative stress on thawed spermatozoa from red deer by using different antioxidant

treatments. Reprod. Fertil. Dev. 22 (5), 856–870. https://doi.org/10.1071/RD09197.

England, G.C.W., Ponzio, P., 1996. Comparison of the quality of frozen-thawed and cooled-rewarmed dog semen. Theriogenology 46 (1), 165–171. https://doi.org/ 10.1016/0093-691X(96)00151-3.

Esterbauer, H., Cheeseman, K.H., 1990. Determination of aldehydic lipid peroxidation products: malonaldehyde and 4-hydroxynonenal. In Academic Press. Methods Enzymol. 407–421.

Hashemzaei, M., Mamoulakis, C., Tsarouhas, K., Georgiadis, G., Lazopoulos, G., Tsatsakis, A., Asrami, E.S., Rezaee, R., 2020. Crocin: A fighter against inflammation and pain. Food Chem. Toxicol. 143, 111521 https://doi.org/10.1016/j.fct.2020.111521.

Henkel, R., 2005. The impact of oxidants on sperm function. Andrologia 37 (6), 205–206. https://doi.org/10.1111/j.1439-0272.2005.00699.x. Linde-Forsberg, C., 2001. Regulations and recommendations for international shipment of chilled and frozen canine semen. A1209.0501. In: Concannon, P.W.,

England, G.C.W., Verstegen, J. (Eds.), Recent Advances in Small Animal Reproduction. Intenational Veterinary Information Service, Ithaca. A1209.0501. http://www.ivis.org/.

Longobardi, V., Zullo, G., Cotticelli, A., Salzano, A., Albero, G., Navas, L., Rufrano, D., Claps, S., Neglia, G., 2020. Crocin improves the quality of cryopreserved goat semen in different breeds. Animals 10 (6), 1101. https://doi.org/10.3390/ani10061101.

Longobardi, V., della Valle, G., Iannaccone, F., Calabria, A., Di Vuolo, G., Damiano, S., Ciarcia, R., Gasparrini, B., 2021. Effects of the antioxidant crocin on frozen-thawed buffalo (Bubalus bubalis) sperm. In: Ital. J. Anim. Sci, 20, pp. 2095–2101. https://doi.org/10.1080/1828051X.2021.1997653.

Mann, T., 1964. Metabolism of semen: fructolysis, respiration, and sperm energetics. The Biochemistry of Semen and the Male Reproductive Tract. Wiley,, New York, USA, pp. 265–307.

Marshburn, P.B., McIntire, D., Carr, B.R., Byrd, W., 1992. Spermatozoal characteristics from fresh and frozen donor semen and their correlation with fertility outcome after intrauterine insemination. Fertil. Steril. 58 (1), 179–186. https://doi.org/10.1016/S0015-0282(16)55157-7.

Mata-Campuzano, M., A´lvarez-Rodríguez, M., A´lvarez, M., Tamayo-Canul, J., Anel, L., de Paz, P., Martínez-Pastor, F., 2015. Post-thawing quality and incubation resilience of cryopreserved ram spermatozoa are

affected by antioxidant supplementation and choice of extender. Theriogenology 83 (4), 520–528. https://doi.org/10.1016/j.theriogenology.2014.10.018.

Michael, A.J., Alexopoulos, C., Pontiki, E.A., Hadjipavlou-Litina, D.J., Saratsis, P., Ververidis, H.N., Boscos, C.M., 2009. Effect of antioxidant supplementation in semen extenders on semen quality and reactive oxygen species of chilled canine spermatozoa. Anim. Reprod. Sci. 112 (1–2), 119–135. https://doi.org/10.1016/j.anireprosci.2008.04.007.

Rahaiee, S., Moini, S., Hashemi, M., Shojaosadati, S.A., 2015. Evaluation of antioxidant activities of bioactive compounds and various extracts obtained from saffron (Crocus sativus L.): a review. J. Food Sci. Technol. 52, 1881–1888. https://doi.org/10.1007/s13197-013-1238-x.

Rota, A., Stro¨m, B., Linde-Forsberg, C., 1995. Effects of seminal plasma and three extenders on canine semen stored at 4C. Theriogenology 44 (6), 885–900. https://doi.org/10.1016/0093-691X(95)00278-G.

Sapanidou, V., Taitzoglou, I., Tsakmakidis, I, Kourtzelis, I., Fletouris, D., Theodoridis, A., Zervos, I., Tsantarliotou, M., 2015. Antioxidant effect of crocin on bovine sperm quality and in vitro fertilization. Theriogenology 84 (8), 1273–1282. https://doi.org/10.1016/j.theriogenology.2015.07.005.

Sapanidou, V., Lavrentiadou, S.N., Errico, M., Panagiotidis, I., Fletouris, D., Efraimidis, I., Zervos, I., Taitzoglou, I., Gasparrini, B., Tsantarliotou, M., 2022. The addition of crocin in the freezing medium extender improves post-thaw semen quality. Reprod. Domest. Anim. 57 (3), 69–276. https://doi.org/10.1111/ rda.14049.

Sheikholeslami, S.A., Soleimanzadeh, A., Rakhshanpour, A., Shirani, D., 2020. The evaluation of lycopene and cysteamine supplementation effects on sperm and oxidative stress parameters during chilled storage of canine semen. Reprod. Domest. Anim. 55 (9), 1229–1239. https://doi.org/10.1111/rda.13770.

Silvestre, M.A., Y´aniz, J.L., Pen˜a, F.J., Santolaria, P., Castello´-Ruiz, M., 2021. Role of antioxidants in cooled liquid storage of mammal spermatozoa. Antioxidants 10 (7), 1096. https://doi.org/10.3390/antiox10071096.

Singla, R.K., Bhat, G.V., 2011. Crocin: an overview. Indo-Glob. Res. J. Pharm. Sci. 1 (4), 281–286.

Tapia, J.A., Macias-Garcia, B., Miro-Moran, A., Ortega-Ferrusola, C., Salido, G.M., Pena, F.J., Aparicio, I.M., 2012. The membrane of the mammalian spermatozoa: much more than an inert envelope. Reprod.

Domest. Anim. 47, 65–75. https://doi.org/10.1111/j.1439-0531.2012.02046.x.

Verstegen, J.P., Onclin, K., Iguer-Ouada, M., 2005. Long-term motility and fertility conservation of chilled canine semen using egg yolk added Tris–glucose extender: In vitro and in vivo studies. Theriogenology 64 (3), 720–733. https://doi.org/10.1016/j.theriogenology.2005.05.035.

Vijayaraghavan, S., 2003. Sperm motility: patterns and regulation. Introduction to Mammalian Reproduction. Springer, US, Boston, MA, pp. 79–91.

Chapter 11

Conclusions and future perspectives

The current thesis delved into several studies to explore and assess the utility and potential of CEUS in a comprehensive multiparametric ultrasonographic approach for evaluating the canine reproductive tract. The technique exhibited promising characteristics for assessing normal conditions and studying the physiology of the targeted organs. While CEUS found successful application in examining the prostate gland, uterus, and ovaries, its routine use in veterinary practice is still pending. Like all ultrasonographic techniques, it heavily depends on the operator's skill, and despite providing quantitative baseline parameters for reproductive organ evaluation, the limited number of studies restricts its integration into routine clinical practice. We strongly believe that the favorable findings of this thesis could encourage and enhance the use of CEUS in veterinary practice, particularly in differentiating between benign and malignant conditions, especially in the prostate gland, thereby avoiding more invasive and anesthesia-requiring techniques such as CT and MR.

Additionally, the results of this thesis displayed promising features regarding the use of CEUS for detecting the vascular blood supply of the prostate gland in neutered dogs, surpassing the capabilities of Color Doppler for small vessel diameter. The distinctions observed between benign and malignant prostatic conditions in intact dogs using CEUS underscore its potential for routine veterinary practice in diagnosing prostatic malignancies in neutered dogs. Incorporating CEUS into clinical practice not only facilitates the identification of lesions undetectable by conventional B-mode and Doppler ultrasound but also proves advantageous in conducting guided biopsies, reducing the need for random sampling, as seen in human medicine.

This manuscript showcases the excellent application of CEUS in female dogs, presenting intriguing results related to ovulation timing monitoring and pregnancy abnormalities. Given the limitations of existing techniques for detecting ovulation in dogs, CEUS emerges as a promising diagnostic tool with increased predictive value. The studies exhibit encouraging outcomes in using CEUS to detect corpora lutea formation, particularly aiding in monitoring luteal function during pregnancy, especially for detecting hypoluteidism.

Regarding CEUS in canine pregnancy, the study within this manuscript reveals promising results in differentiating between placental features in normal and abnormal fetuses. The findings suggest the potential use of this technique for early detection of placental failure in dogs, aiding in determining premature resorption or abortion. Furthermore, the results hint

at the significant role of placental vascularization in fetal abnormalities, as observed in human studies.

In conclusion, this thesis sheds light on the potential use of CEUS and opens new perspectives in the field of small animal reproductive imaging, encouraging further studies to establish an evidence-based approach in routine veterinary practice.